ROLE OF IN VIVO MECHANICAL LOADING IN THE PATHOLOGY, TREATMENT, AND PREVENTION OF OSTEOARTHRITIS

A Dissertation

Presented to the Faculty of the Graduate School

of Cornell University

In Partial Fulfillment of the Requirements for the Degree of

Doctor of Philosophy

by

Derek Timothy Holyoak

December 2018

ROLE OF IN VIVO MECHANICAL LOADING IN THE PATHOLOGY, TREATMENT, AND PREVENTION OF OSTEOARTHRITIS

Derek Timothy Holyoak, Ph. D.

Cornell University 2018

Osteoarthritis (OA) is a degenerative joint disease that affects millions of people worldwide and is the leading cause of disability in the elderly population. To date, no cure exists for OA, and the exact cause is not clearly understood. Mechanical loading at high magnitudes, however, is a primary risk factor for the disease. To better understand the role of mechanical loading in OA, we used an *in vivo* model that applies cyclic axial compression to the knee joints of mice. First, we used the model to study the role of abnormal cartilage matrix properties in load-induced OA. Next, we characterized a novel hydrogel-based drug delivery system and tested the hydrogel's therapeutic efficacy for intra-articular treatment of load-induced OA. Finally, we applied low-level mechanical forces to attenuate OA-like changes after joint injury.

We first sought to understand the effects of an abnormal cartilage matrix on the onset and progression of load-induced OA. The *cho/+* mouse has abnormal collagen fibrils in its cartilage matrix due to a *Col11a1* haploinsufficiency. We hypothesized that *cho/+* mice would develop more severe load-induced OA pathology compared to wildtype (WT) littermates with normal cartilage. Contrary to our hypothesis, *cho/+* mice had less severe load-induced cartilage damage. *Cho/+* mice also had thinner, less dense cortical bone and thicker cartilage. Both characteristics may have played a role in attenuating load-induced OA pathology in *cho/+* mice.

The next goal was to characterize an on-demand hydrogel-based drug delivery system for intra-articular OA treatment. Synthetic hydrogels were made of cross-linked 4-arm maleimide functionalized polyethylene glycol, and we analyzed their mechanical integrity and on-demand release *in vitro*. The hydrogels maintained their mechanical properties after 10,000 cycles of cyclic compression at 80% strain. In addition, they released particles in response to collagenase exposure, highlighting their on-demand release characteristics in the OA joint environment. *In vivo*, hydrogel injections reduced load-induced cartilage damage and osteophyte size. Further work is needed to determine the most effective drugs to combine with the hydrogel system.

Finally, we sought to determine whether low-level loads could attenuate post-traumatic OA. Mice underwent the destabilization of the medial meniscus (DMM) surgery to mimic an injury in the knee joint. These DMM joints were then loaded with low-level cyclic axial compression. The loading regimen attenuated DMM-induced cartilage degradation, osteophyte formation, and subchondral bone sclerosis. Thus, low-level axial loading may be used to slow post-traumatic OA progression.

In summary, *in vivo* cyclic tibial compression allowed us to better understand the role of mechanical loading in the pathology, treatment, and prevention of OA. Our results show that both cartilage and bone are involved in OA progression, and both tissues must be considered when predicting disease severity. Furthermore, synthetic hydrogel systems combined with therapeutics may be an effective approach to improve intra-articular drug retention time. Finally, low-level axial loading has the potential to aid as a preventive intervention for OA, particularly after a joint injury.

BIOGRAPHICAL SKETCH

Derek Timothy Holyoak was born in Blairstown, NJ on October 15, 1990. He graduated as valedictorian from North Warren Regional High School in 2009. In high school, Derek's interests in sports, science, and math sparked his interest in orthopaedic biomechanics. In 2013, he received a Bachelor of Science in Biomedical Engineering with a minor in Electrical Engineering from the University of Connecticut in Storrs, CT. At UConn, Derek was heavily involved in the BMES student chapter and enjoyed playing intramural sports. During his senior year, Derek pursued an internship at Cybex, International, where he and his team completed a study analyzing the biomechanical effects of body position on knee joint stresses during the lunge exercise. In 2013, he entered the Cornell Biomedical Engineering PhD Program. As a graduate student, Derek found a love for teaching and mentoring, and was given the opportunity as a GAANN Fellow to assist in successfully designing a junior-level biomedical engineering course in measurements and instrumentation. Additionally, he served as a Graduate Research and Teaching Fellow and led multiple teaching workshops for other graduate students and postdoctoral fellows. Derek collaborated with many faculty members at Cornell, and his research ranged from orthopaedic mechanobiology to drug delivery-based biomaterials. In his final year at Cornell, he placed 2nd in the 3-minute Thesis Competition and received the PhD Teaching Assistant of the Year Award. In October 2017, Derek got engaged to his incredible fiancé, Lynn, while they were on vacation in Iceland. In July 2018, Derek received his Doctor of Philosophy in Biomedical Engineering with plans to pursue a career in biomedical engineering consulting.

DEDICATION

I dedicate this work to Marty and Lorraine Rabinowitz and Spur.

ACKNOWLEDGMENTS

I could not have completed this PhD without all the love and support from my mentors, colleagues, collaborators, family, friends, and funding sources.

First and foremost, I would like to thank the members of my committee. My PI, Dr. Marjolein van der Meulen, guided me through the entire journey, gave me excellent advice whenever I had issues or needed guidance, and made me feel like an important part of the orthopaedics field. I have never met someone with so much passion for research as Dr. Christopher Hernandez, who provided me with motivation to keep pushing even when nothing was working. Dr. Mary Goldring from the Hospital for Special Surgery (HSS) provided a tremendous pool of knowledge on osteoarthritis. Dr. Ankur Singh was practically my fourth committee member, who taught me everything I need to know about biomaterials-based drug delivery. Also, Dr. Miguel Otero was close to a fifth committee member and was my primary contact for any biological question that arose during my PhD.

In addition to my committee, I need to thank Dr. Mathias Bostrom, Dr. Timothy Wright, and Dr. Steven Goldring from HSS for their expert advice on experimental design and analysis in the orthopaedics field. I also would like to thank Dr. Lawrence Bonassar, Dr. Lisa Fortier, Dr. Eve Donnelly, and Dr. Kirk Gunsallus for their expert opinions in the cartilage, bone, and biomechanics fields. I also need to thank everyone who helped me develop as a teacher. I truly lucked out having Dr. Chris Schaffer as my teaching mentor. Dr. Kimberley Williams and Dr. Derina Samuel taught me how to embrace teaching as research projects and develop teaching workshops. Lastly, I want

to thank Judy Thoroughman, Belinda Floyd, and Marcia Sawyer for all their administrative support.

My friends and fellow lab members at Cornell, UConn, and New Jersey played a major role in this accomplishment. They not only provided the motivation I needed to efficiently perform research, but they also offered relief after the workday and on weekends when I needed to relax and enjoy my time. I want to give special thanks to Dr. Funmi Adebayo for her mentorship, and Carolyn Chlebek, Tibra Wheeler, and Sophia Ziemian for their experimental assistance. My undergraduates, Naa Shidaa Armar, Ariana Otto, and Matthew Kim, played a key role in my success. I also need to thank all my friends, especially the 203 Prospect crew, the Real Graduates, and the basketball crew. Lastly, the UConn Has-Beens and the B-town Crew played a big part in my academic journey.

Finally, I need to thank my family for everything they do for me. My mom, Sharon, continuously cheers me on, and still has my first conference abstract framed at home. My dad, Andy, is hoping to become my first test-subject when our hydrogel system and beneficial loading regimen are translated clinically. My brother, Mike, was and still is the one I look up to as a successful engineer. Lastly, my fiancé, Lynn, gave me the support I needed to kick butt even when things were at their worst.

TABLE OF CONTENTS

LIST OF FIGURES

CHAPTER 1: INTRODUCTION

1.1 Synovial joints

A synovial joint (herein referred to as a joint) is a structure where two bones meet and articulate to allow motion. Synovial joints consist of a synovial capsule, synovial membrane, and articular cartilage. The synovial capsule is a dense, fibrous structure that surrounds the entire joint cavity. The synovial membrane is the inner layer of the joint capsule, and its primary function is to secrete synovial fluid. This fluid contains hyaluronan and lubricin, which interact to serve as a lubricant between the bones that make up the joint. Lastly, articular cartilage is a connective tissue that covers the ends of articulating bones. Cartilage provides a smooth, lubricated surface with minimal friction and aids in transmitting loads.

A number of synovial joints have additional structures that provide further stabilization and support to the joint (Fig. 1.1). For example, ligaments connect bones and prevent certain movements that could be harmful to joints. In the knee, the anterior/posterior cruciate ligaments (ACL/PCL) prevent excessive anterior/posterior motion or twisting, and the medial and lateral collateral ligaments (MCL, LCL) provide lateral support to the joint. Another critical part of the knee is the meniscus. The meniscus is a thin layer of fibrous tissue that lies between the articular cartilage on the tibial plateau and femoral condyles. The meniscus provides additional support to the knee and helps to distribute loads from the cartilage to the bone.

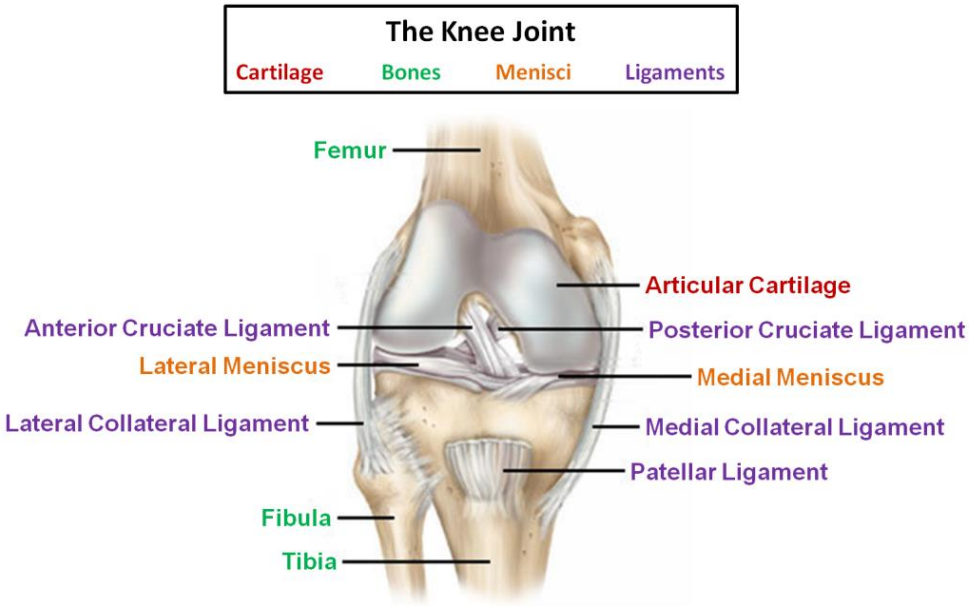

Figure 1.1. Labeled schematic of knee. The knee joint is the articulation between the femur and tibia. Articular cartilage lines the ends of each bone, and menisci provide further support and to the joint. Multiple ligaments serve to stabilize the knee. Adapted from umn.edu.

1.1.1 Articular cartilage

Articular cartilage is the most important feature of synovial joints. Without cartilage present in the joint, bones would not be able to articulate smoothly, and movement would be extremely painful. Collagen and proteoglycans are the two main constituents of the cartilage extracellular matrix (ECM) (Fig. 1.2). Collagen has two functions in the cartilage ECM. Its first function is to provide cartilage with tensile strength to withstand any excessive tensile forces in the joint [1]. Its second function is to entrap the proteoglycans in the ECM and prevent them from leaking out of the matrix [2]. The collagen in cartilage is primarily in the form of collagen II. In addition, collagen IX and XI contribute to the formation of collagen fibrils in the cartilage matrix [3,4]. Collagen serves as the backbone of the cartilage ECM.

Proteoglycans are hydrophilic components of cartilage that attract and retain water in the ECM. The water retained by proteoglycans is responsible for the compressive properties of the cartilage ECM [5]. Proteoglycans possess excellent hydrophilic properties because of their structure [6]. Their functional structural component is the glycosaminoglycan (GAG). Examples of GAGs are chondroitin sulfate and keratin sulfate. These GAGs are tethered to a core protein to form a paintbrush-like structure that behaves like a sponge to retain water during compression. These paintbrush-like structures are attached to long hyaluronic acid chains via linking proteins. Together, these components make up the proteoglycan. Aggrecan is the most abundant proteoglycan in the cartilage ECM.

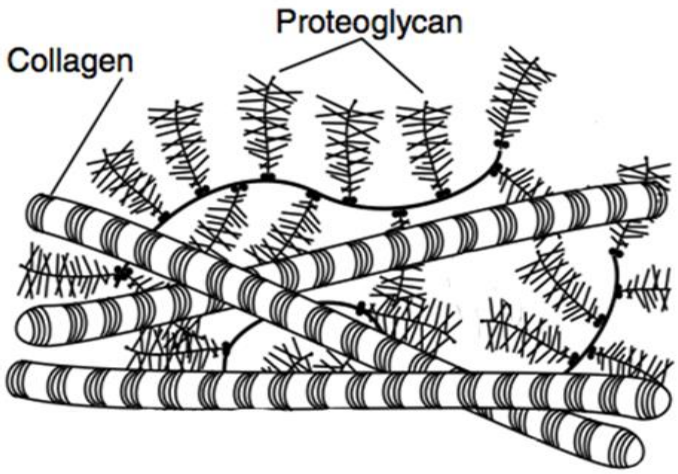

Figure 1.2. Cartilage extracellular matrix components. Collagen fibrils are the backbone of the cartilage ECM, and the paintbrush-like proteoglycans resist compression by attracting water. Adapted from quizlet.com.

In addition to the ECM, the cells in cartilage, or chondrocytes, form and maintain the tissue. Chondrocytes release factors that maintain the cartilage matrix and prevent excessive inflammation in the joint. Specifically, they produce and maintain both collagen and proteoglycans [7]. Furthermore, in a healthy state, chondrocytes release

anti-inflammatory factors, such as interleukin (IL)-10 [8]. Healthy and abundant chondrocytes are critical to cartilage function.

1.1.2 Cortical and cancellous bone

Bones are composite structures that consist of an exterior cortical shell and inner cancellous network. Cortical bone is dense and consists of basic units called osteons. Cancellous bone is porous and is composed of individual trabeculae. Osteoblasts and osteoclasts are cells found on or near the surface of bone. Osteoblasts form bone, and osteoclasts resorb bone. Osteocytes are the cells located within the mineralized bone matrix that play a major role in bone cell-to-cell signaling and facilitate the activity of osteoblasts and osteoclasts (i.e. remodeling). Bone structure and remodeling are both critical factors in the health of synovial joints, because of the direct interaction between bone and cartilage [9].

In this thesis, we focus on two regions of bone near articulating joints, the epiphysis and metaphysis. The epiphysis is the region at the end of a long bone that is separated from the rest of the bone by the growth plate. The epiphyseal cortical bone is commonly called the subchondral bone plate and lies directly underneath the articular cartilage. Epiphyseal cancellous bone consists of a small amount of cancellous bone that lies between the subchondral bone plate and growth plate. The metaphysis is the region on the opposite side of the growth plate that extends approximately 10% of the bone length towards the middle of the bone. The metaphysis contains cancellous bone surrounded by a cortical shell.

1.2 Osteoarthritis

Osteoarthritis (OA) is a progressive, degenerative, and disabling disease that affects synovial joints. Approximately 27 million people in the United States suffer from OA [10]. As the population ages and obesity rates rise, the prevalence of OA will increase, and predictions suggest that 25% of the adult population will have the disease by 2030 [11]. OA not only affects the elderly, but also younger, more active individuals with prolonged participation in high physical-demand activities. The disease can occur in multiple sites, primarily affecting the knees, hips, hands, and spine [12].

OA clinically presents as debilitating pain and stiffness and loss of joint function [13]. The disease is characterized by three main structural changes in the joint. These changes can arise from multiple risk factors that will be discussed in the following section. The first structural change is articular cartilage degeneration, indicated by narrowing of the joint space. The second change is a thickened, dense subchondral bone plate, commonly referred to as subchondral bone sclerosis. The third is the formation of bony spurs adjacent to the joint space, known as osteophytes. Together, these three structural changes help distinguish a healthy joint from an OA joint on an x-ray. In addition to these three hallmarks, changes occur in the menisci, synovium, ligaments, and peri-articular muscle as OA progresses (Fig. 1.3). Currently, no cure exists for OA, primarily due to the complex pathological mechanisms of the disease.

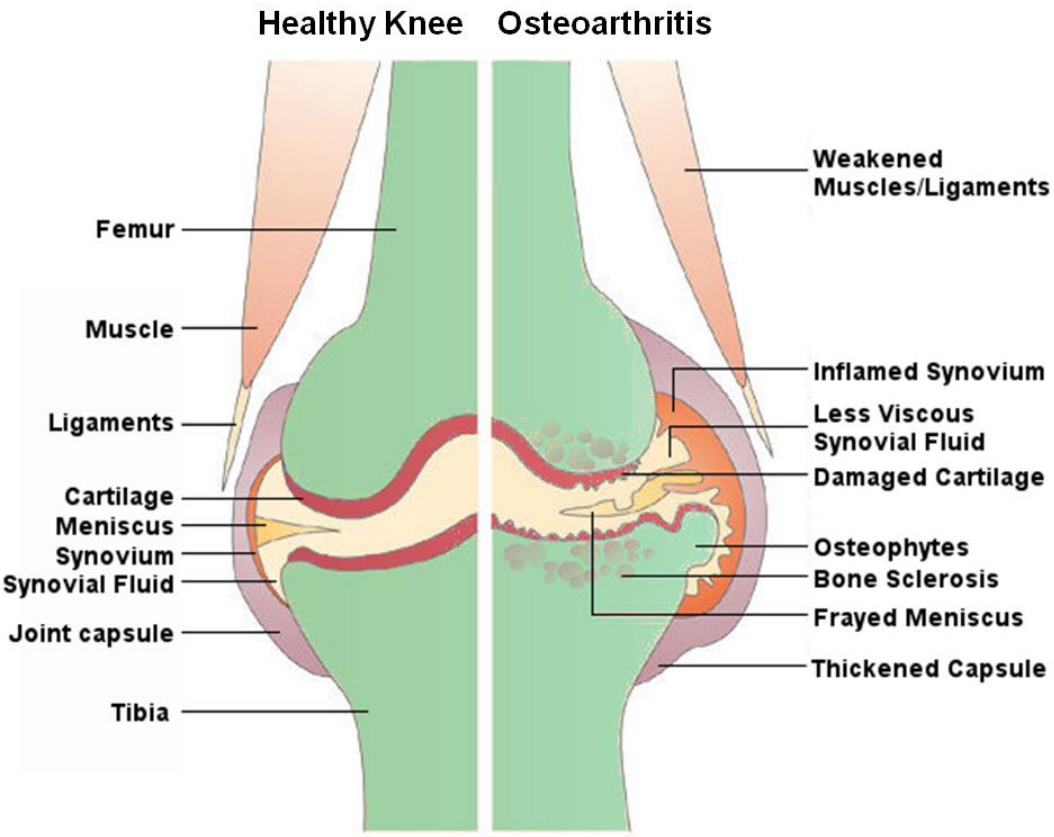

Figure 1.3. Healthy versus OA knee schematic. Cartilage degradation, subchondral bone sclerosis, and osteophyte formation are hallmarks for OA. In addition, many changes occur in the surrounding tissues. Adapted from [14].

1.3 Risk factors for osteoarthritis

Although no cure exists for OA, many risk factors for the disease have been identified based on clinical evidence. Some of these factors include obesity [15,16], aging [17], excessive mechanical loading during occupational activities [18,19], prior joint injuries [20,21], and genetic abnormalities [20]. Although we are aware of these risk factors, predicting disease onset remains extremely difficult, thus limiting effective preventive measures. Studying the interaction of risk factors will help to understand whether individuals with specific genetic backgrounds or physical attributes may be at higher risk for developing OA based on their lifestyles. Furthermore, determining the

interactions of risk factors may aid in the development of new preventive measures and clinical treatment options.

1.3.1 Mechanical loading and OA

Mechanical loading and joint health have a unique relationship. A large spectrum of loading types and magnitudes exists, and each specific load can result in different outcomes (Fig. 1.4). As mentioned previously, excessive mechanical loading is a primary risk factor for developing OA. Specifically, loading at high magnitudes can lead to cartilage degradation by decreasing proteoglycan synthesis [22] and inducing chondrocyte apoptosis [23]. Furthermore, high loads can rupture stabilizing ligaments, such as the ACL [24]. Other forces applied to the joint can directly damage soft tissue in the joint, such as the meniscus or cartilage [25]. Any damage to the joint or tissue surrounding the joint can lead to cartilage degradation.

Despite the consistent agreement that high loads are detrimental to joint health, specific types of loading can benefit joint health and potentially aid in the prevention of cartilage degradation. For example, low levels of mechanical loading, such as mild to moderate exercise or low-level mechanical stimulation, can increase proteoglycan synthesis *in vitro* [26] and maintain thicker cartilage throughout a rodent's lifespan [27]. Treadmill running and low-level loading protocols in rodents have slowed down the progression of injury-induced cartilage degradation [28,29]. Clearly, low levels of mechanical loading have potential to attenuate cartilage degradation. However, further understanding of the specific load levels that result in beneficial effects to the joint is necessary to prescribe rehabilitative loading regimens at the clinical level.

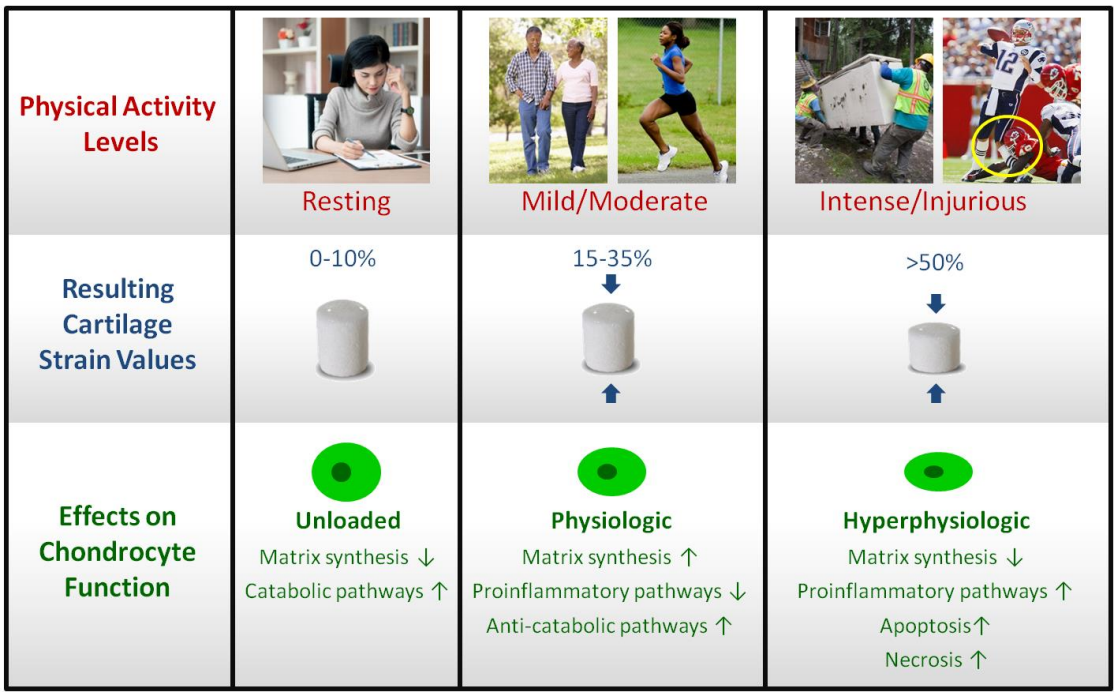

Figure 1.4. Unique relationship between mechanical loading and cartilage health. Chondrocytes exhibit a strain-dependent response. Absence of loading can result in downregulation of matrix synthesis. Mild or moderate levels of physical activity lead to beneficial effects, including increased matrix synthesis and decreased proinflammatory pathways. Intense activities that may lead to injury can cause cell death and increased inflammation. Adapted from [30].

1.3.2 Abnormal tissue properties and OA

The role of cartilage and subchondral bone properties in OA pathology has been a topic of interest for many years [31,32]. Differences in tissue properties often are due to genetics. Epidemiological studies of OA have estimated a heritability of 50% or more depending upon the affected joint, suggesting that half of the variation in disease susceptibility could be explained by genetic factors [33-36]. The collagen network within cartilage can be influenced by genetics. For example, mutations that affect key collagen genes, such as *Col11a1*, lead to abnormally thick collagen fibrils in the cartilage ECM [37], accompanied by reduced tissue tensile properties and OA-like

features early in life. Alterations in other genes that affect collagen II, collagen IX, or proteoglycan structure also lead to abnormal cartilage matrix properties [38].

Subchondral bone properties can vary among individuals. However, whether high or low bone mass increases risk for OA remains unclear. Individuals with extremely elevated bone mass are more susceptible to OA [39–41]. However, women with decreased bone density due to osteoporosis commonly develop OA. In a preclinical model of load-induced OA, higher bone mass protected against cartilage damage [42]. Thus, conflicting evidence makes the interaction between subchondral bone properties and OA onset/progression an important area of OA research.

1.3.3 Joint injury and post-traumatic OA

Joint injuries, especially injuries that occur in the knee, account for a significant subset of OA cases. Examples of injury include tears to stabilizing ligaments such as the ACL, damage to key tissues like the meniscus, or direct impact to subchondral bone or articular cartilage. When these types of injuries occur, an inflammatory cascade commences, and joint mechanics are often altered because of damage to key stabilizing components. Together, excess inflammation and altered joint mechanics resulting from joint trauma lead to a form of OA called post-traumatic OA (PTOA). Approximately 12% of OA cases at the knee are classified as PTOA [43]. Because joint injury is such a common risk factor for OA, many models to study OA involve some type of injury. These models will be discussed further in section 1.6.1.

1.4 Current understanding of OA pathology

During the evolution of OA, inflammatory factors released by cells residing in the synovium, including synovial macrophages and fibroblasts, induce changes in chondrocytes within the cartilage matrix. In a healthy state, these chondrocytes normally benefit the structural integrity of collagen and aggrecan in the tissue. Under OA conditions, however, chondrocytes up-regulate the production of destructive proteases, including matrix metalloproteinases (MMPs) and aggrecanases. These proteases degrade the cartilage matrix, releasing matrix degradation products. Matrix fragments then initiate further inflammatory responses, leading to a vicious cycle of inflammation and cartilage destruction. In addition, inflammatory cytokines act on the adjacent synovium and bone to stimulate synovial inflammation and de-regulate peri-articular bone remodeling. In this section, we briefly review some of the main processes associated with OA, including inflammation, cartilage matrix degradation, and bone adaptation (Fig. 1.5).

1.4.1 Inflammation

Inflammatory factors, including tumor necrosis factor (TNF)-alpha and interleukins (ILs), play a crucial role in OA pathogenesis. TNF-alpha plays a major catabolic role in OA and downregulates production of cartilage extracellular components, including aggrecan and collagen type II [44]. In addition to its direct effects on cartilage matrix synthesis, TNF-alpha also promotes the production of other cytokines, including IL-1 and IL-6. Lastly, TNF-alpha interacts with the receptors

TNFR1 and TNFR2 to activate sensory neurons, leading to pain associated with OA [45].

Similar to TNF-alpha, IL-1 directly affects cartilage by decreasing levels of matrix components and inhibiting anabolic chondrocyte activity [46]. IL-1 also induces production of collagenases and aggrecanases in synovial fibroblasts and chondrocytes, leading to further cartilage destruction [47]. IL-6 is another interleukin that is elevated in the synovial fluid of individuals with OA. The role of IL-6 in disease onset and progression is complex, involving both proinflammatory joint destruction [48] and anti-inflammatory mediation [49].

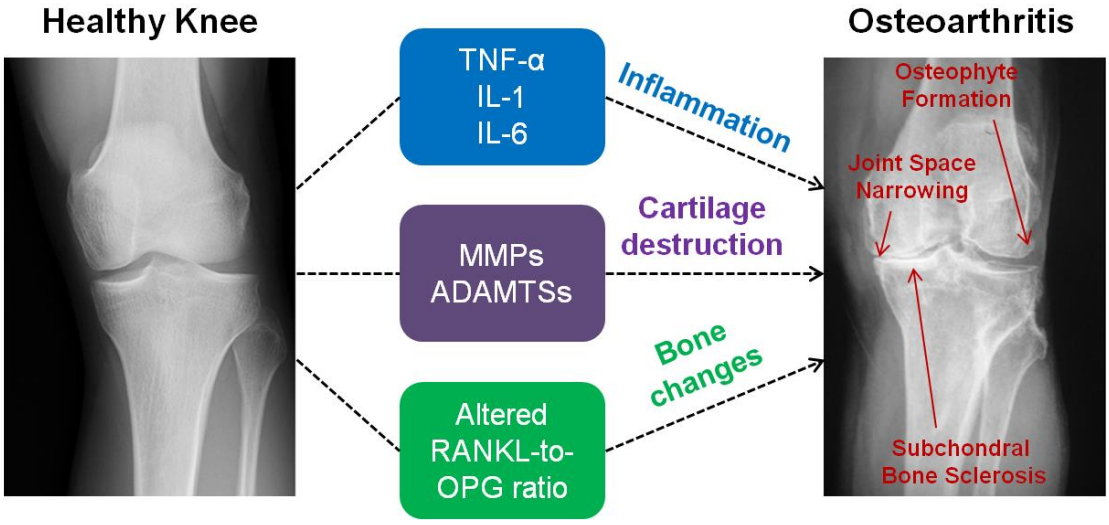

Figure 1.5. Osteoarthritis pathology. Schematic of OA pathology with key factors contributing to disease progression. Human knee joint x-rays depict healthy and OA conditions. Adapted from [50]. (Images courtesy of: Dr. Mathias P. Bostrom at the Hospital for Special Surgery, New York).

1.4.2 Cartilage matrix degradation

Structural damage of the cartilage matrix occurs from a variety of proteolytic enzymes that break down aggrecan, type II collagen, and other key matrix components.

The major aggrecanases in OA include ADAMTS (A Disintegrin and Metalloproteinase with ThromboSpondin type I motifs)-4 and -5, and MMP-3. In general, aggrecanases cleave the aggrecan protein between the G1 and G2 globular domains. This cleaving creates aggrecan fragments that have weakened compressive properties compared to intact aggrecan proteins [51].

The major collagenases associated with OA are MMP-1 and MMP-13, which cleave collagen proteins at specific locations, resulting in two or more collagen fragments [52,53]. Again, these collagen fragments do not provide the structural support or tensile strength that intact collagen fibrils provide to the healthy articular cartilage matrix, resulting in compromised load-bearing properties. Importantly, the presence of matrix fragments in the synovial joint space initiates further inflammation, perpetuating the vicious cycle of inflammation and matrix destruction.

1.4.3 Bone adaptation

In addition to structural and molecular changes that occur in the cartilage, certain enzymes can alter the underlying bone. For example, the RANKL (receptor activator of NF-κβ ligand)-to-OPG (osteoprotegerin) ratio, is altered in the OA state. Under healthy conditions, the RANKL-to-OPG ratio maintains an appropriate balance between osteoblast and osteoclast activity. Under OA conditions, however, osteoblasts in the subchondral bone exhibit an altered RANKL-to-OPG ratio [54]. This promotes excess bone formation, leading to subchondral bone sclerosis.

1.5 Osteoarthritis treatment

Because of the complexity of OA pathology, developing disease-modifying drugs remains extremely difficult. Until we better understand the disease mechanism, traditional treatments will be the most effective in alleviating pain associated with OA (Fig. 1.6). The first suggested treatment involves lifestyle changes [55]. Improvements in diet and more frequent exercise are common non-pharmacologic recommendations to relieve pain [56]. Weight loss from diet and cardiovascular exercise can alleviate pain by reducing forces experienced by the affected joints. Furthermore, strength training targeted at improving quadriceps, hamstring, and calf strength can help absorb forces that would otherwise be transmitted through the knee joint [57,58]. However, clinicians only recommend mild exercise, because high-intensity exercise involving heavy loads may worsen OA-related symptoms.

Oral medications are the first pharmacologic treatment option for OA-associated pain. Some of the most common oral medications are non-steroidal anti-inflammatory drugs (NSAIDs). These drugs target and inhibit cyclo-oxygenase enzyme (COX)-2 activity associated with inflammation. Acetaminophen is another medication commonly used for OA that inhibits the synthesis of prostaglandins and has similar effects to NSAIDs. Nutritional supplements may also help to inhibit OA-associated pain. Glucosamine-chondroitin is one of the most popular supplements and may even aid in production/retention of GAGs in the cartilage ECM [59]. If pain is unbearable, opioids can be prescribed by a clinician, but their use can result in physical dependence and withdrawal symptoms. Overall, some of the main downfalls of oral administration of

drugs is the possibility for gastrointestinal irritation and lack of targeting to the affected joint.

If oral medications fail to relieve pain, intra-articular (IA) injection is the next step. These injections are delivered directly to the joint space and are thus more targeted compared to oral delivery. The most common drugs used for IA injections are corticosteroids, hyaluronic acid (HA), and platelet-rich plasma (PRP) [60-62]. The main limitation of IA injections is the lack of retention time inside the joint, resulting in minimal functional improvement in patients. A large area of current research focuses on engineering novel drug delivery platforms to improve drug retention time inside the joint. Both current drugs used in the clinic and novel drug delivery approaches will be discussed in further detail in the following sections.

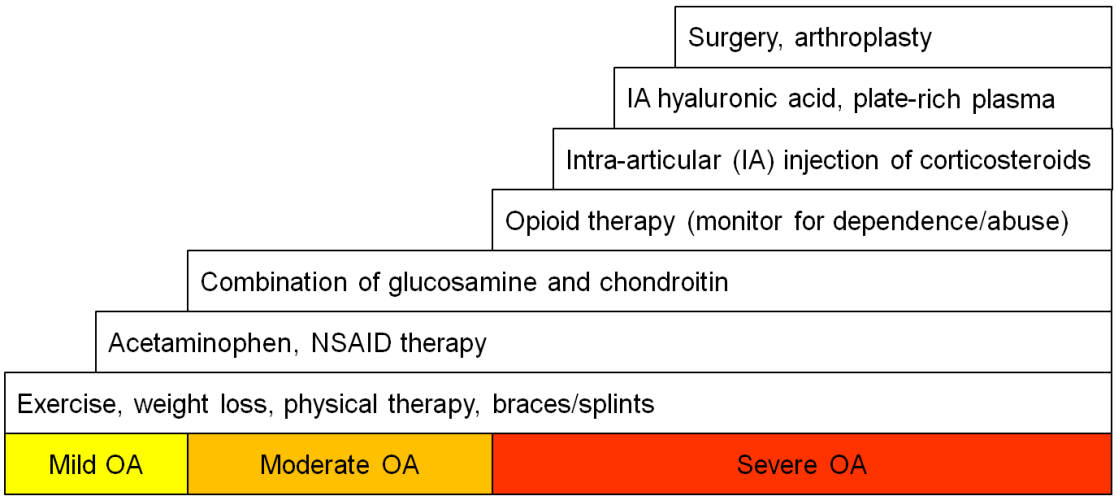

Figure 1.6. Summary of OA treatments. The majority of interventions typically begin when patients present severe OA signs and symptoms. Clearly, earlier, more effective interventions are necessary to better prevent and treat the disease. Adapted from [55].

Surgical intervention is required when both non-pharmacologic and pharmacologic treatments become ineffective in relieving pain. Arthroscopic techniques remove debris in the joint space or create smooth surfaces on the cartilage surface.

Osteotomy removes osteophytes that inhibit physiological joint movement. When damage associated with OA becomes too severe, joint replacement, or arthroplasty, is the most effective option. Hip and knee replacements are the standard treatments for end-stage OA and are generally successful in relieving pain. However, the surgery is invasive, requires drastic lifestyle changes, and results in a major financial burden. Thus, patients generally want to avoid surgery if possible.

1.5.1 Intra-articular drug therapies in the clinic

Corticosteroids, hyaluronic acid (HA), and platelet-rich plasma (PRP) are the most common drugs used for IA drug delivery in the clinic. Corticosteroids function as anti-inflammatory and immunosuppressive agents. Although the mechanism of action is not fully understood, corticosteroids suppress local inflammation by down-regulating arachidonic acids and prostaglandins [60], leading to vasoconstriction [63]. The clinical effects of corticosteroids have been reviewed extensively [64,65]. In general, IA injection of corticosteroids effectively reduces pain up to 3 weeks post injection, but the effect diminishes after longer periods [66]. Yet, no conclusion can be drawn to confirm the improvement in joint function, measured in terms of walking distance, range of motion and several scoring systems.

IA-injected HA has been proposed to alleviate OA symptoms. Physically, HA behaves as a viscoelastic lubricant at low shear rates (resting and walking) and an energy absorber at high shear rates (exercising) [67]. Exogenous HA also mediates inflammation, regulates nerve sensitivity, and enhances synthesis of proteoglycans [68]. The outcome from clinical trials of IA injection of HA has been systematically reviewed

[69]. When combining the results from multiple clinical trials, the injection of HA did not improve joint function at any time point. Like corticosteroids, the benefits of HA injection were limited to pain reduction in patients after exercise, but not pain at rest. The pain-relieving effects of HA were not significant during the first 5 weeks post-injection but became significant after 10 weeks. Therefore, the effect of HA has a delayed initiation and prolonged duration, compared with corticosteroids. Although HA of higher molecular weight (MW) has been suggested to be more effective in alleviating OA from *in vitro* and *in vivo* models [70], no difference between high and low MW HA has been observed in clinical trials [69,70].

Another current IA injectable medication for OA that has recently emerged is platelet-rich plasma (PRP) [71]. PRP can be separated from a patient's blood via centrifugation and injected back into the affected site and potentially increase the rate of healing because of its high concentration of growth factors. In the past, PRP was primarily used to treat chronic tendon injuries. More recently, PRP is being used to treat acute tendon and ligament injuries and chronic knee OA. A recent review discussed how PRP reduced pain and improved function significantly better than HA in OA patients [72]. Further research is still required to fully understand PRP's effects in treating OA.

1.5.2 Novel biomaterials for intra-articular drug delivery

Despite the variety of drugs available for IA injection, this mode of delivery does not consistently relieve OA symptoms due to limited drug retention times in the joint space. Corticosteroids and hyaluronic acid, for example have half lives in suspension of 1 to 2 hours and 22-26 hours, respectively [73]. These problems partly

arise because of the physical and electrical barriers that the articular cartilage ECM provides to the chondrocytes. Specifically, the dense collagen II network, the avascularity, and the negatively charged aggrecan molecules may prevent entrance of therapeutic agents into the cartilage matrix [74]. In addition, the synovial membrane surrounding the intra-articular joint space creates a compartment that can retain larger molecules, but many small molecules such as NSAIDs and other therapeutics can rapidly leak out of the joint space.

To overcome these retention challenges, biomaterials-based drug delivery platforms have been developed, including microparticles, nanoparticles, and injectable hydrogels. Micro- and nano-particle systems involve encapsulating a drug of choice inside or tethered to a biomaterial. Particle size ranges from the nanoscale to the microscale. In general, drugs combined with particle delivery systems demonstrate improved retention time compared to the drug alone [50].

Injectable hydrogels offer unique capabilities as a drug delivery system. Hydrogels can be made of synthetic or natural materials [75]. Synthetic hydrogels offer a few advantages over natural hydrogels, including excellent biocompatibility, inert properties, and tunable mechanical properties based on formulation [76,77]. A goal of this thesis is to engineer and test a synthetic hydrogel drug delivery system to improve retention time inside the joint, and therefore, make IA drug delivery a more effective strategy for OA treatment.

1.6 Preclinical models of osteoarthritis

To better understand OA and to test novel treatments for the disease, preclinical animal models have been developed to recapitulate OA progression. Animal models can be classified under invasive and non-invasive categories (Fig. 1.7). Invasive models primarily use chemically-induced cartilage degeneration or surgical injuries, and non-invasive models involve repetitive joint loading, load-induced impact injury or spontaneously occurring OA progression [50,78,79].

1.6.1 Invasive Preclinical OA Models

Under the invasive models, chemically-induced cartilage degeneration approaches involve intra-articular injection of collagenase [80–82], TGF-β [83], monosodium iodoacetate [84–87], or papain [88–90]. These methods have provided critical knowledge about key molecular and cellular pathways during disease initiation. However, these models do not fully recapitulate human OA progression, limiting their use in understanding clinical scenarios [50,78].

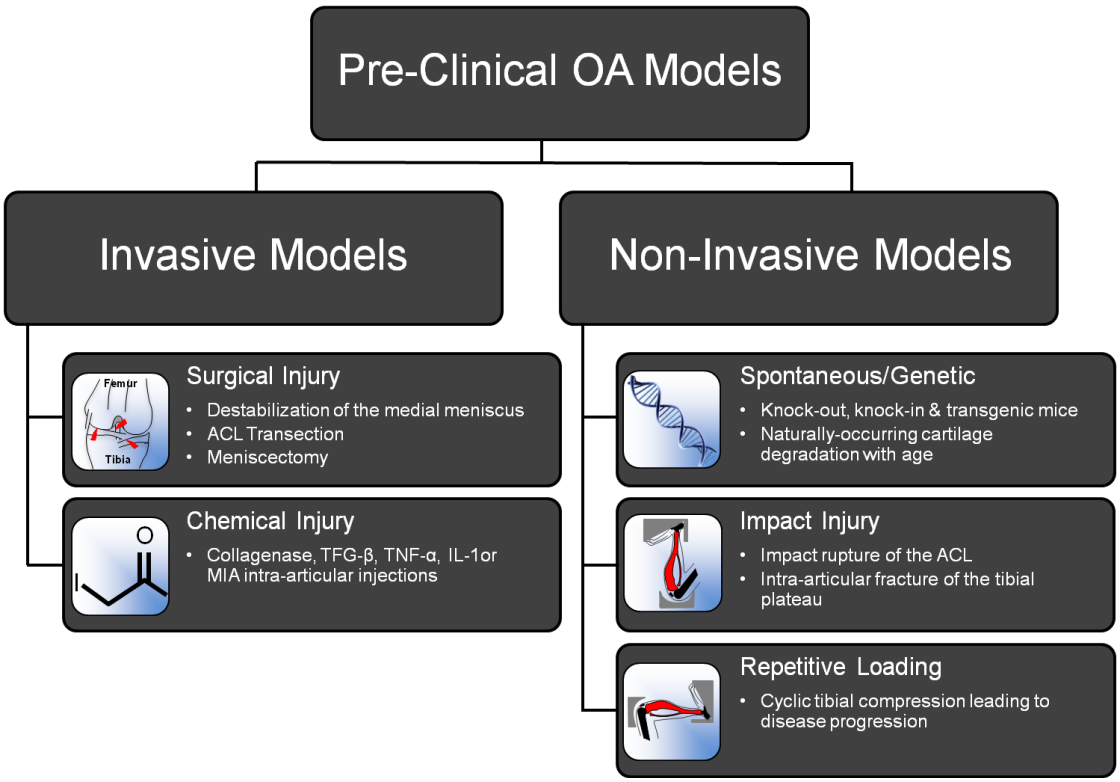

Figure 1.7. Preclinical animal models for OA research. Models can be classified as invasive or non-invasive. They can also represent traumatic injuries or long-term wear and tear of joints. Adapted from [91].

Post-surgical models of OA better mimic clinical injuries and subsequent OA progression. Models, such as anterior cruciate ligament transection (ACLT) [92–95], meniscectomy [93,94], and destabilization of the medial meniscus (DMM) [96,97] involve the use of surgical methods to disrupt or transect stabilizing ligaments, leading to alterations in joint mechanics. With surgical trauma, OA results over time, enabling the investigation of the full time course of post-traumatic OA progression. These surgical injuries have been applied to a variety of animal models [78], and have significantly contributed to the current knowledge of post-traumatic OA progression. However, a major limitation of these models is the difficulty in differentiating the

surgical inflammatory and healing response from the progression of OA, which confounds the understanding of disease etiology.

1.6.2 Non-Invasive Preclinical OA models

Non-invasive models of OA have been developed to elucidate the mechanism of OA progression without the confounding effects of surgical intervention [98]. These models include genetic/spontaneous OA development [99,100], non-invasive impact injury models [24,25,101,102], and the recently-developed cyclic load-induced OA model [103,104].

Genetic/spontaneous models involve the use of animals, such as the guinea pig [100], certain strains of mice (e.g. C57Bl/6 and BALB/c) [105], or mice that have been genetically manipulated and develop the disease throughout their lifespan. Such studies allow for understanding OA pathology without external intervention and exploring genetic pathways for potential therapeutic targets. However, many forms of spontaneous OA can take months or even years to develop, limiting their use in laboratory settings.

Non-invasive impact injury models utilize high compressive loads to induce an intra-articular fracture of the tibial plateau [25] or rupture of the ACL [24], both leading to OA initiation and progression. Each of these non-invasive models provides key advantages in understanding OA pathology, particularly in recapitulating the clinical scenario without invasive measures. However, the exact mechanical environment of the joint within these models is unknown, and thus the relationship between mechanical forces and OA progression is difficult to understand.

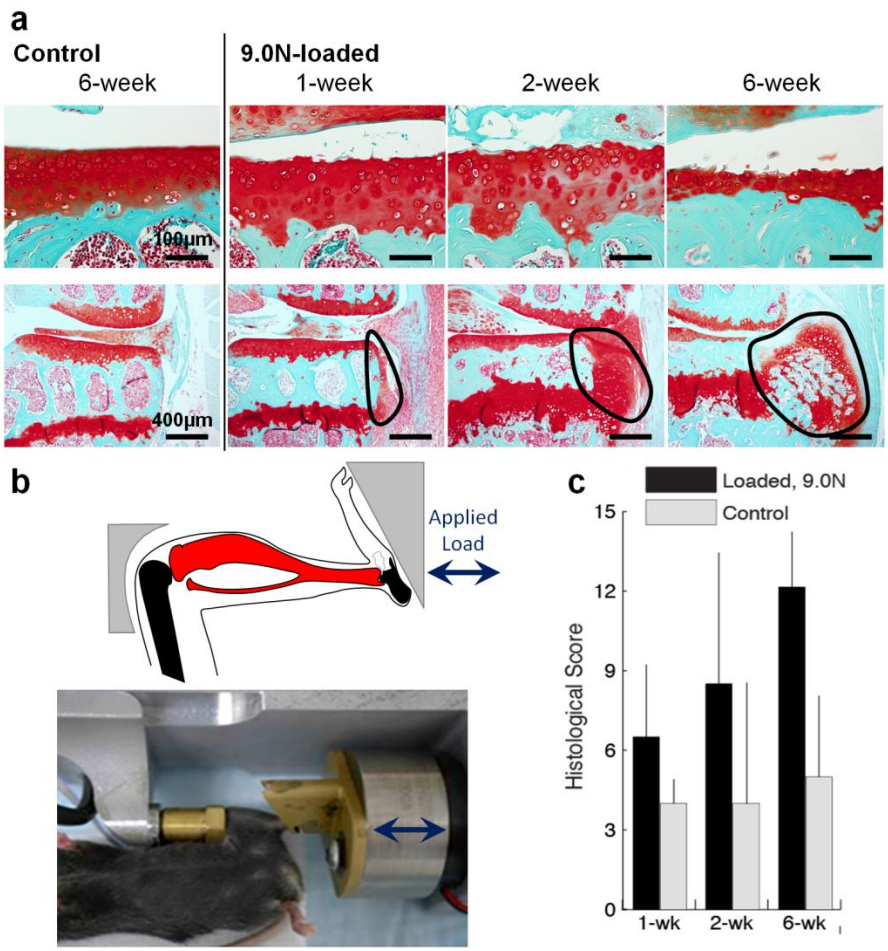

Figure 1.8. *In vivo* cyclic tibial compression. a) Representative histological sections from loading consisting of 9.0N peak loads for 1200 cycles daily at 4.0Hz frequency for either 1, 2, or 6 weeks. Top row shows cartilage (shown in red) thinning and surface damage over time with loading, and bottom row shows osteophyte growth and maturation. b) Schematic and photograph of the mouse leg inside the loading device. c) Histological scores indicating greater severity of OA overtime with 9.0N-loading. Adapted from [104].

The cyclic load-induced model of OA offers a unique platform to specifically elucidate the relationship between mechanical forces and disease initiation (Fig. 1.8). Primarily used in mice, the load-induced model applies controlled, cyclic compressive loading to the tibia, leading to predictable OA progression in the knee joint [103,104]. The next section summarizes the key features of load-induced OA mouse models.

1.6.3 Models of load-induced OA

A common theme in this thesis is the application of cyclic tibial compression. Cyclic loading applied to the tibia of mice noninvasively induces OA-like changes over time [103,104]. This *in vivo* loading model allows the user to specify the load magnitude, number of cycles, frequency of each cycle, and duration of loading. In general, higher loads lasting for longer durations lead to more cartilage degeneration and subchondral bone changes. Importantly, unlike other OA animal models, cartilage degeneration in this model is most likely not due to joint instability or an injury, but is caused by direct mechanical overload of the articular cartilage [106]. The cyclic tibial compression model can produce a range of OA severity. Thus, therapeutics can be tested for efficacy under moderate and severe OA conditions with the model.

To date, cyclic tibial compression has been used to study the initiation and progression of load-induced OA at high and moderate load magnitudes. High (9.0 Newtons) load magnitudes induced OA-like changes, including cartilage degradation, osteophyte formation, and subchondral bone changes, in young (10-week) and adult (26-week) mice. Moderate (4.5 Newtons) loads led to less severe cartilage degradation. No evidence of bone changes was evident after 6 weeks of moderate loading in adult mice. A goal of our lab is to relate these load magnitudes in mice to physical activities in humans (Fig. 1.9). We also seek to determine the effects of mild loads. If we can understand the effects of multiple load levels in mice, we may be able to better distinguish beneficial versus detrimental loading types in humans.

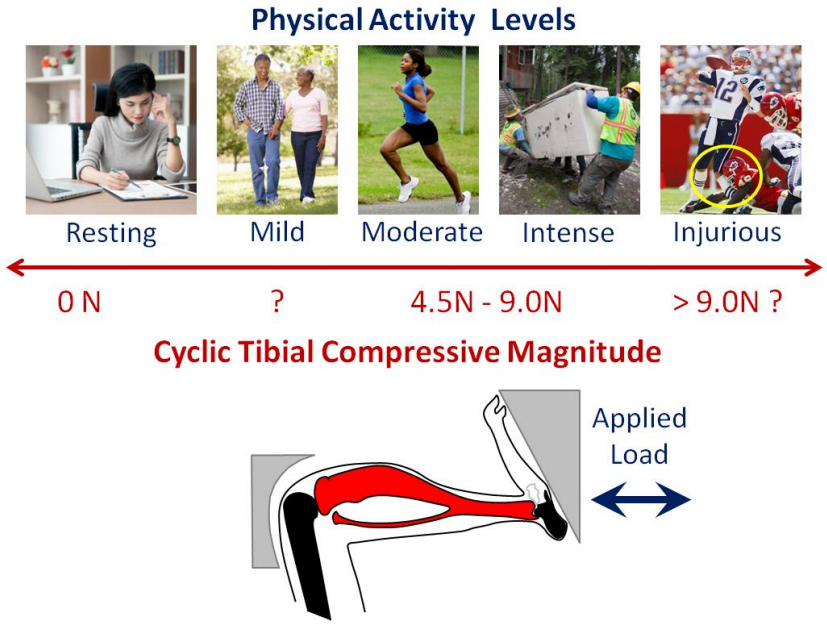

Figure 1.9. Relationship between physical activity levels in humans to cyclic tibial loading magnitudes in mice. Our lab previously showed that both 4.5N- and 9.0N-loading induced cartilage damage in mice. However, further research is necessary to explore loading magnitudes that are beneficial to cartilage health.

1.7 Metrics for determining disease severity

Clinically, the main measures for OA severity include a combination of imaging and self/clinician assessment to determine morphologic features and symptoms related to pain, function, and quality of life. The most common imaging modality to assess OA severity is the radiograph. Clinicians score the severity of a radiograph based on the joint space width and severity of osteophyte formation. For example, Kellgran and Lawrence developed a scoring system that is still used today [107,108]. The scale ranges from 0 to 3, with normal joints receiving a score of 0, and severely diseased joints indicating a score of 3. In addition to x-ray, magnetic resonance imaging and computed tomography scans can further assess 3D structural changes in the bone and soft tissue surrounding the joint.

Self-reported questionnaires and clinician-administered outcome measures also play a key role in identifying pain and function associated with disease. One of the most common self-reported questionnaires is the Western Ontario and McMaster Universities Osteoarthritis Index (WOMAC) score. The questionnaire consists of 24 questions relating to pain, function, and stiffness. The questions are then weighted, and scores are measured to determine disease severity. Other common self-reported questionnaires include the Knee Injury and Osteoarthritis Outcome Score (KOOS) and the American Academy of Orthopaedic Surgeons (AAOS) Outcomes Instruments. Furthermore, clinicians assess functional characteristics such as range of motion, muscle strength, and instability.

Clinical measures of OA are effective in determining OA severity based on radiograph scores and self-reported pain. However, clinical measures do not offer any insights into disease mechanism or tissue-specific changes. On the other hand, preclinical models offer a platform to perform end-stage analyses of tissue morphology and protein levels. The following two sections will describe the structural and cellular/protein-level assays frequently performed in preclinical murine models of OA.

1.7.1 Murine tissue morphology outcome measures

In preclinical murine models, outcome measures include cartilage degradation, bone morphology, and other joint tissue changes upon experiment completion (Fig. 1.10). Mice are euthanized, and the knee joints are harvested and fixed. The joints can be imaged using microcomputed tomography (microCT) and processed for paraffin embedding and histology. MicroCT scans are taken of the knee joints to assess cortical

and trabecular bone morphology. Specifically, the thickness and tissue mineral density of the subchondral bone plate can be determined. The underlying cancellous bone morphology in the epiphysis (distal to the subchondral bone plate and proximal to the growth plate) and metaphysis (distal to the growth plate) can also be analyzed for bone volume fraction, trabecular thickness and separation, and tissue mineral density.

The histological analysis seeks to measure the severity of articular cartilage damage using semi-quantitative scoring methods. Thin sections are typically stained with Safranin O or Toluidine blue and examined for structural and cellular changes in the cartilage. In general, normal healthy cartilage is scored low (0) and the score increases to represent damaged cartilage. Two frequently used scoring systems are the OARSI and Mankin systems [37,109]. The OARSI scoring system is sensitive to structural changes in the cartilage, and the Mankin system focuses on cellular and proteoglycan-level changes. With the OARSI scoring system [109], normal articular cartilage scores a 0, proteoglycan loss is 0.5, small fibrillations on the cartilage surface is 1, vertical clefts down to immediately below the superficial layer is 2, and vertical clefts/erosion to the calcified cartilage extending <25%, 25-50%, 50-75%, and 75-100% of the articular surface are 3, 4, 5 and 6, respectively.

With the Mankin scoring system, proteoglycan content, indicated by the Safranin O staining intensity, is scored 0 to 4, chondrocyte arrangement is scored 0 to 3, and chondrocyte periphery staining is scored 0 to 2 [37]. Scores for these three categories are added together for each tissue section. Both OARSI and Mankin scoring are generally performed across the entire joint using evenly spaced tissue sections. Scores are then averaged, summed, or the maximum is taken to assess OA severity.

Additional histological outcomes include osteophyte severity and changes in the synovial lining, meniscus, and ligaments.

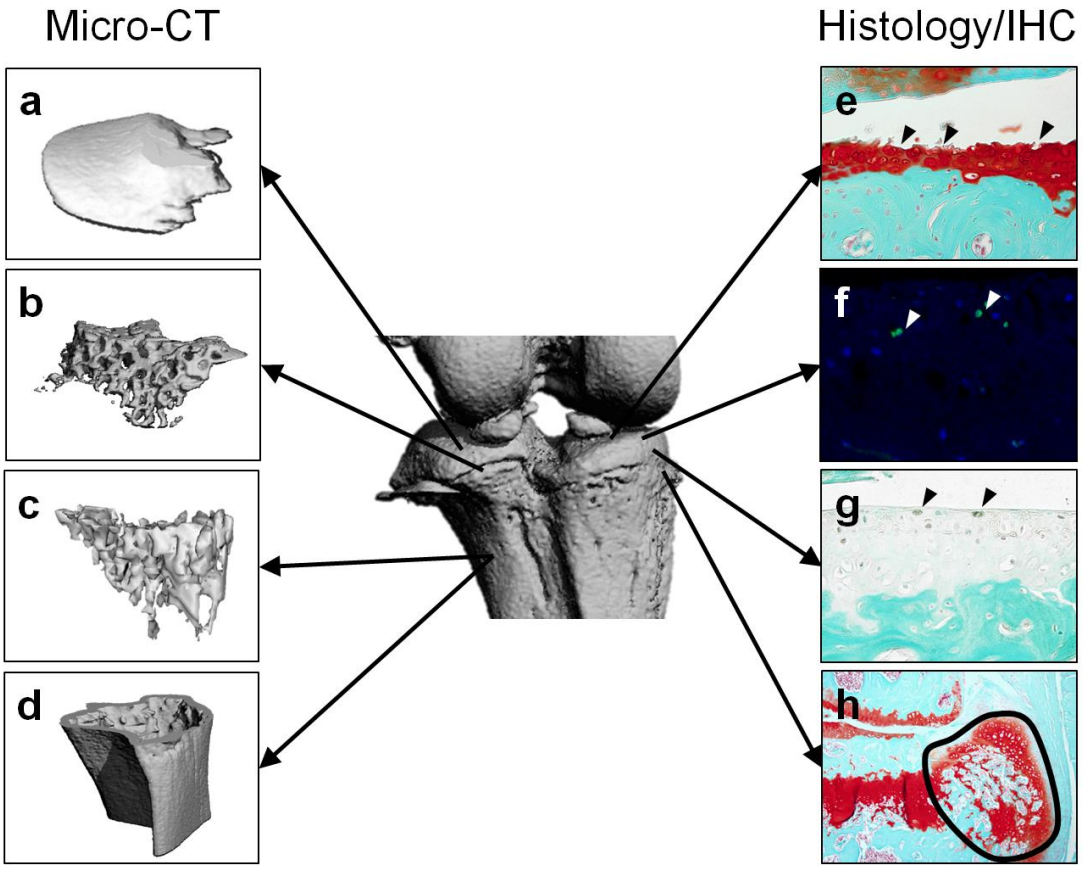

Figure 1.10. Murine outcome measures for assessment of OA severity. MicroCT scans can be used to analyze tissue properties of the a) subchondral bone, b) epiphyseal cancellous bone, c) metaphyseal cancellous bone, and d) metaphyseal cortical shell. Histology and IHC can be used to assess e) cartilage morphology, f) cell death, d) protein levels, and h) osteophyte formation. Adapted from [91].

1.7.2 Murine cellular outcomes

In addition to tissue morphology, efforts have increased to understand the cellular pathways associated with OA. To this end, immunohistochemistry (IHC) has been implemented to further analyze bone, cartilage, synovial and meniscal changes on the protein level [102,110]. Briefly, tissue sections are incubated with a primary antibody for the protein of choice, and then with a secondary antibody and substrate for

visualization. Positive staining in the joint tissues is then quantified and compared to contralateral control joints, thus expanding our understanding of OA progression from the cellular to the tissue scale.

1.8 Aims

This thesis focuses on three key aspects of osteoarthritis: pathology, treatment, and prevention. Regarding pathology, we investigated the effect of abnormal cartilage material properties resulting from altered genetics on load-induced osteoarthritis progression. In terms of treatment, we engineered and tested a novel hydrogel-based drug delivery system to improve intra-articular drug retention times and deliver drugs on-demand. Lastly, we used low-level mechanical loading to attenuate OA progression after joint injury in mice.

1.8.1 Aim 1

Interactions among risk factors for osteoarthritis (OA) are not well understood. We investigated the combined impact of two prevalent risk factors: mechanical loading and genetically abnormal cartilage tissue properties. The *cho/+* mouse has abnormal collagen fibrils in its cartilage matrix due to a point mutation in the *Col11a1* gene. We used cyclic tibial compression to simulate mechanical loading in the *cho/+* (*Col11a1* haploinsufficient) mouse. We hypothesized that the collagen mutation would not alter bone properties and that *cho/+* mice, which develop early onset OA, would develop exacerbated load-induced cartilage damage compared to their littermates. To test our hypotheses, we applied cyclic compression to the left tibiae of 6-month-old *cho/+* male

mice and wild-type (WT) littermates for 1, 2, and 6 weeks at moderate (4.5N) and high (9.0N) peak load magnitudes. We then characterized load-induced cartilage and bone changes by histology, microcomputed tomography, and immunohistochemistry.

1.8.2 Aim 2

Short drug retention times in the joint space have limited the success of intra-articular drug delivery as a treatment for osteoarthritis (OA). Injectable hydrogels recently were developed to overcome this retention challenge. Ideally, an intra-articular hydrogel delivery system should maintain constant size for long durations under hydrolytic conditions, withstand forces that occur in weight-bearing joints, and release therapeutics in the presence of inflammatory markers and/or degradative enzymes, such as collagenases (e.g. matrix metalloproteinase (MMP)-3 or -13). To this end, we engineered an on-demand, biocompatible, injectable hydrogel using crosslinked 4-arm maleimide functionalized polyethlyene glycol (PEG-MAL). To crosslink the hydrogel, we used nondegradable Dithiothreitol (DTT) or MMP-3 and -13 degradable GCRDVPMSMRGGDRCG peptides (VPM). To predict how these hydrogels perform as a drug delivery system, we aimed to 1) determine the effect of PEG-MAL weight percentages on swelling ratios of hydrogels, 2) understand the effects of cyclic compression and hydrolytic degradation on the mechanical properties and particle release from hydrogels, and 3) determine the effect of degradable crosslinker on particle release from hydrogels in the presence of collagenase. Finally, in an *in vivo* mouse model, we 4) determined if the hydrogels could attenuate OA progression after a single bout of high-magnitude cyclic tibial compression.

1.8.3 Aim 3

Mechanical loading and joint health have a unique relationship in OA onset and progression. Intense physical activity or high levels of loading lead to cartilage degradation by decreasing proteoglycan synthesis, inducing chondrocyte apoptosis, and rupturing stabilizing ligaments. On the other hand, mild exercise resulting in low-level loads benefits cartilage by preventing injury-induced cartilage degradation, maintaining thicker cartilage, and increasing proteoglycan synthesis *in vitro*. However, exercise leads to systemic effects, such as muscle growth and weight loss, that are also beneficial to joint health. Therefore, whether low levels of mechanical loading can directly aid cartilage health remains unclear. We sought to understand the beneficial effects of low-level mechanical loading using *in vivo* cyclic tibial compression. We used low-level cyclic compression in combination with a surgically-induced model of post-traumatic OA, the destabilization of the medial meniscus (DMM), to determine whether daily cyclic compression would directly benefit knee joints. We hypothesized that low-level cyclic compression would attenuate post-traumatic OA pathology induced by DMM.

1.9 References

1. Hedlund H, Mengarelli-Widholm S, Reinholt FP, Svensson O. Stereologic studies on collagen in bovine articular cartilage. *APMIS* 1993;101:133–40.
2. Chen MH, Broom N. On the ultrastructure of softened cartilage: a possible model for structural transformation. *J Anat* 1998;192 (Pt 3):329–41.
3. Shaw LM, Olsen BR. FACIT collagens: diverse molecular bridges in extracellular matrices. *Trends Biochem Sci* 1991;16:191–4.
4. Li Y, Lacerda D a, Warman ML, Beier DR, Yoshioka H, Ninomiya Y, Oxford JT, Morris NP, Andrikopoulos K, Ramirez F. A fibrillar collagen gene, Col11a1, is essential for skeletal morphogenesis. *Cell* 1995;80:423–430.
5. Oegema TR. Delayed formation of proteoglycan aggregate structures in human articular cartilage disease states. *Nature* 1980;288:583–5.
6. Pickard J, Ingham E, Egan J, Fisher J. Investigation into the effect of proteoglycan molecules on the tribological properties of cartilage joint tissues. *Proc Inst Mech Eng Part H J Eng Med* 1998;212:177–182.
7. Hunter GK, Rogakou CC, Pritzker KP. Extracellular matrix synthesis by articular chondrocytes and synovial fibroblasts in long-term monolayer culture. *Biochim Biophys Acta* 1984;804:459–65.
8. Iannone F, Bari C De, Dell'Accio F, Covelli M, Cantatore FP, Patella V, Bianco G Lo, Lapadula G. Interleukin-10 and interleukin-10 receptor in human osteoarthritic and healthy chondrocytes. *Clin Exp Rheumatol* 19:139–45.
9. Goldring MB, Goldring SR. Articular cartilage and subchondral bone in the pathogenesis of osteoarthritis. *Ann N Y Acad Sci* 2010;1192:230–237.
10. Lawrence RC, Felson DT, Helmick CG, Arnold LM, Choi H, Deyo RA, Gabriel S, Hirsch R, Hochberg MC, Hunder GG, Jordan JM, Katz JN, Kremers HM, Wolfe F, National Arthritis Data Workgroup. Estimates of the prevalence of arthritis and other rheumatic conditions in the United States. Part II. *Arthritis Rheum* 2008;58:26–35.
11. Hootman JM, Helmick CG. Projections of US prevalence of arthritis and associated activity limitations. *Arthritis Rheum* 2006;54:226–229.
12. Felson DT. Epidemiology of hip and knee osteoarthritis. *Epidemiol Rev* 1988;10:1–28.
13. Hunter DJ, Felson DT. Osteoarthritis. *BMJ* 2006;332:639–42.
14. Wieland HA, Michaelis M, Kirschbaum BJ, Rudolphi KA. Osteoarthritis - an untreatable disease? *Nat Rev Drug Discov* 2005;4:331–44.
15. Felson DT, Anderson JJ, Naimark A, Walker AM, Meenan RF. Obesity and Knee Osteoarthritis. *Ann Intern Med* 1988;109:18.
16. Messier SP, Loeser RF, Miller GD, Morgan TM, Rejeski WJ, Sevick MA, Ettinger WH, Pahor M, Williamson JD. Exercise and dietary weight loss in overweight and obese older adults with knee osteoarthritis: the Arthritis, Diet, and Activity Promotion Trial. *Arthritis Rheum* 2004;50:1501–10.
17. Buckwalter JA, Saltzman C, Brown T. The impact of osteoarthritis: implications for research. *Clin Orthop Relat Res* 2004:S6-15.
18. Kaila-Kangas L, Arokoski J, Impivaara O, Viikari-Juntura E, Leino-Arjas P, Luukkonen R, Heliövaara M. Associations of hip osteoarthritis with history of recurrent exposure to manual handling of loads over 20 kg and work participation: a population-based study of men and women. *Occup Environ Med* 2011;68:734–8.
19. Cameron KL, Hsiao MS, Owens BD, Burks R, Svoboda SJ. Incidence of physician-diagnosed osteoarthritis among active duty United States military service members. *Arthritis Rheum* 2011;63:2974–82.
20. Felson DT. Osteoarthritis: New Insights. Part 1: The Disease and Its Risk Factors.

Ann Intern Med 2000;133:635.
21. Lohmander LS, Englund PM, Dahl LL, Roos EM. The long-term consequence of anterior cruciate ligament and meniscus injuries: osteoarthritis. *Am J Sports Med* 2007;35:1756–69.
22. Kurz B, Jin M, Patwari P, Cheng DM, Lark MW, Grodzinsky AJ. Biosynthetic response and mechanical properties of articular cartilage after injurious compression. *J Orthop Res* 2001;19:1140–1146.
23. Stolberg-Stolberg JA, Furman BD, William Garrigues N, Lee J, Pisetsky DS, Stearns NA, DeFrate LE, Guilak F, Olson SA. Effects of cartilage impact with and without fracture on chondrocyte viability and the release of inflammatory markers. *J Orthop Res* 2013;31:1283–1292.
24. Christiansen B a., Anderson MJ, Lee C a., Williams JC, Yik JHN, Haudenschild DR. Musculoskeletal changes following non-invasive knee injury using a novel mouse model of post-traumatic osteoarthritis. *Osteoarthr Cartil* 2012;20:773–782.
25. Furman BD, Strand J, Hembree WC, Ward BD, Guilak F, Olson SA. Joint degeneration following closed intraarticular fracture in the mouse knee: a model of posttraumatic arthritis. *J Orthop Res* 2007;25:578–92.
26. Sah RL-Y, Kim Y-J, Doong J-YH, Grodzinsky AJ, Plass AHK, Sandy JD. Biosynthetic response of cartilage explants to dynamic compression. *J Orthop Res* 1989;7:619–636.
27. Hubbard-Turner T, Guderian S, Turner MJ. Lifelong physical activity and knee osteoarthritis development in mice. *Int J Rheum Dis* 2015;18:33–39.
28. Hamamura K, Zhang P, Zhao L, Shim JW, Chen A, Dodge TR, Wan Q, Shih H, Na S, Lin C-C, Sun H Bin, Yokota H. Knee loading reduces MMP13 activity in the mouse cartilage. *BMC Musculoskelet Disord* 2013;14:312.
29. Galois L, Etienne S, Grossin L, Watrin-Pinzano A, Cournil-Henrionnet C, Loeuille D, Netter P, Mainard D, Gillet P. Dose-response relationship for exercise on severity of experimental osteoarthritis in rats: a pilot study. *Osteoarthritis Cartilage* 2004;12:779–86.
30. Sanchez-Adams J, Leddy HA, McNulty AL, O'Conor CJ, Guilak F. The mechanobiology of articular cartilage: bearing the burden of osteoarthritis. *Curr Rheumatol Rep* 2014;16:451.
31. Burr DB, Utreja A. Editorial: Wnt Signaling Related to Subchondral Bone Density and Cartilage Degradation in Osteoarthritis. *Arthritis Rheumatol* 2018;70:157–161.
32. Radin EL, Rose RM. Role of subchondral bone in the initiation and progression of cartilage damage. *Clin Orthop Relat Res* 1986:34–40.
33. Felson DT, Zhang Y. An update on the epidemiology of knee and hip osteoarthritis with a view to prevention. *Arthritis Rheum* 1998;41:1343–1355.
34. Meurs JBJ van. Osteoarthritis year in review 2016: genetics, genomics and epigenetics. *Osteoarthr Cartil* 2017;25:181–189.
35. Valdes AM, Spector TD. Genetic epidemiology of hip and knee osteoarthritis. *Nat Rev Rheumatol* 2011;7:23–32.
36. Spector TD, MacGregor AJ. Risk factors for osteoarthritis: genetics. *Osteoarthr Cartil* 2004;12:39–44.
37. Xu L, Flahiff CM, Waldman B a., Wu D, Olsen BR, Setton L a., Li Y. Osteoarthritis-like changes and decreased mechanical function of articular cartilage in the joints of mice with the chondrodysplasia gene (cho). *Arthritis Rheum* 2003;48:2509–2518.
38. Hu K, Xu L, Cao L, Flahiff CM, Brussiau J, Ho K, Setton LA, Youn I, Guilak F, Olsen BR, Li Y. Pathogenesis of osteoarthritis-like changes in the joints of mice deficient in type IX collagen. *Arthritis Rheum* 2006;54:2891–900.
39. Hardcastle SA, Dieppe P, Gregson CL, Davey Smith G, Tobias JH. Osteoarthritis

and bone mineral density: are strong bones bad for joints? *Bonekey Rep* 2015;4:624.
40. Hardcastle SA, Dieppe P, Gregson CL, Arden NK, Spector TD, Hart DJ, Edwards MH, Dennison EM, Cooper C, Sayers A, Williams M, Davey Smith G, Tobias JH. Individuals with high bone mass have an increased prevalence of radiographic knee osteoarthritis. *Bone* 2015;71:171–179.
41. Im G-I, Kim M-K. The relationship between osteoarthritis and osteoporosis. *J Bone Miner Metab* 2014;32:101–109.
42. Adebayo OO, Ko FC, Wan PT, Goldring SR, Goldring MB, Wright TM, Meulen MCH van der. Role of subchondral bone properties and changes in development of load-induced osteoarthritis in mice. *Osteoarthr Cartil* 2017;25:2108–2118.
43. Brown TD, Johnston RC, Saltzman CL, Marsh JL, Buckwalter JA. Posttraumatic osteoarthritis: a first estimate of incidence, prevalence, and burden of disease. *J Orthop Trauma* 2006;20:739–44.
44. Saklatvala J. Tumour necrosis factor alpha stimulates resorption and inhibits synthesis of proteoglycan in cartilage. *Nature* 1986;322:547–549.
45. Sommer C, Kress M. Recent findings on how proinflammatory cytokines cause pain: peripheral mechanisms in inflammatory and neuropathic hyperalgesia. *Neurosci Lett* 2004;361:184–7.
46. Goldring MB, Birkhead JR, Suen LF, Yamin R, Mizuno S, Glowacki J, Arbiser JL, Apperley JF. Interleukin-1 beta-modulated gene expression in immortalized human chondrocytes. *J Clin Invest* 1994;94:2307–16.
47. Ismail HM, Miotla-Zarebska J, Troeberg L, Tang X, Stott B, Yamamoto K, Nagase H, Fosang AJ, Vincent TL, Saklatvala J. Brief Report: JNK-2 Controls Aggrecan Degradation in Murine Articular Cartilage and the Development of Experimental Osteoarthritis. *Arthritis Rheumatol (Hoboken, NJ)* 2016;68:1165–71.
48. Fonseca JE, Santos MJ, Canhão H, Choy E. Interleukin-6 as a key player in systemic inflammation and joint destruction. *Autoimmun Rev* 2009;8:538–542.
49. Opal SM, Depalo VA. Anti-Inflammatory Cytokines. *CHEST J* 2000;118:503–508.
50. Holyoak DT, Tian YF, Meulen MCH van der, Singh A. Osteoarthritis: Pathology, Mouse Models, and Nanoparticle Injectable Systems for Targeted Treatment. *Ann Biomed Eng* 2016;44:2062–75.
51. Huang K, Wu LD. Aggrecanase and aggrecan degradation in osteoarthritis: a review. *J Int Med Res* 2008;36:1149–60.
52. Little CB, Barai A, Burkhardt D, Smith SM, Fosang AJ, Werb Z, Shah M, Thompson EW. Matrix metalloproteinase 13-deficient mice are resistant to osteoarthritic cartilage erosion but not chondrocyte hypertrophy or osteophyte development. *Arthritis Rheum* 2009;60:3723–33.
53. Yang C-C, Lin C-Y, Wang H-S, Lyu S-R. Matrix metalloproteases and tissue inhibitors of metalloproteinases in medial plica and pannus-like tissue contribute to knee osteoarthritis progression. Williams BO, ed. *PLoS One* 2013;8:e79662.
54. Boyce BF, Xing L. The RANKL/RANK/OPG pathway. *Curr Osteoporos Rep* 2007;5:98–104.
55. Sinusas K. Osteoarthritis: diagnosis and treatment. *Am Fam Physician* 2012;85:49–56.
56. Felson DT. Weight Loss Reduces the Risk for Symptomatic Knee Osteoarthritis in Women. *Ann Intern Med* 1992;116:535.
57. Clyman B. Exercise in the treatment of osteoarthritis. *Curr Rheumatol Rep* 2001;3:520–3.
58. Lange AK, Vanwanseele B, Fiatarone singh MA. Strength training for treatment of osteoarthritis of the knee: A systematic review. *Arthritis Rheum* 2008;59:1488–1494.
59. Henrotin Y, Marty M, Mobasheri A. What is the current status of chondroitin

sulfate and glucosamine for the treatment of knee osteoarthritis? *Maturitas* 2014;78:184–187.
60. Hong S-CL, Levine L. Inhibition of arachidonic acid release from cells as the biochemical action of anti-inflammatory corticosteroids (prostaglandins/phospholipids/anti-inflammation/serum). 1976;73:1730–1734.
61. Miller LE, Block JE. US-Approved Intra-Articular Hyaluronic Acid Injections are Safe and Effective in Patients with Knee Osteoarthritis: Systematic Review and Meta-Analysis of Randomized, Saline-Controlled Trials. *Clin Med Insights Arthritis Musculoskelet Disord* 2013;6:57–63.
62. WANG F, HE X. Intra-articular hyaluronic acid and corticosteroids in the treatment of knee osteoarthritis: A meta-analysis. *Exp Ther Med* 2015;9:493–500.
63. Williams TJ, Peck MJ. Role of prostaglandin-mediated vasodilatation in inflammation. *Nature* 1977;270:530–2.
64. Bellamy N, Campbell J, Welch V, Gee TL, Bourne R, Wells GA. Intraarticular corticosteroid for treatment of osteoarthritis of the knee. In: Bellamy N, ed. *Cochrane Database of Systematic Reviews*. Chichester, UK: John Wiley & Sons, Ltd; 2006:CD005328.
65. Jüni P, Hari R, Rutjes AW, Fischer R, Silletta MG, Reichenbach S, Costa BR da. Intra-articular corticosteroid for knee osteoarthritis. *Cochrane Database Syst Rev* 2015:CD005328.
66. Kruse DW. Intraarticular cortisone injection for osteoarthritis of the hip. Is it effective? Is it safe? *Curr Rev Musculoskelet Med* 2008;1:227–33.
67. Balazs EA, Denlinger JL. Viscosupplementation: a new concept in the treatment of osteoarthritis. *J Rheumatol Suppl* 1993;39:3–9.
68. Moreland LW. Intra-articular hyaluronan (hyaluronic acid) and hylans for the treatment of osteoarthritis: mechanisms of action. *Arthritis Res Ther* 2003;5:54–67.
69. Arrich J, Piribauer F, Mad P, Schmid D, Klaushofer K, Müllner M. Intra-articular hyaluronic acid for the treatment of osteoarthritis of the knee: systematic review and meta-analysis. *CMAJ* 2005;172:1039–43.
70. Ghosh P, Guidolin D. Potential mechanism of action of intra-articular hyaluronan therapy in osteoarthritis: are the effects molecular weight dependent? *Semin Arthritis Rheum* 2002;32:10–37.
71. Kon E, Mandelbaum B, Buda R, Filardo G, Delcogliano M, Timoncini A, Fornasari PM, Giannini S, Marcacci M. Platelet-rich plasma intra-articular injection versus hyaluronic acid viscosupplementation as treatments for cartilage pathology: from early degeneration to osteoarthritis. *Arthroscopy* 2011;27:1490–501.
72. Meheux CJ, McCulloch PC, Lintner DM, Varner KE, Harris JD. Efficacy of Intra-articular Platelet-Rich Plasma Injections in Knee Osteoarthritis: A Systematic Review. *Arthrosc J Arthrosc Relat Surg* 2016;32:495–505.
73. Coleman PJ, Scott D, Ray J, Mason RM, Levick JR. Hyaluronan secretion into the synovial cavity of rabbit knees and comparison with albumin turnover. *J Physiol* 1997;503 (Pt 3):645–56.
74. Rothenfluh D a, Bermudez H, O'Neil CP, Hubbell J a. Biofunctional polymer nanoparticles for intra-articular targeting and retention in cartilage. *Nat Mater* 2008;7:248–254.
75. He Z, Wang B, Hu C, Zhao J. An overview of hydrogel-based intra-articular drug delivery for the treatment of osteoarthritis. *Colloids Surfaces B Biointerfaces* 2017;154:33–39.
76. Patel RG, Purwada A, Cerchietti L, Inghirami G, Melnick A, Gaharwar AK, Singh A. Microscale Bioadhesive Hydrogel Arrays for Cell Engineering Applications. *Cell Mol Bioeng* 2014;7:394–408.
77. Yu J, Chen F, Wang X, Dong N, Lu C, Yang G, Chen Z. Synthesis and

characterization of MMP degradable and maleimide cross-linked PEG hydrogels for tissue engineering scaffolds. 2016.
78. Christiansen BA, Guilak F, Lockwood KA, Olson SA, Pitsillides AA, Sandell LJ, Silva MJ, Meulen MCH van der, Haudenschild DR. Non-invasive mouse models of post-traumatic osteoarthritis. *Osteoarthr Cartil* 2015;23:1627–1638.
79. Bendele AM. Animal models of osteoarthritis. *J Musculoskelet Neuronal Interact* 2001;1:363–76.
80. Kraan PM van der, Vitters EL, Putte LB van de, Berg WB van den. Development of osteoarthritic lesions in mice by "metabolic" and "mechanical" alterations in the knee joints. *Am J Pathol* 1989;135:1001–14.
81. Kraan PM van der, Vitters EL, Beuningen HM van, Putte LB van de, Berg WB van den. Degenerative knee joint lesions in mice after a single intra-articular collagenase injection. A new model of osteoarthritis. *J Exp Pathol (Oxford)* 1990;71:19–31.
82. Kikuchi T, Sakuta T, Yamaguchi T. Intra-articular injection of collagenase induces experimental osteoarthritis in mature rabbits. *Osteoarthr Cartil* 1998;6:177–186.
83. Beuningen H. van, Glansbeek H., Kraan P. van der, Berg W. van den. Osteoarthritis-like changes in the murine knee joint resulting from intra-articular transforming growth factor-β injections. *Osteoarthr Cartil* 2000;8:25–33.
84. Clements KM, Ball AD, Jones HB, Brinckmann S, Read SJ, Murray F. Cellular and histopathological changes in the infrapatellar fat pad in the monoiodoacetate model of osteoarthritis pain. *Osteoarthr Cartil* 2009;17:805–812.
85. Little C, Zaki yz Raymond S. What constitutes an " animal model of osteoarthritis " e the need for consensus? 2012.
86. Bove S., Calcaterra S., Brooker R., Huber C., Guzman R., Juneau P., Schrier D., Kilgore K. Weight bearing as a measure of disease progression and efficacy of anti-inflammatory compounds in a model of monosodium iodoacetate-induced osteoarthritis. *Osteoarthr Cartil* 2003;11:821–830.
87. Combe R, Bramwell S, Field MJ. *The monosodium iodoacetate model of osteoarthritis: a model of chronic nociceptive pain in rats?*; 2004.
88. Inoue S, Glimcher MJ. The reaction of cartilage and osteophyte formation after the intraarticular injection of papain. *Nihon Seikeigeka Gakkai Zasshi* 1982;56:415–30.
89. Murat N, Karadam B, Ozkal S, Karatosun V, Gidener S. [Quantification of papain-induced rat osteoarthritis in relation to time with the Mankin score]. *Acta Orthop Traumatol Turc* 2007;41:233–7.
90. Bentley G. Papain-induced degenerative arthritis of the hip in rabbits. *J Bone Joint Surg Br* 1971;53:324–37.
91. Adebayo OO, Holyoak DT, Meulen MCH Van der. Mechanobiological mechanisms of load-induced osteoarthritis. *Submitt Mechanomedicine* 2018.
92. Pond MJ, Nuki G. Experimentally-induced osteoarthritis in the dog. *Ann Rheum Dis* 1973;32:387–8.
93. Kamekura S, Hoshi K, Shimoaka T, Chung U, Chikuda H, Yamada T, Uchida M, Ogata N, Seichi a, Nakamura K, Kawaguchi H. Osteoarthritis development in novel experimental mouse models induced by knee joint instability 4. *OsteoarthritisCartilage* 2005;13:632–641.
94. Hayami T, Pickarski M, Zhuo Y, Wesolowski GA, Rodan GA, Duong LT. Characterization of articular cartilage and subchondral bone changes in the rat anterior cruciate ligament transection and meniscectomized models of osteoarthritis. *Bone* 2006;38:234–243.
95. McErlain DD, Appleton CTG, Litchfield RB, Pitelka V, Henry JL, Bernier SM, Beier F, Holdsworth DW. Study of subchondral bone adaptations in a rodent surgical

model of OA using in vivo micro-computed tomography. *Osteoarthr Cartil* 2008;16:458–469.
96. Glasson SS, Blanchet TJ, Morris E a. The surgical destabilization of the medial meniscus (DMM) model of osteoarthritis in the 129/SvEv mouse. *Osteoarthr Cartil* 2007;15:1061–1069.
97. Culley KL, Dragomir CL, Chang J, Wondimu EB, Coico J, Plumb DA, Otero M, Goldring MB. Mouse models of osteoarthritis: surgical model of posttraumatic osteoarthritis induced by destabilization of the medial meniscus. *Methods Mol Biol* 2015;1226:143–73.
98. Poulet B. Non-invasive Loading Model of Murine Osteoarthritis. *Curr Rheumatol Rep* 2016;18:40.
99. McCoy AM. Animal Models of Osteoarthritis: Comparisons and Key Considerations. *Vet Pathol* 2015;52:803–18.
100. Jimenez PA, Glasson SS, Trubetskoy O V, Haimes HB. Spontaneous osteoarthritis in Dunkin Hartley guinea pigs: histologic, radiologic, and biochemical changes. *Lab Anim Sci* 1997;47:598–601.
101. Lewis JS, Hembree WC, Furman BD, Tippets L, Cattel D, Huebner JL, Little D, DeFrate LE, Kraus VB, Guilak F, Olson SA. Acute joint pathology and synovial inflammation is associated with increased intra-articular fracture severity in the mouse knee. *Osteoarthr Cartil* 2011;19:864–873.
102. Wu P, Holguin N, Silva MJ, Fu M, Liao W, Sandell LJ. Early response of mouse joint tissue to noninvasive knee injury suggests treatment targets. *Arthritis Rheumatol* 2014;66:1256–1265.
103. Poulet B, Hamilton RW, Shefelbine S, Pitsillides AA. Characterizing a novel and adjustable noninvasive murine joint loading model. *Arthritis Rheum* 2011;63:137–47.
104. Ko FC, Dragomir C, Plumb DA, Goldring SR, Wright TM, Goldring MB, Meulen MCH van der. In Vivo Cyclic Compression Causes Cartilage Degeneration and Subchondral Bone Changes in Mouse Tibiae. *Arthritis Rheum* 2013;65:1569–1578.
105. Stoop R, Kraan PM Van Der, Buma P, Hollander AP, Billinghurst RC, Poole AR, Berg WB Van Den. Type II collagen degradation in spontaneous osteoarthritis in C57BL/6 and BALB/c mice. *Arthritis Rheum* 1999;42:2381–2389.
106. Adebayo OO, Ko FC, Goldring SR, Goldring MB, Wright TM, Meulen MCH van der. Kinematics of meniscal- and ACL-transected mouse knees during controlled tibial compressive loading captured using roentgen stereophotogrammetry. *J Orthop Res* 2017;35:353–360.
107. Kellgren JH. The treatment of osteoarthrosis. *Rep Rheum Dis* 1963;15:1–2.
108. Kellgren JH, Lawrence JS. Radiological assessment of osteo-arthrosis. *Ann Rheum Dis* 1957;16:494–502.
109. Glasson SS, Chambers MG, Berg WB Van Den, Little CB. The OARSI histopathology initiative - recommendations for histological assessments of osteoarthritis in the mouse. *Osteoarthritis Cartilage* 2010;18 Suppl 3:S17-23.
110. Ko FC, Dragomir CL, Plumb DA, Hsia AW, Adebayo OO, Goldring SR, Wright TM, Goldring MB, Meulen MCH van der. Progressive cell-mediated changes in articular cartilage and bone in mice are initiated by a single session of controlled cyclic compressive loading. *J Orthop Res* 2016.

CHAPTER 2: COLLAGEN XI MUTATION LOWERS SUSCEPTIBILITY TO LOAD-INDUCED CARTILAGE DAMAGE IN MICE

2.1 Introduction

Osteoarthritis (OA) is a whole joint disease characterized by pain and stiffness due to articular cartilage degradation, subchondral bone changes, and osteophyte formation. OA is the leading cause of disability in the elderly and affects approximately 27 million people in the United States alone [1–5]. The disease primarily affects articulating joints subjected to loading and motion such as the knees, fingers, and hips. OA has many risk factors, including aging, obesity, previous joint injury, joint malalignment, high levels of mechanical loading, and genetic abnormalities that affect cartilage integrity [6]. Determining the interactions of these factors in influencing joint damage is critical to better understanding the disease and developing effective treatment options. In this study, we focused on the combined impact of mechanical loading and a genetically abnormal cartilage matrix in OA pathogenesis.

Mechanical loading and joint health have a unique relationship. Low levels of mechanical loading, such as mild exercise, can benefit cartilage by preventing injury-induced cartilage degradation [7,8], maintaining thicker cartilage [9], and increasing proteoglycan synthesis [10]. However, higher levels of loading can lead to cartilage degradation by decreasing proteoglycan synthesis [11], inducing chondrocyte apoptosis [12], and rupturing critical stabilizing ligaments [13]. To further elucidate the role of mechanical loading in OA, we and others developed a noninvasive preclinical model that applies controlled cyclic compression to mouse knee joints [14,15]. We previously demonstrated that this model recapitulates OA pathology in healthy mouse knees [14].

Epidemiological studies of OA have estimated a heritability of 50% or more depending upon the affected joint, suggesting that half of the variation in disease susceptibility could be explained by genetic factors [16–19]. Collagen XI is essential for collagen fibril formation in articular cartilage [20,21]. Collagen fibrils, containing primarily type II collagen with the alpha 1 collagen XI [α1(XI)] chain incorporated, form a network in the cartilage extracellular matrix (ECM) that contributes to tensile strength and retention of proteoglycans in cartilage tissue. In this study, we focused on a mutation in the gene encoding α1(XI) that results in chondrodysplasia in humans and the development of secondary OA. Mice with the same point mutation in one allele of the *Col11a1* gene (*cho/+*), display abnormally thick collagen fibrils in their cartilage ECM [22], accompanied by reduced tissue tensile properties and OA-like features starting at 3 months of age [22]. The expression levels of both discoidin domain receptor (DDR)-2 and matrix metalloproteinase (MMP)-13 are elevated in the articular cartilage of *cho/+* mice [23] and contribute to degradation of the pericellular matrix [24]. Although mice homozygous for the cho mutation display severe skeletal abnormalities resulting in perinatal lethality [20], *cho/+* mice do not display overt skeletal or extra-skeletal developmental defects besides the aforementioned age-related changes in the cartilage matrix [25]. Thus, *cho/+* mice provide a model to study the contribution of a genetically abnormal cartilage matrix to load-induced OA in a well-controlled manner.

The influence of a genetically abnormal cartilage matrix on the severity of load-induced cartilage damage is unknown. Because cartilage damage was enhanced in mice overexpressing DDR-2 subjected to a surgically-induced posttraumatic model of OA [26], we predicted that *cho/+* cartilage, with elevated levels of DDR-2, would

experience exacerbated load-induced damage. Furthermore, the mechanical properties of the cartilage matrix are impaired in the *cho/+* mouse, so we expected the cartilage to deform more under load, thereby increasing the strains on the chondrocytes, leading to cell death and cartilage degradation. However, the skeletal phenotype has not been carefully examined in adult *cho/+* mice. Our previous RNAseq analyses on total RNA isolated from mouse bone showed that Col11a1 is among the most highly expressed genes in both cancellous and cortical bone [27]. Altered subchondral bone properties in *cho/+* mice could also influence the cartilage response to loading, and thus we could not accurately predict the overall response to load in the knee joints of the *cho/+* mouse.

Therefore, we aimed to 1) determine whether the collagen XI mutation affects the intrinsic cortical and cancellous bone phenotype of *cho/+* mice, and 2) examine the interaction between mechanical loading and genetically abnormal cartilage matrix properties in the onset and progression of OA. We subjected *cho/+* mice and wild-type (WT) littermates to cyclic tibial compression in vivo and used radiographic, histological, and immunohistochemical techniques to assess the phenotypic bone and cartilage changes in the knee joint. We hypothesized that cartilage abnormalities due to the collagen XI mutation would exacerbate cartilage damage and subchondral bone adaptation associated with load-induced OA. However, we found that the development and progression of OA cartilage pathology was less severe in the mutant mice compared to their WT littermates. Our findings indicate that the altered bone and cartilage phenotypes may have contributed to these unexpected results and highlight the complex nature of the interactions between bone and cartilage properties in the evolution of load-induced OA.

2.2 Materials and Methods

2.2.1 Mouse Genotyping

Mouse genotyping was performed as described previously [20]. Heterozygous *cho/+* mice and WT littermates were housed together (2 to 4 mice per cage). Lighting was maintained at a 12-hours-on-12-hours-off schedule. Mice were given food and water *ad libitum*. Male 6-month-old *cho/+* mice and WT littermates were used for the phenotype characterization and loading experiments. We previously confirmed the presence of cartilage damage in response to moderate and high loads in male 6-month-old C57BL/6 mice [14] and the loss of superficial proteoglycan staining in non-loaded male *cho/+* mice by 6 months of age, indicative of early OA-like changes [28].

2.2.2 Mechanical Loading

We applied cyclic compression to the left tibiae of *cho/+* mice [20,22,29] and WT littermates at moderate (4.5N) and high (9.0N) peak load magnitudes for durations of 1, 2, and 6 weeks (n=6/group/genotype). Right limbs served as contralateral controls. With mice under general anesthesia (2% isoflurane, 1.0L/min, Webster), loading was applied to the left tibiae 5 days/week for 1200 cycles at a frequency of 4 Hz. [30] Upon completion of loading, mice were euthanized. Knee joints were harvested and fixed in 4% paraformaldehyde overnight at 4°C. All experimental techniques were approved by the Cornell IACUC.

2.2.3 Cartilage and Bone Morphology Analyses

Microcomputed tomography (microCT) scans were used to assess phenotypic bone morphology and changes in response to loading. After fixation, tissues were transferred to 70% ethanol for short-term storage. Intact knee joints were scanned using microCT, with an isotropic voxel resolution of 10 μm (μCT35, Scanco, Bruttisellen, Switzerland; 55kVp, 145μA, 600ms integration time). The effects of beam hardening were reduced with a 0.5 mm aluminum filter. After scanning, knee joints were decalcified in formic acid and processed for paraffin embedding. Paraffin blocks were sectioned at a thickness of 6 μm from posterior to anterior using a rotary microtome (Leica RM2255, Wetzlar, Germany).

To assess cartilage morphology, sections were stained with Safranin O/Fast Green at 90-μm intervals throughout the joint. Histological scoring was performed on these sections by two blinded researchers to examine cartilage damage in the medial and lateral tibial plateaus. Scores from all sections of each limb were averaged. In control limbs, a modified Mankin scoring system was used to characterize the articular cartilage phenotype of *cho/+* and WT mice [22]. Structural cartilage damage after loading was evaluated in all limbs using the OARSI scoring system [31]. Cartilage thickness was measured in both the medial and lateral plateaus on three representative sections in the joint (posterior, middle, and anterior) as described previously [14,32].

To assess osteophyte formation in response to loading, we examined Safranin O/Fast Green-stained histological sections for ectopic bone formation surrounding the joint. Osteophyte maturity was evaluated as described previously [33]. Briefly, we identified the section from each joint that contained the largest portion of the medial

tibial osteophyte. Using the representative slide, we scored osteophyte maturity: 0 for no osteophyte, 1 for a primarily cartilaginous osteophyte, 2 for a mixture of cartilage and bone, or 3 for primarily bony structure. We also measured the medial-lateral width of the osteophyte, defined as the distance between the medial end of the epiphysis and the end of the ectopic bone. Widths are reported as absolute values.

To assess peri-articular bone morphology, we examined cortical and cancellous bone in the epiphysis and metaphysis of the proximal tibia using microCT. We analyzed the subchondral cortical bone plate (SBP) and metaphyseal cortical shell for thickness and tissue mineral density (TMD). For the SBP, the volume of interest (VOI) encompassed all cortical bone beginning at the proximal end of the tibia extending distally until the epiphyseal cancellous bone was evident. The VOI for the metaphyseal cortical shell began distal to the growth plate and extended 10% of the tibial length, excluding cancellous bone. We analyzed isolated cancellous bone in the epiphysis and metaphysis for bone volume fraction (BV/TV), trabecular thickness (Tb.Th), trabecular separation (Tb.Sp), and TMD. For the epiphysis, the VOI encompassed cancellous bone proximal to the growth plate and distal to the subchondral bone plate, excluding cortical bone. The VOI for metaphyseal cancellous bone encompassed the same region analyzed for the cortical shell, excluding the cortex.

2.2.4 Immunohistochemistry and TUNEL assay

We performed immunohistochemistry (IHC) to assess load-induced changes in cartilage proteins in *cho/+* and WT mice. We evaluated markers of OA disease using specific antibodies against MMP-13 (Abcam, AB39012, Cambridge, MA) and DDR-2

(Abcam, AB5520, Cambridge, MA). We also assessed chondrocyte apoptosis using a TUNEL kit to detect DNA strand breaks (Sigma, 11684795910 Roche, Darmstadt, Germany). We analyzed the medial posterior tibial plateau at early time points under high loads, because the majority of load-induced damage occurs in this region [14], and a single session of 9N cyclic compression leads to progressive cell-mediated changes and cartilage degradation at 1 and 2 weeks [32].

We stained one representative section from the posterior region of control and loaded limbs from animals loaded for 1 or 2 weeks at 9N. For MMP-13 and DDR-2 IHC, sections were deparaffinized, rehydrated, and incubated with 2.5% hyaluronidase at 37°C for antigen retrieval, and quenched for endogenous peroxidase activity. Sections for MMP-13 IHC were then incubated with 1% bovine serum albumin and 0.5% Triton X-100 for 1h. Sections for DDR-2 IHC were incubated with Dako protein block for 5min at room temperature. Then, the samples were incubated overnight at 4°C with specific antibodies against MMP-13 or DDR-2, followed by incubation with anti-rabbit horseradish peroxidase-conjugated secondary antibodies. Color development was performed using the peroxidase substrate DAB. Samples were dehydrated, coverslipped, and the percentage of positive immunostaining in the articular cartilage of the medial tibial plateau was calculated using ImageJ software (NIH) as described previously [34,35].

For the TUNEL assay, sections were deparaffinized, rehydrated, and incubated with proteinase K at 37°C. The samples were then incubated with the TUNEL reaction mixture for 1h at 37°C. Finally, sections were coverslipped with antifade mounting media containing DAPI. TUNEL positive cells were measured in the articular cartilage

of the medial tibial plateau, as described previously [34,35], and normalized to the total number of chondrocytes (DAPI+ signal) to account for potential changes in cellularity.

2.2.5 Statistical analyses

Bone parameters and Mankin scores of control limbs were compared between WT and *cho/+* mice using a Student's *t*-test. To minimize potential systemic effects of loading and aging, we analyzed control limbs only from the 1-week time point for our baseline bone phenotype comparisons. Baseline IHC parameters in control limbs were also compared between WT and *cho/+* mice using a *t*-test.

To understand the effects of loading, we used a four-way ANOVA with load (loaded vs. control limb), magnitude (high vs. moderate), duration (1 vs. 2 vs. 6 weeks), and genotype (WT vs. *cho/+*) as variables, with animal as a random effect. We applied the ANOVA to assess OARSI histological scores, cartilage thickness, and all bone morphological parameters. To analyze the IHC and TUNEL results and osteophyte formation at high loads, we used a three-way ANOVA with load, genotype, and duration as variables, with animal as a random effect. Post-hoc testing was performed with Tukey's tests for interaction effects and *t*-tests for individual effects.

2.3 Results

2.3.1 Bone and Cartilage Phenotypes

Cortical bone thickness and TMD were different between genotypes. The metaphyseal cortical shell was thinner ($p=0.029$) and had lower TMD ($p=0.002$) in *cho/+* mice compared to WT littermates (Fig. 2.1A). Similarly, the medial subchondral

bone plate was thinner (p=0.041) with a trend towards lower TMD (p=0.051) in *cho/+* mice (Fig. 2.1B). Cancellous bone morphology in the proximal tibia was similar between WT and *cho/+* mice. Specifically, cancellous BV/TV, Tb.Th, Tb.Sp, and TMD were not different in the epiphyseal and metaphyseal regions of either genotype (Fig. S-2.7). In addition, tibial length was not different between *cho/+* and WT mice (17.70±0.32 vs. 17.75±0.34mm).

Consistent with previous reports [22], loss of proteoglycan in the articular cartilage in *cho/+* mice occurred spontaneously at 6 months of age, resulting in higher Mankin scores (p=0.011, Fig. S-2.8). Proteoglycan loss was localized to the superficial layer of the articular cartilage, as evident from the representative Safranin O/Fast Green images of control limbs (Fig. S-2.8). *Cho/+* mice also had ~10% thicker cartilage than WT on the medial side of the joint in the posterior (78.49 vs. 71.28μm, p=0.028, Fig. 2.2C), middle (93.15 vs. 87.16μm, p=0.036), and anterior (93.07 vs. 84.97μm, p=0.071) regions. Cartilage in *cho/+* mice was also thicker on the lateral side in the posterior region (75.94 vs. 68.63μm, p=0.012). In the medial tibial plateau, calcified cartilage thickness was not different between genotypes (data not shown), indicating that the thickened articular cartilage in *cho/+* mice was due to thicker hyaline cartilage.

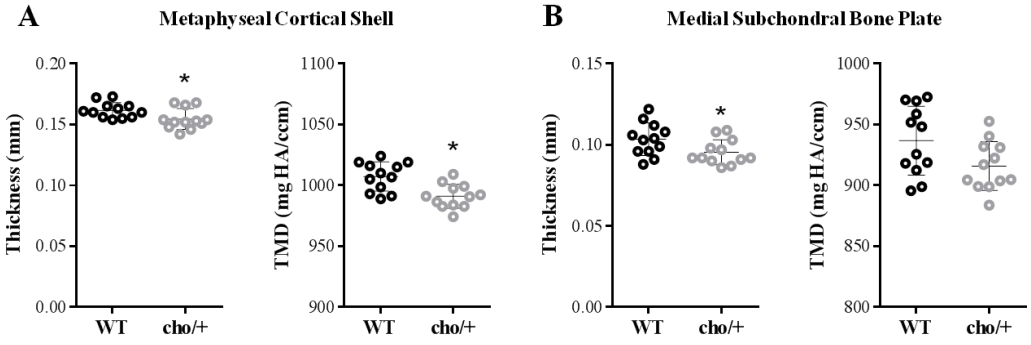

Figure 2.1. Cortical bone phenotypes were different between *cho/+* mice and WT littermates. Cortical bone in the (A) metaphyseal shell and (B) medial subchondral bone plate in *cho/+* mice was thinner and less dense compared to WT littermates. Lines behind the dots show the mean ± SD of 24 mice (n=12/group). TMD = Tissue Mineral Density. *p<0.05 vs. WT by *t*-test.

2.3.2 Load-Induced Articular Cartilage Morphological Changes

Mechanical loading induced articular cartilage degradation in the tibial plateaus of both WT and *cho/+* mice (Fig. 2.2A). Moderate loading (4.5N) caused little damage after 1 and 2 weeks, but fibrillation of the articular surface was present after 6 weeks. Load-induced damage under moderate loads was similar in both genotypes. With high loads (9.0N), cartilage fibrillation occurred by 1 week. Erosion of the articular surface occurred after 2 weeks. At the 6-week time point, the articular cartilage was completely eroded to the tidemark, and in some cases, erosion occurred through the entire calcified cartilage layer, most often on the medial tibial plateau of WT mice. Under high loads, the medial tibial plateau of loaded limbs in *cho/+* mice had significantly less cartilage damage than in WT (OARSI score 1.22 vs. 1.67, p=0.016, Fig. 2.2B).

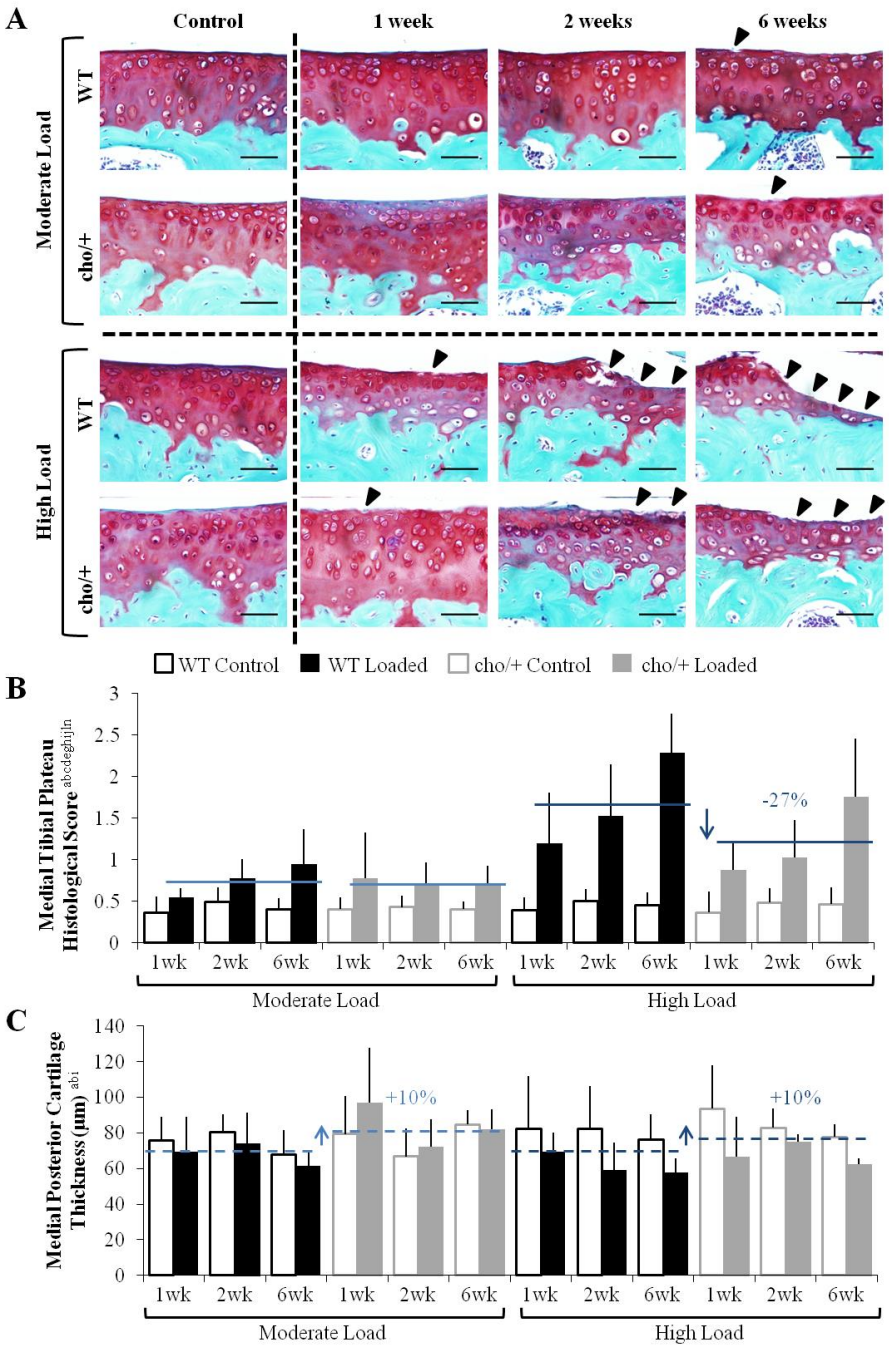

Figure 2.2. *Cho/+* mice were less susceptible to load-induced cartilage degradation. (A) Moderate loading led to fibrillation after 6 weeks. High loads led to fibrillation after 1 week and progressed to erosion after 2 and 6 weeks. Damage is indicated by arrow heads. (B) Under high load magnitudes, *cho/+* mice experienced less severe cartilage damage compared to WT mice, but moderate loads caused similar damage between genotypes. (C) High loads caused thinning in the posterior region of the tibial plateau. *Cho/+* mice had approximately 10% thicker cartilage than WT mice. Scale Bars = 50 µm. Bars show the mean ± SD of 72 mice (n=6/group). Solid and dashed lines indicate post-hoc comparisons of the effect of genotype and genotype*load,

respectively. $p<0.05$ by ANOVA indicated on vertical axis for effects of [a]Genotype, [b]Load, [c]Duration, [d]Magnitude, [e]Genotype*Load, [f]Genotype*Duration, [g]Genotype*Magnitude, [h]Load*Duration, [i]Load*Magnitude, [j]Duration*Magnitude, [k]Genotype*Load*Duration, [l]Genotype*Load*Magnitude, [m]Genotype*Duration*Magnitude, [n]Load*Duration*Magnitude, [o]Genotype*Load*Duration*Magnitude.

The high load caused localized cartilage thinning in the posterior region of the tibial plateau (Fig. 2.2C). Cartilage thinning was also evident in cartilage in the middle region of the joint on the medial side with loading. The majority of thinning occurred in the hyaline cartilage (Fig. 2.2A). Load-induced cartilage thinning was similar in both genotypes. In contrast, moderate loading caused little to no thinning.

2.3.3 Osteophyte formation

Osteophyte formation was evident only in limbs loaded at high load magnitudes (Fig. 2.3A). After 1 week of high loads, small cartilaginous pre-osteophytes were present on the medial tibial plateau of all loaded joints. After 2 weeks, medial osteophytes grew significantly in size, but remained primarily cartilaginous with little to no mineralization. After 6 weeks of loading, osteophytes had undergone ossification and were predominantly bone. In the knees of a few animals, these bony osteophytes extended along the entire medial side of the joint. Osteophyte size and maturity was similar between genotypes (Fig. 2.3B,C), with a slight trend towards smaller osteophytes in *cho/+* mice ($p=0.185$, Fig. 2.3B).

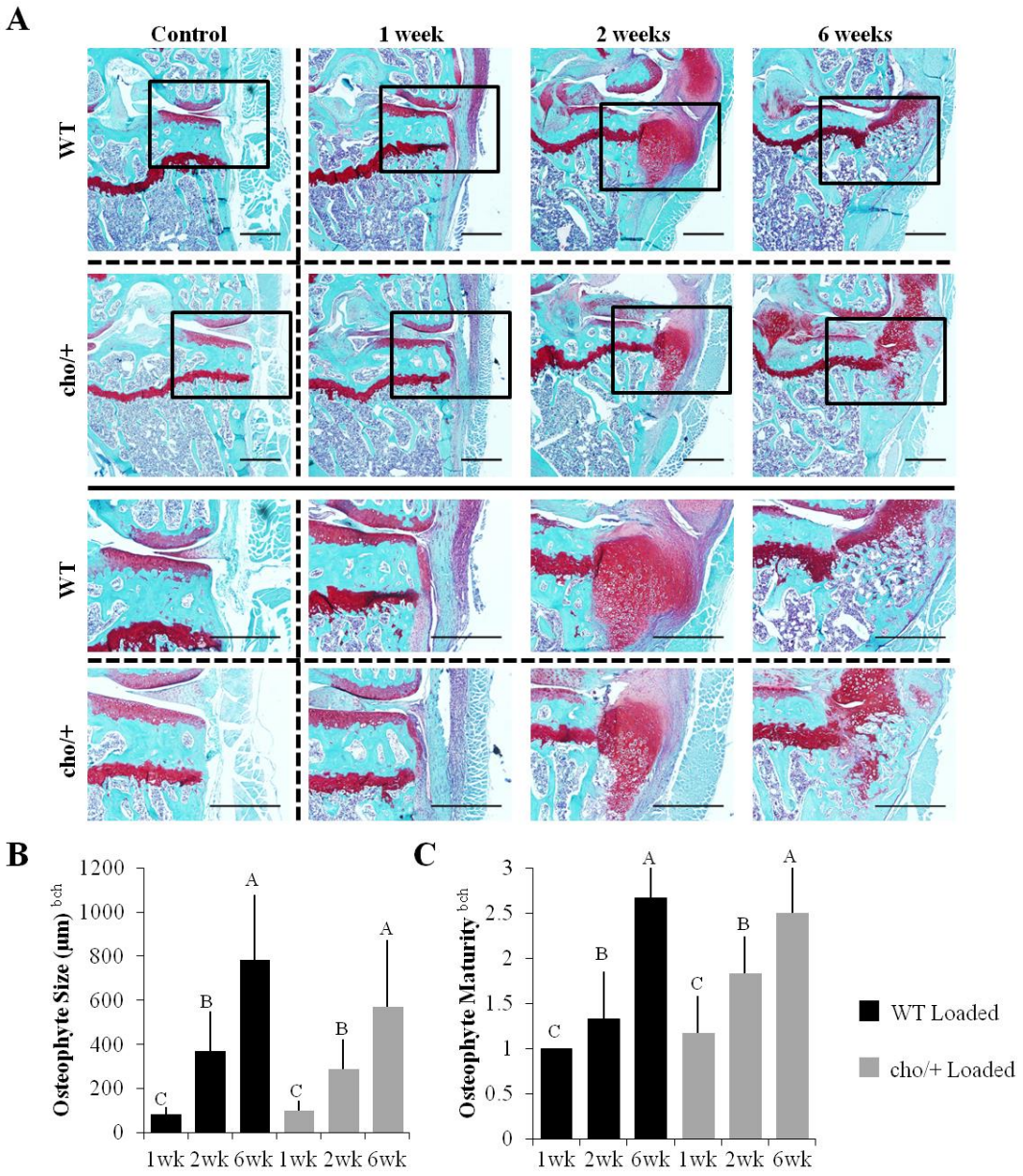

Figure 2.3. Osteophyte formation was similar between genotypes. (A) Osteophytes formed on the medial tibial plateau of loaded limbs. (B,C) After 1 week, osteophytes were small and primarily cartilagenous. After 6 weeks, osteophytes were larger and more mineralized. Scale Bars = 500 μm Bars show the mean ± SD of 36 mice (n=6/group). Same letters over the bars indicate similar mean values, and groupings with different letters indcate that the difference is significant by post-hoc comparisons of the effect of load*duration. $p<0.05$ by ANOVA indicated on vertical axis for effects of [a]Genotype, [b]Load, [c]Duration, [f]Genotype*Duration, [g]Genotype*Load, [h]Load*Duration, [k]Genotype*Load*Duration.

2.3.4 Load-Induced Peri-Articular Bone Morphological Changes

High loads had no effect on medial subchondral cortical bone plate thickness (Fig. 2.4A), but decreased TMD (Fig. 2.4B). Moderate loads did not change SBP thickness (Fig. S-2.9A) or TMD (Fig. S-2.9B). Load-induced changes in the SBP were similar between the genotypes.

High loads maintained thickness in the metaphyseal cortical shell (Fig. 2.4C), whereas moderate loads had no effect on metaphyseal cortical thickness (Fig. S-2.9C). TMD was not affected by either load level (Fig. 2.4D, Fig. S-2.9D). The cortical shell changed similarly in response to loading in both genotypes. When pooled by genotype, *cho/+* mice had thinner ($p=0.002$) and less dense ($p<0.0001$) cortical bone in the metaphyseal region.

Loading led to epiphyseal cancellous bone loss in both *cho/+* and WT mice (Fig. 2.5A). Bone loss in the epiphysis was primarily trabecular thinning ($p=0.038$) with a trend towards greater separation ($p=0.054$, Fig. 2.5B) as a result of both high and moderate loads (Fig. S-10A,B). Load-induced epiphyseal cancellous bone changes were similar in both genotypes. When pooled by genotype, *cho/+* mice had a trend towards thinner trabeculae compared to WT (0.053 vs. 0.054mm, $p=0.095$).

Unlike the epiphysis, metaphyseal cancellous BV/TV was unaffected by loading in either genotype (Fig. 2.5C). However, loading increased Tb.Th and TMD (Fig. 2.5D). Tb.Sp did not change with loading in the metaphysis. These changes were not different between high and moderate loads (Fig. S-10C,D). Load-induced metaphyseal cancellous bone changes were similar between genotypes. When pooled by genotype,

metaphyseal trabeculae were thinner in *cho/+* than WT mice (0.051 vs. 0.054mm, p=0.014), similar to the epiphysis.

Bone loss occurred over time in all four regions of bone we analyzed. Specifically, cortical bone thickness in the subchondral bone plate decreased over time in control and loaded limbs, and metaphyseal cortical shell thickness decreased in control limbs. In addition, epiphyseal and metaphyseal cancellous BV/TV decreased over time in both control and loaded limbs.

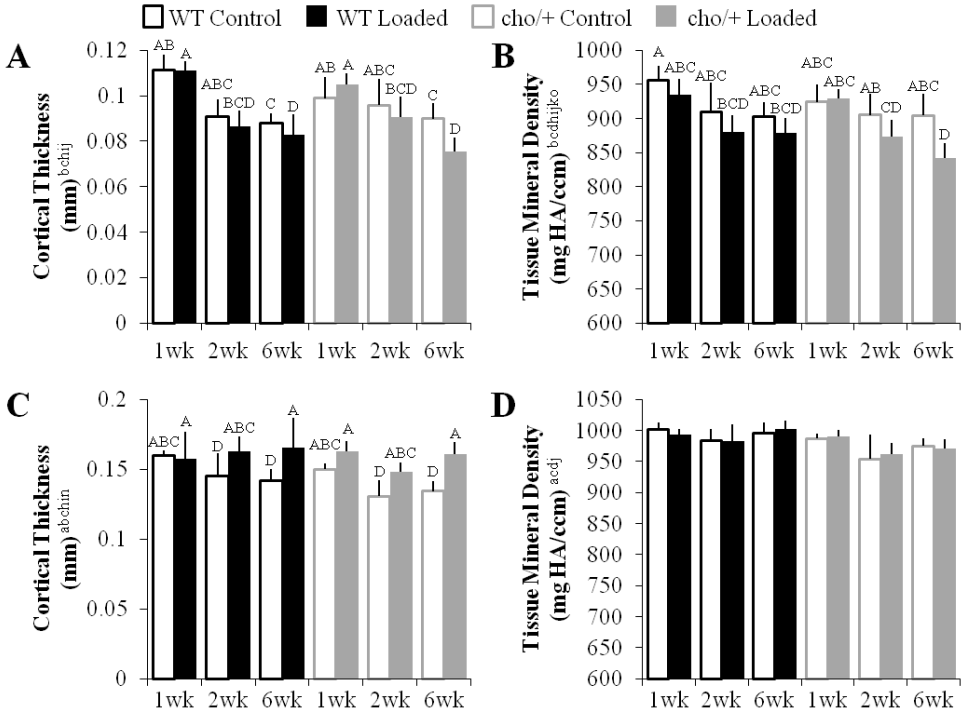

Figure 2.4. Cortical bone in the subchondral bone plate and metaphyseal cortical shell responded differently to high loads. (A,B) The subchondral cortical bone plate thinned and became less dense with loading. (C,D) The metaphyseal cortical shell maintained thickness and its density remained the same with loading. Bars show the mean ± SD of 36 mice (n=6/group). Same letters over the bars indicate similar mean values, and groupings with different letters indcate that the difference is significant by post-hoc comparisons of the effect of (A) load*duration, (B) genotype*load*duration*magnitude, and (C) load*duration*magnitude. $p<0.05$ by ANOVA indicated on vertical axis for effects of [a]Genotype, [b]Load, [c]Duration, [d]Magnitude, [e]Genotype*Load, [f]Genotype*Duration, [g]Genotype*Magnitude, [h]Load*Duration, [i]Load*Magnitude, [j]Duration*Magnitude, [k]Genotype*Load*Duration, [l]Genotype*Load*Magnitude, [m]Genotype*Duration*Magnitude, [n]Load*Duration*Magnitude, [o]Genotype*Load*Duration*Magnitude.

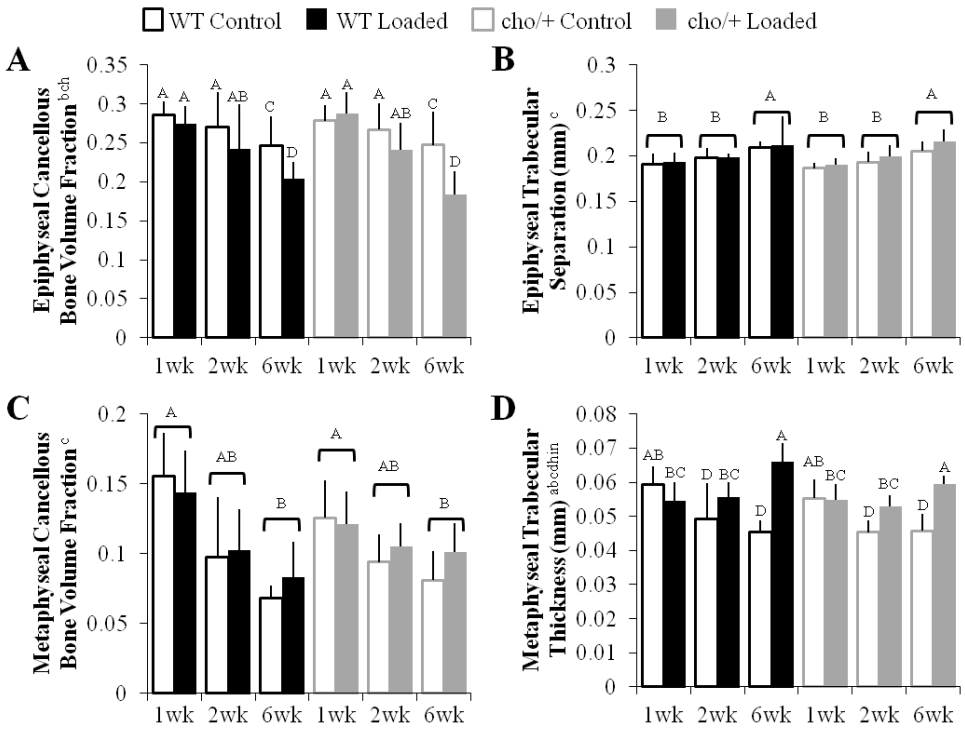

Figure 2.5. Cancellous bone in the epiphysis and metaphysis responded differently to high loads. (A) Epiphyseal cancellous bone decreased in bone volume fraction with high load magnitudes. (B) Epiphyseal trabecular separation increased with duration. (C) Cancellous bone in the metaphysis decreased with duration, but (D) trabecular thickness increased with loading. Bars show the mean ± SD of 36 mice (n=6/group). Same letters over the bars, or pooled bars, indicate similar mean values, and groupings with different letters indcate that the difference is significant by post-hoc comparisons of the effect of (A) load*duration, (B,C) duration, and (D) load*duration*magnitude. $p<0.05$ by ANOVA indicated on vertical axis for effects of [a]Genotype, [b]Load, [c]Duration, [d]Magnitude, [e]Genotype*Load, [f]Genotype*Duration, [g]Genotype*Magnitude, [h]Load*Duration, [i]Load*Magnitude, [j]Duration*Magnitude, [k]Genotype*Load*Duration, [l]Genotype*Load*Magnitude, [m]Genotype*Duration*Magnitude, [n]Load*Duration*Magnitude, [o]Genotype*Load*Duration*Magnitude.

2.3.5 Immunohistochemical and TUNEL analyses

Control *cho/+* limbs had high MMP-13 levels ($p=0.031$) and a trend towards increased DDR-2 immunostaining ($p=0.111$) compared to WT littermates, consistent with previous reports [28]. Loading induced a trend towards decreased MMP-13 (1.3 vs. 1.9%) and DDR-2 (1.3 vs. 2.9%) immunostaining in *cho/+* mice, whereas MMP-13

and DDR-2 levels were not altered with loading in WT littermates (Fig. 2.6). In addition, loading decreased cellularity in both genotypes (data not shown), and high loads also increased chondrocyte apoptosis in both genotypes (p=0.009), with a greater percentage of TUNEL+ cells in *cho/+* mice compared to WT littermates after 2 weeks of loading (1.8 vs. 0.8μm^2/cell #, Fig. 2.6).

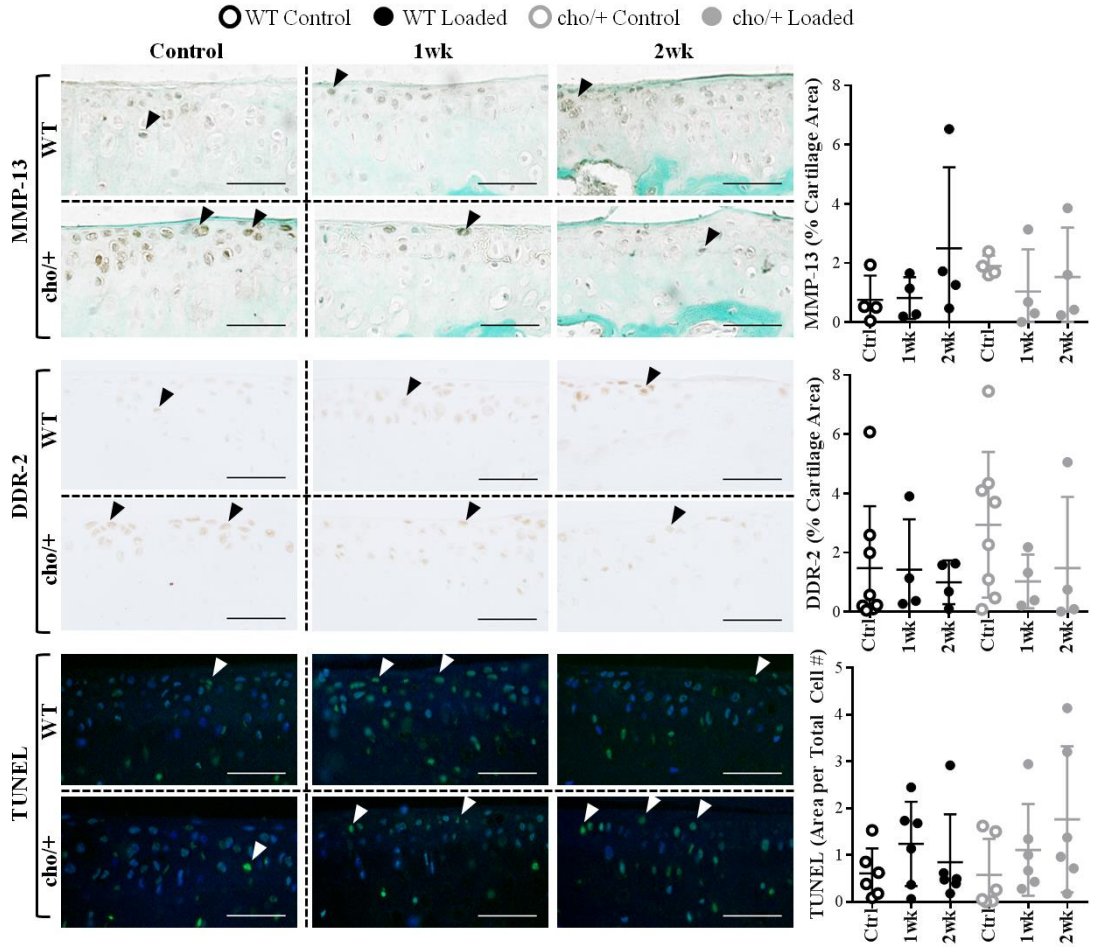

Figure 2.6. MMP-13 and DDR-2 levels were higher in control limbs of *cho/+* mice compared to WT littermates. Loading induced a trend towards decreased MMP-13 and DDR-2 immunostaining in *cho/+* mice, whereas it did not alter MMP-13 and DDR-2 levels in WT littermates. Apoptosis increased in loaded limbs, with slightly higher levels of apoptosis in *cho/+* mice after 2 weeks of loading. Scale Bars = 50 μm. Lines behind the dots show the mean ± SD of 16-24 mice (n=4-8/group).

2.4 Discussion

We sought to determine whether the mutant alpha XI collagen chain incorporated into the cartilage collagen fibrillar network and resultant changes in articular cartilage composition in *cho/+* mice altered the responses in the cartilage and bone in knee joints subjected to cyclic tibial compression compared to WT littermates. We confirmed the presence of differences in cartilage morphology and the development of the spontaneous onset of OA-like features between 6-month-old *cho/+* mice and WT littermates as previously reported [28]. Unexpectedly, we found that prior to loading, the cortical bone in the subchondral bone plate and metaphysis was thinner and less dense in *cho/+* mice compared to their WT littermates, whereas the collagen XI mutation was not associated with any change in cancellous bone structure.

We originally hypothesized that the collagen XI mutation would not affect bone phenotype based on collagen XI's key role in fibril formation in cartilage [21,28,36]. Our results, however, suggest that collagen XI plays a role in the formation and/or maintenance of cortical bone. Indeed, previous studies support our results that fibrillar collagen components play a role in bone morphogenesis and structure [20,37]. Mice homozygous for the *Col11a1* mutation (*cho/cho*) do not survive after birth because of improper skeletal formation, including a shortened spine and shortened bones in the appendicular and thoracic skeleton [20]. *Col11a1*-deficient mice also have altered bone microarchitecture during embryonic development [38]. In addition, mice with a deficiency in collagen IX, another key component of collagen fibrils in the cartilage ECM, have abnormal skeletal properties [37]. Lastly, *Col11a2* mutations lead to mild dwarfism in Labrador retrievers [39]. Consistent with these previous findings, *cho/+*

mice had thinner and less dense cortical bone compared to WT littermates. These results emphasize the involvement of collagen XI in the development and potentially the composition and properties of bone in the mature skeleton.

Contrary to our hypothesis, *cho/+* mice were less susceptible to load-induced cartilage damage compared to WT littermates, despite the spontaneous proteoglycan loss and increased DDR-2 and MMP-13 levels associated with the collagen XI mutation. One explanation for the less severe cartilage damage may be related to the differences in cartilage thickness between genotypes. *Cho/+* mice had ~10% thicker cartilage in the medial tibial plateau compared to WT littermates. Cartilage swelling correlates with proteoglycan loss in early-stage experimental OA [40]; thus, the cartilage in 6-month-old *cho/+* mice may experience swelling concurrently with the associated spontaneous proteoglycan loss typical of the early OA-like phenotype of *cho/+* mice at this age. Whereas load-induced cartilage thinning was not different between genotypes, the overall thicker cartilage in *cho/+* mice may have reduced the load-induced structural cartilage stresses. Our observation is consistent with previous reports, also based on *in vivo* loading experiments, that showed thicker cartilage decreased the peak contact pressures and shear forces in the articular cartilage [41]. Furthermore, mice susceptible to spontaneous cartilage lesions (Str/ort) were protected from load-induced mechanical trauma compared to control mice (CBA) because of thicker articular cartilage [41]. In both studies, the decreased susceptibility to load-induced cartilage damage may be due, partly, to dissipation of mechanical stresses by the thicker articular cartilage.

The thinner, less dense cortical bone in the metaphyseal shell and medial subchondral bone plate in *cho/+* mice may also have played a role in attenuating load-

induced cartilage damage. Subchondral cortical bone stiffness is important in initiating OA [42–44]. Clinically, individuals with extremely elevated bone density are more likely to develop OA in the hip and knee [45,46], and bone density and OA incidence may be inversely related [47]. Thus, the thinner, less dense cortical bone in *cho/+* mice could have contributed to the reduced severity of load-induced cartilage damage. Of interest, these results differ from previous findings showing enhanced cartilage damage in transgenic mice conditionally overexpressing DDR-2 in the articular cartilage subjected to the surgical destabilization of the medial meniscus (DMM) OA model [26]. However, the bone properties of these transgenic mice prior to DMM surgery were not assessed and most likely differed from those of *cho/+* mice, which could account for our different results.

Our findings confirm the mechanistic connection of DDR-2 and MMP-13 in cartilage degradation in *cho/+* mice. DDR-2 is a cell surface receptor that drives MMP-13 expression and activity and is elevated in OA disease in both human articular cartilage and murine models, including the *cho/+* mouse [23,24,28,48]. We found that elevated DDR-2 and MMP-13 levels correlated with spontaneous proteoglycan loss in *cho/+* mice but were not associated with the OA-like changes induced by loading in either genotype. In loaded limbs, we observed trends towards decreased MMP-13 and DDR-2 levels in *cho/+* mice, whereas loading did not alter MMP-13 or DDR-2 levels in WT littermates. Independent of the differences in DDR-2 and MMP-13 levels between genotypes, loading decreased cellularity and increased cell death similarly in *cho/+* and WT cartilage, with only minor differences in apoptosis at 2 weeks post-loading, when *cho/+* mice showed a trend towards increased numbers of TUNEL+ cells

compared to WT. Taken together, differences in susceptibility to load-induced cartilage damage may be due to tissue-level characteristics rather than the cellular responses we examined. Specifically, the thicker cartilage and the thinner, less dense cortical bone in *cho/+* mice were likely the driving factors in lowering the susceptibility of *cho/+* mice to load-induced cartilage degradation, in agreement with previous findings [41].

We clearly observed two distinct etiologies of OA and an unexpected interaction in the development of cartilage damage in our study. *Cho/+* mice developed spontaneous OA from genetically weaker matrix properties that resulted in DDR-2-driven collagenase activity and gradual proteoglycan loss throughout their lifespan [28]. On the other hand, cyclic tibial compression at high-load levels led to rapid structural changes in the cartilage matrix with little evidence of proteoglycan loss [14]. The lack of correlation between loading and DDR2/MMP13 levels was unexpected but was likely an example of the different mechanisms involved in load-induced versus genetic OA. We can only speculate that other receptors and cartilage-degrading enzymes (i.e., collagenases and aggrecanases) not analyzed in the context of this study contributed to load-induced cartilage degradation. Ultimately, the contribution of the genetic abnormalities of the cartilage in the *cho/+* mouse was not additive to load-induced cartilage damage, suggesting that these two risk factors do not act synergistically or additively [49].

Our study had several limitations, potential alternative strategies, and strengths. With our microCT analysis of subchondral bone, we analyzed the full volume of the subchondral cortical bone plate but could not isolate specific regions within the subchondral bone. To examine location-specific changes, we measured localized

subchondral bone thickness from histology slides in the anterior, middle, and posterior regions. The histology measurements matched our microCT findings. In particular, loading did not affect subchondral bone plate thickness in any of these three regions, and thickness decreased over time. Similarly, cortical and cancellous bone in the epiphysis and metaphysis decreased with time in this study. The changes in bone architecture over time can be attributed to aging, as rapid bone changes can occur in mice around 6 months of age [50].

The mechanical loading regimen is not representative of all forms of joint loading. Cyclic tibial compression allows for precise control of the loading regimen, produces consistent cartilage damage, and does not depend on mouse activity levels or willingness to run on a treadmill or wheel. However, alternative techniques for applying elevated loads could be considered. For example, excessive treadmill running leads to OA in C57Bl/6 mice [51] and could have produced a different response in *cho/+* mice compared to cyclic tibial compression, but treadmill running also has a multitude of systemic effects [52]. Cyclic tibial compression allowed us to focus solely on the specific characteristics of mechanical loading, including duration and magnitude, and their effects on the progression of load-induced OA.

Alternative forms of genetic OA also should be considered. Mice that are deficient in type IX collagen (C*ol9a1*-/-) also develop abnormal collagen fibrils in the cartilage matrix leading to OA [53] and show trabecular bone deterioration [54]. Mice with mutations in other matrix-related genes, such as lubricin, have decreased cellularity in the superficial layer of their articular cartilage [55]. Lastly, investigating the effects of cyclic tibial compression in older *cho/+* mice at more advanced stages of OA [28]

may provide insights into the interaction between genetics and loading during the progression of OA.

To our knowledge, this study is the first to examine the cortical and cancellous bone properties in the *cho/+* mouse strain. We demonstrated that mice with mutant collagen XI exhibit changes in cortical bone, with limited changes in cancellous bone. Our study provides evidence that thinner, less dense cortical bone and thicker cartilage may be associated with decreased severity of load-induced OA. Genetically abnormal cartilage matrix properties due to the collagen XI mutation were not additive to load-induced cartilage damage. The modes of damage involved in spontaneous OA in *cho/+* mice and load-induced OA differed from each other at both the tissue and cellular levels. Our findings provide further insights into the complex nature of the interactions between bone and cartilage properties in the evolution of load-induced OA and demonstrate the utility of using mice with intrinsic alterations in cartilage and bone properties and defined loading conditions to elucidate the role of mechanobiological factors in OA development and progression.

2.5 Acknowledgments

We thank Lyudamila Lukashova of the Hospital for Special Surgery and the CARE staff at Cornell University. We would also like to thank our funding sources: NIH R21-AR064034, the Clark and Kirby Foundations, Office of Academic and Diversity Initiatives (NSA), and the Howard Hughes Medical Institute (AO).

2.6 References

1. Lawrence RC, Felson DT, Helmick CG, Arnold LM, Choi H, Deyo RA, Gabriel S, Hirsch R, Hochberg MC, Hunder GG, Jordan JM, Katz JN, Kremers HM, Wolfe F, National Arthritis Data Workgroup. Estimates of the prevalence of arthritis and other rheumatic conditions in the United States. Part II. *Arthritis Rheum* 2008;58:26–35.
2. Turkiewicz A, Petersson IF, Björk J, Hawker G, Dahlberg LE, Lohmander LS, Englund M. Current and future impact of osteoarthritis on health care: a population-based study with projections to year 2032. *Osteoarthr Cartil* 2014;22:1826–1832.
3. Felson DT. Osteoarthritis: Priorities for osteoarthritis research: much to be done. *Nat Rev Rheumatol* 2014;10:447–448.
4. Hunter DJ, Schofield D, Callander E. The individual and socioeconomic impact of osteoarthritis. *Nat Rev Rheumatol* 2014;10:437–41.
5. Hootman JM, Helmick CG. Projections of US prevalence of arthritis and associated activity limitations. *Arthritis Rheum* 2006;54:226–229.
6. Felson DT. Risk Factors for Osteoarthritis. *Clin Orthop Relat Res* 2004;427:S16–S21.
7. Hamamura K, Zhang P, Zhao L, Shim JW, Chen A, Dodge TR, Wan Q, Shih H, Na S, Lin C-C, Sun H Bin, Yokota H. Knee loading reduces MMP13 activity in the mouse cartilage. *BMC Musculoskelet Disord* 2013;14:312.
8. Galois L, Etienne S, Grossin L, Watrin-Pinzano A, Cournil-Henrionnet C, Loeuille D, Netter P, Mainard D, Gillet P. Dose-response relationship for exercise on severity of experimental osteoarthritis in rats: a pilot study. *Osteoarthritis Cartilage* 2004;12:779–86.
9. Hubbard-Turner T, Guderian S, Turner MJ. Lifelong physical activity and knee osteoarthritis development in mice. *Int J Rheum Dis* 2015;18:33–39.
10. Sah RL-Y, Kim Y-J, Doong J-YH, Grodzinsky AJ, Plass AHK, Sandy JD. Biosynthetic response of cartilage explants to dynamic compression. *J Orthop Res* 1989;7:619–636.
11. Kurz B, Jin M, Patwari P, Cheng DM, Lark MW, Grodzinsky AJ. Biosynthetic response and mechanical properties of articular cartilage after injurious compression. *J Orthop Res* 2001;19:1140–1146.
12. Stolberg-Stolberg JA, Furman BD, William Garrigues N, Lee J, Pisetsky DS, Stearns NA, DeFrate LE, Guilak F, Olson SA. Effects of cartilage impact with and without fracture on chondrocyte viability and the release of inflammatory markers. *J Orthop Res* 2013;31:1283–1292.
13. Christiansen B a., Anderson MJ, Lee C a., Williams JC, Yik JHN, Haudenschild DR. Musculoskeletal changes following non-invasive knee injury using a novel mouse model of post-traumatic osteoarthritis. *Osteoarthr Cartil* 2012;20:773–782.
14. Ko FC, Dragomir C, Plumb DA, Goldring SR, Wright TM, Goldring MB, Meulen MCH van der. In Vivo Cyclic Compression Causes Cartilage Degeneration and Subchondral Bone Changes in Mouse Tibiae. *Arthritis Rheum* 2013;65:1569–1578.
15. Poulet B, Hamilton RW, Shefelbine S, Pitsillides AA. Characterizing a novel and adjustable noninvasive murine joint loading model. *Arthritis Rheum* 2011;63:137–47.
16. Felson DT, Zhang Y. An update on the epidemiology of knee and hip osteoarthritis with a view to prevention. *Arthritis Rheum* 1998;41:1343–1355.

17. Meurs JBJ van. Osteoarthritis year in review 2016: genetics, genomics and epigenetics. *Osteoarthr Cartil* 2017;25:181–189.
18. Valdes AM, Spector TD. Genetic epidemiology of hip and knee osteoarthritis. *Nat Rev Rheumatol* 2011;7:23–32.
19. Spector TD, MacGregor AJ. Risk factors for osteoarthritis: genetics. *Osteoarthr Cartil* 2004;12:39–44.
20. Li Y, Lacerda D a, Warman ML, Beier DR, Yoshioka H, Ninomiya Y, Oxford JT, Morris NP, Andrikopoulos K, Ramirez F. A fibrillar collagen gene, Col11a1, is essential for skeletal morphogenesis. *Cell* 1995;80:423–430.
21. Blaschke UK, Eikenberry EF, Hulmes DJS, Galla HJ, Bruckner P. Collagen XI nucleates self-assembly and limits lateral growth of cartilage fibrils. *J Biol Chem* 2000;275:10370–10378.
22. Xu L, Flahiff CM, Waldman BA, Wu D, Olsen BR, Setton LA, Li Y. Osteoarthritis-like changes and decreased mechanical function of articular cartilage in the joints of mice with the chondrodysplasia gene (cho). *Arthritis Rheum* 2003;48:2509–2518.
23. Lam NP, Li Y, Waldman AB, Brussiau J, Lee PL, Olsen BR, Xu L. Age-dependent increase of discoidin domain receptor 2 and matrix metalloproteinase 13 expression in temporomandibular joint cartilage of type IX and type XI collagen-deficient mice. *Arch Oral Biol* 2007;52:579–584.
24. Xu L, Peng H, Wu D, Hu K, Goldring MB, Olsen BE, Li Y. Activation of the discoidin domain receptor 2 induces expression of matrix metalloproteinase 13 associated with osteoarthritis in mice. *J Biol Chem* 2005;280:548–555.
25. Szymko-Bennett YM, Kurima K, Olsen B, Seegmiller R, Griffith AJ. Auditory function associated with Col11a1 haploinsufficiency in chondrodysplasia (cho) mice. *Hear Res* 2003;175:178–182.
26. Xu L, Polur I, Servais JM, Hsieh S, Lee PL, Goldring MB, Li Y. Intact pericellular matrix of articular cartilage is required for unactivated discoidin domain receptor 2 in the mouse model. *Am J Pathol* 2011;179:1338–1346.
27. Kelly NH, Schimenti JC, Ross FP, Meulen MCH Van Der. Transcriptional profiling of cortical versus cancellous bone from mechanically-loaded murine tibiae reveals differential gene expression. 2016.
28. Xu L, Flahiff CM, Waldman B a., Wu D, Olsen BR, Setton L a., Li Y. Osteoarthritis-like changes and decreased mechanical function of articular cartilage in the joints of mice with the chondrodysplasia gene (cho). *Arthritis Rheum* 2003;48:2509–2518.
29. Fernandes RJ, Weis M, Scott MA, Seegmiller RE, Eyre DR. Collagen XI chain misassembly in cartilage of the chondrodysplasia (cho) mouse. *Matrix Biol* 2007;26:597–603.
30. Lynch ME, Main RP, Xu Q, Walsh DJ, Schaffler MB, Wright TM, Meulen MCH van der. Cancellous bone adaptation to tibial compression is not sex dependent in growing mice. *J Appl Physiol* 2010;109:685–91.
31. Glasson SS, Chambers MG, Berg WB Van Den, Little CB. The OARSI histopathology initiative - recommendations for histological assessments of osteoarthritis in the mouse. *Osteoarthritis Cartilage* 2010;18 Suppl 3:S17-23.

32. Ko FC, Dragomir CL, Plumb DA, Hsia AW, Adebayo OO, Goldring SR, Wright TM, Goldring MB, Meulen MCH van der. Progressive cell-mediated changes in articular cartilage and bone in mice are initiated by a single session of controlled cyclic compressive loading. *J Orthop Res* 2016.
33. Little CB, Barai A, Burkhardt D, Smith SM, Fosang AJ, Werb Z, Shah M, Thompson EW. Matrix metalloproteinase 13-deficient mice are resistant to osteoarthritic cartilage erosion but not chondrocyte hypertrophy or osteophyte development. *Arthritis Rheum* 2009;60:3723–33.
34. Girish V, Vijayalakshmi A. Affordable image analysis using NIH Image/ImageJ. *Indian J Cancer* 41:47.
35. Varghese F, Bukhari AB, Malhotra R, De A. IHC Profiler: an open source plugin for the quantitative evaluation and automated scoring of immunohistochemistry images of human tissue samples. *PLoS One* 2014;9:e96801.
36. Rodriguez RR, Seegmiller RE, Stark MR, Bridgewater LC. A type XI collagen mutation leads to increased degradation of type II collagen in articular cartilage. *Osteoarthr Cartil* 2004;12:314–320.
37. Kamper M, Hamann N, Prein C, Clausen-Schaumann H, Farkas Z, Aszodi A, Niehoff A, Paulsson M, Zaucke F. Early changes in morphology, bone mineral density and matrix composition of vertebrae lead to disc degeneration in aged collagen IX -/- mice. *Matrix Biol* 2016;49:132–143.
38. Hafez A, Squires R, Pedracini A, Joshi A, Seegmiller RE, Oxford JT. Col11a1 Regulates Bone Microarchitecture during Embryonic Development HHS Public Access. *J Dev Biol J Dev Biol* 2015;3:158–176.
39. Frischknecht M, Niehof-Oellers H, Jagannathan V, Owczarek-Lipska M, Drögemüller C, Dietschi E, Dolf G, Tellhelm B, Lang J, Tiira K, Lohi H, Leeb T. A COL11A2 mutation in Labrador retrievers with mild disproportionate dwarfism. *PLoS One* 2013;8:e60149.
40. Calvo E, Palacios I, Delgado E, Sánchez-Pernaute O, Largo R, Egido J, Herrero-Beaumont G. Histopathological correlation of cartilage swelling detected by magnetic resonance imaging in early experimental osteoarthritis. *Osteoarthr Cartil* 2004;12:878–886.
41. Poulet B, Westerhof T a T, Hamilton RW, Shefelbine SJ, Pitsillides a. a. Spontaneous osteoarthritis in Str/ort mice is unlikely due to greater vulnerability to mechanical trauma. *Osteoarthr Cartil* 2013;21:756–763.
42. Radin EL, Rose RM. Role of subchondral bone in the initiation and progression of cartilage damage. *Clin Orthop Relat Res* 1986:34–40.
43. Day JS, Linden JC van der, Bank RA, Ding M, Hvid I, Sumner DR, Weinans H. Adaptation of subchondral bone in osteoarthritis. *Biorheology* 2004;41:359–368.
44. Hayami T, Pickarski M, Wesolowski GA, Mclane J, Bone A, Destefano J, Rodan GA, Duong LT. The role of subchondral bone remodeling in osteoarthritis: Reduction of cartilage degeneration and prevention of osteophyte formation by alendronate in the rat anterior cruciate ligament transection model. *Arthritis Rheum* 2004;50:1193–1206.
45. Hardcastle SA, Dieppe P, Gregson CL, Hunter D, Thomas GER, Arden NK, Spector TD, Hart DJ, Laugharne MJ, Clague GA, Edwards MH, Dennison EM, Cooper C, Williams M, Davey Smith G, Tobias JH. Prevalence of radiographic hip

osteoarthritis is increased in high bone mass. *Osteoarthr Cartil* 2014;22:1120–1128.
46. Hardcastle SA, Dieppe P, Gregson CL, Arden NK, Spector TD, Hart DJ, Edwards MH, Dennison EM, Cooper C, Sayers A, Williams M, Davey Smith G, Tobias JH. Individuals with high bone mass have an increased prevalence of radiographic knee osteoarthritis. *Bone* 2015;71:171–179.
47. Im G-I, Kim M-K. The relationship between osteoarthritis and osteoporosis. *J Bone Miner Metab* 2014;32:101–109.
48. Xu L, Peng H, Glasson S, Lee PL, Hu K, Ijiri K, Olsen BR, Goldring MB, Li Y. Increased expression of the collagen receptor discoidin domain receptor 2 in articular cartilage as a key event in the pathogenesis of osteoarthritis. *Arthritis Rheum* 2007;56:2663–2673.
49. Mobasheri A, Rayman MP, Gualillo O, Sellam J, Kraan P van der, Fearon U. The role of metabolism in the pathogenesis of osteoarthritis. *Nat Rev Rheumatol* 2017.
50. Glatt V, Canalis E, Stadmeyer L, Bouxsein ML. Age-related changes in trabecular architecture differ in female and male C57BL/6J mice. *J Bone Miner Res* 2007;22:1197–207.
51. Takasu N. [Experimental study on the effect of forced running on occurrence of osteoarthritis in the knee of C 57 BL mice]. *Nihon Seikeigeka Gakkai Zasshi* 1992;66:1165–75.
52. Boveris A, Navarro A. Systemic and mitochondrial adaptive responses to moderate exercise in rodents. *Free Radic Biol Med* 2008;44:224–229.
53. Hu K, Xu L, Cao L, Flahiff CM, Brussiau J, Ho K, Setton LA, Youn I, Guilak F, Olsen BR, Li Y. Pathogenesis of osteoarthritis-like changes in the joints of mice deficient in type IX collagen. *Arthritis Rheum* 2006;54:2891–900.
54. Wang CJ, Iida K, Egusa H, Hokugo A, Jewett A, Nishimura I. Trabecular Bone Deterioration in col9a1+/− Mice Associated With Enlarged Osteoclasts Adhered to Collagen IX-Deficient Bone. *J Bone Miner Res* 2008;23:837–849.
55. Karamchedu NP, Tofte JN, Waller KA, Zhang LX, Patel TK, Jay GD. Superficial zone cellularity is deficient in mice lacking lubricin: a stereoscopic analysis. *Arthritis Res Ther* 2016;18:64.

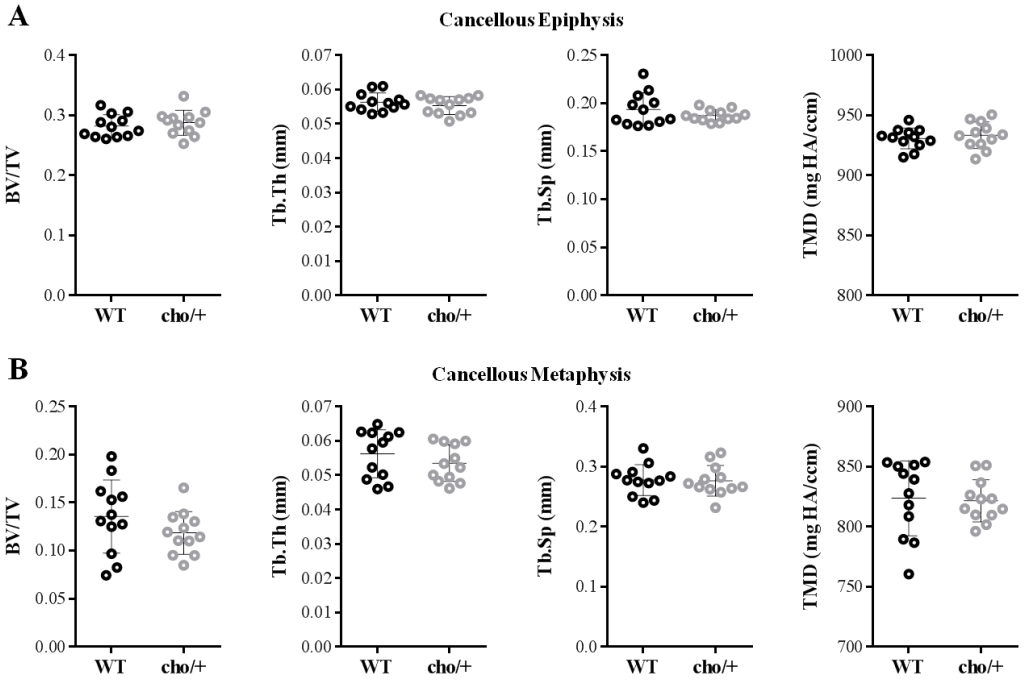

Figure S-2.7. Cancellous bone phenotypes were similar between *cho/+* mice and WT littermates. (A) Epiphyseal and (B) metaphyseal cancellous bone in control limbs of both genotypes was similar. BV/TV = Bone Volume Fraction, Tb.Th = Trabecular Thickness, Tb.Sp = Trabecular Separation, TMD = Tissue Mineral Density. Lines behind the dots show the mean ± SD of 24 mice (n=12/group). *p<0.05 vs. WT by *t*-test.

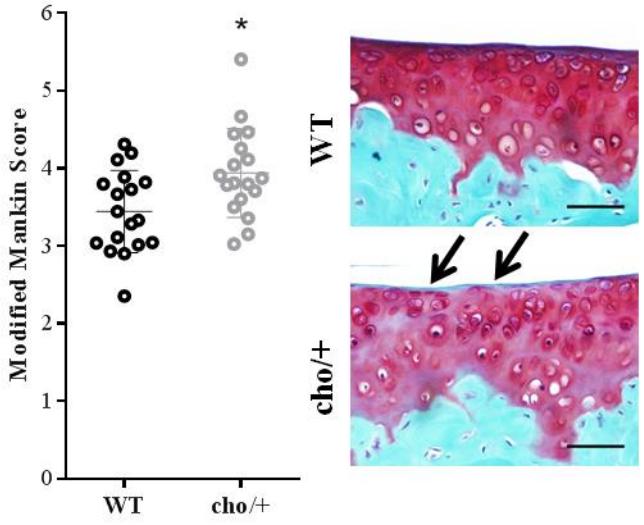

Figure S-2.8. Spontaneous proteoglycan loss occurred in cartilage of *cho/+* mice at 6 months of age. (A) *Cho/+* mice had higher Modified Mankin Score in control limbs compared to WT mice. (B) Arrow indicates proteoglycan loss in the superficial layer of articular cartilage in *cho/+* mice. Scale Bars = 50 μm. Lines behind the dots show the mean ± SD of 36 mice (n=18/group). *p<0.05 vs. WT by *t*-test.

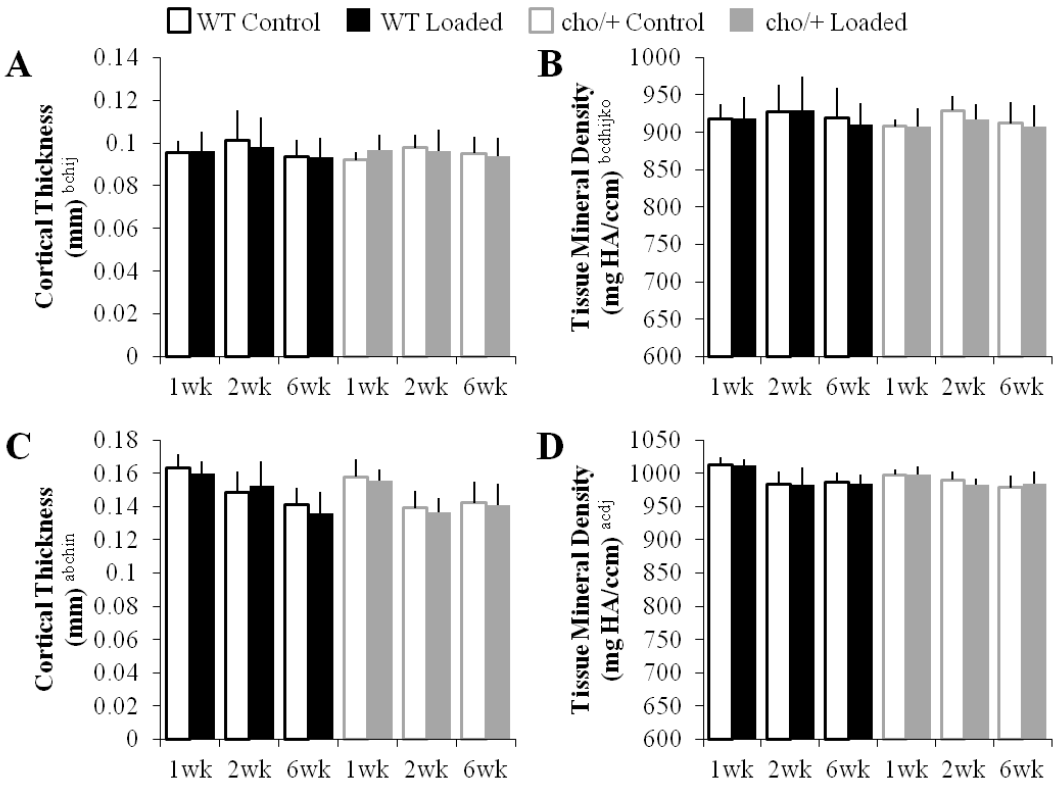

Figure S-2.9. Moderate loading did not affect subchondral bone or metaphyseal cortical shell properties. (A,B) Moderate loading had no effect on cortical bone thickness or tissue mineral density in the medial subchondral bone plate. (C,D) Thickness and tissue mineral density in the metaphyseal cortical shell decreased with duration, similarly in both gentoypes. Bars show the mean ± SD of 36 mice (n=6/group). $p<0.05$ by ANOVA indicated on vertical axis for effects of [a]Genotype, [b]Load, [c]Duration, [d]Magnitude, [e]Genotype*Load, [f]Genotype*Duration, [g]Genotype*Magnitude, [h]Load*Duration, [i]Load*Magnitude, [j]Duration*Magnitude, [k]Genotype*Load*Duration, [l]Genotype*Load*Magnitude, [m]Genotype*Duration*Magnitude, [n]Load*Duration*Magnitude, [o]Genotype*Load*Duration*Magnitude.

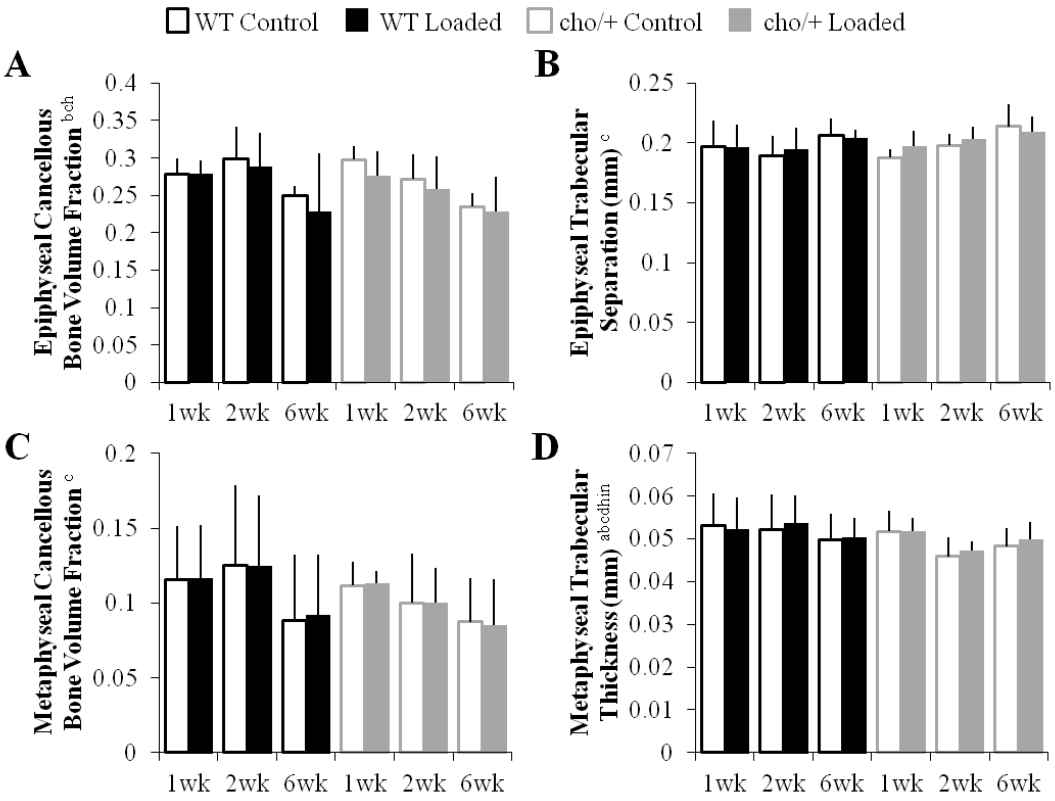

Figure S-2.10. Moderate loading had little effect on cancellous bone in the epiphysis and metaphysis, but bone did change with duration. (A) Epiphyseal cancellous bone volume fraction decreased and (B) trabecular separation increased with duration. Similarly, (C) metaphyseal cancellous bone volume fraction decreased with duration, and (D) trabecular thickness was unaffected by moderate loads. Bars show the mean ± SD of 36 mice (n=6/group). $p<0.05$ by ANOVA indicated on vertical axis for effects of [a]Genotype, [b]Load, [c]Duration, [d]Magnitude, [e]Genotype*Load, [f]Genotype*Duration, [g]Genotype*Magnitude, [h]Load*Duration, [i]Load*Magnitude, [j]Duration*Magnitude, [k]Genotype*Load*Duration, [l]Genotype*Load*Magnitude, [m]Genotype*Duration*Magnitude, [n]Load*Duration*Magnitude, [o]Genotype*Load*Duration*Magnitude.

CHAPTER 3: MECHANICALLY STABLE, INJECTABLE HYDROGELS FOR ATTENUATION OF LOAD-INDUCED OSTEOARTHRITIS

3.1 Introduction

Osteoarthritis (OA) is a degenerative joint disease that affects 27 million individuals in the United States and is the leading cause of disability in the elderly population [1]. Three primary characteristics of OA are cartilage degradation, osteophyte formation, and synovial inflammation. During the development of OA, enzymes such as aggrecanases (e.g. matrix metalloproteinase (MMP)-3) and collagenases (e.g. MMP-13), degrade the cartilage matrix and are elevated in the joint space [2–4]. Post-traumatic osteoarthritis (PTOA) is a subset of OA associated with instability due to mechanical trauma [5]. Providing interventions following mechanical trauma may be beneficial to attenuate PTOA.

Intra-articular (IA) injections for OA treatment are advantageous because of the low drug dosage and reduced risk of side effects, but fast drug clearance from the joint space limits their functional outcome [6,7]. Recent strategies to improve IA drug retention include biomaterials-based drug delivery systems, such as microparticles, nanoparticles, and hydrogels [8]. Micro- and nanoparticles can be engineered to target drug delivery locally to the joint tissues, resulting in longer retention of drugs [9–11]. Injectable hydrogels provide a unique platform with tunable mechanical properties and degradation profiles [12,13]. However, biomaterials in the joint space are subject to daily mechanical loading that leads to undesirable drug release into circulation [14]. Here, we sought to engineer a hydrogel that could withstand the environment in weight-bearing joints and therefore improve IA drug retention.

Ideally, an IA hydrogel delivery system should withstand routine forces in weight-bearing joints (up to 40% strain in cartilage) [15], maintain constant volume for long durations under hydrolytic conditions, and release therapeutics in the presence of degradative proteases, such as aggrecanases and collagenases (e.g. MMP-3 and -13). However, the ability of injectable hydrogels to withstand cyclic mechanical loading in weight-bearing joints remains unknown. Optimizing mechanical integrity and controlling the rate of hydrogel degradation with a collagenase-specific crosslinking system would improve retention time and enable on-demand therapeutic release under OA conditions.

We engineered an on-demand, biocompatible, injectable hydrogel using crosslinked 4-arm maleimide functionalized polyethylene glycol (PEG-MAL). We used either non-degradable or MMP-3- and -13-specific dithiolated crosslinkers to control degradation rates under OA-like conditions. We first characterized the mechanical properties, swelling, and degradation characteristics of these hydrogels *in vitro*. Specifically, we 1) examined the effects of cyclic compression on the mechanical properties and particle release from hydrogels, 2) characterized the effect of PEG-MAL weight percentage on swelling ratios of hydrogels, and 3) determined the effect of degradable crosslinker on particle release from hydrogels in the presence of collagenase. Then, using an *in vivo* mouse model, we 4) determined whether injectable, MMP-degradable hydrogels combined with a commonly used corticosteroid, dexamethasone (DEX), could attenuate OA progression after a single bout of high-magnitude mechanical loading [16]. We hypothesized that the PEG-MAL hydrogel drug-delivery

system would withstand routine forces in weight-bearing joints, maintain constant volume, release therapeutics in response to collagenase, and attenuate load-induced OA.

3.2 Methods

3.2.1 PEG-MAL Hydrogel Synthesis

PEG-MAL hydrogels were synthesized, as described previously [17–20].

For our *in vitro* dynamic cyclic compression and swelling experiments, 50 μL synthetic hydrogels with 2.5, 5, 10, and 20% (w/v) macromer concentration were fabricated using PEG-MAL (Laysan Bio, Inc., >90% purity) and thiolated crosslinkers. We fabricated hydrogels by crosslinking PEG-MAL to non-degradable Dithiothreitol (DTT) using a 1:1.5 macromer-to-crosslinker molar ratio. All components were diluted in 1% HEPES buffer with a pH 7.4; the HEPES buffer was composed of PBS (+/+)and HEPES chemical agent. Each hydrogel contained fluorescent FITC particles (5 μm, Duke Scientific Corporation) suspended in the crosslinker solution at a 2000/μL concentration. After 25 μL of macromer solution was placed in the middle of each well on a nontreated 24-well plate, 25 μL of particle-containing crosslinker solution was injected into the initial droplet and mixed. Hydrogel droplets were prepared and cured at 37°C inside a cell culture incubator for complete crosslinking. PBS was then added to each well to cover the hydrogels (n=6/group).

For our *in vitro* collagenase experiments, 10 μL hydrogels with 10% (w/v) macromer concentration were fabricated by crosslinking PEG-MAL to non-degradable Dithiothreitol (DTT) and MMP-degradable GCRDVPMSMRGGDRCG peptides

(VPM) (AAPPTec, LLC, >90% purity). PEG-MAL was combined with DTT and/or VPM at a 1:1.5 ratio with 0, 50, and 100% VPM (n=4/group).

For our *in vivo* experiments, we used 2 μL hydrogels with 10% (w/v) macromer concentration and 50% VPM (n=5/group) [18].

3.2.2 Dynamic Cyclic Compression

Immediately after fabrication, hydrogels were placed in PBS. Hydrogels underwent unconfined cyclic compression at 37°C with a custom-built, displacement-controlled bioreactor, as described previously [21,22] (Fig. 3.1A). We applied cyclic compression at strain levels of 0, 20, 40, and 80% at a 1 Hz frequency for 10,000 cycles. Particle release was measured in the supernatant from each well following loading of the hydrogel. The supernatant was analyzed by flow cytometry (BD Accuri C6 flow cytometer, BD Biosciences). The resulting particle counts were then gated to output the number of particles in the FITC fluorescent range (Accuri software). In addition, we measured storage and loss modulus of each hydrogel, also described below.

3.2.3 Mechanical properties

Mechanical properties of the hydrogels were measured in shear (Discovery Hybrid Rheometer, TA Instruments, New Castle, DE). We used a parallel plate geometry of 8 mm diameter. The oscillatory degree of rotation (5 degrees), frequency (0.1 Hz), and temperature (37°C) were constant throughout all tests. All samples underwent one cycle of preconditioning. We recorded shear storage (G') and loss (G") moduli as a function of time and calculated average moduli over four cycles for each hydrogel.

3.2.4 Swelling ratio

Immediately after fabrication, we measured the initial hydrogel weight. We then incubated the hydrogels in 1 mL PBS (-/-) at 37°C. For the next 15 days, we removed the PBS, weighed the swollen hydrogels, and replaced the PBS. We calculated the swelling ratio according to the follow equation:

$$Swelling\ ratio = \frac{Swollen\ weight}{Initial\ weight} * 100$$

3.2.5 Collagenase exposure

Hydrogels were subjected to collagenase at 0 U/μL, 0.1 U/μL, or 10 U/μL. After 3 hours of collagenase exposure, particle release was measured in the supernatant from each well. The supernatant was analyzed by flow cytometry (BD Accuri C6 flow cytometer, BD Biosciences). The resulting particle counts were then gated to output the number of particles in the FITC fluorescent range (Accuri software). Gels were then resuspended in PBS for 21 hours. We then reintroduced the hydrogels to collagenase for another 3 hours, and the supernatant was collected and analyzed again. This process was repeated daily for 4 days.

3.2.6 In vivo mechanical loading

To test the therapeutic potential of the hydrogel system, we first induced OA in mice using cyclic tibial compression [16]. We applied a single session of cyclic compression to the tibia of 26-week-old C57Bl/6 male mice (n=5/group; Jackson Laboratory). With the mice under general anesthesia (2% isoflurane, 1.0 L/min, Webster), loading was

applied to the left or right tibia at a 9.0 N-peak load magnitude for 1200 cycles at a 4 Hz frequency. Contralateral limbs served as controls. All experimental techniques were approved by the Cornell IACUC.

3.2.7 Intra-articular injections

Approximately 48 hours after the single loading session, both mouse knee joints received intra-articular injections. With mice under general anesthesia (2% isoflurane, 1.0 L/min), a 2 mm skin incision was made with a #15 blade to expose the patellar tendon. Then, 2 µl of formulation (described in the following section) was injected into the joint space with a Hamilton syringe. The injection location was immediately medial to the patellar tendon. Skin incisions were closed with 6-0 prolene suture (8706H, Ethicon). Buprenorphine (0.1 mg/kg, Reckitt) was administered for two days following surgery. Two weeks after injection, mice were euthanized, and knee joints were harvested and fixed in 4% paraformaldehyde overnight at 4°C.

3.2.8 Treatment groups

To determine the therapeutic efficacy of the hydrogel system, mice were divided into five groups (Fig 3.3A): 1) saline; 2) bolus DEX; 3) DEX-loaded nanoparticles; 4) hydrogel with DEX-loaded nanoparticles; 5) hydrogel alone. For bolus injections, DEX (5 mg/mL, Sigma D1881) was dissolved in PBS [23,24]. For the DEX-loaded nanoparticles (described below), the final concentration of DEX in the nanoparticles was approximately 4.8 mg/mL. The hydrogel group with DEX-loaded nanoparticles contained approximately 10% nanoparticles.

3.2.9 PLGA-DEX nanoparticle fabrication

Nanoparticles were synthesized based on established protocols with modifications [25]. PLGA (30 mg) and DEX (10 mg) were co-dissolved in 1 mL acetone. The solution was vortexed and sonicated for 7 min to create a water-in-oil emulsion. This emulsion was added to 6 mL 2% PVA solution in PBS and sonicated for 7 min. The resulting solution was stirred at 900 rpm for 4 hr, followed by stirring at 900 rpm for 1 hr in a vacuum desiccator. The nanoparticles were centrifuged at 20,000g, resuspended in PBS, and sonicated for 30 sec. The wash step was repeated three times.

3.2.10 Cartilage degradation

Knee joints were decalcified in EDTA (10%) for 2 weeks and embedded in paraffin. Paraffin blocks were sectioned at a thickness of 6 μm from posterior to anterior using a rotary microtome (Leica RM2255, Wetzlar, Germany). Cartilage morphology in the tibial plateau was assessed using Safranin O/Fast Green-stained sections at 90 μm intervals throughout the joint. The OARSI scoring system was used to assess structural cartilage damage [26]. Scores were measured in the medial tibial plateau and averaged across all sections of each limb.

3.2.11 Osteophyte formation

We examined Safranin-O/Fast Green-stained sections for osteophyte formation on the medial aspect of the tibia. We analyzed medial osteophytes from three representative sections in the joint (posterior, middle, and anterior). We measured the medial-lateral

width of the osteophyte, defined as the distance between the medial end of the epiphysis and the end of the osteophyte [27]. Overall osteophyte size is reported as mean width of the three sections.

3.2.12 Synovial Inflammation

We analyzed synovial thickness and pathology using three representative Safranin-O/Fast Green stained sections (posterior, middle, and anterior). Alterations in thickness and cellularity at the synovial insertion of medial tibia were rated with a previously-established synovitis scoring system [28]. Briefly, the synovitis score (maximum score of 6) was the sum of the synovial lining thickness on a scale of 0 to 3 (0: thickness 1-2 cells, 1: thickness 2-4 cells, 2: thickness 4-9 cells, 3: thickness ≥ 10 cells) and cellular density in the synovial stroma on a scale of 0 to 3 (0: normal cellularity, 1: slightly increased cellularity, 2: moderately increased cellularity, 3: greatly increased cellularity). The synovitis score is reported as a whole joint average from 3 evenly spaced slides per limb.

3.2.13 Statistical Analyses

To analyze the effects of cyclic compression on cartilage mechanical properties and particle release, we used a 2-way ANOVA, with PEG-MAL weight percentage and loading condition as variables. To analyze the effects of collagenase exposure on the hydrogels, we used a 3-way ANOVA, with crosslinker, collagenase concentration, and day as variables. For *in vivo* joint morphology, a linear mixed-effects model was used to assess the effects of loading, the effects of hydrogel vs. no hydrogel nested by loading,

and the effects of DEX vs. no DEX nested by loading and the presence of hydrogel. Alpha levels for significance were set to p=0.05.

3.3 Results

3.3.1 Hydrogels maintained mechanical properties after dynamic cyclic compression

Hydrogels of all PEG-MAL weight percentages withstood mechanical loading. Hydrogels maintained overall structure even after cyclic compression at 80% strain levels (Fig. 3.1B). Shear storage and loss moduli did not change after cyclic compression (p=0.996) (Fig. 3.1D,E). Furthermore, hydrogels with higher PEG-MAL weight percentage had greater shear storage and loss moduli (Fig. 3.1D,E). Particle release was below 20% in all groups besides 2.5% PEG-MAL group in response to mechanical loading of up to 40% strain (Fig. 3.1C). However, approximately half of the encapsulated particles were released after cyclic compression with 80% strain.

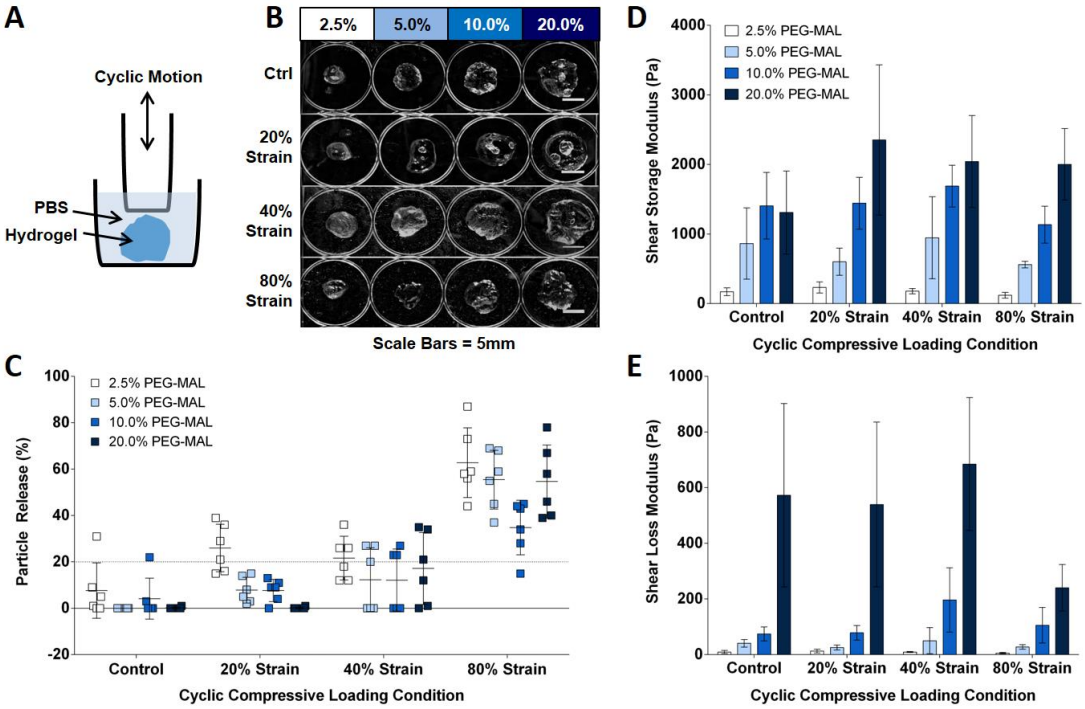

Figure 3.1. Hydrogels maintained mechanical integrity after *in vitro* dynamic cyclic compression. A) Schematic of custom made bioreactor. Adapted from DiDomenico et al. 2017 [22]. B) Hydrogels of all PEG-MAL weight percentages overall structure even after cyclic compression at 80% strain levels. C) Particle release was under 20% (indicated by dotted line) in all hydrogel groups besides the 2.5% PEG-MAL group with cyclic compression up to 40% strain. Approximately half of the particles were released with cyclic compression at 80% strain, but the 10% PEG-MAL group released approximately 20% fewer particles compared to the other groups. D/E) Hydrogels maintained viscoelastic properties with mechanical loading. Shear storage and loss moduli increased with increased PEG-MAL weight percentages.

3.3.2 Swelling ratio increased with PEG-MAL weight percentage

Initially, all gels were similar weight. After 1 day in excess PBS, hydrogel weight increased. Higher PEG-MAL weight percentages resulted in larger swelling ratios (Fig. 3.2A). Hydrogel weight remained constant thereafter for 16 days.

3.3.3 On-demand particle release occurred following collagenase exposure

Particle release in response to collagenase exposure depended on hydrogel formulation, collagenase concentration, and days of exposure (Fig. 3.2B). Hydrogels made with 100% VPM demonstrated greater particle release at all doses of collagenase ($p<0.0001$). Higher concentrations of collagenase led to greater degradation and significantly more release from the gels ($p=0.002$). Particle release was maximum after the first collagenase exposure ($p<0.0001$) and remained relatively constant at a lower level after additional exposures.

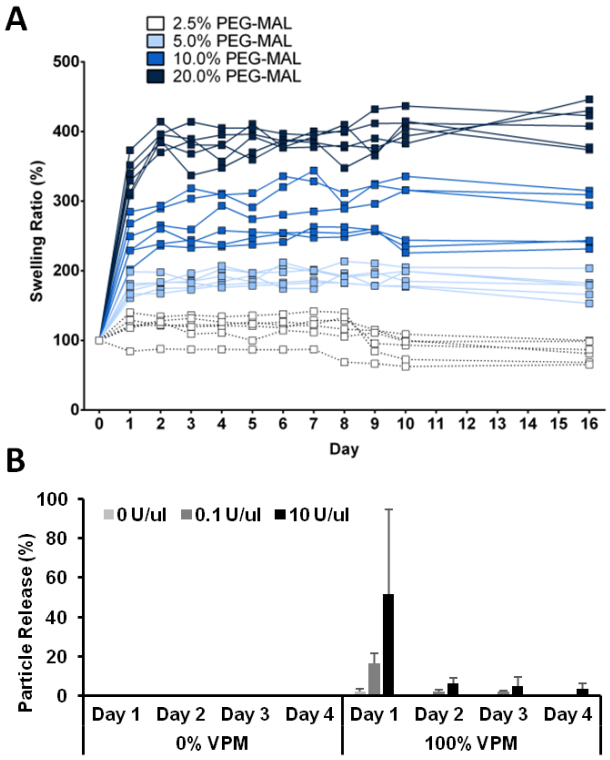

Figure 3.2. A) The majority of swelling occurred within the first 24 hours after hydrogel fabrication. Higher PEG-MAL weight percentages resulted in larger swelling ratios. B) Hydrogels fabricated with 0% VPM crosslinker did not degrade with collagenase exposure. Hydrogels made with 100% VPM degraded at each collagenase concentration. Particle release was dependent on the presence of degradable crosslinker, collagenase concentration, and day of exposure.

3.3.4 Hydrogel-containing formulations attenuated in vivo load-induced cartilage degradation

Cartilage degradation occurred in all groups two weeks after a single bout of cyclic compression at 9.0 N (Fig. 3.3). In general, loading induced cartilage erosion extending to the tidemark in the posteromedial aspect of the tibial plateau. Specifically, loading followed by injection with non-hydrogel formulations increased OARSI scores compared to control limbs ($p=0.0037$). However, less cartilage damage occurred in loaded limbs injected with hydrogel-containing formulations versus non-hydrogel formulations ($p=0.0316$). Treatment with DEX, regardless of formulation, did not affect cartilage degradation compared to groups treated without DEX.

3.3.5 Hydrogel-containing formulations attenuated load-induced osteophyte formation

Osteophytes formed on the medial tibial plateau of loaded limbs in all groups (Fig. 3.3). However, osteophyte size was significantly smaller in the hydrogel-containing injection groups than the non-hydrogel groups ($p=0.0095$). Treatment with DEX, regardless of formulation, did not affect osteophyte size compared to groups treated without DEX.

3.3.6 Hydrogels had no effect on load-induced synovial inflammation

Synovium thickness and synovium cellularity increased in all groups following loading, with no effect of hydrogel (Fig. 3.3). Treatment with DEX, regardless of formulation, did not affect synovitis scores compared to groups treated without DEX.

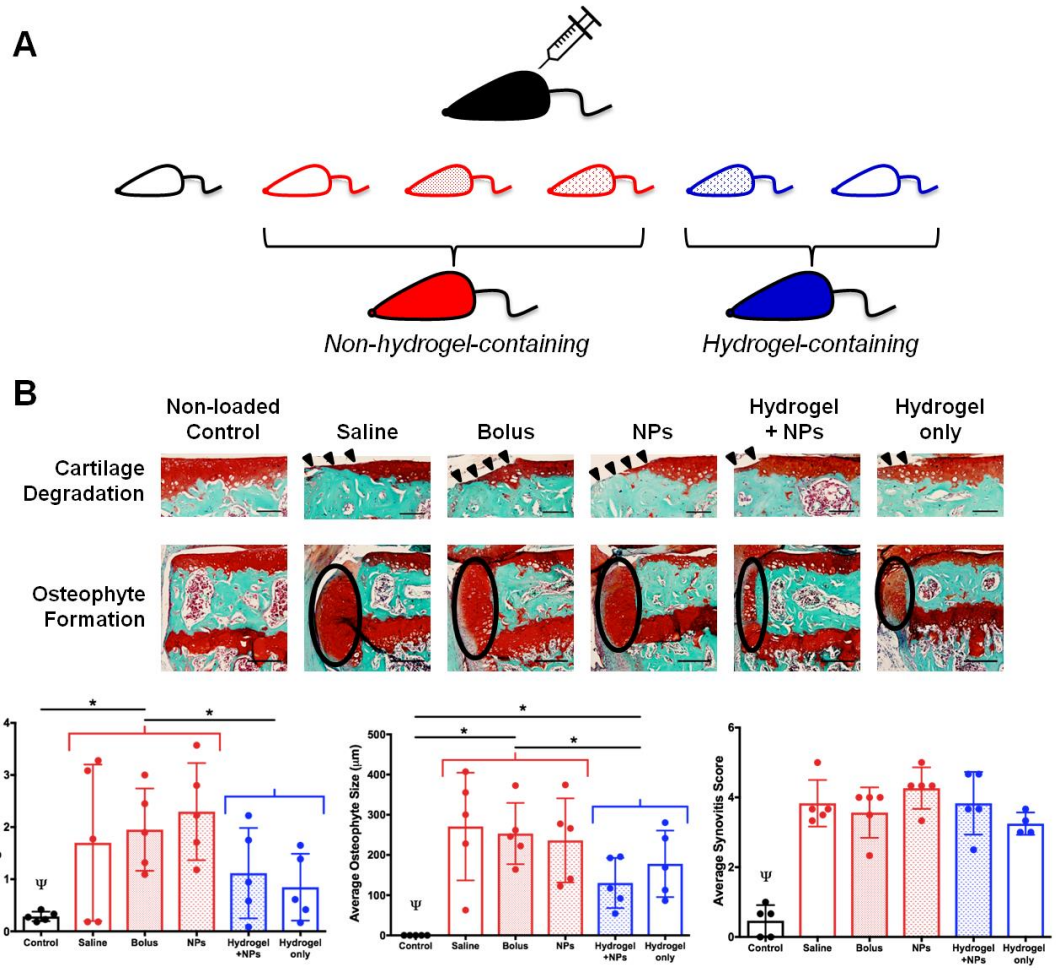

Figure 3.3. IA injections of PEG-MAL hydrogels attenuated load-induced OA. A) Schematic of 5 injection formulations: saline, bolus DEX (5 mg/mL in PBS), DEX-loaded nanoparticles (4.8 mg/mL), hydrogel with DEX-loaded nanoparticles, and hydrogel alone. Hydrogel groups were 10% w/v PEG-MAL with 1:1 DTT:VPM ratio [18]. The hydrogel group with DEX NPs was approximately 10% NPs. B) Hydrogel-containing IA injections had beneficial effects on both cartilage degradation and osteophyte formation, but not synovial thickening induced by a single bout of loading. Red groups = non-hydrogel injections; blue groups = hydrogel-containing injections. Ψ = $p<0.05$ for loading; and * = $p<0.05$ for hydrogel vs. no hydrogel nested by loading. Cartilage scale bars = 100μm. Osteophyte scale bars = 200 μm.

3.4 Discussion

We sought to characterize and test the therapeutic efficacy of an on-demand PEG-MAL hydrogel for IA drug delivery. Our *in vitro* results showed that increased PEG-MAL weight percentage led to greater mechanical properties and higher swelling ratios. Hydrogels maintained their mechanical properties after 10,000 cycles of cyclic

compression at strain levels ranging from 0 to 80%. Furthermore, hydrogels demonstrated on-demand particle release in response to daily collagenase exposure. *In vivo*, hydrogels reduced the severity of cartilage damage and osteophyte formation after a single session of high-level cyclic compression. DEX did not have any protective effects on joint tissues, regardless of formulation. Our results support that the PEG-MAL hydrogel system has potential to improve IA injections for OA treatment.

First, we ensured our hydrogels could withstand mechanical loading. All hydrogel groups maintained their viscoelastic properties after dynamic cyclic compression. Both storage and loss moduli increased with higher PEG-MAL weight percentages, due to greater crosslinking density and the inter-chain entanglements of the components [29–31]. Joint loading can result in cartilage strains up to 40% during normal activity and 80% during injurious activity [15]. All hydrogel groups besides the 2.5% PEG-MAL group demonstrated minimal particle release (<20%) with up to 40% strain. Therefore, hydrogels would release minimal therapeutics during typical daily activities. Importantly, 10% PEG-MAL hydrogels released approximately 20% fewer particles compared to other groups after cyclic compression at 80% strain.

Next, we sought to find a balance between hydrogel swelling and mechanical properties. We wanted to ensure minimal swelling because of the limited space in the joint cavity. The majority of swelling occurred within the first 24 hours after crosslinking before reaching equilibrium, consistent with previous reports [32]. Previously, higher PEG-MAL weight percentage resulted in lower swelling ratios [33]. However, higher PEG-MAL weight percentage also increased the number of hydrophilic groups [34]. Therefore, the increased swelling ratio with higher PEG-MAL

weight percentage observed in our system may be due to increased numbers of hydrophilic groups. Furthermore, the addition of DTT increased the molecular weight between crosslinks [35]. Thus, the high percentage of DTT in these hydrogels also may have increased the swelling ratio with higher PEG-MAL weight percentages. Combining the mechanical and swelling results, the 10% PEG-MAL hydrogel was the optimal balance between mechanical integrity and limited swelling.

We used MMP-degradable hydrogels to improve drug release in the OA environment. MMP-responsive hydrogels have been used for other *in vivo* applications, including bone regeneration [36], myocardial infarction [37], and inflammatory arthritis [38]. We chose crosslinker peptides that degrade in the presence of MMP-3 and -13, because these MMPs are elevated in the joint space during early and late stages of OA [3,4]. Therefore, the most rapid degradation and drug release would occur in an OA joint environment where MMP levels are elevated. Hydrogels demonstrated minimal particle release upon *in vitro* collagenase exposure with non-degradable crosslinkers, whereas higher percentages of particle release occurred with MMP-degradable crosslinkers. Furthermore, the amount of particle release decreased with each collagenase exposure, consistent with previous reports [38]. Thus, PEG-MAL hydrogels demonstrated prolonged, on-demand drug release *in vitro*.

PEG-MAL hydrogels had protective effects on the joint after a single session of *in vivo* high-level cyclic compression. We first compared the therapeutic efficacy of hydrogel-containing vs. non-hydrogel-containing formulations in the load-induced OA joint environment. Hydrogel treatment with or without DEX-loaded nanoparticles attenuated load-induced cartilage damage and osteophyte formation but did not affect

synovitis. On the contrary, injections of bolus DEX or DEX-loaded nanoparticles did not have any beneficial effects on any load-induced tissue changes. Therefore, PEG-MAL hydrogels protected the joints independent of the presence of drug. Natural hydrogels made from hyaluronic acid (HA) have shown similar protective effects in joints without additional therapeutics [39,40]. Thus, our synthetic PEG-MAL hydrogel may possess similar lubricating or cushioning effects as HA hydrogels [12] and future studies will focus on direct comparison to HA. The combination of the hydrogel's protective effects in the joint space and its inert, biocompatible properties provides an excellent platform for an IA drug delivery system.

The lack of response to DEX may be attributed to the severity of load-induced OA and the mechanism of corticosteroids. Previous approaches using IA injections of corticosteroids with or without hydrogels attenuated surgically-induced OA [23,41] and inflammatory arthritis [38,42]. Here, DEX had no beneficial effects on load-induced OA, regardless of formulation (i.e. hydrogel, NPs, or bolus). A single bout of cyclic tibial compression at 9.0 N induced cartilage erosion extending to the tidemark after 2 weeks [16]. This severity of cartilage erosion is an indicator of more advanced or severe stages of OA [26]. Although corticosteroids are OARSI-recommended treatment options for knee OA [43], corticosteroids are most effective in treating milder, but not severe, forms of OA [44–46]. In addition, the primary biochemical action of corticosteroids is the local suppression of inflammation [47]. Although cyclic loading increased synovitis, whether inflammation is a driving factor of load-induced OA remains unclear. Thus, the anti-inflammatory effects of corticosteroids may not be sufficient to attenuate load-induced OA progression.

Future work will focus on improving the hydrogel system and understanding its efficacy in larger preclinical models of OA. First, although our hydrogels maintained mechanical properties after cyclic compression, a high percentage of particle release occurred at the 80% strain level. Depending on where the hydrogel resides in the joint and the degree of physical activity, physiological strains in cartilage could result in 80% strain levels [15] and cause particle release. However, based on preliminary retrieval studies, the hydrogel resides near the fat pad, but further work is necessary to determine whether the hydrogel needs to withstand forces induced by tibiofemoral contact. Second, although our collagenase studies demonstrated daily on-demand release, a high percentage of particles were released on Day 0. Future work can focus on achieving a constant 5-10% particle release for each collagenase exposure, leading to approximately 3 weeks of therapeutics in the joint. The release profile can be controlled with peptides of varying levels of MMP-sensitivity [36]. Here, we used a fast-degrading peptide, but slow-degrading peptides may attenuate therapeutic particle release with collagenase exposure. Third, we used a mouse model of load-induced OA because of its non-invasive means and reproducibility. Future work will focus on larger animal models of OA. Larger joint spaces will allow for greater volumes of injectable hydrogel and more closely mimic the human joint environment. Fourth, we can use alternative drugs to better inhibit OA-like changes. For example, combinatorial approaches involving hydrogels with growth factors [48,49] and glucosamine/chondroitin [39] attenuated OA progression in preclinical animal models. The PEG-MAL hydrogel system may be more effective in combination with other therapeutics compared to DEX.

In summary, we developed an on-demand hydrogel-based drug delivery system that maintained its mechanical properties in response to high levels of cyclic compression. The hydrogel system attenuated load-induced OA, and future work will investigate its efficacy with other therapeutics and loading protocols. Ultimately, this synthetic PEG-MAL hydrogel system is a promising drug delivery strategy for the treatment of OA.

3.5 Acknowledgments

We thank Dr. Lawrence Bonassar, Chris DiDomenico, Natalia Rebollo, and Philip Carubia for experimental assistance. We acknowledge Cornell CCMR (NSF DMR-1719875), NSF CAREER Award (DMR-1554275 (AS)), 3M Non-Tenured Faculty Award (AS), Cornell Sloan and Colman Diversity Fellowships (TW), GAANN Fellowship (DH), and NIH R21-AR064034 (MvdM).

3.6 References

1. Lawrence RC, Felson DT, Helmick CG, Arnold LM, Choi H, Deyo RA, Gabriel S, Hirsch R, Hochberg MC, Hunder GG, Jordan JM, Katz JN, Kremers HM, Wolfe F, National Arthritis Data Workgroup. Estimates of the prevalence of arthritis and other rheumatic conditions in the United States. Part II. *Arthritis Rheum* 2008;58:26–35.
2. Goldring MB, Goldring SR. Osteoarthritis. *J Cell Physiol* 2007;213:626–634.
3. Mehraban F, Kuo SY, Riera H, Chang C, Moskowitz RW. Prostromelysin and procollagenase genes are differentially up-regulated in chondrocytes from the knees of rabbits with experimental osteoarthritis. *Arthritis Rheum* 1994;37:1189–97.
4. Reboul P, Pelletier JP, Tardif G, Cloutier JM, Martel-Pelletier J. The new collagenase, collagenase-3, is expressed and synthesized by human chondrocytes but not by synoviocytes. A role in osteoarthritis. *J Clin Invest* 1996;97:2011–2019.
5. Brown TD, Johnston RC, Saltzman CL, Marsh JL, Buckwalter JA. Posttraumatic osteoarthritis: a first estimate of incidence, prevalence, and burden of disease. *J Orthop Trauma* 2006;20:739–44.
6. Kruse DW. Intraarticular cortisone injection for osteoarthritis of the hip. Is it effective? Is it safe? *Curr Rev Musculoskelet Med* 2008;1:227–33.
7. Arrich J, Piribauer F, Mad P, Schmid D, Klaushofer K, Müllner M. Intra-articular hyaluronic acid for the treatment of osteoarthritis of the knee: systematic review and meta-analysis. *CMAJ* 2005;172:1039–43.
8. Kang ML, Im I. Drug delivery systems for intra-articular treatment of osteoarthritis. *Expert Opin Drug Deliv* 2014;11:269–282.
9. Holyoak DT, Tian YF, Meulen MCH van der, Singh A. Osteoarthritis: Pathology, Mouse Models, and Nanoparticle Injectable Systems for Targeted Treatment. *Ann Biomed Eng* 2016;44:2062–75.
10. Whitmire RE, Scott Wilson D, Singh A, Levenston ME, Murthy N, García AJ. Self-assembling nanoparticles for intra-articular delivery of anti-inflammatory proteins. *Biomaterials* 2012;33:7665–7675.
11. Singh A, Agarwal R, Diaz-Ruiz CA, Willett NJ, Wang P, Lee LA, Wang Q, Guldberg RE, García AJ. Nanoengineered particles for enhanced intra-articular retention and delivery of proteins. *Adv Healthc Mater* 2014;3:1562–7, 1525.
12. He Z, Wang B, Hu C, Zhao J. An overview of hydrogel-based intra-articular drug delivery for the treatment of osteoarthritis. *Colloids Surfaces B Biointerfaces* 2017;154:33–39.
13. Seliktar D. Designing Cell-Compatible Hydrogels for Biomedical Applications.
14. Gerwin N, Hops C, Lucke A. Intraarticular drug delivery in osteoarthritis B. 2006.
15. Sanchez-Adams J, Leddy HA, McNulty AL, O'Conor CJ, Guilak F. The mechanobiology of articular cartilage: bearing the burden of osteoarthritis. *Curr Rheumatol Rep* 2014;16:451.
16. Ko FC, Dragomir CL, Plumb DA, Hsia AW, Adebayo OO, Goldring SR, Wright TM, Goldring MB, Meulen MCH van der. Progressive cell-mediated changes in articular cartilage and bone in mice are initiated by a single session of controlled cyclic compressive loading. *J Orthop Res* 2016.
17. Purwada A, Shah SB, Beguelin W, Melnick AM, Singh A. Modular Immune

Organoids with Integrin Ligand Specificity Differentially Regulate Ex Vivo B Cell Activation. *ACS Biomater Sci Eng* 2017;3:214–225.
18. Purwada A, Shah SB, Béguelin W, August A, Melnick AM, Singh A. Ex vivo synthetic immune tissues with T cell signals for differentiating antigen-specific, high affinity germinal center B cells. *Biomaterials* 2018.
19. Lee TT, García JR, Paez JI, Singh A, Phelps EA, Weis S, Shafiq Z, Shekaran A, Campo A Del, García AJ. Light-triggered in vivo activation of adhesive peptides regulates cell adhesion, inflammation and vascularization of biomaterials. *Nat Mater* 2015;14:352–60.
20. Phelps EA, Enemchukwu NO, Fiore VF, Sy JC, Murthy N, Sulchek TA, Barker TH, García AJ. Maleimide cross-linked bioactive PEG hydrogel exhibits improved reaction kinetics and cross-linking for cell encapsulation and in situ delivery. *Adv Mater* 2012;24:64–70, 2.
21. Ballyns JJ, Bonassar LJ. Dynamic compressive loading of image-guided tissue engineered meniscal constructs. 2011.
22. DiDomenico CD, Xiang Wang Z, Bonassar LJ. Cyclic Mechanical Loading Enhances Transport of Antibodies Into Articular Cartilage. *J Biomech Eng* 2017;139:011012.
23. Huebner KD, Shrive NG, Frank CB. Dexamethasone inhibits inflammation and cartilage damage in a new model of post-traumatic osteoarthritis. *J Orthop Res* 2014;32:566–572.
24. Stephens MB, Beutler AI, O'Connor FG. Musculoskeletal injections: a review of the evidence. *Am Fam Physician* 2008;78:971–6.
25. Vasir JK, Labhasetwar V. Preparation of biodegradable nanoparticles and their use in transfection. *Cold Spring Harb Protoc* 2008;3:1–5.
26. Glasson SS, Chambers MG, Berg WB Van Den, Little CB. The OARSI histopathology initiative - recommendations for histological assessments of osteoarthritis in the mouse. *Osteoarthritis Cartilage* 2010;18 Suppl 3:S17-23.
27. Holyoak DT, Otero M, Armar NS, Ziemian SN, Otto A, Cullinane D, Wright TM, Goldring SR, Goldring MB, Meulen MCH van der. Collagen XI mutation lowers susceptibility to load-induced cartilage damage in mice. *J Orthop Res* 2017;36:711–720.
28. Lewis JS, Hembree WC, Furman BD, Tippets L, Cattel D, Huebner JL, Little D, DeFrate LE, Kraus VB, Guilak F, Olson SA. Acute joint pathology and synovial inflammation is associated with increased intra-articular fracture severity in the mouse knee. *Osteoarthr Cartil* 2011;19:864–873.
29. Daniele MA, Adams AA, Naciri J, North SH, Ligler FS. Interpenetrating networks based on gelatin methacrylamide and PEG formed using concurrent thiol click chemistries for hydrogel tissue engineering scaffolds. *Biomaterials* 2014;35:1845–1856.
30. Yang QS, Ma LH, Shang JJ. The chemo-mechanical coupling behavior of hydrogels incorporating entanglements of polymer chains. *Int J Solids Struct* 2013;50:2437–2448.
31. Cha C, Shin SR, Gao X, Annabi N, Dokmeci MR, Tang X, Khademhosseini A. Controlling mechanical properties of cell-laden hydrogels by covalent incorporation of graphene oxide. *Small* 2014;10:514–523.

32. Peppas NA, Keys KB, Torres-Lugo M, Lowman AM. Poly(ethylene glycol)-containing hydrogels in drug delivery. *J Control Release* 1999;62:81–7.
33. Phelps EA, Templeman KL, Thulé PM, García AJ. Engineered VEGF-releasing PEG-MAL hydrogel for pancreatic islet vascularization. *Drug Deliv Transl Res* 2015;5:125–36.
34. Yu J, Chen F, Wang X, Dong N, Lu C, Yang G, Chen Z. Synthesis and characterization of MMP degradable and maleimide cross-linked PEG hydrogels for tissue engineering scaffolds. 2016.
35. Barbucci R. *Hydrogels*.; 2008.
36. Lutolf MP, Lauer-Fields JL, Schmoekel HG, Metters AT, Weber FE, Fields GB, Hubbell JA. Synthetic matrix metalloproteinase-sensitive hydrogels for the conduction of tissue regeneration: engineering cell-invasion characteristics. *Proc Natl Acad Sci U S A* 2003;100:5413–8.
37. Purcell BP, Lobb D, Charati MB, Dorsey SM, Wade RJ, Zellars KN, Doviak H, Pettaway S, Logdon CB, Shuman JA, Freels PD, Gorman JH, Gorman RC, Spinale FG, Burdick JA. Injectable and bioresponsive hydrogels for on-demand matrix metalloproteinase inhibition. *Nat Mater* 2014;13:653–61.
38. Joshi N, Yan J, Levy S, Bhagchandani S, Slaughter K V, Sherman NE, Amirault J, Wang Y, Riegel L, He X, Rui TS, Valic M, Vemula PK, Miranda OR, Levy O, Gravallese EM, Aliprantis AO, Ermann J, et al. Towards an arthritis flare-responsive drug delivery system.
39. Şükür E, Talu C, Akman YE, Çirci E, Öztürkmen Y, Tüzüner T. Comparison of the chondroprotective effect of a novel hydrogel compound and traditional hyaluronate on rat cartilage in a papain-induced osteoarthritis model. *Acta Orthop Traumatol Turc* 2016;50:458–463.
40. Kang M-L, Jeong S-Y, Im G-I. Hyaluronic Acid Hydrogel Functionalized with Self-Assembled Micelles of Amphiphilic PEGylated Kartogenin for the Treatment of Osteoarthritis.
41. Zhang Z, Wei X, Gao J, Zhao Y, Zhao Y, Guo L, Chen C, Duan Z, Li P, Wei L. Intra-Articular Injection of Cross-Linked Hyaluronic Acid-Dexamethasone Hydrogel Attenuates Osteoarthritis: An Experimental Study in a Rat Model of Osteoarthritis. *Int J Mol Sci* 2016;17:411.
42. Reum Son A, Yeon Kim D, Hun Park S, Yong Jang J, Kim K, Ju Kim B, Yun Yin X, Ho Kim J, Hyun Min B, Keun Han D, Suk Kim M. Direct chemotherapeutic dual drug delivery through intra-articular injection for synergistic enhancement of rheumatoid arthritis treatment. *Nat Publ Gr* 2015.
43. Mcalindon TE, Bannuru RR, Sullivan MC, Arden NK, Berenbaum F, Bierma-Zeinstra SM, Hawker GA, Henrotin Y, Hunter DJ, Kawaguchi H, Kwoh {{ K, Lohmander ## S, Rannou F, Roos Zzz EM, Underwood M. OARSI guidelines for the non-surgical management of knee osteoarthritis. *Osteoarthr Cartil* 2014;22:363–388.
44. Iannitti T, Lodi D, Palmieri B. Intra-Articular Injections for the Treatment of Osteoarthritis. *Drugs R D* 2011;11:13–27.
45. Arden NK, Reading IC, Jordan KM, Thomas L, Platten H, Hassan A, Ledingham J. A randomised controlled trial of tidal irrigation vs corticosteroid injection in knee osteoarthritis: the KIVIS Study. *Osteoarthr Cartil* 2008;16:733–9.

46. Eyigor S, Hepguler S, Sezak M, Oztop F, Capaci K. Effects of intra-articular hyaluronic acid and corticosteroid therapies on articular cartilage in experimental severe osteoarthritis. *Clin Exp Rheumatol* 24:724.
47. Hong SL, Levine L. Inhibition of arachidonic acid release from cells as the biochemical action of anti-inflammatory corticosteroids. *Proc Natl Acad Sci U S A* 1976;73:1730–4.
48. Inoue A, Takahashi KA, Arai Y, Tonomura H, Sakao K, Saito M, Fujioka M, Fujiwara H, Tabata Y, Kubo T. The therapeutic effects of basic fibroblast growth factor contained in gelatin hydrogel microspheres on experimental osteoarthritis in the rabbit knee. *Arthritis Rheum* 2006;54:264–270.
49. Feng Q, Lin S, Zhang K, Dong C, Wu T, Huang H, Yan X, Zhang L, Li G, Bian L. Sulfated hyaluronic acid hydrogels with retarded degradation and enhanced growth factor retention promote hMSC chondrogenesis and articular cartilage integrity with reduced hypertrophy. *Acta Biomater* 2017;53:329–342.

CHAPTER 4: LOW-LEVEL CYCLIC TIBIAL COMPRESSION ATTENUATES OSTEOARTHRITIS PROGRESSION AFTER JOINT INJURY IN MICE

4.1 Introduction

Osteoarthritis (OA) is degenerative joint disease that affects millions of individuals and is the leading cause of disability in the elderly population [1–4]. The three hallmarks of the end-stage disease are cartilage degradation, osteophyte formation, and subchondral bone sclerosis. During the OA process, chondrocyte apoptosis occurs [5], and collagenases and aggrecanases degrade the cartilage matrix, resulting in cleaved aggrecan and collagen [6,7]. Post-traumatic osteoarthritis (PTOA) is a subset of OA associated with joint injury and instability due to mechanical trauma [8]. Individuals who experience a joint injury, such as anterior cruciate ligament (ACL) rupture or meniscal tear, are at risk for developing PTOA due to altered joint kinematics and any trauma directly to the cartilage or adjacent bone [9,10]. Providing interventions following joint injury may be beneficial to attenuate PTOA.

Mechanical loading, exercise, and joint health have a unique relationship in OA onset and progression. Excessive mechanical loading is a primary risk factor for OA [11]. Loading at high levels can decrease aggrecan synthesis and induce chondrocyte apoptosis [12,13]. Furthermore, high loads can rupture stabilizing ligaments or damage joint tissue, such as the meniscus or cartilage [14]. Conversely, mild exercise is a recommended intervention for early-stage OA [15]. Mild exercise involving low-level loading can increase aggrecan synthesis *in vitro* and maintain thicker cartilage *in vivo* [16,17]. In rodents, treadmill running slowed the progression of injury-induced cartilage degradation [18]. Although low-level mechanical loading has potential to

attenuate OA, most experiments investigating the effects of beneficial loading have been either *in vitro* or have involved exercise. *In vitro* studies using cartilage explants and/or chondrocyte culture do not recapitulate the response of the entire joint [12,19]. In addition, exercise leads to systemic effects, including peri-articular muscular strengthening, improvements in proprioception, and weight reduction [20,21]. These multiple effects obscure the contribution of factors that specifically benefit the joint [21]. Here, we sought to isolate the beneficial effects of low-level loading using *in vivo* cyclic tibial compression.

To date, *in vivo* cyclic tibial compression has been an effective approach to study the initiation and progression of load-induced OA. Cyclic compression at moderate (4.5N) and high (9.0N) load magnitudes induced OA-like joint pathology, including cartilage degradation, osteophyte formation, and subchondral bone changes, in young (10-week) and adult (26-week) mice [22-25]. This same approach has the potential to benefit cartilage health at lower load levels. Thus, we sought to determine whether daily cyclic compression at low load magnitudes (1.0N and 2.0N) would attenuate PTOA. To accomplish this objective, we used low-level cyclic compression in combination with a surgically-induced model of PTOA, the destabilization of the medial meniscus (DMM) [26]. We assessed tissue-level changes in the cartilage, peri-articular bone, and menisci. In addition, we analyzed for chondrocyte apoptosis, aggrecan cleavage, and surface collagen loss. We hypothesized that cyclic compression at low load magnitudes would attenuate DMM-induced PTOA.

4.2 Methods

4.2.1 Animals

We used fifty-one 10-week-old male C57BL/6J mice (The Jackson Laboratory, Bar Harbor, ME, USA). Mice were housed in groups of 3 to 5 per cage. Lighting was maintained at a 12-hours-on-12-hours-off schedule. Mice were given food and water *ad libitum*. All experimental techniques were approved by the Cornell IACUC. Briefly, animals underwent DMM surgery [26]. Starting five days after surgery, cyclic tibial compression was applied to the operated limbs for either 2 or 6 weeks. Upon completion of loading, mice were euthanized, and knee joints harvested for histological and architectural analyses.

4.2.2 Surgical destabilization of the medial meniscus

We performed DMM surgery on the right knee joints of all mice [26]. A 3mm skin incision was made with a #15 blade to expose the patellar tendon. Then a soft tissue incision was made immediately medial to the patellar tendon from the distal patella to the proximal tibial plateau. While a second researcher gently pulled the patellar tendon laterally with a Tyrell Hook (without dislocating the patella), the fat pad was shifted laterally with a #11 scalpel blade until the medial meniscotibial ligament (MMTL) was in view. Then, we positioned the scalpel blade inferior to the MMTL with the sharp edge facing laterally. Finally, we rotated the blade clockwise until the MMTL was ruptured. To verify each surgery, we translated the medial meniscus medially using the blunt edge of the scalpel blade. We closed the soft tissue and skin incisions with 6-0 and

7-0 prolene suture, respectively (8706H, 8708H, Ethicon). Buprenorphine (0.1 mg/kg) was administered during recovery, immediately after surgery and once daily for the following 4 days.

4.2.3 Mechanical loading

After the 5-day recovery period from DMM, mice were divided into seven groups (n=7-8/group) (Fig. 4.1). One group was euthanized immediately after the recovery period to investigate short-term damage caused by DMM (*DMM-only:* +0-weeks). Two groups were used for +2-week time points (after the 5-day recovery period). For one +2-week group, cyclic compression was applied to DMM-treated tibiae at peak loads of 1.0N for 2 weeks (*DMM+1.0N:* +2-weeks). The second +2-week group received daily 5-minute doses of anesthesia without cyclic tibial compression (*DMM-only:* +2-weeks). The remaining four groups were used for +6-week time points (after the 5-day recovery period). For three of the +6-week groups, cyclic compression was applied to the DMM-treated right tibiae at 1.0N, 2.0N, or 4.5N peak loads for 6 weeks (*DMM+1.0N, DMM+2.0N, DMM+4.5N:* +6-weeks). The final +6-week group received daily anesthesia without cyclic tibial compression (*DMM-only:* +6-weeks). For all loaded groups, cyclic compression was performed with mice under general anesthesia (2% isoflurane, 1.0L/min, Webster) and consisted of 1200 cycles/day at 4 Hz for 5 days/week. All load waveforms were triangular with load/unload ramps for 0.075 seconds each and dwell times of 0.100 seconds. Contralateral limbs served as controls. Mice were euthanized, and knee joints were harvested and fixed in 4%

paraformaldehyde. After fixation, tissues were transferred to 70% ethanol for short-term storage.

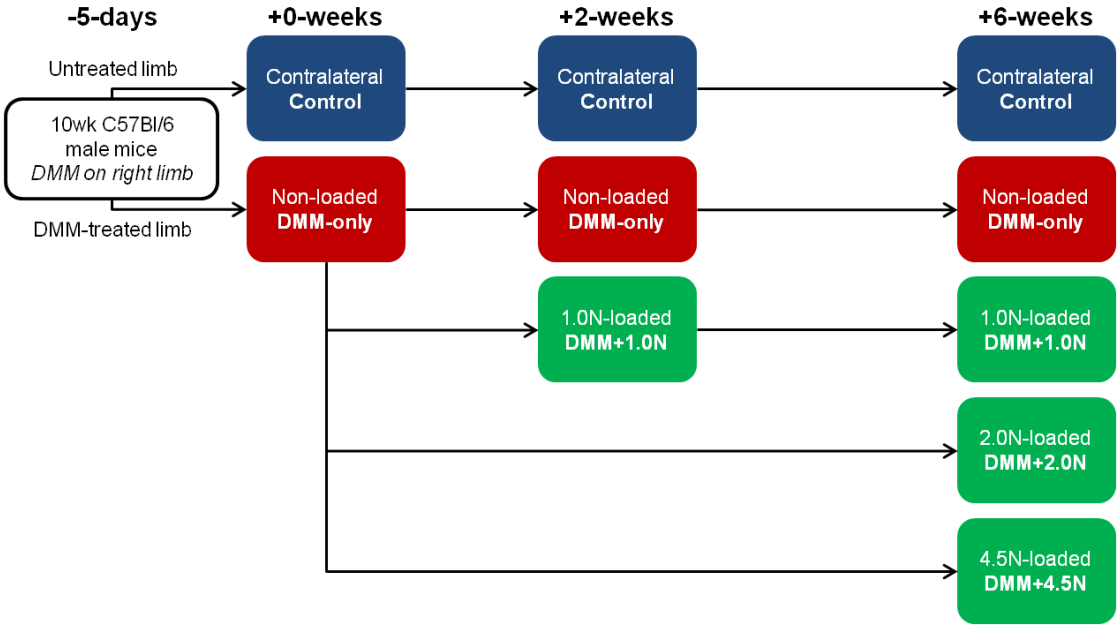

Figure 4.1. Experimental design. 10wk C57Bl/6 male mice underwent DMM surgery on their right limbs. Five days later (+0-weeks), DMM-treated limbs were either subjected to no loading (*DMM-only*),1.0N-loading (*DMM+1.0N*), 2.0N-loading (*DMM+2.0N*), or 4.5N-loading (*DMM+4.5N*) for 2 or 6 weeks. Contralateral limbs served as controls at each time point. n=7-8 mice per group.

4.2.4 Cartilage morphological changes

Knee joints were decalcified in EDTA, processed, and paraffin-embedded. Paraffin blocks were sectioned at a 6-µm-thickness from posterior to anterior using a rotary microtome (Leica RM2255, Wetzlar, Germany). To assess cartilage morphology, sections were stained with Safranin-O/Fast Green at 90-µm intervals. Histological scoring was performed to examine structural cartilage damage in the medial tibial plateau, using the OARSI scoring system [27]. Average and maximum scores of each limb were calculated.

4.2.5 Osteophyte formation

We examined Safranin-O/Fast Green-stained histological sections for osteophyte formation surrounding the joint. We analyzed osteophytes in the medial tibial plateau from three representative sections in the joint (anterior, middle, posterior). Osteophyte maturity was evaluated as described previously: 0 for no osteophyte, 1 for a primarily cartilaginous osteophyte, 2 for a mixture of cartilage and bone, or 3 for primarily bony structure [28]. We also measured the medial-lateral width of the osteophyte, defined as the distance between the medial end of the epiphysis and the end of the osteophyte. Widths are reported as absolute values [24].

4.2.6 Peri-articular bone morphological changes

Bone architecture changes at the +6-week time point were determined by microcomputed tomography (microCT). Prior to decalcification, intact knee joints were scanned by microCT, with an isotropic voxel resolution of 10 μm (μCT35, Scanco, Bruttisellen, Switzerland; 55kVp, 145μA, 600ms integration time). We examined bone in the epiphysis and metaphysis of the proximal tibia. In the epiphysis, we analyzed the subchondral bone plate (SBP) and epiphyseal cancellous bone. For the SBP, the volume of interest (VOI) encompassed all cortical bone below the cartilage surface at the proximal end of the tibia extending distally until epiphyseal cancellous bone was evident. The VOI for epiphyseal cancellous bone encompassed cancellous bone distal to the SBP and proximal to the growth plate, excluding cortical bone. In the metaphysis, we analyzed cancellous bone. The VOI for metaphyseal cancellous bone began distal to the growth plate and extended 10% tibial length, excluding the cortex. Outcome

parameters for the SBP included thickness and tissue mineral density (TMD). Cancellous bone parameters included bone volume fraction (BV/TV), trabecular thickness (Tb.Th), trabecular separation (Tb.Sp), and cancellous TMD (TMD).

4.2.7 Chondrocyte apoptosis

We assessed chondrocyte apoptosis after DMM surgery and 1.0N-loading using a TUNEL kit to detect DNA strand breaks (Sigma, 11684795910 Roche, Darmstadt, Germany). We stained representative sections from the middle region of each limb at all time points. Sections were deparaffinized, rehydrated, and incubated with proteinase K at 37°C. Then, samples were incubated with the TUNEL reaction mixture for 1h at 37°C. Finally, sections were coverslipped with antifade mounting media containing DAPI. DAPI+ cells were measured in the articular cartilage of the medial tibial plateau [29,30]. The DAPI+ signal was normalized to cartilage area. Similarly, TUNEL+ cells were measured and normalized to the total number of chondrocytes (DAPI+ signal) to account for potential changes in cellularity.

4.2.8 Cleaved Aggrecan

Cleaved aggrecan levels after DMM and 1.0N-loading were assessed using immunohistochemistry (IHC). We stained representative sections from the middle region of control and DMM-treated limbs from animals in the *DMM-only* and *DMM+1.0N* groups at the +2-week and +6-week time points [31]. Sections were deparaffinized and rehydrated. Antigen retrieval was performed with a mild temperature retrieval solution at 60°C for 30 minutes (UNI-TRIEVE, Innovex, Richmond,

California). Endogenous peroxidase activity was quenched for 15 minutes at room temperature (RT) (PEROX-BLOCK, Innovex). Background staining was minimized using Background Buster for 30 minutes at RT (STAT Animal IHC Kit, Innovex). Detection of cleaved aggrecan was performed using an anti-NITEGE primary antibody (ThermoFisher PA-1-1746) diluted 1:100 in immunodiluent (Immuno Diluent and Block, Innovex) for 2 hours at RT. Secondary linking antibody and horseradish peroxidase-enzyme (STAT Animal IHC Kit, Innovex) were used for 10 minutes each at RT. Fresh DAB solution was applied and incubated for 5 minutes at RT, and staining intensity was enhanced for 3 minutes at RT (Quick DAB Enhancer, Innovex). Sections were washed with water and mounted (Advantage Mounting Medium, Innovex). Percentage of positive immunostaining in the articular cartilage of the medial tibial plateau was calculated using ImageJ software (NIH) [29,30]. Positive signal was normalized to cartilage area.

4.2.9 Surface collagen content

We assessed surface collagen content using picrosirius red staining. We stained representative sections from the middle region of each limb at all time points. Sections were deparaffinized, rehydrated, and incubated with 0.1% Direct Red 80 (Sigma-Aldrich, 365548) in saturated picric acid for 60 minutes at RT, followed by dehydration and coverslipping. Using custom software (MATLAB, MathWorks), the number of positively stained pixels in the cartilage surface was counted. Positive staining was normalized to the total number of pixels in the cartilage surface.

4.2.10 Meniscal ossicle morphology

MicroCT scans were used to characterize the anterior meniscal ossicle after DMM and loading. The VOI included all positive signal in the medial joint space, excluding the fabella. We assessed meniscus volume and density [32].

4.2.11 Statistical analyses

For histological evaluations, we compared limbs across groups using a one-way ANOVA with animal as a random effect. We applied the ANOVA to analyze OARSI scores, osteophytes, cellularity, apoptosis, cleaved aggrecan, and surface collagen content. Contralateral limbs from the *DMM-only* group were used as our control group for histological evaluations. For microCT comparisons, we used a two-way ANOVA with limb and group as variables, and animal as a random effect. The two-way ANOVA was used to analyze the subchondral bone plate, cancellous bone, and meniscal ossicles.

4.3 Results

4.3.1 Low-level cyclic compression attenuated DMM-induced cartilage degradation

After the 5-day recovery period post-DMM surgery (+0-weeks), cartilage damage was minimal (Fig. 4.2A,B,C). Mild localized proteoglycan loss occurred in some limbs, but neither average nor maximum OARSI scores were different from control limbs at +0-weeks. Two weeks after the 5-day recovery (+2-weeks), proteoglycan loss and mild erosion were present in *DMM-only* limbs, and average OARSI scores were greater compared to + control limbs at +0-weeks. In the

DMM+1.0N group at +2-weeks, moderate proteoglycan was visible in the cartilage, but average OARSI scores were not different from control limbs at +0-weeks. At the +6-week time point, severe cartilage erosion occurred in *DMM-only* limbs. In the *DMM+1.0N* group at +6-weeks, the cartilage surface was generally intact, and structural changes were limited to focal proteoglycan loss. At +6-weeks, average and max OARSI scores in the *DMM+1.0N* group were significantly lower than scores from the *DMM-only* limbs.

Cyclic compression at 2.0N had similar effects to 1.0N-loading at +6-weeks (Fig. 4.2A,D,E). The cartilage surface from 2.0N-loaded limbs was generally intact, but proteoglycan loss was evident. At +6-weeks, average OARSI scores were significantly lower in the *DMM+2.0N* group compared to the *DMM-only* group, but maximum OARSI scores were not different between the two groups. Loading at 4.5N led to moderate cartilage erosion and proteoglycan loss. At +6-weeks, neither average nor maximum OARSI scores were significantly different between the *DMM-only* and *DMM+4.5N* groups.

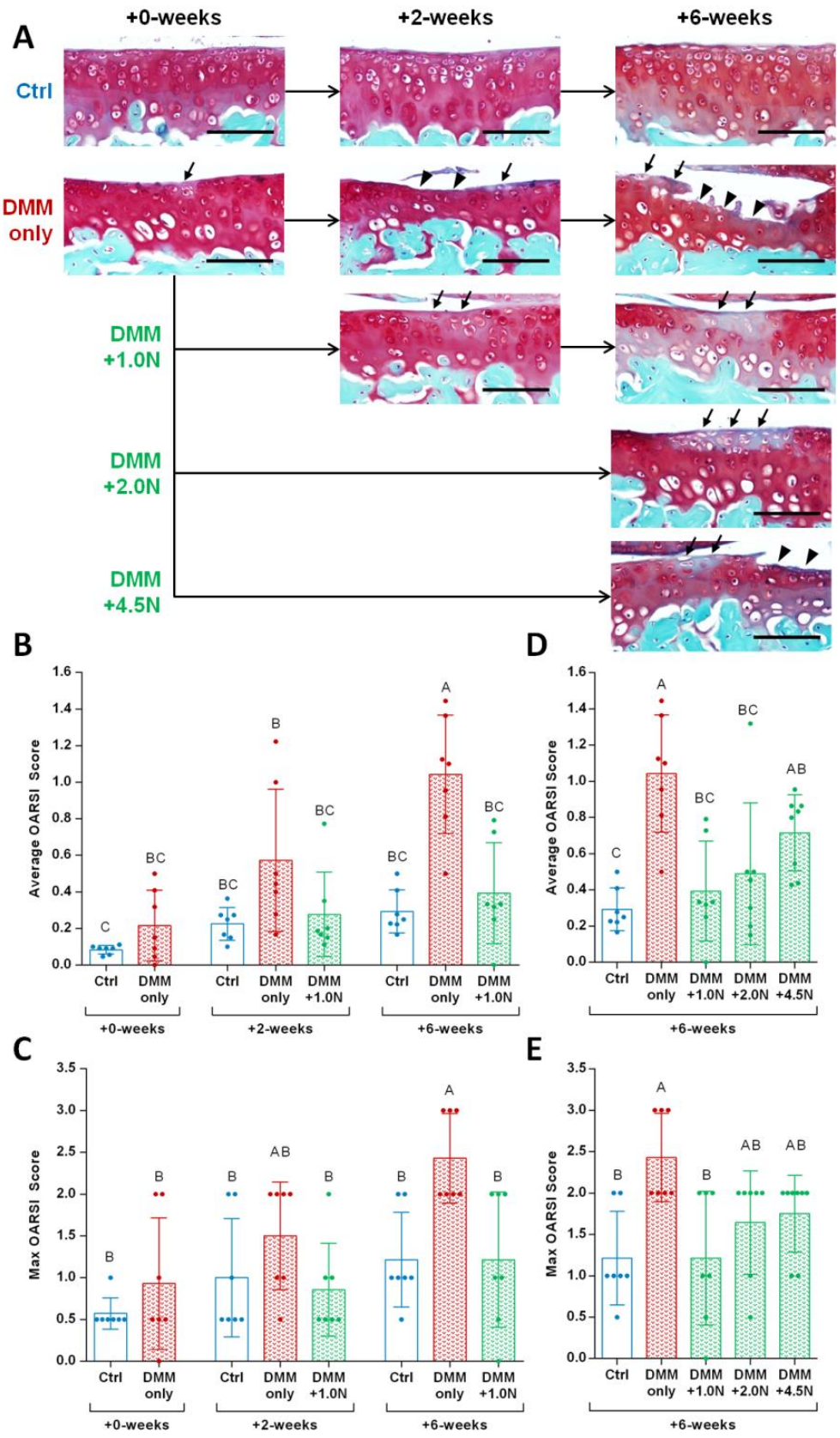
A
+0-weeks
+2-weeks
+6-weeks
Ctrl
DMM only
DMM +1.0N
DMM +2.0N
DMM +4.5N
B
Average OARSI Score
Ctrl
DMM only
DMM +1.0N
+0-weeks
+2-weeks
+6-weeks
C
Max OARSI Score
D
Average OARSI Score
DMM +2.0N
DMM +4.5N
E
Max OARSI Score

Figure 4.2. Low-level cyclic compression attenuated post-traumatic cartilage degradation. (A) Representative Safranin O/Fast Green histological images show that DMM surgery led to focal erosion extending to the tidemark in the medial tibial plateau in the *DMM-only* group. Loading at 1.0N attenuated DMM-induced cartilage erosion, evident from the intact cartilage surface. Loading at 2.0N had similar effects to 1.0N-loading, with an intact cartilage surface after 6 weeks. Moderate loading at 4.5N resulted in mild erosion and proteoglycan loss that was not different from *DMM-only*. (B) Average and (C) max OARSI scores for cartilage damage were significantly different between the *DMM-only* vs. *DMM+1.0N* groups at +6-weeks. (D) 2.0N-loading also led to lower average OARSI scores than *DMM-only*, (E) but not lower max OARSI scores. Scale bars = 100 μm. Arrows indicate proteoglycan loss; arrow heads indicate erosion. Groups with the same letters over the bars are not significantly different; groups with different letters indicate that the means are significantly different by post-hoc comparisons.

4.3.2 Low-level cyclic compression attenuated DMM-induced osteophyte formation

Low-level tibial compression attenuated osteophyte growth (Fig. 4.3). DMM surgery led to osteophytes that extended the length of the medial aspect of the tibial plateau. On the anterior portion of the tibial plateau, medial osteophyte size increased after the 5-day recovery period in the *DMM-only* group (+0-weeks) compared to controls (Fig. 4.3A-B). Anteromedial osteophyte size continued to increase in the *DMM-only* group after 2 and 6 weeks. However, anteromedial size was not different between the +0-week *DMM-only* group and *DMM+1.0N* groups at +2-weeks or +6-weeks. Anteromedial osteophyte maturity was not different between *DMM-only* and *DMM+1.0N* groups.

On the posterior portion of the tibial plateau, medial osteophytes formed in the *DMM-only* groups at all time points, but growth was inhibited with 1.0N-loading at the +2-week and +6-week time points in nearly all animals (Fig. 4.3C,D). In addition, osteophyte maturity at +6-weeks was lower in the *DMM+1.0N* group compared to the *DMM-only* group.

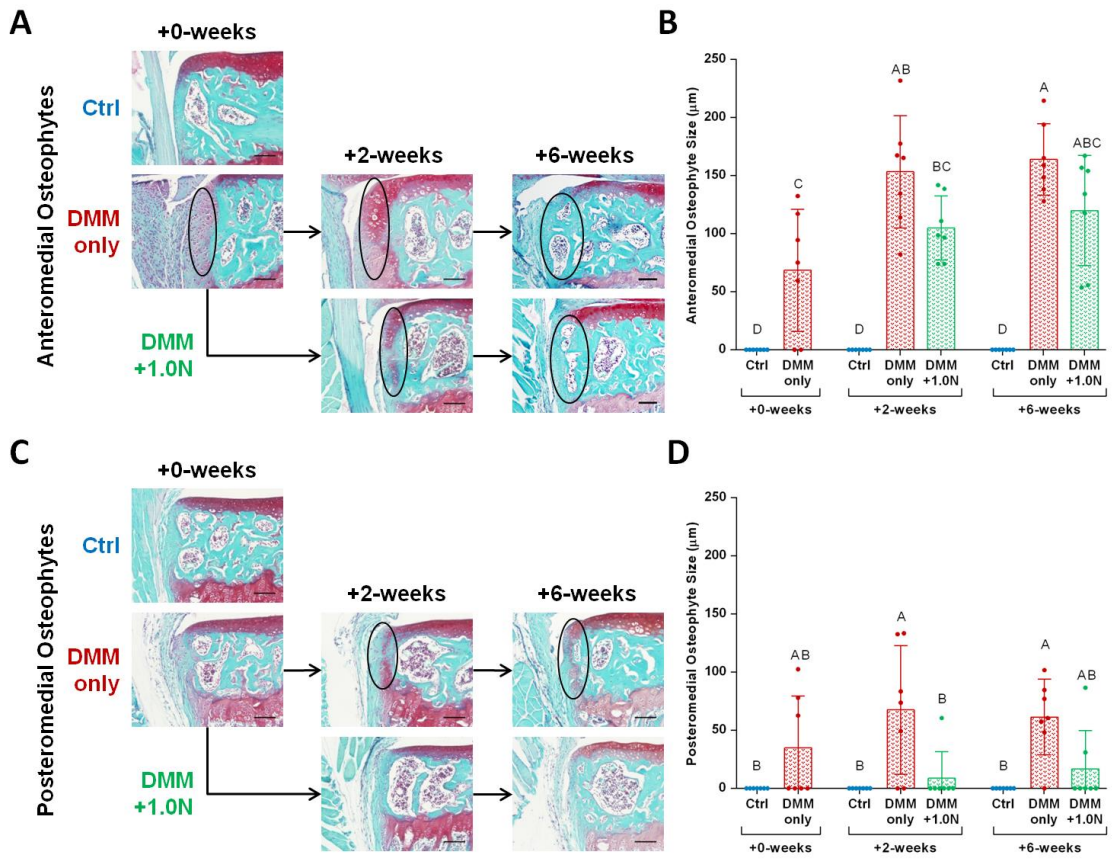

Figure 4.3. Low-level cyclic compression attenuated post-traumatic osteophyte formation. (A) Representative Safranin O/Fast Green histological images indicate that DMM surgery led to osteophyte formation on the anteromedial aspect of the tibial plateau as quickly as 5 days post-surgery. (B) Anteromedial osteophyte size increased in the *DMM-only* groups after 2 and 6 weeks but was not different between the *DMM+1.0N* groups and +0-week *DMM-only* group (C) Low-level cyclic compression completely suppressed posteromedial osteophyte formation in nearly all animals. (D) Posteromedial osteophyte size in the *DMM+1.0N* group was lower compared to *DMM-only* groups. Scale bars = 100 μm. Groups with the same letters over the bars are not significantly different; groups with different letters indicate that the means are significantly different by post-hoc comparisons.

4.3.3 Loading attenuated DMM-induced subchondral bone sclerosis but not cancellous bone loss

Cyclic compression at all load levels attenuated subchondral bone sclerosis after DMM surgery (Fig. 4.4). At +6-weeks, DMM led to a significant increase in tissue mineral density (TMD) in the medial subchondral bone plate compared to control limbs in the *DMM-only* group (Fig. 4.4A). DMM surgery followed by 1.0N-, 2.0N-, or 4.5N-

loading, however, did not result in increased TMD in DMM-treated limbs compared to control limbs. Subchondral bone plate thickness was greater in the *DMM-only* group than the *DMM+4.5N* group (Fig. 4.4B).

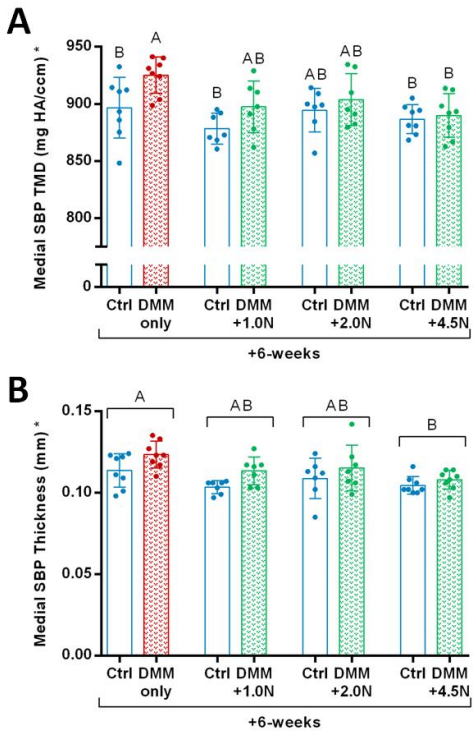

Figure 4.4. Low-level cyclic compression attenuated post-traumatic subchondral bone sclerosis. (A) At the +6-week time point, subchondral bone plate TMD increased in the medial tibial plateau in *DMM-only* limbs compared to contralateral control limbs. TMD was not different between control and treated limbs in the 1.0N-, 2.0N-, or 4.5N-loaded groups. (B) Mice in the *DMM-only* group had thicker medial subchondral cortical bone compared to mice in the moderate load group (*DMM+4.5N*). Groups with the same letters over the bars or pooled bars are not significantly different; groups with different letters indicate that the means are significantly different by post-hoc comparisons. Asterisk on y-axis title indicates significance by post-hoc comparisons for control vs. DMM-treated limbs.

At +6-weeks, cancellous bone volume fraction (BV/TV) in the epiphysis decreased in DMM-treated limbs compared to control limbs in all groups, regardless of whether the limbs underwent loading (Fig. 4.S-7A). The decreased BV/TV was due to increased trabecular separation (Tb.Sp) following DMM (Fig. 4.S-7B). Trabecular

thickness (Tb.Th) was not different between any of the groups (Fig. 4.S-7C). The *DMM-only* group had higher TMD compared to the three loaded groups (Fig. 4.S-7D).

Similarly, bone loss occurred in the metaphysis at +6-weeks after DMM surgery, regardless of whether the limbs underwent loading (Fig. 4.S-8A). Tb.Sp was greater in all DMM-treated limbs compared to control limbs (Fig. 4.S-8B). DMM surgery did not induce any changes in metaphyseal Tb.Th (Fig. 4.S-8C). Lastly, TMD was lower in all DMM-treated limbs compared to control limbs, regardless of whether the limbs underwent loading (Fig. 4.S-8D).

4.3.4 Low-level loading had subtle beneficial effects on chondrocyte loss and apoptosis

Chondrocyte numbers decreased following DMM surgery, indicated by a loss of DAPI+ signal (Fig. 4.5A,B). At +0-weeks, cellularity was not different between *DMM-only* and control limbs. At +2-weeks, small localized areas of the cartilage had decreased cellularity in the *DMM-only* and *DMM+1.0N* groups. At +6-weeks, the *DMM-only* group had the least number of remaining cells with large portions of the tibial plateau lacking cellularity. DAPI+ stained cells in the +6-week *DMM-only* group were significantly lower compared to the +0-week *DMM-only* group. DAPI+ stained cells in the +6-week *DMM+1.0N* group were not significantly different from the +0-week *DMM-only* group but were lower than the +0-week controls.

Subtle differences in chondrocyte apoptosis were evident between groups (Fig. 4.5A,C). Minimal apoptosis occurred in the +0-week *DMM-only* group. TUNEL+ staining increased slightly at +2-weeks in the *DMM-only* group but was not significantly different from +0-week levels. At +6-weeks, the *DMM-only* group had higher levels of

apoptosis compared to the +0-week control group, whereas the *DMM+1.0N* group was not different from the +0-week control group. However, apoptosis levels at +6-weeks were not significantly different between the *DMM-only* and *DMM+1.0N* groups.

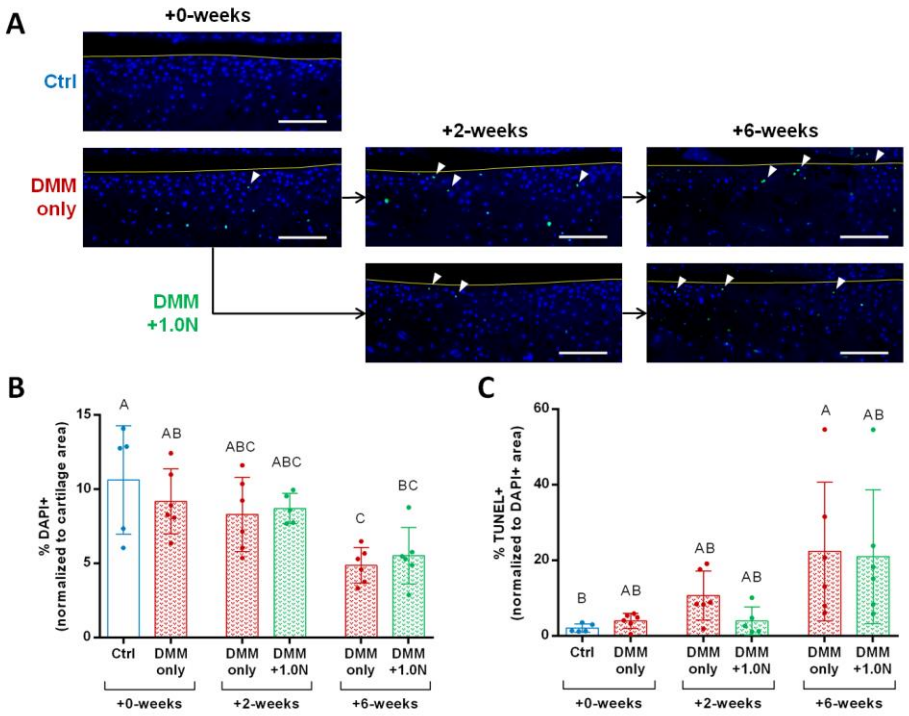

Figure 4.5. Low-level cyclic compression had subtle beneficial effects on cellularity and apoptosis**.** (A) Representative DAPI (blue) overlaid with TUNEL (green) images show chondrocyte loss and apoptosis with DMM surgery, with the greatest degree of cell loss in the +6-week *DMM-only* group. (B) Cellularity decreased in the +6-week *DMM-only* group compared to the +0-week *DMM-only* group, whereas cellularity in the +6-week *DMM+1.0N* group was not different from the +0-week *DMM-only* group. However, cell loss was not different between the and *DMM-only* and *DMM+1.0N* groups at the +2-week and +6-week time points. (C) Chondrocyte apoptosis increased with DMM surgery. Only the +6-week *DMM-only* group was different from the +0-week control group. Scale bars = 100 μm. Arrow heads indicate apoptosis. Yellow curves indicate tibial cartilage surface. Groups with the same letters over the bars are not significantly different; groups with different letters indicate that the means are significantly different by post-hoc comparisons.

4.3.5 Low-level loading had subtle beneficial effects on cleaved aggrecan levels

Cleaved aggrecan levels in the *DMM-only* and *DMM+1.0N* were not significantly different from control limbs (Fig. 4.6). However, *DMM-only* limbs had a

mean increase of 116% in cleaved aggrecan levels compared to control limbs, whereas *DMM+1.0N* limbs had an increase of 53% compared to control limbs. In addition, cleaved aggrecan levels decreased by 59% from +2-weeks to +6-weeks.

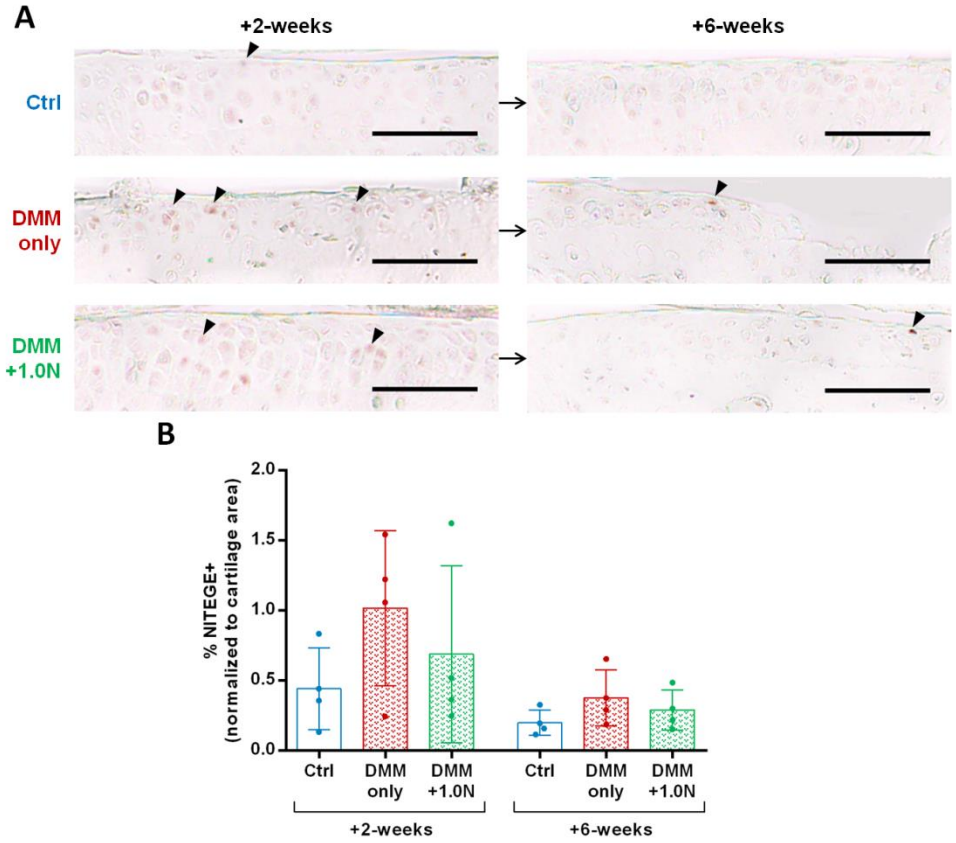

Figure 4.6. Low-level cyclic compression had subtle beneficial effects on cleaved aggrecan levels. (A) Representative IHC images show cleaved aggrecan levels in control, *DMM-only*, and *DMM+1.0N* at the +2-week and +6-week time point, with the highest levels of positive immunostaining in the *DMM-only* group. (B) Cleaved aggrecan levels were 116% higher in *DMM-only* limbs compared to control limbs, and only 53% higher in *DMM+1.0N* limbs compared to controls. However, these changes were not significant due to small sample size. Scale bars = 100 μm. Arrow heads indicate positive signal.

4.3.6 Loading had no effect on surface collagen content

Surface collagen content decreased with time in both *DMM-only* and *DMM+1.0N* groups (Fig. 4.S-9). At +6-weeks, limbs from the *DMM-only* and

DMM+1.0N groups had lower surface staining compared to the +0-week *DMM-only* group. However, picrosirius red staining between the *DMM-only* and *DMM+1.0N* groups was not different.

4.3.7 Loading had no effect on DMM-induced meniscal ossicle expansion

At +6-weeks, DMM surgery increased anteromedial meniscal ossicle volume compared to control limbs in all groups, regardless of whether the limbs underwent loading (Fig. 4.S-10A,B). Meniscus volume in DMM-treated limbs was approximately 1.5x the volume of control limbs. In addition, meniscal ossicles decreased in density after DMM surgery (Fig. 4.S-10C).

4.4 Discussion

We examined whether non-invasive axial compression at low load magnitudes could attenuate PTOA progression following DMM. We hypothesized that low-level cyclic tibial compression would slow DMM-induced OA-like changes. After 6 weeks, limbs that underwent DMM surgery without additional loading had cartilage erosion extending to the tidemark, osteophytes present on medial aspect of the tibial plateau, and sclerotic subchondral bone, consistent with previous studies [26]. In addition, *DMM-only* limbs had decreased cellularity, a trend towards increased cleaved aggrecan levels, loss of surface collagen, meniscal growth, and cancellous bone loss. Low-level cyclic compression initiated 5 days after DMM surgery attenuated many of these DMM-induced factors, including the three hallmarks of OA: cartilage erosion, osteophyte formation, and subchondral bone sclerosis. Furthermore, low-level loading had subtle

beneficial effects on cellularity, and a trend towards decreased aggrecan cleavage compared to *DMM-only* limbs. However, loading did not attenuate DMM-induced cancellous bone loss, meniscal growth, or surface collagen loss. Overall, our results support our hypothesis that low-level axial cyclic compression can slow the progression of multiple OA-like features induced by DMM.

The effect of low-level cyclic tibial compression in the knee was the opposite of tibial compression at higher load magnitudes. Previously, cyclic tibial compression focused on the induction of OA-like damage following high levels of mechanical loading [22,23]. Loading at 9.0N caused cartilage erosion, osteophyte formation, and subchondral bone changes in both 10- and 26-week-old mice. In addition, moderate loading at 4.5N caused mild cartilage surface degradation in 26-week-old mice, but minimal bone changes. Here, moderate loads did not exacerbate DMM-induced cartilage damage in 10-week-old mice, although we expected DMM-induced cartilage damage to worsen with 4.5N-loading based on previous studies using 26-week-old mice [22,24]. Both the younger mouse age and the addition of DMM may have altered the cartilage response to 4.5N-loading. In contrast to prior tibial loading studies, we applied low-level cyclic compression at 1.0N or 2.0N. The low loads attenuated many of the damaging effects of DMM surgery. Therefore, low-level (1.0N) and high-level (9.0N) loading resulted in opposite responses in terms of cartilage, osteophytes, and subchondral bone. These results demonstrate the importance of load magnitude in determining the knee joint response to tibial loading. In addition, the constant load/unload and dwell times between waveforms caused lower strain rates for lower magnitudes. Because strain rate is an important parameter in the cartilage response to

compressive forces [12], the lower strain rate during the lower-magnitude loading also may have benefited the cartilage.

The beneficial effects of cyclic axial compression were comparable to other noninvasive preclinical loading regimens. To our knowledge, the only other studies to focus directly on the beneficial effects of *in vivo* cyclic loading in isolation involved transverse loading of the knee at 1.0N for 2 weeks after surgical induction of OA in mice [33,34]. Low-level transverse knee loading attenuated post-traumatic cartilage damage and bone mineral density changes. Furthermore, transverse knee loading accelerated bone healing after a surgical wound of the tibia [35]. Therefore, low-level loading of the knee joint in both the transverse and axial directions can attenuate cartilage and bone changes after injury. However, no study involving transverse knee loading has reported effects on osteophyte formation. In addition, transverse knee loading rarely occurs during exercise, whereas axial joint loading occurs in most lower extremity exercises (i.e. walking, running, etc.). Thus, our findings support the direct beneficial effects of axial loading on articular cartilage during exercise.

Controlled, low-level loading was equally as effective, if not more effective, compared to preclinical exercise regimens used to benefit joint tissues. Activities involving mild to moderate mechanical loading of joints benefited articular cartilage in multiple preclinical studies [17,18,36,37]. Mice with lifelong access to running wheels maintained thicker cartilage compared to mice without running wheels [17]. In addition, low- (15min/day) and moderate-intensity (30min/day) treadmill exercise at 12-18m/min attenuated cartilage degeneration in rats after ACL transection or DMM surgery [18,36]. Lastly, treadmill exercise reduced pain associated with chemically-induced OA in rats

[37]. Although these preclinical exercise studies showed beneficial effects in articular cartilage, none of these studies showed protective effects at the osteophyte level. In fact, gentle treadmill walking had no effect on osteophyte formation after DMM surgery [36], whereas low-level cyclic compression significantly attenuated DMM-induced posteromedial osteophyte formation in our study. The posterior region most likely showed the most significant changes, because the contact point during tibial loading occurs in the posterior region of the tibial plateau [38]. Nonetheless, although exercise is beneficial to articular cartilage, low-level cyclic compression resulted in additional benefits in the joint, possibly due to the controlled nature of the loading protocol.

The cartilage response to mechanical loading at the cellular and protein levels depends on load-induced strain levels [39]. Low-level cyclic compression likely resulted in a beneficial response in large part due to tissue strain. Static tibial compression at 1.0N-loads resulted in cartilage strain levels of approximately 15%, estimated by linear elastic computational models [40]. During the stance phase of human gait, deformation ranged between 7 and 23% of resting cartilage thickness [41]. Hence, we achieved normal physiologic strains in murine cartilage using cyclic tibial compression. In turn, these dynamic physiologic strains may have induced anabolic, anti-catabolic, or anti-inflammatory effects [39], resulting in attenuation of PTOA. Therefore, we should have observed beneficial effects from loading at the cellular and protein levels. Based on our TUNEL data, low-level loading had subtle protective effects on cellularity and apoptosis. In addition, although significance was not observed due to small sample size, cleaved aggrecan levels increased by approximately twice as much in *DMM-only* limbs compared to *DMM+1.0N* limbs. However, the surface

collagen content was not retained with 1.0N-loading, but more intact cartilage tissue remained in the *DMM+1.0N* groups compared to the *DMM-only* groups. Therefore, the strain induced by low-level loading resulted in subtle protective effects at the cellular and protein levels that most likely contributed to the beneficial effects at the tissue level.

The translation of these findings from mice to humans is an important question. Further understanding of the mouse loading conditions is required. Although cartilage strain levels during static tibial compression have been approximated using computational models [40], stresses and strains resulting from dynamic cyclic compression should be quantified. Clinically, novel imaging modalities can determine cartilage strain after physical activities [41–43], and computational models can be used to predict load-induced cartilage stresses and strains [44,45]. Using these techniques, the load magnitude required to achieve healthy physiologic strain levels can be determined. With the appropriate load magnitudes, controlled loading regimens could improve pre- and post-operative treatment of joint injuries. For example, knee immobilization is generally required for 4 weeks following ACL reconstruction surgery [46]. Weight-bearing activity during these first 4 weeks is restricted to touch-down weight bearing [47]. Although immobilization is critical to preventing unwanted stresses on the graft during rehabilitation, low-magnitude cyclic forces that minimize stresses on the graft but produce healthy tissue strains may maintain healthy cartilage. However, the success of loading following DMM in mice may reflect the limited joint instability associated with the model [38]. Loading following ligament injuries associated with increased instability, such as ACL rupture, could lead to detrimental

effects. Thus, understanding the degree of instability associated with the injury is critical before applying compressive loading to the joint.

In conclusion, controlled low-level cyclic loading was beneficial to joint health and attenuated PTOA following DMM. Although protection was not observed in all regions of the knee joint, cartilage erosion, osteophyte formation, and subchondral bone sclerosis were attenuated. Low-level cyclic compression was equally as effective, if not more effective, in attenuating OA-like changes compared to similar non-invasive approaches. The beneficial effects were likely due to tissue strain achieved by the low load magnitudes. Future work needs to focus on determining the molecular events that result from daily beneficial loading and translating these loads to clinical use. Ultimately, rehabilitation protocols following joint injury may benefit from controlled, low-level cyclic compression to maintain healthy cartilage and attenuate the development of PTOA.

4.5 Acknowledgments

We thank Drs. Christopher Hernandez, Mary Goldring, Mathias Bostrom, Larry Bonassar, and Lisa Fortier for valuable input. We also thank Camila Carballo, Lyudamila Lukashova and the Cornell CARE staff for experimental assistance. Funding provided by NIH R21-AR064034, Robert and Helen Appel Fellowship, and the Clark and Kirby Foundations.

4.6 References

1. Lawrence RC, Felson DT, Helmick CG, Arnold LM, Choi H, Deyo RA, Gabriel S, Hirsch R, Hochberg MC, Hunder GG, Jordan JM, Katz JN, Kremers HM, Wolfe F, National Arthritis Data Workgroup. Estimates of the prevalence of arthritis and other rheumatic conditions in the United States. Part II. *Arthritis Rheum* 2008;58:26–35.
2. Turkiewicz A, Petersson IF, Björk J, Hawker G, Dahlberg LE, Lohmander LS, Englund M. Current and future impact of osteoarthritis on health care: a population-based study with projections to year 2032. *Osteoarthr Cartil* 2014;22:1826–1832.
3. Hootman JM, Helmick CG. Projections of US prevalence of arthritis and associated activity limitations. *Arthritis Rheum* 2006;54:226–9.
4. Hunter DJ, Schofield D, Callander E. The individual and socioeconomic impact of osteoarthritis. *Nat Rev Rheumatol* 2014;10:437–41.
5. Kim HA, Blanco FJ. Cell death and apoptosis in osteoarthritic cartilage. *Curr Drug Targets* 2007;8:333–45.
6. Mitchell PG, Magna HA, Reeves LM, Lopresti-Morrow LL, Yocum SA, Rosner PJ, Geoghegan KF, Hambor JE. Cloning, expression, and type II collagenolytic activity of matrix metalloproteinase-13 from human osteoarthritic cartilage. *J Clin Invest* 1996;97:761–768.
7. Nagase H, Kashiwagi M. Aggrecanases and cartilage matrix degradation. *Arthritis Res Ther* 2003;5:94–103.
8. Brown TD, Johnston RC, Saltzman CL, Marsh JL, Buckwalter JA. Posttraumatic osteoarthritis: a first estimate of incidence, prevalence, and burden of disease. *J Orthop Trauma* 2006;20:739–44.
9. Driban JB, Eaton CB, Lo GH, Ward RJ, Lu B, McAlindon TE. Association of knee injuries with accelerated knee osteoarthritis progression: data from the Osteoarthritis Initiative. *Arthritis Care Res (Hoboken)* 2014;66:1673–9.
10. Punzi L, Galozzi P, Luisetto R, Favero M, Ramonda R, Oliviero F, Scanu A. Post-traumatic arthritis: overview on pathogenic mechanisms and role of inflammation. *RMD open* 2016;2:e000279.
11. Felson DT. Risk Factors for Osteoarthritis. *Clin Orthop Relat Res* 2004;427:S16–S21.
12. Kurz B, Jin M, Patwari P, Cheng DM, Lark MW, Grodzinsky AJ. Biosynthetic response and mechanical properties of articular cartilage after injurious compression. *J Orthop Res* 2001;19:1140–1146.
13. Stolberg-Stolberg JA, Furman BD, William Garrigues N, Lee J, Pisetsky DS, Stearns NA, DeFrate LE, Guilak F, Olson SA. Effects of cartilage impact with and without fracture on chondrocyte viability and the release of inflammatory markers. *J Orthop Res* 2013;31:1283–1292.
14. Christiansen B a., Anderson MJ, Lee C a., Williams JC, Yik JHN, Haudenschild DR. Musculoskeletal changes following non-invasive knee injury using a novel mouse model of post-traumatic osteoarthritis. *Osteoarthr Cartil* 2012;20:773–782.
15. Uthman OA, Windt DA van der, Jordan JL, Dziedzic KS, Healey EL, Peat GM, Foster NE. Exercise for lower limb osteoarthritis: systematic review incorporating trial sequential analysis and network meta-analysis. *BMJ* 2013;347:f5555.
16. Sah RL-Y, Kim Y-J, Doong J-YH, Grodzinsky AJ, Plass AHK, Sandy JD.

Biosynthetic response of cartilage explants to dynamic compression. *J Orthop Res* 1989;7:619–636.
17. Hubbard-Turner T, Guderian S, Turner MJ. Lifelong physical activity and knee osteoarthritis development in mice. *Int J Rheum Dis* 2015;18:33–39.
18. Galois L, Etienne S, Grossin L, Watrin-Pinzano A, Cournil-Henrionnet C, Loeuille D, Netter P, Mainard D, Gillet P. Dose-response relationship for exercise on severity of experimental osteoarthritis in rats: a pilot study. *Osteoarthritis Cartilage* 2004;12:779–86.
19. Freeman PM, Natarajan RN, Kimura JH, Andriacchi TP. Chondrocyte cells respond mechanically to compressive loads. *J Orthop Res* 1994;12:311–320.
20. Beckwée D, Vaes P, Cnudde M, Swinnen E, Bautmans I. Osteoarthritis of the knee: why does exercise work? A qualitative study of the literature. *Ageing Res Rev* 2013;12:226–36.
21. Boveris A, Navarro A. Systemic and mitochondrial adaptive responses to moderate exercise in rodents. *Free Radic Biol Med* 2008;44:224–229.
22. Ko FC, Dragomir C, Plumb DA, Goldring SR, Wright TM, Goldring MB, Meulen MCH van der. In Vivo Cyclic Compression Causes Cartilage Degeneration and Subchondral Bone Changes in Mouse Tibiae. *Arthritis Rheum* 2013;65:1569–1578.
23. Poulet B, Hamilton RW, Shefelbine S, Pitsillides A a. Characterizing a novel and adjustable noninvasive murine joint loading model. *Arthritis Rheum* 2011;63:137–147.
24. Holyoak DT, Otero M, Armar NS, Ziemian SN, Otto A, Cullinane D, Wright TM, Goldring SR, Goldring MB, Meulen MCH van der. Collagen XI mutation lowers susceptibility to load-induced cartilage damage in mice. *J Orthop Res* 2017;36:711–720.
25. Adebayo OO, Ko FC, Wan PT, Goldring SR, Goldring MB, Wright TM, Meulen MCH van der. Role of subchondral bone properties and changes in development of load-induced osteoarthritis in mice. *Osteoarthr Cartil* 2017;25:2108–2118.
26. Glasson SS, Blanchet TJ, Morris E a. The surgical destabilization of the medial meniscus (DMM) model of osteoarthritis in the 129/SvEv mouse. *Osteoarthr Cartil* 2007;15:1061–1069.
27. Glasson SS, Chambers MG, Berg WB Van Den, Little CB. The OARSI histopathology initiative - recommendations for histological assessments of osteoarthritis in the mouse. *Osteoarthritis Cartilage* 2010;18 Suppl 3:S17-23.
28. Little CB, Barai A, Burkhardt D, Smith SM, Fosang AJ, Werb Z, Shah M, Thompson EW. Matrix metalloproteinase 13-deficient mice are resistant to osteoarthritic cartilage erosion but not chondrocyte hypertrophy or osteophyte development. *Arthritis Rheum* 2009;60:3723–33.
29. Girish V, Vijayalakshmi A. Affordable image analysis using NIH Image/ImageJ. *Indian J Cancer* 41:47.
30. Varghese F, Bukhari AB, Malhotra R, De A. IHC Profiler: an open source plugin for the quantitative evaluation and automated scoring of immunohistochemistry images of human tissue samples. *PLoS One* 2014;9:e96801.
31. Stock M, Menges S, Eitzinger N, Geßlein M, Botschner R, Wormser L, Distler A, Schlötzer-Schrehardt U, Dietel K, Distler J, Beyer C, Gelse K, Engelke K, Koenders MI, Berg W van den, Mark K von der, Schett G. A Dual Role of Upper Zone of Growth

Plate and Cartilage Matrix-Associated Protein in Human and Mouse Osteoarthritic Cartilage: Inhibition of Aggrecanases and Promotion of Bone Turnover. *Arthritis Rheumatol* 2017;69:1233–1245.
32. Donato S, Pacilè S, Colombo F, Garrovo C, Monego SD, Macor P, Tromba G, Biffi S. Meniscal ossicles as micro-CT imaging biomarker in a rodent model of antigen-induced arthritis: A synchrotron-based x-ray pilot study. *Sci Rep* 2017;7:1–7.
33. Hamamura K, Zhang P, Zhao L, Shim JW, Chen A, Dodge TR, Wan Q, Shih H, Na S, Lin C-C, Sun H Bin, Yokota H. Knee loading reduces MMP13 activity in the mouse cartilage. *BMC Musculoskelet Disord* 2013;14:312.
34. Li X, Yang J, Liu D, Li J, Niu K, Feng S, Yokota H, Zhang P. Knee loading inhibits osteoclast lineage in a mouse model of osteoarthritis. *Sci Rep* 2016;6:24668.
35. Zhang P, Sun Q, Turner CH, Yokota H. Knee loading accelerates bone healing in mice. *J Bone Miner Res* 2007;22:1979–87.
36. Iijima H, Aoyama T, Ito A, Yamaguchi S, Nagai M, Tajino J, Zhang X, Kuroki H. Effects of short-term gentle treadmill walking on subchondral bone in a rat model of instability-induced osteoarthritis. *Osteoarthr Cartil* 2015;23:1563–74.
37. Allen J, Imbert I, Havelin J, Henderson T, Stevenson G, Liaw L, King T. Effects of Treadmill Exercise on Advanced Osteoarthritis Pain in Rats. *Arthritis Rheumatol* 2017;69:1407–1417.
38. Adebayo OO, Ko FC, Goldring SR, Goldring MB, Wright TM, Meulen MCH van der. Kinematics of meniscal- and ACL-transected mouse knees during controlled tibial compressive loading captured using roentgen stereophotogrammetry. *J Orthop Res* 2017;35:353–360.
39. Sanchez-Adams J, Leddy HA, McNulty AL, O'Conor CJ, Guilak F. The mechanobiology of articular cartilage: bearing the burden of osteoarthritis. *Curr Rheumatol Rep* 2014;16:451.
40. Adebayo OO, Goldring MB, Goldring SR, Wright TM, Meulen MCH Van Der. Computational Models for the Analysis of Load-Induced Osteoarthritis. *Unpubl Manuscr*.
41. Lad NK, Liu B, Ganapathy PK, Utturkar GM, Sutter EG, Moorman CT, Garrett WE, Spritzer CE, DeFrate LE. Effect of normal gait on in vivo tibiofemoral cartilage strains. *J Biomech* 2016;49:2870–2876.
42. Cher WL, Utturkar GM, Spritzer CE, Nunley JA, DeFrate LE, Collins AT. An analysis of changes in in vivo cartilage thickness of the healthy ankle following dynamic activity. *J Biomech* 2016;49:3026–3030.
43. Halonen KS, Mononen ME, Jurvelin JS, Töyräs J, Salo J, Korhonen RK. Deformation of articular cartilage during static loading of a knee joint – Experimental and finite element analysis. *J Biomech* 2014;47:2467–2474.
44. Besier TF, Pal S, Draper CE, Fredericson M, Gold GE, Delp SL, Beaupre GS. The Role of Cartilage Stress in Patellofemoral Pain. *Med Sci Sport Exerc* 2015;47:2416–2422.
45. Klets O, Mononen ME, Tanska P, Nieminen MT, Korhonen RK, Saarakkala S. Comparison of different material models of articular cartilage in 3D computational modeling of the knee: Data from the Osteoarthritis Initiative (OAI). *J Biomech* 2016;49:3891–3900.

46. Smith MA, Smith WT, Kosko P. Anterior cruciate ligament tears: reconstruction and rehabilitation. *Orthop Nurs* 2014;33:14–24.
47. Andrews J, Harrelson G, Wilk K. *Physical rehabilitation of the injured athlete*. 3rd ed. Pennsylvania, PA: Saunders; 2004.

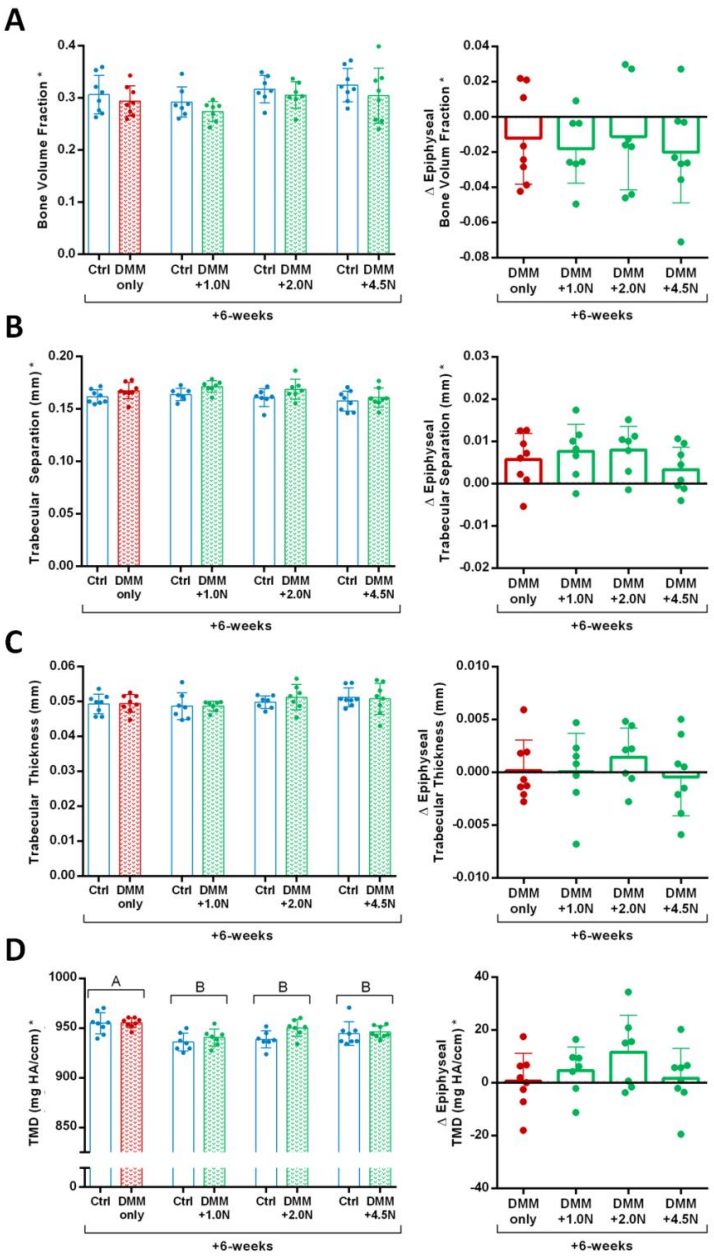

Figure 4.S-7. Low-level loading had no effect on epiphyseal cancellous bone mass. (A) At +6-weeks, DMM-treated limbs had significantly lower cancellous bone volume fraction in the epiphysis compared to control limbs, regardless of whether the limbs underwent loading. (B) Cancellous bone loss was primarily due to greater trabecular separation in the epiphysis. (C) Trabecular thickness was not affected by DMM or loading. (D) The *DMM-only* group had higher TMD in the epiphysis compared to the three loaded groups. Graphs on the left show raw data for each limb; graphs on the right show deltas between control and DMM-treated limbs. Groups with the same letters over the bars or pooled bars are not significantly different; groups with different letters indicate that the means are significantly different by post-hoc comparisons. Asterisk on y-axis title indicates significance by post-hoc comparisons for control vs. DMM-treated limbs.

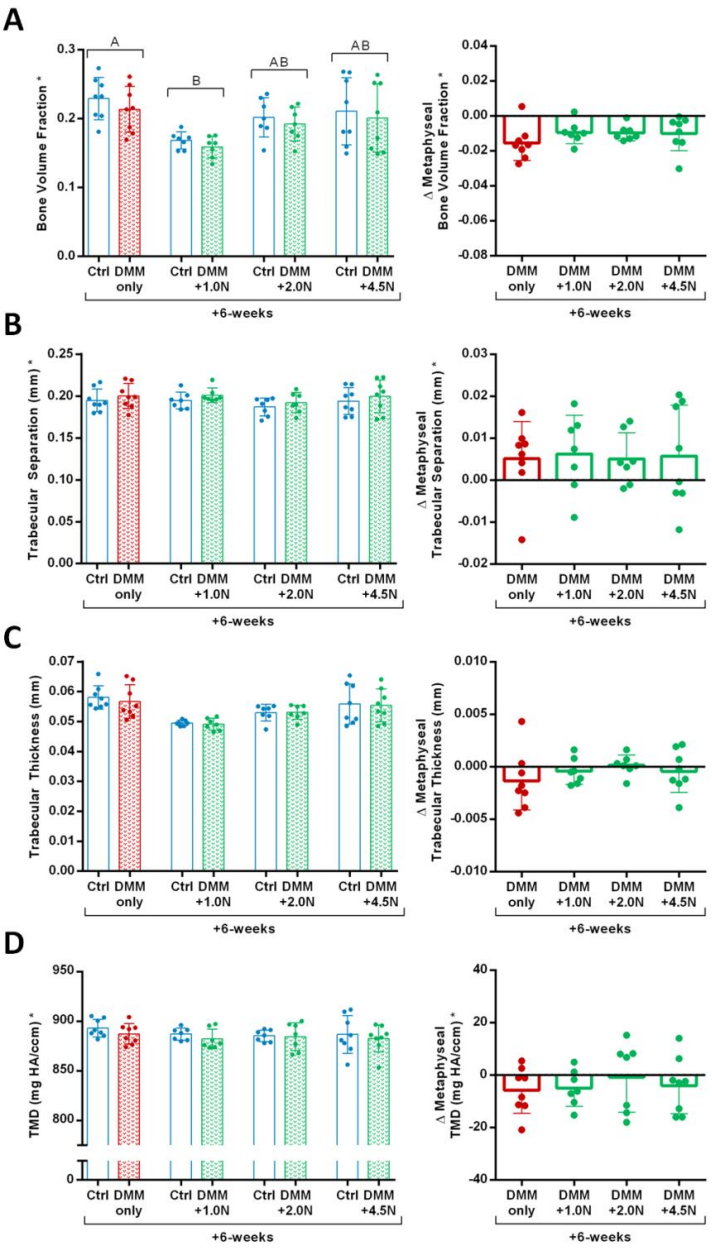

Figure 4.S-8. Low-level loading had no effect on metaphyseal cancellous bone mass. (A) At +6-weeks, DMM-treated limbs had significantly lower cancellous bone volume fraction in the metaphysis compared to control limbs, regardless of whether the limbs underwent loading. (B) Cancellous bone loss was primarily due to greater trabecular separation in the metaphysis. (C) Trabecular thickness was not affected by DMM or loading. (D) DMM-treated limbs had significantly lower TMD in the metaphysis compared to control limbs, regardless of whether the limbs underwent loading. Graphs on the left show raw data for each limb; graphs on the right show deltas between control and DMM-treated limbs. Groups with the same letters over the bars or pooled bars are not significantly different; groups with different letters indicate that the means are significantly different by post-hoc comparisons. Asterisk on y-axis title indicates significance by post-hoc comparisons for control vs. DMM-treated limbs.

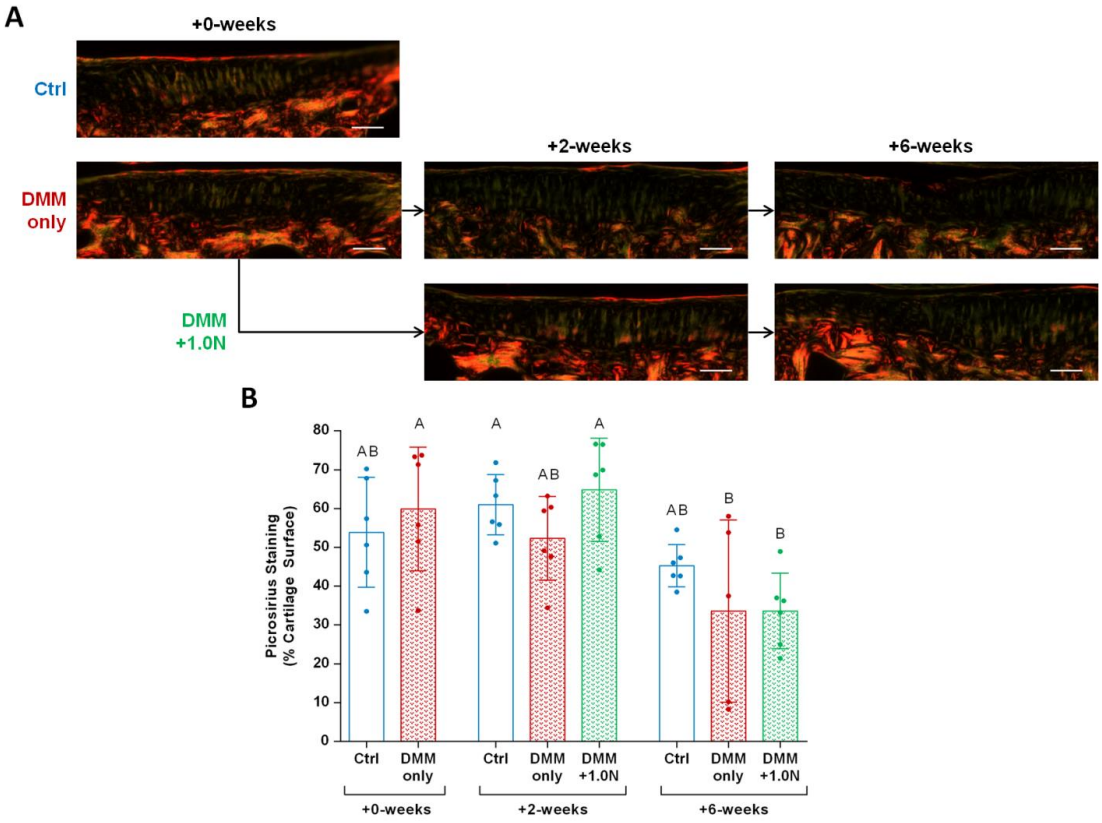

Figure 4.S-9. DMM surgery led to reduced surface collagen content. (A) Representative picrosirius red images show surface collagen content, indicated by the red staining at the cartilage surface. (B) Picrosirius red staining at the cartilage surface decreased after 6 weeks in both the *DMM-only* and *DMM+1.0N* groups compared to the +0-week *DMM-only* group. Scale bars = 100 μm.

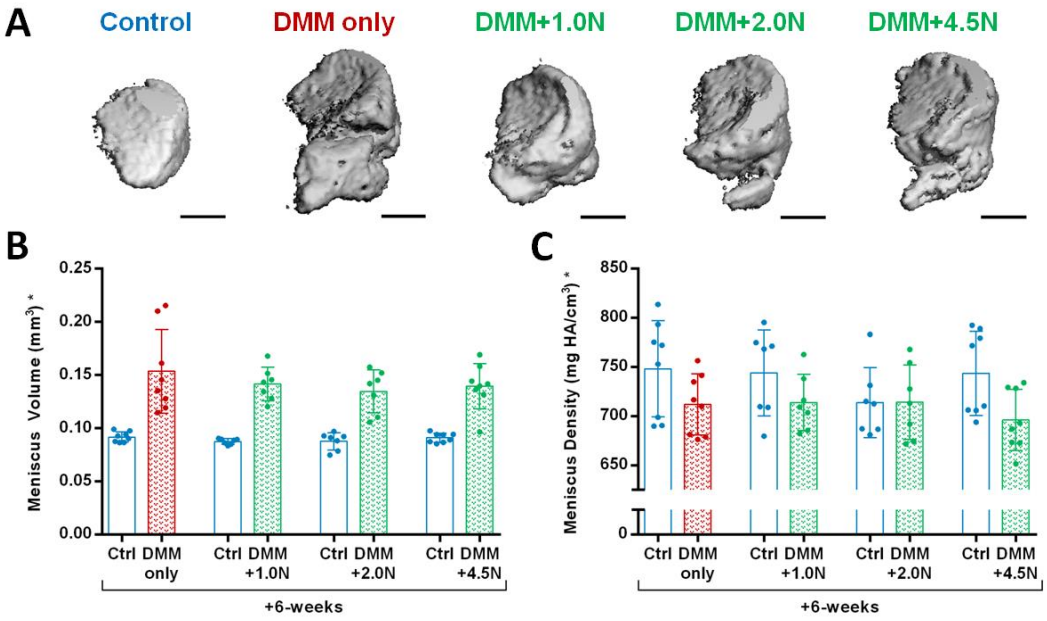

Figure 4.S-10. DMM surgery led to increased anteromedial meniscal ossicle volume. (A) Representative microCT 3-D reconstructions show significant changes between control and DMM-treated meniscal ossicle sizes for all groups. (B) Menisci in DMM-treated limbs were approximately 1.5 times larger than in control limbs, regardless of whether the limbs underwent loading. (C) Meniscal ossicle density decreased after DMM surgery in all groups. Scale bars = 250 μm. Asterisk on y-axis title indicates significance by post-hoc comparisons for control vs. DMM-treated limbs.

CHAPTER 5: CONCLUSIONS AND DISCUSSION

5.1 Summary

This thesis focused on three key aspects of osteoarthritis: pathology, treatment, and prevention. These OA questions were addressed by three aims: 1) determine the effects of altered cartilage matrix properties on the severity of load-induced OA, 2) design and test the efficacy of a hydrogel-based intra-articular on-demand drug delivery system, and 3) determine whether low-level cyclic tibial compression can attenuate surgically-induced OA. Together, these three aims advanced our knowledge and understanding of load-induced OA and created a path for promising OA therapeutic strategies. This final chapter will summarize the findings from each research project, discuss key strengths and limitations of the studies, and conclude with future directions.

5.1.1 Aim 1: Load-induced osteoarthritis in mice with altered cartilage tissue

Our first aim was to investigate the influence of genetically abnormal cartilage matrix properties on load-induced OA onset and progression. Mechanical loading and abnormal tissue properties resulting from genetics are two prevalent risk factors for OA [1,2]. Understanding interactions between risk factors is critical to predict, prevent, and treat OA. We used the *cho/+* mouse that has abnormal collagen fibrils and reduced tensile properties in its cartilage due to a point mutation in the *Coll11a1* gene [3,4]. We first characterized the musculoskeletal phenotype. 6-month-old *cho/+* mice had OA-like proteoglycan loss and increased MMP-13 levels in their cartilage, as expected from previous studies [3]. However, the mutant mice also had thicker cartilage and thinner, less dense subchondral bone compared to wildtype (WT) littermates.

Contrary to our hypothesis, *cho/+* mice developed less severe load-induced cartilage damage after cyclic tibial compression at high load magnitudes. The combination of two characteristics of the *cho/+* mouse could explain this finding. First, when mice with different genetic backgrounds were compared, mice with thicker cartilage developed less-severe load-induced cartilage damage, because thicker cartilage resulted in decreased contact pressures [5]. Second, high bone mass has been linked to increased OA risk clinically [6,7]. *Cho/+* mice had both thicker cartilage and thinner, less dense cortical bone compared to WT littermates, which may explain the development of less severe load-induced OA. Overall, this study showed that the collagen XI mutation in *cho/+* mice did not exacerbate load-induced OA progression, suggesting that loading and the altered cartilage tissue properties induced by the genetic abnormality in collagen may be independent risk factors for OA.

5.1.2 Aim 2: Hydrogels for on-demand drug delivery

Our second aim was to characterize and test the therapeutic efficacy of an injectable hydrogel-based intra-articular drug delivery system. Intra-articular injection is a common treatment to alleviate pain associated with severe OA of the knee prior to surgical intervention. Although these injections can be effective long-term for a subset of patients, the efficacy in most individuals is generally inconsistent due to the lack of drug retention time in the joint space [8,9]. Thus, we sought to improve retention time using a hydrogel-based drug delivery system. The hydrogel backbone featured maleimide-functionalized polyethylene glycol (PEG-MAL) and collagenase-specific crosslinkers to induce on-demand therapeutic release under OA conditions [10].

We first determined the effects of cyclic compression on hydrogel mechanical properties and measured therapeutic release with collagenase exposure. After subjecting our hydrogels to 10,000 cycles of dynamic cyclic compression up to 80% strain, the mechanical properties were not different from non-loaded gels. In response to daily collagenase exposure, particle release occurred in hydrogels fabricated with collagenase-specific crosslinkers. Our *in vitro* results suggest that these PEG-MAL hydrogels can withstand routine forces in the knee joint that occur during physical activity and can release drugs on-demand in response to OA-associated inflammation/degradation.

We also tested the therapeutic efficacy of our hydrogel system in combination with a common corticosteroid, dexamethasone (DEX). Our *in vivo* results indicated that DEX, either in bolus form or encapsulated in nanoparticles, did not attenuate load-induced OA pathological changes. However, hydrogel injections with or without DEX attenuated load-induced cartilage degradation and osteophyte formation. Therefore, the lubricating effects of the hydrogel were beneficial to joint health. Overall, our combined *in vitro* and *in vivo* results suggest that this hydrogel system is a promising therapeutic strategy to treat OA.

5.1.3 Aim 3: Low-level loading to attenuate osteoarthritis in vivo

Our third aim was to attenuate OA progression using low-level cyclic compression. Exercise is recommended to alleviate pain associated with mild to moderate OA. Effects of exercise include weight loss and muscle strengthening surrounding the joint [11,12]. Together, these effects reduce loading experienced by

weight-bearing joints. However, exercise has an additional beneficial effect that is commonly overlooked. Mild to moderate exercise induced low-level loads in the joint that directly benefited cartilage health by stimulating chondrocytes to upregulate cartilage matrix synthesis and decrease proinflammatory pathways [13]. The specific characteristics of these beneficial loads, however, are not well understood. Preclinical models to isolate the effects of beneficial loading associated with exercise do not exist. Therefore, we investigated the effects of low-level loading using cyclic tibial compression.

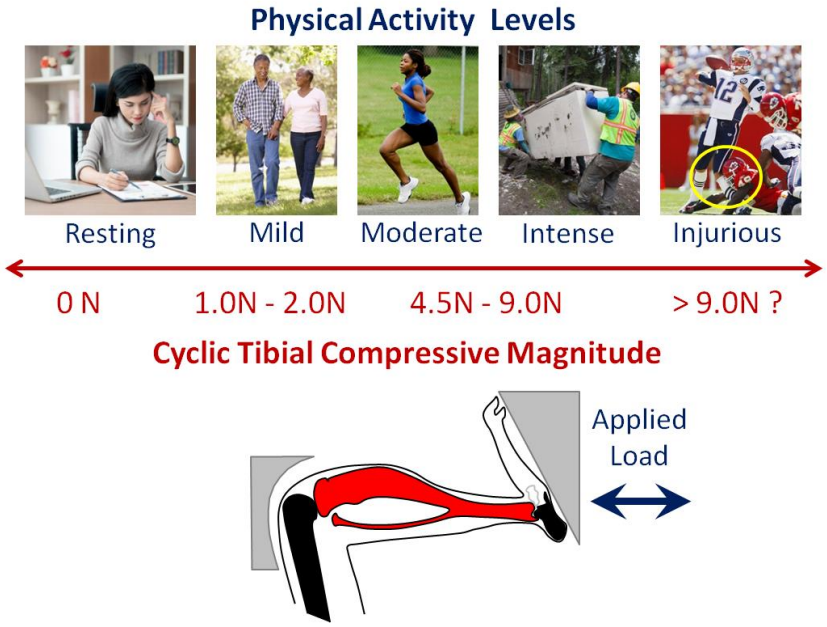

Figure 5.1. Improved understanding of relationship between cyclic tibial compression and physiological activities. To date, cyclic tibial compression was not used to investigate low load magnitudes that mimic mild exercise in humans and result in beneficial cartilage responses. We determined that cyclic compression at 1.0N or 2.0N resulted in cartilage protection after injury.

Low-level cyclic compression slowed the progression of surgically-induced OA. Specifically, cyclic loading at 1.0N and 2.0N attenuated cartilage degradation, osteophyte formation, and subchondral bone changes associated with DMM-induced

OA. These results indicate that controlled loading at the correct magnitude can be beneficial to joint health (Fig. 5.1). We can now directly compare the specific tissue-level and molecular responses of beneficial versus detrimental mechanical loading *in vivo*. Overall, this study showed that low-level mechanical loading can be used as a rehabilitative approach after joint injury.

5.1.4 Discussion

Although this thesis consisted of three distinct projects, tissue strain in the cartilage matrix was a key factor in each aim. The degree of cartilage deformation during mechanical loading plays a major role in determining a beneficial versus detrimental response [13]. Physiologic dynamic activities lead to cartilage tissue strains of 15-35% and result in matrix synthesis and reduction of inflammation. However, hyperphysiologic or injurious activities produce cartilage strains greater than 50% and cause matrix catabolism, increased activity of proinflammatory pathways, and chondrocyte apoptosis [13]. Therefore, we believe that the relationship between load magnitude, tissue strain, and cartilage response contributed to the results throughout this thesis.

Based on our findings from Aim 1 and previous studies [14–17], tibial loading at high load magnitudes (9.0N) results in OA-like joint pathology, including cartilage damage, osteophyte formation, and subchondral bone changes. These tissue-level changes suggest that cartilage strains reach hyperphysiologic levels during cyclic compression at high load magnitudes. Although further work is necessary to understand the exact degree of cartilage deformation at these high load levels, we can speculate that

tissue strains had an influence in the responses to high-level cyclic compression in Aims 1 and 2.

In Aim 1, *cho/+* mice developed less severe load-induced cartilage damage compared to their WT littermates, despite abnormal cartilage matrix properties in *cho/+* mice. We believe that cartilage thickness and its influence on tissue strain may have been a key factor in these results. Thicker cartilage resulted in increased contact area and lower contact pressure in finite element models of similar tibial loading models [5]. In our study, cartilage was 10% thicker in *cho/+* mice compared to WT littermates. Taken together, the thicker cartilage in *cho/+* mice may have resulted in increased contact area in the cartilage. The increased contact area led to decreased pressure and tissue strain. To this end, the area of cartilage contact, the thickness of the tissue, and the tissue properties contribute to tissue strains in response to high-level tibial compression.

In Aim 2, intra-articular injection of hydrogels attenuated cartilage damage and osteophyte formation after a single bout of high-level loading. Although the exact reasons behind this result are not clear, the hydrogel clearly had a beneficial effect on joint health. Again, we can speculate that the hydrogel influenced cartilage tissue strain. Like Aim 1, the hydrogel in the joint space may have led to increased contact area between the cartilage surfaces during cage activities post-loading. In addition, the hydrogel may have effectively "thickened" the joint space after injection. The increased contact area and thickened joint space would have resulted in more highly distributed loads, leading to decreased tissue strain.

In Aim 3, low-level cyclic compression induced a beneficial response in the knee joint. These results suggest that we achieved healthy physiologic levels of strain in the cartilage during cyclic compression. Based on tissue-level results, low-level loading decreased DMM-induced matrix catabolism. Furthermore, low-level loading had a subtle beneficial effect on chondrocyte apoptosis. Finite element models from our lab estimated that tibial loading at 1.0N produced approximately 15% cartilage strain [18]. These combined experimental and computational data are consistent with previous literature that indicates cartilage strains of 15-35% results in healthy responses [13]. Overall, the beneficial and detrimental effects of mechanical loading in this thesis were most likely the result of modulating cartilage tissue strain.

5.2 Strengths

The research described in this thesis contributed significantly to the understanding of OA pathology, treatment, and prevention. A key theme throughout the thesis was addressing the questions with an integrative approach. We combined biomedical engineering, mechanical engineering, biomaterials, biology, and physiology to solve key problems associated with OA. In Aim 1 (Chapter 2), we combined genetically-induced abnormal material properties with an altered mechanical environment to study the interaction of risk factors in OA onset and progression. In Aim 2 (Chapter 3), we used biomaterials characterization techniques, i*n vitro* and *in vivo* dynamic cyclic compression, and collagenase-driven degradation inspired by disease pathology to develop a novel approach for IA drug delivery. In Aim 3 (Chapter 4), we used surgical techniques to induce OA and novel loading regimens to successfully slow

down post-traumatic OA. Overall, the interdisciplinary nature and integrative approaches of this work are major strengths.

Another consistent strength of this thesis was the focus on load-induced OA using *in vivo* cyclic tibial compression. Prior studies showed that repetitive loading [14,19] or a single bout of loading [15] both induce OA-like pathology in mice. Based on these findings, we used repetitive and single bouts of load in this thesis to study disease progression and test novel treatments. This model of OA offers several advantages over traditional OA models. Cyclic tibial compression at high load levels offers a noninvasive, nontraumatic approach to induce OA [20]. This allows researchers to investigate the direct relationship between controlled mechanical loading and cartilage damage [21]. Furthermore, the OA model closely mimics the well-known clinical "wear and tear" form of OA.

The use of cyclic tibial compression allowed a spectrum of load-induced responses to be studied. In addition to the damaging effects of high loads, we explored the positive effects of loading. Aim 3 (Chapter 4) is the first use of *in vivo* cyclic tibial compression to benefit cartilage health. To date, most experiments investigating the beneficial effects of loading either have been *in vitro* [22–24] or examined exercise, such as treadmill running or mouse running wheels [25,26]. *In vitro* experiments using cartilage explants and chondrocyte culture cannot recapitulate the response of the multiple tissues that comprise the joint. Furthermore, exercise induces systemic effects, including muscle gain and weight loss. Isolating the independent contribution of low to moderate loading is difficult with studies involving exercise. In this thesis, we demonstrated that controlled low-level loads applied by *in vivo* cyclic tibial compression

attenuated OA-like changes after an injury. The translation of this loading regimen to the human level could result in improvements in physical therapy techniques after traumatic joint injury, or maintenance of cartilage health throughout a lifetime.

5.3 Limitations

This thesis combined *in vitro* and *in vivo* techniques to analyze specific aspects of OA. The entirety of the *in vivo* work was performed using preclinical murine models of OA. Although the mouse is an extremely common *in vivo* model to study human diseases, distinct differences between mouse and human knee joint morphology must be considered. First, mouse cartilage is thinner than human cartilage. Therefore, the distinct zones in human cartilage (i.e. superficial, middle, and deep) are not as distinguishable in mouse cartilage. In humans, each of these zones plays a distinct role in responding to specific types of loads [27]. Thus, the mechanics of the overall cartilage structure in the mouse may be different from humans. Second, the chondrocyte density is approximately 24-times higher in mice compared to humans [28]. The increased number of chondrocytes makes mouse cartilage more responsive to changes in environment, contributing to the rapid development of OA in mice. Finally, animal size and body weight differ between mice and humans. Because humans are more than three orders of magnitude heavier than mice, determining the appropriate mechanical properties of a drug delivery system, such as the hydrogel system described in Aim 2, is difficult in a mouse model of OA.

Although these limitations of the mouse are important to consider, mouse cartilage also shares several key characteristics with human tissue. Specifically, the

composition of the cartilage matrix, including the collagen II fibrils and proteoglycans, is similar between the two species. Furthermore, OA disease pathology is similar between mice and humans, and a tremendous amount of OA knowledge has come from mouse studies [29]. Therefore, despite the limitations, the mouse is an excellent preclinical model to study OA.

OA is a complex disease with many etiologies. For example, the disease can be divided into six different phenotypes: aging-, cartilage-, subchondral bone-, traumatic injury-, inflammation-, and metabolic-driven OA [30]. Recapitulating the full range of these phenotypes in a single research project is nearly impossible, but understanding which phenotypes are relevant to a specific research question is important to consider. Although the load-induced OA model in Aims 1 and 2 does not fit into a single phenotype based on Mobasheri et al.'s definitions [30], the model has attributes of the aging phenotype and demonstrates both cartilage- and subchondral bone-driven changes. The DMM model in Aim 3 is an example of the traumatic injury-driven phenotype. Thus, although we were not able to investigate all OA etiologies in this thesis, we are aware of what these mouse models represent in a clinical scenario.

5.4 Future Work

This work examined two novel treatments for OA. The first was a hydrogel-based on-demand delivery system for sustained intra-articular drug retention. The second involved the application of low-level loading to attenuate cartilage degradation after a traumatic injury. Both projects demonstrated promising results, but further research is necessary to understand their potential impact in treating OA in the clinic.

Specifically, we need to determine whether *in vivo* drug retention time of our PEG-MAL hydrogels is improved compared to bolus drug injections under both healthy and OA conditions. In addition, we need to continue preclinical testing of the low-level loading approach to understand the underlying mechanism and develop potential clinical applications of the loading regimen.

5.4.1 Determining intra-articular drug retention time with in vivo imaging

Improving the clinical outcome of intra-articular injection requires increasing intra-articular retention time of drugs. To further characterize our hydrogel-based drug delivery system, a future goal is to quantify drug retention with the hydrogel compared to a bolus drug alone. To accomplish this goal, we have been working with a fluorescent *in vivo* imaging system (IVIS). With the system, we are able to visualize fluorescently labeled markers inside a knee joint [31]. To date, we have focused on quantifying fluorescent signal intensity in the knee joints of mice. However, due to the small size of the intra-articular joint space in mice, we are only able to inject 2 μL of drug or hydrogel into the knee. No matter the intensity of the fluorescent label used, a 2-μl volume is extremely difficult to visualize with IVIS. Therefore, I propose that future work needs to be shifted to a larger animal model to quantify drug retention with the hydrogel system. Larger animal models allow higher volumes to be injected and have shown success in tracking intra-articular drug retention previously [32].

The proposed project would involve injecting five different preparations into the knee joints of rats. Previous studies involving intra-articular injections in rat knee joints have used up to 100 μL [33]. The proposed study would be designed similarly to the *in*

vivo study in Chapter 3 with slight modifications. The injection groups would be 1) hydrogel + drug-loaded nanoparticles, 2) hydrogel + drug, 3) drug-loaded nanoparticles, 4) drug, and 5) saline. The drug would be labeled with a fluorescent dye, such as DyLight 650 (ThermoFisher). The fluorescent intensity in the knee joint would be visualized and quantified with daily IVIS images. We would expect that the drug-loaded nanoparticles inside the hydrogel would lead to the longest drug retention, and the bolus drug would leave the joint rapidly. This proposed experiment is critical in determining whether the hydrogel system extends the retention time of drugs inside the joint space.

Upon completion of the drug retention studies, further work needs to focus on the translation of this therapeutic approach to animal models that more closely mimic the human joint environment. The hydrogel system showed promise in attenuating load-induced OA pathology in mice. To move the hydrogel system closer to clinical use, similar studies with other therapeutics should be performed in the rat/rabbit, and ultimately the pig because of its similarities to humans [34]. If the PEG-MAL hydrogel system attenuates OA more effectively compared to bolus drug in these larger animal models, the hydrogel system can be moved to clinical trials.

5.4.2 Translating beneficial loads to clinical scenarios

In Aim 3, low-level cyclic tibial compression attenuated OA progression. Future preclinical studies need to focus on further developing the approach for clinical scenarios. One example is combining the loading approach with immobilization after a joint injury and determining cartilage health long-term after injury. Current clinical protocols immobilize the joint after surgical repair. Confined mouse cages restrict

movement and have decreased OA severity in mice after joint injury [35]. We believe that controlled loading combined with immobilization of the affected joint may aid in long-term protection of cartilage. A proposed experiment would be similar to the project described in Aim 3. The major modification would be the addition of hindlimb unloading after DMM [36], rather than normal cage activity. Three groups would be compared: 1) DMM + loading, 2) DMM + hindlimb suspension, and 3) DMM + loading + hindlimb suspension. Comparing the severity of DMM-induced cartilage damage would determine whether controlled loading adds to the beneficial effects of immobilization after an injury.

In addition to preclinical studies, a future direction is translation of controlled, low-level axial loading from mice to humans. The strain levels in the cartilage resulting from 1.0N tibial compression are approximately equal to ~15% [18]. Because cartilage tissue strain is generally translatable across species [34], future work needs to determine load magnitudes that result in ~15% strain in human cartilage. New technologies, such as magnetic resonance imaging and biplanar fluoroscopy, will allow us to determine loads that result in beneficial cartilage strains [37]. Then, fixtures capable of applying controlled, cyclic compression at these load magnitudes to human tibiae need to be designed. These loading fixtures would contribute to physical therapy post-injury or rehabilitation centers for the elderly population to maintain cartilage health. Ultimately, the approach has potential to help both younger individuals fully recover from injury and older individuals who are unable to actively move their joints.

5.5 Conclusion

In this thesis, we not only learned about OA progression, but we also showed promising results for novel treatment options and preventive measures. Overall, the findings from this research will hopefully play a role in treating clinical OA in the future. To conclude, I want to end with a quote from my three-minute thesis title that we should continue telling ourselves to overcome this painful disease: “OA, no way!”

5.6 References

1. Felson DT. Risk Factors for Osteoarthritis. *Clin Orthop Relat Res* 2004;427:S16–S21.
2. Felson DT, Zhang Y. An update on the epidemiology of knee and hip osteoarthritis with a view to prevention. *Arthritis Rheum* 1998;41:1343–1355.
3. Xu L, Flahiff CM, Waldman B a., Wu D, Olsen BR, Setton L a., Li Y. Osteoarthritis-like changes and decreased mechanical function of articular cartilage in the joints of mice with the chondrodysplasia gene (cho). *Arthritis Rheum* 2003;48:2509–2518.
4. Lam NP, Li Y, Waldman AB, Brussiau J, Lee PL, Olsen BR, Xu L. Age-dependent increase of discoidin domain receptor 2 and matrix metalloproteinase 13 expression in temporomandibular joint cartilage of type IX and type XI collagen-deficient mice. *Arch Oral Biol* 2007;52:579–584.
5. Poulet B, Westerhof T a T, Hamilton RW, Shefelbine SJ, Pitsillides a. a. Spontaneous osteoarthritis in Str/ort mice is unlikely due to greater vulnerability to mechanical trauma. *Osteoarthr Cartil* 2013;21:756–763.
6. Hardcastle SA, Dieppe P, Gregson CL, Arden NK, Spector TD, Hart DJ, Edwards MH, Dennison EM, Cooper C, Sayers A, Williams M, Davey Smith G, Tobias JH. Individuals with high bone mass have an increased prevalence of radiographic knee osteoarthritis. *Bone* 2015;71:171–179.
7. Hardcastle SA, Dieppe P, Gregson CL, Hunter D, Thomas GER, Arden NK, Spector TD, Hart DJ, Laugharne MJ, Clague GA, Edwards MH, Dennison EM, Cooper C, Williams M, Davey Smith G, Tobias JH. Prevalence of radiographic hip osteoarthritis is increased in high bone mass. *Osteoarthr Cartil* 2014;22:1120–1128.
8. Kruse DW. Intraarticular cortisone injection for osteoarthritis of the hip. Is it effective? Is it safe? *Curr Rev Musculoskelet Med* 2008;1:227–33.
9. Arrich J, Piribauer F, Mad P, Schmid D, Klaushofer K, Müllner M. Intra-articular hyaluronic acid for the treatment of osteoarthritis of the knee: systematic review and meta-analysis. *CMAJ* 2005;172:1039–43.
10. Patel RG, Purwada A, Cerchietti L, Inghirami G, Melnick A, Gaharwar AK, Singh A. Microscale Bioadhesive Hydrogel Arrays for Cell Engineering Applications. *Cell Mol Bioeng* 2014;7:394–408.
11. Felson DT. Weight Loss Reduces the Risk for Symptomatic Knee Osteoarthritis in Women. *Ann Intern Med* 1992;116:535.
12. Uthman OA, Windt DA van der, Jordan JL, Dziedzic KS, Healey EL, Peat GM, Foster NE. Exercise for lower limb osteoarthritis: systematic review incorporating trial sequential analysis and network meta-analysis. *BMJ* 2013;347:f5555.
13. Sanchez-Adams J, Leddy HA, McNulty AL, O'Conor CJ, Guilak F. The mechanobiology of articular cartilage: bearing the burden of osteoarthritis. *Curr Rheumatol Rep* 2014;16:451.
14. Ko FC, Dragomir C, Plumb DA, Goldring SR, Wright TM, Goldring MB, Meulen MCH van der. In Vivo Cyclic Compression Causes Cartilage Degeneration and Subchondral Bone Changes in Mouse Tibiae. *Arthritis Rheum* 2013;65:1569–1578.
15. Ko FC, Dragomir CL, Plumb DA, Hsia AW, Adebayo OO, Goldring SR, Wright TM, Goldring MB, Meulen MCH van der. Progressive cell-mediated changes in

articular cartilage and bone in mice are initiated by a single session of controlled cyclic compressive loading. *J Orthop Res* 2016.
16. Adebayo OO, Ko FC, Wan PT, Goldring SR, Goldring MB, Wright TM, Meulen MCH van der. Role of subchondral bone properties and changes in development of load-induced osteoarthritis in mice. *Osteoarthr Cartil* 2017;25:2108–2118.
17. Holyoak DT, Otero M, Armar NS, Ziemian SN, Otto A, Cullinane D, Wright TM, Goldring SR, Goldring MB, Meulen MCH van der. Collagen XI mutation lowers susceptibility to load-induced cartilage damage in mice. *J Orthop Res* 2017;36:711–720.
18. Adebayo OO, Goldring MB, Goldring SR, Wright TM, Meulen MCH Van Der. Computational Models for the Analysis of Load-Induced Osteoarthritis. *Unpubl Manuscr*.
19. Poulet B, Hamilton RW, Shefelbine S, Pitsillides A a. Characterizing a novel and adjustable noninvasive murine joint loading model. *Arthritis Rheum* 2011;63:137–147.
20. Adebayo OO, Holyoak DT, Meulen MCH Van der. Mechanobiological mechanisms of load-induced osteoarthritis. *Submitt Mechanomedicine* 2018.
21. Adebayo OO, Ko FC, Goldring SR, Goldring MB, Wright TM, Meulen MCH van der. Kinematics of meniscal- and ACL-transected mouse knees during controlled tibial compressive loading captured using roentgen stereophotogrammetry. *J Orthop Res* 2017;35:353–360.
22. Sah RL-Y, Kim Y-J, Doong J-YH, Grodzinsky AJ, Plass AHK, Sandy JD. Biosynthetic response of cartilage explants to dynamic compression. *J Orthop Res* 1989;7:619–636.
23. Kurz B, Jin M, Patwari P, Cheng DM, Lark MW, Grodzinsky AJ. Biosynthetic response and mechanical properties of articular cartilage after injurious compression. *J Orthop Res* 2001;19:1140–1146.
24. Freeman PM, Natarajan RN, Kimura JH, Andriacchi TP. Chondrocyte cells respond mechanically to compressive loads. *J Orthop Res* 1994;12:311–320.
25. Galois L, Etienne S, Grossin L, Watrin-Pinzano A, Cournil-Henrionnet C, Loeuille D, Netter P, Mainard D, Gillet P. Dose-response relationship for exercise on severity of experimental osteoarthritis in rats: a pilot study. *Osteoarthritis Cartilage* 2004;12:779–86.
26. Hubbard-Turner T, Guderian S, Turner MJ. Lifelong physical activity and knee osteoarthritis development in mice. *Int J Rheum Dis* 2015;18:33–39.
27. Raizman I, Croos JNA De, St-Pierre J-P, Pilliar RM, Kandel RA. Articular cartilage subpopulations respond differently to cyclic compression in vitro. *Tissue Eng Part A* 2009;15:3789–98.
28. Stockwell RA. The interrelationship of cell density and cartilage thickness in mammalian articular cartilage. *J Anat* 1971;109:411–21.
29. Christiansen BA, Guilak F, Lockwood KA, Olson SA, Pitsillides AA, Sandell LJ, Silva MJ, Meulen MCH van der, Haudenschild DR. Non-invasive mouse models of post-traumatic osteoarthritis. *Osteoarthr Cartil* 2015;23:1627–1638.
30. Mobasheri A, Rayman MP, Gualillo O, Sellam J, Kraan P van der, Fearon U. The role of metabolism in the pathogenesis of osteoarthritis. *Nat Rev Rheumatol* 2017.
31. Cho H, Pinkhassik E, David V, Stuart JM, Hasty KA. Detection of early cartilage

damage using targeted nanosomes in a post-traumatic osteoarthritis mouse model. *Nanomedicine Nanotechnology, Biol Med* 2015;11:939–946.
32. Singh A, Agarwal R, Diaz-Ruiz CA, Willett NJ, Wang P, Lee LA, Wang Q, Guldberg RE, García AJ. Nanoengineered particles for enhanced intra-articular retention and delivery of proteins. *Adv Healthc Mater* 2014;3:1562–7, 1525.
33. Riggin CN, Tucker JJ, Soslowsky LJ, Kuntz AF. Intra-articular tibiofemoral injection of a nonsteroidal anti-inflammatory drug has no detrimental effects on joint mechanics in a rat model. *J Orthop Res* 2014;32:1512–1519.
34. Ronken S, Arnold MP, Ardura García H, Jeger A, Daniels AU, Wirz D. A comparison of healthy human and swine articular cartilage dynamic indentation mechanics. *Biomech Model Mechanobiol* 2012;11:631–639.
35. Kim BJ, Kim D-W, Kim SH, Cho JH, Lee HJ, Park DY, Park SR, Choi BH, Min B-H. Establishment of a reliable and reproducible murine osteoarthritis model. *Osteoarthr Cartil* 2013;21:2013–2020.
36. Morey-Holton ER, Globus RK. Hindlimb unloading rodent model: technical aspects. *J Appl Physiol* 2002;92:1367–77.
37. Lad NK, Liu B, Ganapathy PK, Utturkar GM, Sutter EG, Moorman CT, Garrett WE, Spritzer CE, DeFrate LE. Effect of normal gait on in vivo tibiofemoral cartilage strains. *J Biomech* 2016;49:2870–2876.

APPENDIX A: CHAPTER 2 DATA

Histological (OARSI) Score (Scorer #1): OARSI scoring of articular cartilage damage measured by Safranin O/Fast Green stain for wildtype (WT) and *cho*/+ (HET) mice. Each column corresponds to a slide separated at a 90 μm interval, with start and end slides indicated. Average (Avg) and maximum (Max) scores reported for articular cartilage in the medial (M) and lateral (L) tibial plateaus.

ID	Genotype	Duration	Magnitude	Limb	Plateau	Start	End	1	2	3	4	5	6	7	8	9	10	11	12	13	14	Avg	Max
5546	WT	1 week	4.5N	control	M	2	11	0.5	0	0	0	0	0	0	0	0	0.5					0.10	0.5
					L	3	10	1	0.5	0	0	0.5	0	0	0.5							0.31	1
				loaded	M	1	11	1	1	0	1	0.5	0.5	0.5	0	0.5	0.5	0.5				0.55	1
					L	1	11	1	1	2	1	0.5	1	0.5	0.5	0.5	0.5	0.5				0.82	2
5547	WT	1 week	4.5N	control	M	7	15	0	0.5	0	0	0	0	0	0	0.5						0.11	0.5
					L	4	11	0.5	0	0.5	1	1	0.5	0.5	0							0.50	1
				loaded	M	2	12	0.5	0.5	0.5	0	0	0.5	1	0.5	0.5	0.5	0.5				0.45	1
					L	2	10	3	0.5	0.5	1	1	0.5	1	0.5	0.5	0.5					0.90	3
5556	WT	1 week	4.5N	control	M	2	12	0.5	0.5	0.5	0	0	1	0.5	0	0	0.5	1				0.41	1
					L	1	10	0.5	0.5	1	0	0.5	1	0.5	0.5	0.5	0.5					0.55	1
				loaded	M	2	12	0.5	0.5	0	0	0	0.5	0.5	0	0.5	0	0.5				0.27	0.5
					L	3	13	1	2	2	2	2	1	1	0.5	0.5	0.5	0.5				1.18	2
5567	WT	1 week	4.5N	control	M	3	13	0.5	0	0	0	0	0	0	0.5	0	0	0				0.09	0.5
					L	3	13	0.5	0.5	0.5	0.5	0.5	0.5	1	0.5	0	0.5	0.5				0.50	1
				loaded	M	2	11	1	0.5	0	0	0.5	0.5	1	2	0.5	0.5					0.65	2
					L	2	11	2	1	1	0.5	2	2	2	0.5	0.5	0.5					1.20	2
5554	WT	1 week	4.5N	control	M	2	12	0	0	0	0	0	0	1	1	1	0	0.5				0.32	1
					L	1	9	1	0.5	0.5	1	0	0.5	1	0.5	0.5						0.61	1
				loaded	M	1	12	0.5	0.5	0	0	0.5	0.5	0.5	2	0.5	0.5	0.5	0.5			0.54	2
					L	2	12	0.5	1	2	1	2	1	0	1	0.5	0.5					0.95	2
5557	WT	1 week	4.5N	control	M	2	11	0	0.5	0	0	0	0.5	0	0	0	0					0.10	0.5
					L	6	16	1	0.5	0	0.5	0.5	0	0.5	0	0	0.5	0.5				0.36	1
				loaded	M	1	5	0.5	0.5	0.5	0.5	0.5	0.5	0.5								0.50	0.5
					L	3	11	0.5	1	1	1	2	0	1	0.5	0.5	0.5					0.80	2
5545	HET	1 week	4.5N	control	M	3	12	0	0	0	0	0	0	0	0	0	0.5					0.05	0.5
					L	2	10	0.5	0.5	0	0.5	0	0	0	0.5	0.5						0.28	0.5
				loaded	M	6	15	2	0.5	0.5	0	0	1	0.5	0.5	0.5	0.5					0.60	2
					L	4	12	2	0.5	1	0.5	0.5	1	1	0.5	1	0.5					0.85	2
5561	HET	1 week	4.5N	control	M	4	11	0	0	0	0	0	0	0	0.5							0.06	0.5
					L	3	11	1	0	1	1	0	1	0.5	0	0.5						0.56	1
				loaded	M	8	14	0.5	0.5	0	0.5	0.5	0.5	0.5	0.5							0.44	0.5
					L	5	11	1	1	1	2	1	2	0.5								1.21	2
5559	HET	1 week	4.5N	control	M	4	12	0.5	0.5	0.5	0.5	0.5	0	0.5	0	0.5						0.39	0.5
					L	2	8	0.5	0.5	0.5	0.5	0.5	1	0								0.50	1

				loaded	M	5	12	0.5	0	0.5	0.5	0.5	1	0.5	0.5	0.5						0.50	1
					L	3	9	2	0.5	0.5	0.5	0.5	0.5	0.5	0.5	0.5						0.67	2
5558	HET	1 week	4.5N	control	M	2	10	0.5	0.5	0	0	0	0	0	0	0.5						0.17	0.5
					L	5	11	0.5	0.5	0	0	0	0.5	0	0	0						0.17	0.5
				loaded	M	10	15	0.5	0.5	0	0	0.5	1									0.42	1
					L	4	8	1	2	0.5	0.5	2	0.5									1.08	2
5562	HET	1 week	4.5N	control	M	10	16	0.5	0.5	0	0.5	0	0	0								0.21	0.5
					L	3	8	0	0.5	0.5	0.5	0	0.5									0.33	0.5
				loaded	M	7	15	0.5	1	0	0.5	0	0.5	1	2	0.5						0.67	2
					L	3	9	1	2	2	2	1	1	0	0.5	0.5						1.11	2
5565	HET	1 week	4.5N	control	M	7	13	0	0.5	0	0.5	0	0	0.5								0.21	0.5
					L	4	9	0	0	0	0	0	0									0.00	0
				loaded	M	1	11	0	0.5	1	0	0.5	0.5	0.5	0	0.5	0.5	0	0.5	0.5		0.38	1
					L	2	13	0.5	0	0.5	0.5	0.5	0.5	0.5	0.5	0.5	0.5	0.5	0.5			0.46	0.5
5539	WT	2 week	4.5N	control	M	9	15	0	0	0	0	0	0.5	0								0.07	0.5
					L	5	12	0	0	2	0.5	0.5	0.5	0	0							0.44	2
				loaded	M	6	14	0.5	0.5	0	0.5	1	2	0.5	0	0.5						0.61	2
					L	4	10	2	1	0.5	0.5	1	1	1	0.5							0.94	2
5537	WT	2 week	4.5N	control	M	4	13	0	0	0	0	0	0	1	0	0	0					0.10	1
					L	2	11	0	1	1	0	1	1	2	0.5	0	0.5					0.70	2
				loaded	M	1	12	1	0.5	0.5	0.5	0.5	0.5	0.5	1	1	0.5	0.5	0.5			0.63	1
					L	3	13	0.5	0.5	1	2	1	1	2	2	1	0.5	0.5				1.09	2
5538	WT	2 week	4.5N	control	M	11	15	0	0	1	1	0.5										0.50	1
					L	2	7	1	0	0	1	1	0									0.50	1
				loaded	M	1	9	2	1	0	0.5	2	1	0.5	0	0.5	0.5					0.80	2
					L	4	12	2	2	2	2	2	2	1	2	0.5	0.5					1.60	2
5541	WT	2 week	4.5N	control	M	6	14	0	0	0	0.5	1	1	0	0	0						0.28	1
					L	2	9	1	1	1	0.5	2	2	0	0.5							1.00	2
				loaded	M	1	11	0.5	0.5	0	1	1	1	0.5	0	0.5	0.5	0.5				0.55	1
					L	3	12	2	2	2	1	1	1	2	1	2	0.5	0.5	0.5			1.29	2
5518	WT	2 week	4.5N	control	M	3	16	0.5	0	0	0	0	0	0	0	0	0	0	0	0	0.5	0.07	0.5
					L	3	14	1	0.5	0.5	0.5	0.5	0	0.5	0.5	0	0	0	0			0.33	1
				loaded	M	6	15	0.5	0.5	0	0	0	0.5	0.5	0	0.5	0.5	0.5				0.32	0.5
					L	3	10	2	0	0.5	0.5	1	0	1	0.5	0.5	0.5					0.65	2
5522	WT	2 week	4.5N	control	M	4	14	0	0	0	0	0	0	0	0	0	0	0.5				0.05	0.5
					L	2	10	0	1	0.5	0.5	0.5	1	0.5	0	0.5						0.50	1
				loaded	M	3	14	0.5	0.5	0.5	0	0	1	0.5	0.5	0.5	0	0.5	0.5			0.42	1
					L	1	7	2	1	0.5	0.5	2	2									1.33	2
5472	HET	2 week	4.5N	control	M	2	10	0	0	0	0	0	0	0	0	0.5						0.06	0.5
					L	1	8	1	0.5	0.5	0	0.5	2	0	0							0.56	2

				loaded	M	1	7	0.5	0.5	0.5	0.5	0.5	0.5	0.5	0.5	0.5	0.5					0.50	0.5
					L	5	12	1	1	1	0.5	2	2	0.5	0.5	0.5	0.5					0.95	2
5474	HET	2 week	4.5N	control	M	1	6	0	0	0	0.5	0.5	0.5									0.25	0.5
					L	9	14	1	1	0	0.5	2	1									0.92	2
				loaded	M	1	11	0.5	0.5	1	0	0.5	0.5	0.5	0	0.5	0.5	0.5				0.45	1
					L	2	10	0.5	2	2	2	0.5	2	2	2	0.5	0.5					1.40	2
5475	HET	2 week	4.5N	control	M	2	12	0.5	0	0	0	0	0	0	0	0	0	0.5				0.09	0.5
					L	2	9	1	0.5	0	0	0.5	2	2	0							0.75	2
				loaded	M	8	14	1	0.5	0.5	0.5	0.5	0.5	0.5	0.5	0.5						0.56	1
					L	2	7	0.5	1	1	2	2	2	0.5								1.29	2
5490	HET	2 week	4.5N	control	M	8	15	0	0	0	0	1	0.5	0.5	0.5							0.31	1
					L	1	5	0	0	0.5	0.5	1										0.40	1
				loaded	M	3	12	0.5	1	0.5	2	1	0.5	0.5	0.5	0.5	0.5					0.75	2
					L	1	6	0.5	2	2	0.5	0.5	0.5	0.5								0.93	2
5491	HET	2 week	4.5N	control	M	1	9	0	0	0	0	0.5	0	0	0	0.5						0.11	0.5
					L	2	10	0	0	0	1	0.5	0	1	0.5	0						0.33	1
				loaded	M	2	8	0.5	0	0.5	0.5	0.5	1	0.5	0.5	0.5						0.50	1
					L	7	13	0.5	0.5	0.5	2	2	2	2	2	0.5	0.5					1.25	2
5493	HET	2 week	4.5N	control	M	11	15	0	0	0	1	0										0.20	1
					L	2	5	0	0	1	1											0.50	1
				loaded	M	3	7	0.5	0.5	0.5	0.5	1	1	0.5	5							1.19	5
					L	11	16	2	0.5	2	0	1	2									1.25	2
5535	WT	6 week	4.5N	control	M	11	17	0	0	0	1	0.5	0	0.5								0.29	1
					L	4	11	0	2	1	1	1	2	2	1							1.25	2
				loaded	M	8	14	1	0.5	1	1	1	2	0.5								1.00	2
					L	15	18	2	0.5	1	0.5											1.00	2
5524	WT	6 week	4.5N	control	M	4	12	0	0	0	0	0	0	0	0	0.5						0.06	0.5
					L	5	13	0	1	0.5	0.5	1	0.5	0.5	0	0.5						0.50	1
				loaded	M	14	19	0.5	0.5	0	0	2	2	0.5								0.79	2
					L	10	16	2	2	1	1	2	1	2	2							1.63	2
5529	WT	6 week	4.5N	control	M	4	12	0	0	0	0	0	0	0.5	0	0						0.06	0.5
					L	9	14	0.5	0.5	0.5	0.5	0.5	0									0.42	0.5
				loaded	M	14	20	0.5	2	0.5												1.00	2
					L	16	20	2	0.5	1	0.5											1.00	2
5532	WT	6 week	4.5N	control	M	10	18	0	0	0	0	0	0	0.5	0	0.5						0.11	0.5
					L	12	18	0.5	0.5	0.5	0	0.5	0	1								0.43	1
				loaded	M	6	13	0	1	0	1	0.5	0	0	0.5	0.5	0.5					0.40	1
					L	6	14	2	2	2	1	0.5	1	2	2	0.5						1.44	2
5534	WT	6 week	4.5N	control	M	4	16	0	0	0	0	0	0	0	1	0	0	0	0	0		0.08	1
					L	4	16	0	0	0	1	1	1	1	1	1	0.5	0.5	0	0.5		0.58	1

				loaded	M	1	9	0	0.5	1	1	0	2	1	0.5	0.5	0.5	0.5				0.68	2
					L	5	14	4	0	0	1	0	0.5	1	2	0.5	0.5					0.95	4
5528	WT	6 week	4.5N	control	M	3	14	0.5	0.5	0	0	0	0	0	1	0.5	0	0	0			0.21	1
					L	7	16	2	1	1	0	0	0	0.5	0	0	0.5					0.50	2
				loaded	M	14	20	0.5	0	0.5	0	1	2	2	0.5							0.81	2
					L	8	14	2	3	2	2	1	2	2	0.5	0.5						1.67	3
5531	HET	6 week	4.5N	control	M	8	17	0	0	0	0	0	0	0	0	0	0.5					0.05	0.5
					L	8	15	0	0.5	0	0	0	0.5	1	0							0.25	1
				loaded	M	7	18	1	0.5	1	0	0.5	2	0.5	0.5	0.5	0.5	0.5	0.5			0.67	2
					L	8	15	3	1	1	2	2	0.5	0.5	0.5	0.5	0	0.5				1.05	3
5526	HET	6 week	4.5N	control	M	3	12	0.5	0.5	0.5	0.5	0.5	1	0	0	0	0					0.35	1
					L	5	13	2	2	0.5	0.5	0.5	1	0.5	1	0						0.89	2
				loaded	M	7	16	0.5	1	0	0	0.5	0.5	0.5	2	0.5	0.5	0.5				0.59	2
					L	5	13	4	2	0.5	1	1	2	2	1	0.5	0.5					1.45	4
5527	HET	6 week	4.5N	control	M	2	10	0.5	0	0.5	0.5	1	0.5	0	0.5	0.5						0.44	1
					L	3	11	0.5	1	1	0.5	0.5	1	0.5	0	0.5						0.61	1
				loaded	M	9	18	0.5	0.5	0.5	0.5	0.5	2	1	0.5	0.5	0.5	0.5	0.5			0.67	2
					L	8	15	3	2	2	1	0.5	1	0.5	1	0.5	0.5					1.20	3
5536	HET	6 week	4.5N	control	M	7	16	0.5	0.5	0.5	0.5	0	0	0	0	0	0					0.20	0.5
					L	4	14	0.5	0	1	0	0.5	0	1	0	1	0	0.5				0.41	1
				loaded	M	5	12	2	1	0.5	1	2	2	0	1	1	0.5					1.10	2
					L	5	12	4	1	2	2	0	2	0.5	2	0.5						1.56	4
5544	HET	6 week	4.5N	control	M	8	17	0.5	1	0.5	0	0	0	0	0	0	0					0.20	1
					L	8	17	0.5	0.5	1	0.5	0.5	1	1	1	0	0.5					0.65	1
				loaded	M	5	15	0.5	0.5	0	0	0	0.5	0.5	0.5	0.5	0.5	0.5				0.36	0.5
					L	4	13	2	1	1	1	1	2	1	2	2	0.5	0.5				1.27	2
5560	HET	6 week	4.5N	control	M	8	17	0.5	0.5	0.5	0	0	0	0.5	0	0	0.5					0.25	0.5
					L	6	14	0	0	0	0	0	0.5	1	0	0						0.17	1
				loaded	M	3	11	0.5	0.5	0.5	0	0.5	1	0.5	0.5	0.5	0.5					0.50	1
					L	8	13	2	2	0.5	0	0.5	0.5									0.92	2
5578	WT	1 week	9.0N	control	M	4	13	0	0.5	0	0	0	0	1	0	0	0					0.15	1
					L	4	11	2	1	0.5	0.5	1	0.5	0	0							0.69	2
				loaded	M	7	15	4	0.5	0	0.5	0	1	0.5	0.5	0.5						0.83	4
					L	12	15	3	2	1	1											1.75	3
5576	WT	1 week	9.0N	control	M	1	10	0	0	0.5	0	1	1	0	0	0	0.5					0.30	1
					L	1	10	1	1	1	1	0.5	0.5	1	1	0	0					0.70	1
				loaded	M	9	14	3	3	3	0	2	1									2.00	3
					L	8	14	3	2	1	1	0.5	1	2								1.50	3
5579	WT	1 week	9.0N	control	M	7	15	0	0	0	0	0	0.5	0	0	0.5						0.11	0.5
					L	4	12	0	0	1	1	1	1	1	0	0						0.56	1

				loaded	M	6	13	2	1	1	0	1	0	2	0.5							0.94	2
					L	3	9	2	1	2	2	2	2	0.5	0.5							1.50	2
5571	WT	1 week	9.0N	control	M	4	12	0.5	0	0	0	0	0	0	0	0.5						0.11	0.5
					L	2	9	0	1	1	0.5	0.5	1	1	0							0.63	1
				loaded	M	7	15	3	3	0.5	1	1	0.5	0.5	1	0.5						1.22	3
					L	7	15	2	1	2	2	0.5	0.5	1	2	2						1.44	2
5572	WT	1 week	9.0N	control	M	8	14	0	0	0	0	0	0	0								0.00	0
					L	8	14	0	0.5	0.5	0	0.5	1	0								0.36	1
				loaded	M	12	15	3	2	0	0											1.25	3
					L	13	15	3	1	1												1.67	3
5570	WT	1 week	9.0N	control	M	7	16	0.5	0	0	0	0	0	0	0	0	0.5					0.10	0.5
					L	4	12	0	0	1	0.5	1	0.5	0	1	0						0.44	1
				loaded	M	7	16	0.5	0	1	0	0	0	0.5	0	0	0.5					0.25	1
					L	4	12	2	3	0.5	0	1	1	0.5	1	0						1.00	3
5564	HET	1 week	9.0N	control	M	8	16	0	0	0	0	0	0	0	0	0						0.00	0
					L	5	13	0	0	0	0	0	0	0.5	0.5	0						0.11	0.5
				loaded	M	8	16	0	0	0.5	2	0.5	0.5	1	0.5	0.5	0.5					0.60	2
					L	5	13	4	0.5	0.5	0.5	1	1									1.25	4
5577	HET	1 week	9.0N	control	M	13	16	0	0	0	0											0.00	0
					L	10	15	0.5	0	1	1	1	0									0.58	1
				loaded	M	13	16	2	0.5	0	2	0										0.90	2
					L	10	15	2	4	2	1	0.5	1									1.75	4
5574	HET	1 week	9.0N	control	M	7	13	0	0	0	0	0	0	0								0.00	0
					L	4	9	1	0.5	1	2	1	0.5									1.00	2
				loaded	M	7	13	3	2	2	1	0.5	1	0								1.36	3
					L	4	9	2	2	2	2	2	1									1.83	2
5580	HET	1 week	9.0N	control	M	10	16	0	0	0	0.5	0	0.5	0								0.14	0.5
					L	6	12	0	0	1	0	1	2	0								0.57	2
				loaded	M	10	16	0	0	0	0.5	0.5	0.5	1	0							0.31	1
					L	6	12	2	1	1	1	0	0	1	2							1.00	2
5573	HET	1 week	9.0N	control	M	2	8	0	0	0	0	0	0	0.5								0.07	0.5
					L	4	10	0	1	0	0.5	1	1	0								0.50	1
				loaded	M	9	14	1	1	0.5	0.5	0.5	0.5									0.67	1
					L	4	12	2	3	2	2	1	1	2	2	2						1.89	3
5569	HET	1 week	9.0N	control	M	3	10	0.5	0	0	0	0	0	0.5	0.5							0.19	0.5
					L	2	7	0.5	0.5	0	1	2	0.5									0.75	2
				loaded	M	15	20	0.5	3	2	0	0.5	1									1.17	3
					L	11	18	1	2	0.5	1	1	2	0.5	0.5							1.06	2
5519	WT	2 week	9.0N	control	M	2	8	0	0	0	0	1	0	0.5								0.21	1
					L	3	8	0.5	0.5	0	0	0	0.5									0.25	0.5

				loaded	M	14	21	2	2	2	0	1	2	0.5	2							1.44	2
					L	14	21	2	1	0.5	0	2	0.5	0.5	0.5							0.88	2
5521	WT	2 week	9.0N	control	M	7	15	0	0	0	0	0	1	0	0	0.5						0.17	1
					L	6	13	1	1	0.5	0.5	0.5	0.5	0	0							0.50	1
				loaded	M	9	15	3	4	2	2	1	2	2								2.29	4
					L	7	15	3	3	2	2	2	1	2	2	0.5						1.94	3
5523	WT	2 week	9.0N	control	M	1	10	0.5	0	0	0	0	0.5	0	0	0	0					0.10	0.5
					L	2	13	0.5	1	1	2	0	1	1	1	0	0	0.5				0.73	2
				loaded	M	14	18	3	2	3	2	2	0.5									2.08	3
					L	5	10	0.5	1	2	2	2	1									1.42	2
5563	WT	2 week	9.0N	control	M	7	15	0.5	0.5	0	0	0	0.5	0.5	0.5	0						0.28	0.5
					L	7	15	0.5	0.5	0.5	1	0.5	0.5	0.5	0.5	1						0.61	1
				loaded	M	9	16	0.5	1	2	2	0	0.5	0.5	0.5							0.88	2
					L	10	16	6	5	0.5	0.5	1	0.5	0.5								2.00	6
5566	WT	2 week	9.0N	control	M	7	15	2	0.5	0	0	0.5	0.5	0	0.5	0.5						0.50	2
					L	11	17	0.5	0.5	0.5	0.5	0.5	0.5	0.5								0.50	0.5
				loaded	M	14	19	2	0.5	0.5	2	0	0.5									0.92	2
					L	13	19	5	2	0	0.5	0.5	2	2								1.71	5
5549	WT	2 week	9.0N	control	M	9	17	0	0	0	0	0.5	0	0	0	0						0.06	0.5
					L	5	11	0	1	0	0.5	0.5	0.5	0								0.36	1
				loaded	M	12	16	2	2	2	0.5	1										1.50	2
					L	9	14	0.5	2	1	1	0.5	1									1.00	2
5482	HET	2 week	9.0N	control	M	5	14	0.5	0	0	0.5	0	0.5	0	0	0.5	1					0.30	1
					L	3	11	0	0.5	1	0.5	0.5	1	0	0.5	0.5						0.50	1
				loaded	M	5	15	2	2	2	1	0.5	0	1	0.5	1	0.5	0.5				1.00	2
					L	3	12	3	2	2	2	2	2	2	2	0	0.5	0.5				1.64	3
5483	HET	2 week	9.0N	control	M	3	12	0	0	0.5	0	0	0	0	0.5	0.5	0.5					0.20	0.5
					L	1	9	0.5	1	0.5	1	0.5	0.5	0.5	0.5	1						0.67	1
				loaded	M	4	12	2	0.5	0.5	0.5	1	1	1	1	0.5	0.5	0.5	0.5			0.79	2
					L	6	14	2	0.5	1	1	2	2	2	1	0.5						1.33	2
5520	HET	2 week	9.0N	control	M	1	7	0	0	0	0	0.5	0.5	0.5								0.21	0.5
					L	1	4	0.5	1	0.5	0.5											0.63	1
				loaded	M	7	16	1	0.5	1	0.5	0	0.5	0	0	0.5	0.5	0.5				0.45	1
					L	5	15	0.5	1	0.5	2	1	0.5	0.5	0.5	1	1	0.5				0.82	2
5550	HET	2 week	9.0N	control	M	7	14	0	2	0.5	0.5	0.5	0.5	0	0							0.50	2
					L	3	9	0.5	0.5	0.5	1	1	1	2								0.93	2
				loaded	M	8	13	1	1	3	0	0.5	0.5	0.5								0.93	3
					L	5	10	3	0.5	0.5	0.5	1	3									1.42	3
5551	HET	2 week	9.0N	control	M	4	13	0.5	1	0	0	0.5	0.5	1	0	0	0.5					0.40	1
					L	3	11	0.5	0.5	0.5	0.5	0.5	0.5	0.5	0.5	0.5						0.50	0.5

				loaded	M	8	14	3	2	0	0	0	1	1	0.5	0.5						0.89	3
					L	8	16	2	3	0.5	2	0.5	0.5	0.5	0.5	2						1.28	3
5553	HET	2 week	9.0N	control	M	8	16	0.5	0	0	0	0	0	2	0.5	0						0.33	2
					L	3	8	0	0	0.5	0	1	2									0.58	2
				loaded	M	12	16	3	2	2	2	2	2									2.17	3
					L	8	14	4	3	2	1	0.5	2	2	2							2.06	4
5509	WT	6 week	9.0N	control	M	16	20	0.5	0	0	0	0.5										0.20	0.5
					L	11	16	0.5	0	0.5	1	1	0.5									0.58	1
				loaded	M	19	24	2	1	0.5	1	0	1	2								1.07	2
					L	17	24	3	3	0.5	0.5	1	0.5	0.5	1	1						1.22	3
5512	WT	6 week	9.0N	control	M	7	17	0	0.5	0	0	0	0	0.5	2	0	0	0				0.27	2
					L	7	15	0.5	0.5	0.5	1	1	0	0	0	0						0.39	1
				loaded	M	22	27	3	4	2	2	0.5	1									2.08	4
					L	20	27	4	2	2	0.5	2	0.5	0.5	1							1.56	4
5513	WT	6 week	9.0N	control	M	2	13	0	0	0	0	0	0	0	0	0	0	0	0.5			0.04	0.5
					L	4	13	0.5	0.5	0.5	0.5	0	0	0.5	0	0	0.5					0.30	0.5
				loaded	M	15	19	4	3	0.5	0.5	1										1.80	4
					L	16	19	5	4	1	0.5	0.5										2.20	5
5514	WT	6 week	9.0N	control	M	5	15	0.5	0	0	0	0	0	0.5	0.5	0	0	0				0.14	0.5
					L	8	15	0	0	0	0.5	0.5	0.5	0.5	0							0.25	0.5
				loaded	M	16	21	3	3	2	0.5	0	0.5									1.50	3
					L	13	18	4	2	3	0.5	0.5	2	2								2.00	4
5515	WT	6 week	9.0N	control	M	5	14	0.5	0	0	0	0.5	0	0	0	0	0					0.10	0.5
					L	7	14	0.5	0	0.5	0.5	0.5	0	0.5	0							0.31	0.5
				loaded	M	11	13	2	3	1	2	0										1.60	3
					L	13	15	2	2	2												2.00	2
5517	WT	6 week	9.0N	control	M	4	14	0	0.5	0	0	0	0.5	1	0	0	0	0				0.18	1
					L	4	12	0.5	0.5	0.5	0	0	0.5	0	0	0.5						0.28	0.5
				loaded	M	17	20	2	3	3	3	0.5										2.30	3
					L	13	19	3	3	2	1	0.5	1	1	2							1.69	3
5510	HET	6 week	9.0N	control	M	10	18	0.5	0.5	0.5	0.5	0.5	0.5	1	0	0.5						0.50	1
					L	6	14	0	0	0.5	0	0.5	0.5	1	2	0.5						0.56	2
				loaded	M	20	24	0.5	1	1	0.5	1										0.80	1
					L	18	24	3	2	1	0.5	0.5	0.5	0.5								1.14	3
5511	HET	6 week	9.0N	control	M	3	14	1	0	0	0	0	0.5	0.5	0.5	0	0	0	0.5			0.25	1
					L	3	13	0.5	0.5	0.5	1	0	0.5	0	0	0.5	0.5	0				0.36	1
				loaded	M	19	24	3	1	2	2	1	3									2.00	3
					L	18	24	5	3	2	2	2	2	2								2.57	5
5516	HET	6 week	9.0N	control	M	8	16	0.5	0.5	0.5	0	0	0	0	0	0						0.17	0.5
					L	9	16	0.5	0	0	0.5	0	0	0	0.5							0.19	0.5

				loaded	M	11	18	4	2	1	0	0.5	1	1	2							1.44	4
					L	13	18	4	3	2	0.5	2	0.5									2.00	4
5530	HET	6 week	9.0N	control	M	2	12	0.5	0.5	0	0	0	0	0	0.5	0	0.5					0.20	0.5
					L	5	13	0	0	0.5	0	0	0.5	1	0.5	0						0.28	1
				loaded	M	16	21	3	2	0.5	1	1	1									1.42	3
					L	11	18	2	3	3	1	2	2	2	2	2						2.11	3
5533	HET	6 week	9.0N	control	M	16	21	0	0	0	0	0	0									0.00	0
					L	9	16	0.5	0	0	0.5	1	0.5	1	0.5							0.50	1
				loaded	M	11	19	0.5	0.5	0	0	1	1	1	0.5	2						0.72	2
					L	13	19	4	2	0	1	0.5	0.5	1								1.29	4
5525	HET	6 week	9.0N	control	M	4	15	0	0	0	0	0	0	0	0	0	0	0	0.5			0.04	0.5
					L	5	15	0	0.5	1	1	0.5	0	1	1	2	0	0.5				0.68	2
				loaded	M	12	17	3	3	3	0	0	1									1.67	3
					L	12	17	4	2	2	2	1	1									2.00	4

Histological (OARSI) Score (Scorer #2): OARSI scoring of articular cartilage damage measured by Safranin O/Fast Green stain for wildtype (WT) and *cho*/+ (HET) mice. Each column corresponds to a slide separated at a 90 μm interval, with start and end slides indicated. Average (Avg) and maximum (Max) scores reported for articular cartilage in the medial (M) and lateral (L) tibial plateaus.

ID	Genotype	Duration	Magnitude	Limb	Plateau	Start	End	1	2	3	4	5	6	7	8	9	10	11	12	13	14	Avg	Max
5546	WT	1 week	4.5N	control	M	2	11	0.5	0.5	1	0	0.5	0.5	0.5	0.5	0	1	0.5				0.50	1
					L	3	10	0.5	2	0.5	2	1	1	0.5	0.5	0.5	1	0.5				0.91	2
				loaded	M	1	11	0.5	1	0	2	0.5	0.5	0	1	0.5	0.5					0.65	2
					L	1	11	2	2	2	2	1	1	0.5	0.5	0.5	0.5					1.20	2
5547	WT	1 week	4.5N	control	M	7	15	0.5	0.5	0.5	0	0	0.5									0.33	0.5
					L	4	11	1	0.5	1	1	2	0.5	0.5	0.5							0.88	2
				loaded	M	2	12	1	0.5	0.5	0	0	0	1	0.5	0	0.5	1				0.45	1
					L	2	10	0.5	0.5	1	1	1	2	0.5	0.5	0.5						0.83	2
5556	WT	1 week	4.5N	control	M	2	12	0.5	0.5	0.5	0.5	0	0.5	1	1	0.5	0.5	1				0.59	1
					L	1	10	0.5	1	1	1	1	2	1	0.5	0.5	0.5					0.90	2
				loaded	M	2	12	0.5	0.5	0.5	0.5	2	1	1	0.5	0.5	0.5	0.5				0.73	2
					L	3	13	2	2	2	3	2	2	2	1	0.5	0.5	0.5				1.59	3
5567	WT	1 week	4.5N	control	M	3	13	0.5	0.5	0	0	0	0	0.5	0.5	0	0.5	0.5				0.27	0.5
					L	3	13	0.5	2	1	1	0.5	2	1	0.5	0.5	0.5	0.5				0.91	2
				loaded	M	2	11	0.5	0.5	0.5	0.5	0.5	0.5	1	1	0.5	0.5					0.60	1
					L	2	11	4	0.5	0.5	0.5	2	1	0.5	0.5	0.5	0.5					1.05	4
5554	WT	1 week	4.5N	control	M	2	12	1	0.5	0.5	0.5	1	1	1	2	2	0.5					1.00	2
					L	1	9	2	2	2	2	1	1	0.5	0.5							1.38	2
				loaded	M	1	12	0.5	0.5	0.5	0.5	0.5	0.5	2	0.5	0.5	0.5	0.5	0.5			0.63	2
					L	2	12	0.5	1	2	2	1	0.5	1	2	0.5	0.5					1.10	2
5557	WT	1 week	4.5N	control	M	2	11	0.5	0.5	0.5	0.5	0.5	0.5	0.5	0.5	0.5	0.5	0.5				0.50	0.5
					L	6	16	2	1	1	1	1	0.5	1	1	0.5	0.5					0.95	2
				loaded	M	1	5	0.5	0.5	0.5	0.5	0.5										0.50	0.5
					L	3	11	1	1	1	0.5	0.5	1	0.5	0.5							0.75	1
5545	HET	1 week	4.5N	control	M	3	12	1	0	0	0.5	0.5	0.5	0.5	0	0.5	0.5					0.40	1
					L	2	10	0.5	0.5	0.5	0.5	1	0.5	2	2	0.5	0.5					0.85	2
				loaded	M	6	15	2	0.5	0.5	0.5	0.5	2	0.5	0.5	1	2					1.00	2
					L	4	12	2	0.5	1	0.5	1	1	2	2	2						1.33	2
5561	HET	1 week	4.5N	control	M	4	11	0.5	0	0.5	0.5	0.5	2	0.5	0.5	1						0.67	2
					L	3	11	1	0	2	1	0.5	2	2	0.5	0.5						1.06	2
				loaded	M	8	14	0.5	0.5	0.5	0.5	0.5	0.5	0.5								0.50	0.5
					L	5	11	0.5	1	1	2	3	3									1.75	3
5559	HET	1 week	4.5N	control	M	4	12	2	1	0.5	0.5	0.5	1	0.5	0.5							0.81	2
					L	2	8	0.5	1	0.5	0.5	0.5	0.5	2	0.5							0.75	2

				loaded	M	5	12	0.5	0.5	0.5	0.5	0.5	0.5	0.5	0.5	0.5						0.50	0.5
					L	3	9	0.5	0.5	0.5	0.5	0.5	0.5									0.50	0.5
5558	HET	1 week	4.5N	control	M	2	10	0.5	0.5	0.5	0.5	0.5	0.5	0.5	0.5	0.5						0.50	0.5
					L	5	11	0.5	0.5	2	2	1	0.5	0.5	0.5							0.94	2
				loaded	M	10	15	1	2	0.5	2	1	0.5									1.17	2
					L	4	8	2	3	0.5	2	2										1.90	3
5562	HET	1 week	4.5N	control	M	10	16	0.5	0.5	0.5	0.5	0.5	0.5									0.50	0.5
					L	3	8	0.5	0.5	2	0.5	0.5										0.80	2
				loaded	M	7	15	1	0.5	0.5	0.5	0.5	1	0.5	0.5							0.63	1
					L	3	9	3	2	3	1	3	0.5	0.5								1.86	3
5565	HET	1 week	4.5N	control	M	7	13	0.5	0.5	0.5	0.5	0.5	0.5	0.5								0.50	0.5
					L	4	9	0.5	0.5	0.5	1	0.5	0.5									0.58	1
				loaded	M	1	11	0.5	0.5	0.5	0.5	0.5	0.5	0.5	0.5	0.5	0.5	0.5	0.5			0.50	0.5
					L	2	13	3	3	0.5	0.5	0.5	0.5	0.5	0.5	0.5	0.5					1.00	3
5539	WT	2 week	4.5N	control	M	9	15	0.5	0.5	0.5	0.5	2	2	0.5								0.93	2
					L	5	12	0.5	2	2	2	2	3	1	1	0.5						1.56	3
				loaded	M	6	14	1	0.5	0.5	1	2	0.5	1								0.93	2
					L	4	10	3	4	2	2	3	3	2								2.71	4
5537	WT	2 week	4.5N	control	M	4	13	0.5	0.5	1	0	0.5	1	1	0.5	0.5	0.5	1				0.64	1
					L	2	11	2	2	2	1	2	2	2	2	0.5	1					1.65	2
				loaded	M	1	12	0.5	0.5	0.5	0.5	0.5	0.5	1	2	0.5	2	0.5				0.82	2
					L	3	13	2	0.5	2	3	2	1	1	1	0.5	0.5	0.5				1.27	3
5538	WT	2 week	4.5N	control	M	11	15	0.5	0.5	2	2	0.5										1.10	2
					L	2	7	2	0.5	1	2	3	3									1.92	3
				loaded	M	1	9	3	2	1	0.5	2	2	1	0.5	2						1.56	3
					L	4	12	4	2	3	3	3	2	2	3	0.5						2.50	4
5541	WT	2 week	4.5N	control	M	6	14	0.5	0.5	0.5	1	1	2	0.5	0.5							0.81	2
					L	2	9		1	2	2	2	2	2	2							1.86	2
				loaded	M	1	11	0.5	0.5	0.5	1	2	2	1	0.5	1	0.5					0.95	2
					L	3	12	2	2	2	1	2	1	2	3	2	0.5					1.75	3
5518	WT	2 week	4.5N	control	M	3	16	0.5	2	0.5	0.5	0.5	0.5	0.5	0	0.5	1	0.5	0.5			0.63	2
					L	3	14	1	1	2	2	2	1	1	1	1	0.5	0.5				1.18	2
				loaded	M	6	15	1	2	3	0.5	0.5	1	0.5	0.5	0.5	0.5					1.00	3
					L	3	10	3	1	0.5	2	2	2	2	2							1.81	3
5522	WT	2 week	4.5N	control	M	4	14	0.5	0.5	2	0.5	0.5	0.5	0.5	1	0.5	0.5	1				0.73	2
					L	2	10	0.5	1	1	1	1	2	2	1	1						1.17	2
				loaded	M	3	14	0.5	0.5	0.5	0.5	1	1	1	2	0.5	0.5	0.5				0.77	2
					L	1	7	1	2	3	2	1	3	0.5								1.79	3
5472	HET	2 week	4.5N	control	M	2	10	0.5	0.5	1	0.5	0.5	0.5	1	1	0.5						0.67	1
					L	1	8	1	2	2	0.5	2	3	2	0.5							1.63	3

				loaded	M	1	7	0.5	0.5	0.5	0.5	0.5	0.5	0.5	1	0.5						0.56	1
					L	5	12	1	2	2	1	1	1	1	0.5	0.5						1.11	2
5474	HET	2 week	4.5N	control	M	1	6	0.5	0.5	0.5	0.5	0.5	0.5									0.50	0.5
					L	9	14	2	2	1	0.5	2	2									1.58	2
				loaded	M	1	11	0.5	0.5	1	0.5	1	0.5	0.5	0.5	0.5	0.5					0.60	1
					L	2	10	3	3	2	1	1	2	0.5	0.5	0.5						1.50	3
5475	HET	2 week	4.5N	control	M	2	12	1	1	1	1	0.5	0.5	1		0.5						0.81	1
					L	2	9	2	2	2	1	2	3	1								1.86	3
				loaded	M	8	14	0.5	0.5	0.5	0.5	1	0.5	0.5	0.5							0.56	1
					L	2	7	0.5	2	3	4	2	1	0.5								1.86	4
5490	HET	2 week	4.5N	control	M	8	15	0.5	0.5	0.5	0.5	0.5	0.5									0.50	0.5
					L	1	5	0.5	0.5	0.5	1	1										0.70	1
				loaded	M	3	12	0.5	0.5	2	2	0.5	0.5	0.5	0.5	0.5	1					0.85	2
					L	1	6	1	2	2	3	4	1	0.5								1.93	4
5491	HET	2 week	4.5N	control	M	1	9	0.5	1	1	1	2	0.5	1	0.5	1	1					0.95	2
					L	2	10	1	1	0.5	3	1	3	3	2	1						1.72	3
				loaded	M	2	8	1	1	2	1	0.5	0.5	0.5								0.93	2
					L	7	13	2	1	0.5	1	2	2	1	0.5							1.25	2
5493	HET	2 week	4.5N	control	M	11	15	0.5	0.5	1	1	0.5										0.70	1
					L	2	5	0.5	0.5	2	2											1.25	2
				loaded	M	3	7	0.5	0.5	0.5	2	2										1.10	2
					L	11	16	1	0.5	0.5	1	2	1	2								1.14	2
5535	WT	6 week	4.5N	control	M	11	17	0.5	1	0.5	0.5	0.5	0	0	0	0.5						0.39	1
					L	4	11	0.5	0.5	0	1	2	3	3								1.43	3
				loaded	M	8	14	0.5	4	4	0.5	2	2									2.17	4
					L	15	18	5	3	2	1	1	2	4								2.57	5
5524	WT	6 week	4.5N	control	M	4	12	0.5	0.5	0.5	1	0	1	2	2	0.5						0.89	2
					L	5	13	2	2	2	1	1	1	1	1							1.38	2
				loaded	M	14	19	1	0.5	1	1	3	2	2								1.50	3
					L	10	16	3	3	3	3	2	3	2	2	3						2.67	3
5529	WT	6 week	4.5N	control	M	4	12	0	0	1	0.5	0	1	2	0.5	0.5	0.5					0.60	2
					L	9	14	3	4	1	0.5	1	2	1								1.79	4
				loaded	M	14	20	1	0.5	0.5	0.5	2	0.5	2								1.00	2
					L	16	20	2	5	3	2	2	2									2.67	5
5532	WT	6 week	4.5N	control	M	10	18	2	0.5	0.5	0.5	0.5	0.5	0.5								0.71	2
					L	12	18	0.5	1	0.5	2	0.5										0.90	2
				loaded	M	6	13	1	0.5	1	0.5	0.5	0.5	0.5	0.5							0.63	1
					L	6	14	2	2	1	2	1	1	2	2	0.5						1.50	2
5534	WT	6 week	4.5N	control	M	4	16	0.5	1	1	1	0.5	0.5	0.5	2	0.5	0.5	0.5	0.5	2		0.85	2
					L	4	16	0.5	2	2	3	3	1	0.5	3	3	2	1	0.5	1		1.73	3

				loaded	M	1	9	0.5	0.5	0.5	0.5	0.5	0.5	1	0.5	0.5	0.5					0.55	1
					L	5	14	0.5	0.5	2	0.5	2	2	2	2	3						1.61	3
5528	WT	6 week	4.5N	control	M	3	14	0.5	0.5	0.5	0.5	0.5	0.5	1	1	0.5	0.5	0.5	0.5			0.58	1
					L	7	16	1	1	1	1	0.5	0.5	1	0.5	0.5	0.5					0.75	1
				loaded	M	14	20	0.5	0.5	0.5	0.5	1	2	1	0.5							0.81	2
					L	8	14	3	2	2	2	2	2	0.5								1.93	3
5531	HET	6 week	4.5N	control	M	8	17	1	1	0	0	0	0.5	0	1	0.5	2					0.60	2
					L	8	15	2	2	1	2	1	2	3	2	0.5						1.72	3
				loaded	M	7	18	2	1	0.5	0.5	1	0.5	2	0.5	1	1	0	0.5			0.88	2
					L	8	15	2	1	2	0.5	1	1	0.5	2	2						1.33	2
5526	HET	6 week	4.5N	control	M	3	12	0.5	0.5	0.5	0.5	0.5	2	0.5	0.5	0.5	0.5					0.65	2
					L	5	13	2	2	1	0.5	1	1	2	2	0.5						1.33	2
				loaded	M	7	16	0.5	1	0.5	0.5	0.5	0.5	1	2	0.5	2	0.5				0.86	2
					L	5	13	4	2	1	1	2	3	3	3	0.5						2.17	4
5527	HET	6 week	4.5N	control	M	2	10	1	0.5	0.5	0.5	0.5	0.5	0.5	0.5	0.5	0.5					0.55	1
					L	3	11	1	1	2	0.5	0.5	1	2	1	0.5	0.5					1.00	2
				loaded	M	9	18	0.5	0.5	0.5	0.5	0.5	0.5	0.5	0.5	0.5	0.5					0.50	0.5
					L	8	15	2	2	1	0.5	0.5	0.5	0.5	0.5							0.94	2
5536	HET	6 week	4.5N	control	M	7	16	0.5	0.5	0.5	0.5	0.5	0.5	0.5	0.5	0.5	0.5	0.5				0.50	0.5
					L	4	14	0.5	2	2	0.5	0.5	0.5	2	0.5	0.5	0.5	0.5				0.91	2
				loaded	M	5	12	1	1	0.5	2	2	0.5	1	0.5							1.06	2
					L	5	12	0.5	2	2	0.5	2	0.5	2	0.5							1.25	2
5544	HET	6 week	4.5N	control	M	8	17	0.5	0.5	1	0.5	0.5	0.5	0.5	0.5	0.5	0.5					0.55	1
					L	8	17	0.5	2	1	1	1	1	1	2	0.5	0.5					1.05	2
				loaded	M	5	15	0.5	0.5	0.5	0.5	0.5	0.5	0.5	1	0.5	0.5					0.55	1
					L	4	13	4	1	1	0.5	1	1	1	2	2	0.5					1.40	4
5560	HET	6 week	4.5N	control	M	8	17	0.5	0.5	0.5	0.5	0.5	0.5	0.5	0.5	0.5	0.5					0.50	0.5
					L	6	14	0.5	1	1	0.5	0.5	0.5	0.5	0.5	0.5						0.61	1
				loaded	M	3	11	1	0.5	1	0.5	0.5	0.5	0.5	0.5	0.5						0.61	1
					L	8	13	4	4	0.5	0.5	0.5	0.5									1.67	4
5578	WT	1 week	9.0N	control	M	4	13	1	0.5	0	1	0	2	1	0.5	1	0					0.70	2
					L	4	11	2	2	2	2	2	2	1	0.5	1	0.5					1.50	2
				loaded	M	7	15	4	1	1	0.5	0.5	1	0.5	0.5	2						1.22	4
					L	12	15	5	3	3	2	2										3.00	5
5576	WT	1 week	9.0N	control	M	1	10	1	0	0.5	0.5	2	0.5	0.5	0.5	0.5	0.5					0.65	2
					L	1	10	2	2	2	2	2	2	2	2	1	0.5					1.75	2
				loaded	M	9	14	3	4	3	0.5	2	2									2.42	4
					L	8	14	2	2	2	2	2	3	4								2.43	4
5579	WT	1 week	9.0N	control	M	7	15	0.5	0.5	0.5	0	0.5	2	0.5	0.5	0.5						0.61	2
					L	4	12	0.5	0.5	2	1	1	2	1	2							1.25	2

				loaded	M	6	13	0.5	3	2	1	2	1	2	2							1.69	3
					L	3	9	0.5	0.5	2	3	2	2	2	2							1.75	3
5571	WT	1 week	9.0N	control	M	4	12	1	1	1	1	0.5	2	2	1	0.5	0.5					1.05	2
					L	2	9	2	1	1	0.5	1	2	2	2	1						1.39	2
				loaded	M	7	15	1	0.5	0	0.5	1	1	2	0.5	1						0.83	2
					L	7	15	3	1	1	2	1	2	2	2	2						1.78	3
5572	WT	1 week	9.0N	control	M	8	14	0.5	0.5	0.5	0.5	0	0.5	0.5								0.43	0.5
					L	8	14	0.5	0.5	2	2	1	1	0.5								1.07	2
				loaded	M	12	15	2	1	0.5	0.5											1.00	2
					L	13	15	4	3	0.5												2.50	4
5570	WT	1 week	9.0N	control	M	7	16	0.5	0.5	0.5	0.5	0	0.5	0.5	0.5	0.5	1					0.50	1
					L	4	12	0.5	0.5	1	2	1	1	0.5	2	0.5						1.00	2
				loaded	M	7	16	2	0.5	0.5	0.5	0.5	0.5	0.5								0.71	2
					L	4	12	6	5	3	1	1	2	1								2.71	6
5564	HET	1 week	9.0N	control	M	8	16	0.5	0.5	0	0.5	0.5	0.5	0.5	0	0.5						0.39	0.5
					L	5	13	0.5	1	0.5	0.5	0.5	0.5	0.5	0.5	0.5						0.56	1
				loaded	M	8	16	1	1	1	3	2	1	1	1	0.5	0.5					1.20	3
					L	5	13	4		0.5	0.5	1	2									1.60	4
5577	HET	1 week	9.0N	control	M	13	16	3	2	1	0.5	1	0.5									1.33	3
					L	10	15	4	5	3	2	2	2									3.00	5
				loaded	M	13	16	3	1	0.5	0.5	0.5										1.10	3
					L	10	15	5	5	2	3	3	2									3.33	5
5574	HET	1 week	9.0N	control	M	7	13	0.5	0.5	1	0	0	0.5	0.5								0.43	1
					L	4	9	2	2	1	2	3	3									2.17	3
				loaded	M	7	13	2	1	0.5	0.5	1	2									1.17	2
					L	4	9	1	2	2	2	2	2									1.83	2
5580	HET	1 week	9.0N	control	M	10	16	0.5	0.5	0.5	0	0	0.5	0.5								0.36	0.5
					L	6	12	1	2	2	0.5	2	3	0.5								1.57	3
				loaded	M	10	16	0.5	0.5	0.5	0	0.5	0.5	1	0.5							0.50	1
					L	6	12	5	2	1	1	0.5	0.5	1	0.5							1.44	5
5573	HET	1 week	9.0N	control	M	2	8	0.5	0	0.5	0	0.5	0.5	0.5	0.5							0.38	0.5
					L	4	10	0.5	2	0.5	0.5	2	1	0.5	0.5							0.94	2
				loaded	M	9	14	0.5	0.5	2	0.5	0.5	0.5									0.75	2
					L	4	12	3	3	3	2	2	2	3	3	2						2.56	3
5569	HET	1 week	9.0N	control	M	3	10	0.5	0.5	1	1	2	0.5	2								1.07	2
					L	2	7	0.5	1	0.5	2	3	1									1.33	3
				loaded	M	15	20	0.5	1	0.5	0.5	0.5	2									0.83	2
					L	11	18	5	3	1	4	2	3	3	3							3.00	5
5519	WT	2 week	9.0N	control	M	2	8	1	1	0.5	2	0.5	1	0.5								0.93	2
					L	3	8	1	1	1	1	1	3									1.33	3

				loaded	M	14	21	0.5	1	0.5	0.5	2	0.5	2								1.00	2
					L	14	21	2	1	1	2	2	2	1								1.57	2
5521	WT	2 week	9.0N	control	M	7	15	1	0.5	0	0.5	1	2	0.5	0.5	0.5						0.72	2
					L	6	13	2	2	2	3	2	3	1	0.5	0.5						1.78	3
				loaded	M	9	15	2	2	2	1	2	3	0.5								1.79	3
					L	7	15	5	4	5	4	3	2	1	2	2						3.11	5
5523	WT	2 week	9.0N	control	M	1	10	1	1	0.5	0	0.5	2	2	0.5	0.5	0.5					0.85	2
					L	2	13	1	1	2	2	2	2	2	2	1	0.5					1.55	2
				loaded	M	14	18	2	3	3	2											2.50	3
					L	5	10	1	2	3	3	3	3									2.50	3
5563	WT	2 week	9.0N	control	M	7	15	0.5	1	1	0.5	0.5	1	1	2							0.94	2
					L	7	15	0.5	0.5	0.5	0.5	0.5	1	0.5	0.5							0.56	1
				loaded	M	9	16	1	1	2	2	1	0.5	1	1							1.19	2
					L	10	16	6	5	3	2	2	1	0.5								2.79	6
5566	WT	2 week	9.0N	control	M	7	15	2	0.5	0.5	0.5	0.5	0.5	0.5	0.5	0.5						0.67	2
					L	11	17	3	0.5	0.5	0.5	0.5	1	0.5	0.5							0.88	3
				loaded	M	14	19	5	4	1	1	0.5	0.5									2.00	5
					L	13	19	5	3	1	1	1	0.5									1.92	5
5549	WT	2 week	9.0N	control	M	9	17	0.5	0.5	0.5	1	0.5	0.5	0.5	1	1	0.5	0.5				0.64	1
					L	5	11	1	1	0.5	0.5	0.5	0.5	0.5	0.5	0.5	0.5					0.60	1
				loaded	M	12	16	0.5	0.5	0.5	0.5	0.5	2	1	0.5							0.75	2
					L	9	14	3	2	2	2	2	1	0.5								1.79	3
5482	HET	2 week	9.0N	control	M	5	14	3	1	0.5	0.5	0.5	0.5	1	1	1	2					1.10	3
					L	3	11	1	2	3	1	0.5	2	1	1	0.5	0.5					1.25	3
				loaded	M	5	15	2	1	0.5	1	0.5	0.5	1	2	1	0.5	1				1.00	2
					L	3	12	2	3	3	2	2	2	2	2	1	1					2.00	3
5483	HET	2 week	9.0N	control	M	3	12	0.5	0.5	0.5	0.5	0.5	0.5	0.5	0.5	0.5	0.5	0.5				0.50	0.5
					L	1	9	0.5	3	1	2	0.5	2	1	1	0.5						1.28	3
				loaded	M	4	12	3	1	1	1	1	2	3	1	0.5						1.50	3
					L	6	14	2	3	1	2	1	2	2	2	0.5						1.72	3
5520	HET	2 week	9.0N	control	M	1	7	0.5	0.5	0.5	0.5	0.5	1	0.5								0.57	1
					L	1	4	1	2	0.5	0.5											1.00	2
				loaded	M	7	16	1	1	0.5	0.5	0.5	1	0.5	0.5	0.5	0.5	0.5				0.64	1
					L	5	15	5	4	3	2	0.5	0.5	0.5	0.5	0.5	0.5	0.5				1.59	5
5550	HET	2 week	9.0N	control	M	7	14	0.5	0.5	0.5	0.5	0.5	0.5	0.5	0.5	0.5						0.50	0.5
					L	3	9	0.5	0.5	0.5	1	1	2	0.5								0.86	2
				loaded	M	8	13	0.5	0.5	0.5	0.5	0.5	2	0.5								0.71	2
					L	5	10	4	1	1	0.5	0.5	2									1.50	4
5551	HET	2 week	9.0N	control	M	4	13	0.5	0.5	0.5	0.5	0	0.5	0.5	2	0.5	0.5	0.5				0.59	2
					L	3	11	0.5	0.5	0.5	0.5	0.5	0.5	0.5	0.5	0.5						0.50	0.5

				loaded	M	8	14	3	3	0.5	0.5	0.5	0.5	0.5								1.21	3
					L	8	16	3	4	1	2	1	0.5	1	2							1.81	4
5553	HET	2 week	9.0N	control	M	8	16	0.5	2	0.5	0.5	0.5	0.5	0.5	0	0.5	1	0.5	0.5			0.63	2
					L	3	8	1	1	2	2	2	1	1	1	1	0.5	0.5				1.18	2
				loaded	M	12	16	1	2	3	0.5	0.5	1	0.5	0.5	0.5	0.5					1.00	3
					L	8	14	3	1	0.5	2	2	2	2	2							1.81	3
5509	WT	6 week	9.0N	control	M	16	20	0.5	2	0.5	0.5	2	0.5									1.00	2
					L	11	16	2	0.5	2	3	4										2.30	4
				loaded	M	19	24	2	3	5	5	3	3	3								3.43	5
					L	17	24	1	2	5	4	3	4	3								3.14	5
5512	WT	6 week	9.0N	control	M	7	17	0.5	0.5	1	1	1	2	0.5	2	1						1.06	2
					L	7	15	1	2	0.5	2	1	1	1	2	0.5						1.22	2
				loaded	M	22	27	1	5	5	0.5	3										2.90	5
					L	20	27	5	5	5	5	5										5.00	5
5513	WT	6 week	9.0N	control	M	2	13	0.5	0.5	1	0.5	0.5	0.5	0.5	0.5	0.5	0.5	0.5				0.55	1
					L	4	13	1	1	2	2	2	2	1	2	0.5	0.5					1.40	2
				loaded	M	15	19	5	5	5	2	0.5	1									3.08	5
					L	16	19	6	5	5	2	1										3.80	6
5514	WT	6 week	9.0N	control	M	5	15	0.5	0.5	0.5	0.5	0.5	0.5	0.5	0.5	1	0.5					0.55	1
					L	8	15	0.5	0.5	0.5	0.5	0.5	0.5	1	0.5							0.56	1
				loaded	M	16	21	4	3	2	1	0.5	1									1.92	4
					L	13	18	6	4	2	1	0.5	1	2	1							2.19	6
5515	WT	6 week	9.0N	control	M	5	14	1	1	0.5	0.5	0.5	1	2	0.5	0.5	0.5					0.80	2
					L	7	14	2	1	2	2	3	2	2	0.5							1.81	3
				loaded	M	11	13	5	3	1	3											3.00	5
					L	13	15	3	3	3												3.00	3
5517	WT	6 week	9.0N	control	M	4	14	0.5	0.5	0.5	0.5	0.5	0.5	1	0.5	0.5						0.56	1
					L	4	12	2	1	2	1	1	1	0.5	0.5							1.13	2
				loaded	M	17	20	3	3	3	2											2.75	3
					L	13	19	2	3	2	2	1	2	2								2.00	3
5510	HET	6 week	9.0N	control	M	10	18	1	1	0.5	0.5	0.5	2	2	1	0.5						1.00	2
					L	6	14	1	2	0.5	0.5	2	3	2	4	1						1.78	4
				loaded	M	20	24	4	2	2	1	2										2.20	4
					L	18	24	6	5	4	4	2	2	1								3.43	6
5511	HET	6 week	9.0N	control	M	3	14	1	0.5	0.5	0.5	0	0.5	0.5	0.5			0.5	1			0.55	1
					L	3	13	1	0.5	0.5	2	0.5	0.5	0.5	1			0.5	0.5			0.75	2
				loaded	M	19	24	2	6	6	4	1	2	2	0.5	0.5						2.67	6
					L	18	24	3	2	5	5	3	3	2	3	3	2					3.10	5
5516	HET	6 week	9.0N	control	M	8	16	0.5	0.5	0.5	0.5	0.5	0.5	0.5	0	0.5	0.5					0.45	0.5
					L	9	16	0.5	0.5	0.5	0.5	0.5	0.5	1	1	0.5						0.61	1

				loaded	M	11	18	4	4	2	3	0.5	0.5	2	1	2						2.11	4
					L	13	18	6	4	3	4	3	1	0.5								3.07	6
5530	HET	6 week	9.0N	control	M	2	12	0.5	0.5	0.5	0.5	2	0.5	0.5	0.5	0.5	0.5					0.65	2
					L	5	13	0.5	0.5	2	2	2	2	2	0.5							1.44	2
				loaded	M	16	21	3	1	0.5	2	1	0.5									1.33	3
					L	11	18	4	3	4	1	2	2	2	2							2.50	4
5533	HET	6 week	9.0N	control	M	16	21	2	2	0.5	0.5	0.5	0.5									1.00	2
					L	9	16	1	0.5	1	1	2	1	1	2							1.19	2
				loaded	M	11	19	0.5	0.5	1	1	2	2	1	1							1.13	2
					L	13	19	6	4	2	2	2	2	2								2.86	6
5525	HET	6 week	9.0N	control	M	4	15	0.5	2	2	1	0	0.5	0.5	0.5	0.5	1	0.5	0.5			0.79	2
					L	5	15	1	1	2	2	1	1	1	2	1	0.5	1				1.23	2
				loaded	M	12	17	5	4	3	5	1										3.60	5
					L	12	17	4	4	5	5	4										4.40	5

Histological (OARSI) Score (Average): OARSI scoring of articular cartilage damage measured by Safranin O/Fast Green stain for wildtype (WT) and *cho*/+ (HET) mice. Average scores of Scorers #1 and #2 reported for articular cartilage in the medial (M) and lateral (L) tibial plateaus.

Magnitude	Duration	Genotype	Limb	Medial	Lateral
4.5N	1wk	WT	Control	0.30	0.61
		WT	Control	0.22	0.69
		WT	Control	0.50	0.73
		WT	Control	0.18	0.70
		WT	Control	0.66	0.99
		WT	Control	0.30	0.66
	2wk	WT	Control	0.50	1.00
		WT	Control	0.37	1.18
		WT	Control	0.80	1.21
		WT	Control	0.55	1.43
		WT	Control	0.35	0.76
		WT	Control	0.39	0.83
	6wk	WT	Control	0.34	1.34
		WT	Control	0.47	0.94
		WT	Control	0.33	1.10
		WT	Control	0.41	0.66
		WT	Control	0.46	1.15
		WT	Control	0.40	0.63
9N	1wk	WT	Control	0.43	1.09
		WT	Control	0.48	1.23
		WT	Control	0.36	0.90
		WT	Control	0.58	1.01
		WT	Control	0.21	0.71
		WT	Control	0.30	0.72
	2wk	WT	Control	0.57	0.79
		WT	Control	0.44	1.14
		WT	Control	0.48	1.14
		WT	Control	0.61	0.59
		WT	Control	0.58	0.69
		WT	Control	0.35	0.48
	6wk	WT	Control	0.60	1.44
		WT	Control	0.66	0.81
		WT	Control	0.29	0.85
		WT	Control	0.34	0.41
		WT	Control	0.45	1.06

		WT	Control	0.37	0.70
4.5N	1wk	HET	Control	0.43	1.05
		HET	Control	0.36	0.81
		HET	Control	0.60	0.63
		HET	Control	0.33	0.55
		HET	Control	0.36	0.57
		HET	Control	0.36	0.29
	2wk	HET	Control	0.36	1.09
		HET	Control	0.38	1.25
		HET	Control	0.45	1.30
		HET	Control	0.41	0.55
		HET	Control	0.53	1.03
		HET	Control	0.45	0.88
	6wk	HET	Control	0.33	0.99
		HET	Control	0.50	1.11
		HET	Control	0.50	0.81
		HET	Control	0.35	0.66
		HET	Control	0.38	0.85
		HET	Control	0.38	0.39
9N	1wk	HET	Control	0.19	0.33
		HET	Control	0.67	1.79
		HET	Control	0.21	1.58
		HET	Control	0.25	1.07
		HET	Control	0.22	0.72
		HET	Control	0.63	1.04
	2wk	HET	Control	0.70	0.88
		HET	Control	0.35	0.97
		HET	Control	0.39	0.81
		HET	Control	0.50	0.89
		HET	Control	0.50	0.50
		HET	Control	0.48	0.88
	6wk	HET	Control	0.75	1.17
		HET	Control	0.40	0.56
		HET	Control	0.31	0.40
		HET	Control	0.43	0.86
		HET	Control	0.50	0.84
		HET	Control	0.42	0.95
4.5N	1wk	WT	Loaded	0.60	1.01
		WT	Loaded	0.45	0.87
		WT	Loaded	0.50	1.39

		WT	Loaded	0.63	1.13
		WT	Loaded	0.58	1.03
		WT	Loaded	0.50	0.78
	2wk	WT	Loaded	0.77	1.83
		WT	Loaded	0.72	1.18
		WT	Loaded	1.18	2.05
		WT	Loaded	0.75	1.52
		WT	Loaded	0.66	1.23
		WT	Loaded	0.59	1.56
	6wk	WT	Loaded	1.58	1.79
		WT	Loaded	1.14	2.15
		WT	Loaded	1.00	1.83
		WT	Loaded	0.51	1.47
		WT	Loaded	0.62	1.28
		WT	Loaded	0.81	1.80
9N	1wk	WT	Loaded	1.03	2.38
		WT	Loaded	2.21	1.96
		WT	Loaded	1.31	1.63
		WT	Loaded	1.03	1.61
		WT	Loaded	1.13	2.08
		WT	Loaded	0.48	1.86
	2wk	WT	Loaded	1.22	1.22
		WT	Loaded	2.04	2.53
		WT	Loaded	2.29	1.96
		WT	Loaded	1.03	2.39
		WT	Loaded	1.46	1.82
		WT	Loaded	1.13	1.39
	6wk	WT	Loaded	2.25	2.18
		WT	Loaded	2.49	3.28
		WT	Loaded	2.44	3.00
		WT	Loaded	1.71	2.09
		WT	Loaded	2.30	2.50
		WT	Loaded	2.53	1.84
4.5N	1wk	HET	Loaded	1.80	1.93
		HET	Loaded	0.47	1.48
		HET	Loaded	0.50	0.58
		HET	Loaded	0.79	1.49
		HET	Loaded	0.65	1.48
		HET	Loaded	0.44	0.73
	2wk	HET	Loaded	0.53	1.03

		HET	Loaded	0.53	1.45
		HET	Loaded	0.56	1.57
		HET	Loaded	0.80	1.43
		HET	Loaded	0.71	1.25
		HET	Loaded	1.14	1.20
	6wk	HET	Loaded	0.77	1.19
		HET	Loaded	0.73	1.81
		HET	Loaded	0.58	1.07
		HET	Loaded	1.08	1.40
		HET	Loaded	0.46	1.34
		HET	Loaded	0.56	1.29
9N	1wk	HET	Loaded	0.90	1.43
		HET	Loaded	1.00	2.54
		HET	Loaded	1.26	1.83
		HET	Loaded	0.41	1.22
		HET	Loaded	0.71	2.22
		HET	Loaded	1.00	2.03
	2wk	HET	Loaded	1.00	1.82
		HET	Loaded	1.15	1.53
		HET	Loaded	0.55	1.20
		HET	Loaded	0.82	1.46
		HET	Loaded	1.05	1.55
		HET	Loaded	1.58	1.94
	6wk	HET	Loaded	1.50	2.29
		HET	Loaded	2.33	2.84
		HET	Loaded	1.77	2.54
		HET	Loaded	1.38	2.31
		HET	Loaded	0.92	2.07
		HET	Loaded	2.63	3.20

Localized Articular Cartilage Thickness: Cartilage thickness (μm) in the posterior (Post), middle (Mid), and anterior (ant) regions of the medial and lateral tibial plateaus in wildtype (WT) and *cho*/+ (HET) mice.

					Medial			Lateral		
ID	**Genotype**	**Duration**	**Magnitude**	**Limb**	**Post**	**Mid**	**Ant**	**Post**	**Mid**	**Ant**
5546	WT	1wk	4.5N	control	56.85	74.50	106.85	72.15	86.53	75.28
5547	WT	1wk	4.5N	control	76.65	77.15	127.00	86.18	83.70	33.78
5556	WT	1wk	4.5N	control	73.55	108.53	72.58	87.40	118.58	70.15
5567	WT	1wk	4.5N	control	74.15	89.98	67.75	62.93	107.88	53.28
5554	WT	1wk	4.5N	control	98.78	103.23	55.98	107.08	94.28	29.28
5557	WT	1wk	4.5N	control	74.60	81.53	55.55	70.35	79.40	39.80
5539	WT	2wk	4.5N	control	83.53	86.70	71.95	67.10	98.63	36.53
5537	WT	2wk	4.5N	control	84.50	47.68	63.80	72.63	104.20	75.18
5538	WT	2wk	4.5N	control	63.80	79.48	65.05	61.43	44.28	70.68
5541	WT	2wk	4.5N	control	82.03	83.05	81.73	62.48	71.30	55.83
5518	WT	2wk	4.5N	control	93.50	65.10	83.63	74.08	87.63	53.70
5522	WT	2wk	4.5N	control	75.40	82.85	89.53	53.15	91.08	48.65
5535	WT	6wk	4.5N	control	72.98	99.35	95.28	69.15	113.80	69.90
5524	WT	6wk	4.5N	control	75.83	90.18	92.18	73.40	89.05	63.45
5529	WT	6wk	4.5N	control	72.93	84.90	75.75	75.48	86.08	84.35
5532	WT	6wk	4.5N	control	42.35	73.45	78.70	58.08	64.20	90.75
5534	WT	6wk	4.5N	control	70.48	99.78	106.10	74.58	102.03	66.08
5528	WT	6wk	4.5N	control	72.38	99.53	85.80	96.03	104.58	89.85
5578	WT	1wk	9N	control	126.58	97.98	71.10	75.85	95.73	76.50
5576	WT	1wk	9N	control	70.68	97.68	88.45	93.63	84.55	73.98
5579	WT	1wk	9N	control	102.60	117.73	70.13	65.48	102.98	72.10
5571	WT	1wk	9N	control	53.80	86.98	75.45	58.80	105.85	73.65
5572	WT	1wk	9N	control	50.15	74.55	91.55	80.1	79.925	58.575
5570	WT	1wk	9N	control	89.38	125.10	152.45	71.53	125.13	96.75
5519	WT	2wk	9N	control	78.38	97.50	90.35	96.65	86.90	84.65
5521	WT	2wk	9N	control	119.85	102.68	93.78	108.73	94.10	62.20
5523	WT	2wk	9N	control	86.93	75.70	72.80	60.25	66.65	56.50
5563	WT	2wk	9N	control	48.30	92.80	84.48	80.90	94.55	89.83
5566	WT	2wk	9N	control	68.18	87.70	56.20	87.80	101.90	76.23
5549	WT	2wk	9N	control	91.60	80.70	89.90	101.85	94.58	65.38
5509	WT	6wk	9N	control	65.58	88.80	95.78	54.65	125.73	91.40
5512	WT	6wk	9N	control	72.43	49.23	41.60	52.05	38.35	19.33
5513	WT	6wk	9N	control	86.33	93.03	68.98	70.40	94.85	56.28
5514	WT	6wk	9N	control	91.53	100.35	103.75	91.58	85.55	85.98
5515	WT	6wk	9N	control	55.08	105.38	86.03	94.23	80.70	47.30

5517	WT	6wk	9N	control	85.83	100.03	85.40	94.18	110.15	51.10
5545	HET	1wk	4.5N	control	80.55	86.55	74.90	82.48	101.28	89.73
5561	HET	1wk	4.5N	control	114.35	116.10	124.35	97.83	96.15	74.85
5559	HET	1wk	4.5N	control	76.70	108.38	98.25	45.55	63.65	24.83
5558	HET	1wk	4.5N	control	48.70	66.05	32.47	97.825	96.15	74.85
5562	HET	1wk	4.5N	control	83.35	100.85	103.68	95.08	99.65	66.15
5565	HET	1wk	4.5N	control	72.55	87.225	92.225	95.075	99.65	66.15
5472	HET	2wk	4.5N	control	90.85	96.775	83.275	83.28	78.15	47.70
5474	HET	2wk	4.5N	control	60.55	97.35	60.525	69.25	67.20	71.00
5475	HET	2wk	4.5N	control	85.60	68.55	73.75	78.25	69.50	69.88
5490	HET	2wk	4.5N	control	65.13	74.85	74.28	76.30	103.40	71.98
5491	HET	2wk	4.5N	control	42.70	107.70	82.00	74.63	86.18	61.38
5493	HET	2wk	4.5N	control	55.98	101.40	74.78	66.83	78.70	51.40
5531	HET	6wk	4.5N	control	83.50	100.15	70.03	86.95	102.40	78.00
5526	HET	6wk	4.5N	control	73.70	94.75	99.48	93.38	86.53	64.08
5527	HET	6wk	4.5N	control	93.70	118.18	91.48	112.98	99.08	55.90
5536	HET	6wk	4.5N	control	86.55	78.48	47.30	81.78	110.15	103.70
5544	HET	6wk	4.5N	control	93.55	99.33	112.10	88.98	87.20	54.05
5560	HET	6wk	4.5N	control	76.53	85.65	90.58	72.58	89.78	45.50
5564	HET	1wk	9N	control	78.58	92.15	125.50	65.65	98.55	69.25
5577	HET	1wk	9N	control	94.65	93.50	90.00	78.65	134.83	89.43
5574	HET	1wk	9N	control	80.73	123.38	105.88	105.23	66.43	77.93
5580	HET	1wk	9N	control	99.10	71.95	110.30	64.33	92.43	67.90
5573	HET	1wk	9N	control	69.80	92.33	85.30	117.83	108.28	85.55
5569	HET	1wk	9N	control	138.85	124.78	104.43	111.10	100.85	79.90
5482	HET	2wk	9N	control	82.13	55.38	45.23	48.03	60.83	19.10
5483	HET	2wk	9N	control	70.40	101.15	105.13	95.68	89.75	63.88
5520	HET	2wk	9N	control	96.25	96.25	91.23	97.95	95.13	53.65
5550	HET	2wk	9N	control	74.93	99.22	119.06	100.24	99.42	82.35
5551	HET	2wk	9N	control	76.87	110.50	71.98	59.18	109.60	73.23
5553	HET	2wk	9N	control	96.15	97.33	108.35	65.15	122.88	74.03
5510	HET	6wk	9N	control	83.35	100.85	103.68	73.60	119.13	71.13
5511	HET	6wk	9N	control	67.03	91.83	105.30	51.98	102.63	54.35
5516	HET	6wk	9N	control	80.98	91.28	95.73	84.90	100.85	71.03
5530	HET	6wk	9N	control	71.83	102.25	84.28	99.55	93.35	84.05
5533	HET	6wk	9N	control	79.80	87.25	142.50	62.55	67.20	97.78
5525	HET	6wk	9N	control	83.93	95.98	96.28	77.68	79.03	56.45
5546	WT	1wk	4.5N	loaded	81.95	87.98	38.25	80.25	72.28	64.13
5547	WT	1wk	4.5N	loaded	102.50	103.15	115.60	78.13	91.25	60.53
5556	WT	1wk	4.5N	loaded	65.65	100.15	81.95	68.95	102.83	54.13

5567	WT	1wk	4.5N	loaded	57.25	91.53	87.09	64.83	93.30	71.03
5554	WT	1wk	4.5N	loaded	59.43	89.38	91.13	81.90	104.05	32.05
5557	WT	1wk	4.5N	loaded	50.40	83.75	70.78	68.95	78.85	57.88
5539	WT	2wk	4.5N	loaded	64.18	114.63	79.63	74.13	86.58	75.65
5537	WT	2wk	4.5N	loaded	79.45	95.28	94.95	63.03	92.95	66.38
5538	WT	2wk	4.5N	loaded	47.65	78.50	64.13	85.38	70.50	62.05
5541	WT	2wk	4.5N	loaded	69.95	93.83	90.73	97.10	85.78	49.58
5518	WT	2wk	4.5N	loaded	83.65	84.05	64.73	66.75	77.18	61.48
5522	WT	2wk	4.5N	loaded	98.50	65.80	80.48	84.40	82.70	75.10
5535	WT	6wk	4.5N	loaded	56.45	116.03	102.80	89.40	109.25	94.63
5524	WT	6wk	4.5N	loaded	61.00	70.68	93.13	62.88	99.68	110.65
5529	WT	6wk	4.5N	loaded	65.00	73.20	110.35	51.95	77.35	95.23
5532	WT	6wk	4.5N	loaded	49.20	78.08	78.28	53.93	74.93	79.75
5534	WT	6wk	4.5N	loaded	62.10	81.58	85.35	48.70	82.95	48.65
5528	WT	6wk	4.5N	loaded	73.90	94.20	99.50	43.68	90.88	60.43
5578	WT	1wk	9N	loaded	74.43	111.48	128.83	71.00	115.90	123.15
5576	WT	1wk	9N	loaded	68.20	63.60	88.98	64.13	107.73	86.35
5579	WT	1wk	9N	loaded	63.30	80.35	100.95	66.75	81.28	78.88
5571	WT	1wk	9N	loaded	60.08	99.98	69.85	59.35	81.60	73.33
5572	WT	1wk	9N	loaded	60.78	87.15	83.03	86.45	89.05	75.48
5570	WT	1wk	9N	loaded	88.23	111.15	55.20	21.75	80.45	88.93
5519	WT	2wk	9N	loaded	58.40	52.75	103.58	53.38	94.73	91.58
5521	WT	2wk	9N	loaded	65.38	91.78	120.35	36.95	88.98	124.53
5523	WT	2wk	9N	loaded	61.38	96.88	66.55	66.60	95.38	37.85
5563	WT	2wk	9N	loaded	46.63	92.83	91.33	36.23	95.33	83.00
5566	WT	2wk	9N	loaded	41.80	86.63	116.58	29.90	59.58	101.73
5549	WT	2wk	9N	loaded	80.75	76.23	95.28	50.33	104.85	67.73
5509	WT	6wk	9N	loaded	80.75	76.23	95.28	50.33	104.85	67.73
5512	WT	6wk	9N	loaded	50.13	62.15	77.25	71.88	37.15	107.83
5513	WT	6wk	9N	loaded	47.53	100.95	107.18	38.00	67.95	97.55
5514	WT	6wk	9N	loaded	54.83	60.93	102.75	64.80	94.03	100.58
5515	WT	6wk	9N	loaded	47.58	58.73	89.78	N/A	N/A	N/A
5517	WT	6wk	9N	loaded	66.60	62.83	72.15	49.23	87.63	96.73
5545	HET	1wk	4.5N	loaded	157.13	103.08	102.08	82.03	134.10	45.73
5561	HET	1wk	4.5N	loaded	101.38	131.33	119.95	105.00	121.53	70.80
5559	HET	1wk	4.5N	loaded	83.08	92.20	122.93	100.53	111.88	57.43
5558	HET	1wk	4.5N	loaded	75.90	94.98	117.30	58.20	97.15	95.25
5562	HET	1wk	4.5N	loaded	83.35	100.85	103.68	73.60	119.13	71.13
5565	HET	1wk	4.5N	loaded	82.55	124.00	116.90	74.70	78.88	81.18
5474	HET	2wk	4.5N	loaded	57.38	105.80	45.65	94.53	86.55	39.63

5475	HET	2wk	4.5N	loaded	86.48	79.68	84.77	37.85	82.43	70.83
5490	HET	2wk	4.5N	loaded	66.10	88.70	63.43	113.03	91.58	58.60
5491	HET	2wk	4.5N	loaded	90.80	96.35	103.10	111.58	80.33	51.50
5493	HET	2wk	4.5N	loaded	59.68	96.70	98.70	65.28	87.75	108.85
5531	HET	6wk	4.5N	loaded	107.80	108.75	82.03	76.30	94.68	43.60
5526	HET	6wk	4.5N	loaded	67.55	93.33	114.58	64.50	75.73	68.53
5527	HET	6wk	4.5N	loaded	93.68	114.78	50.13	82.65	94.98	96.78
5536	HET	6wk	4.5N	loaded	78.10	91.05	83.55	85.18	85.18	67.05
5544	HET	6wk	4.5N	loaded	79.38	96.13	71.03	101.18	92.15	75.28
5560	HET	6wk	4.5N	loaded	66.15	91.40	70.10	62.75	86.43	66.18
5564	HET	1wk	9N	loaded	45.45	94.08	70.70	54.88	94.93	89.08
5577	HET	1wk	9N	loaded	77.85	65.78	102.73	81.38	67.33	88.50
5574	HET	1wk	9N	loaded	67.28	65.80	121.50	72.98	82.53	110.53
5580	HET	1wk	9N	loaded	35.03	53.00	50.60	66.38	79.78	63.83
5573	HET	1wk	9N	loaded	83.83	85.13	38.33	58.75	120.85	70.28
5569	HET	1wk	9N	loaded	91.63	85.03	125.88	33.75	128.98	83.53
5482	HET	2wk	9N	loaded	78.55	100.03	115.73	61.58	95.48	68.35
5483	HET	2wk	9N	loaded	75.95	101.83	106.48	74.25	108.28	74.68
5520	HET	2wk	9N	loaded	74.98	72.10	107.03	52.70	93.25	86.95
5550	HET	2wk	9N	loaded	79.62	80.35	109.78	49.27	97.11	100.94
5551	HET	2wk	9N	loaded	67.53	83.35	114.80	64.70	82.05	115.63
5553	HET	2wk	9N	loaded	71.90	79.93	95.70	45.60	120.13	105.48
5510	HET	6wk	9N	loaded	65.53	76.25	101.28	61.30	76.90	101.38
5511	HET	6wk	9N	loaded	65.08	119.33	87.90	27.50	93.75	110.48
5516	HET	6wk	9N	loaded	56.80	89.58	96.95	39.60	78.83	77.15
5530	HET	6wk	9N	loaded	60.90	88.45	92.93	66.13	36.65	117.43
5533	HET	6wk	9N	loaded	62.83	93.45	89.58	64.23	95.58	100.23
5525	HET	6wk	9N	loaded	64.65	53.95	99.58	62.50	76.83	95.55

Osteophyte Measurements: Osteophyte size and maturity (mat) measured by Safranin O/Fast Green stain in wildtype (WT) and *cho*/+ (HET) mice. Size reported as absolute width (μm); maturity reported on a scale of 0 to 3. Measurements reported for largest osteophytes in the medial (M) tibial plateau.

ID	Genotype	Duration	Magnitude	Limb	Plateau	Size	Mat
5546	WT	1wk	4.5N	Loaded	M	0	0
5547	WT	1wk	4.5N	Loaded	M	0	0
5556	WT	1wk	4.5N	Loaded	M	0	0
5567	WT	1wk	4.5N	Loaded	M	0	0
5554	WT	1wk	4.5N	Loaded	M	0	0
5557	WT	1wk	4.5N	Loaded	M	0	0
5539	WT	2wk	4.5N	Loaded	M	0	0
5537	WT	2wk	4.5N	Loaded	M	0	0
5538	WT	2wk	4.5N	Loaded	M	0	0
5541	WT	2wk	4.5N	Loaded	M	0	0
5518	WT	2wk	4.5N	Loaded	M	0	0
5522	WT	2wk	4.5N	Loaded	M	0	0
5535	WT	6wk	4.5N	Loaded	M	0	0
5524	WT	6wk	4.5N	Loaded	M	0	0
5529	WT	6wk	4.5N	Loaded	M	0	0
5532	WT	6wk	4.5N	Loaded	M	0	0
5534	WT	6wk	4.5N	Loaded	M	0	0
5528	WT	6wk	4.5N	Loaded	M	0	0
5578	WT	1wk	9N	Loaded	M	66	1
5576	WT	1wk	9N	Loaded	M	74	1
5579	WT	1wk	9N	Loaded	M	50	1
5571	WT	1wk	9N	Loaded	M	52	1
5572	WT	1wk	9N	Loaded	M	102	1
5570	WT	1wk	9N	Loaded	M	144	1
5519	WT	2wk	9N	Loaded	M	290	1
5521	WT	2wk	9N	Loaded	M	685	1
5523	WT	2wk	9N	Loaded	M	363	1
5563	WT	2wk	9N	Loaded	M	136	2
5566	WT	2wk	9N	Loaded	M	379	2
5549	WT	2wk	9N	Loaded	M	365	1
5509	WT	6wk	9N	Loaded	M	1068	3
5512	WT	6wk	9N	Loaded	M	856	2
5513	WT	6wk	9N	Loaded	M	534	3
5514	WT	6wk	9N	Loaded	M	908	3
5515	WT	6wk	9N	Loaded	M	311	2

5517	WT	6wk	9N	Loaded	M	1013	3
5545	HET	1wk	4.5N	Loaded	M	0	0
5561	HET	1wk	4.5N	Loaded	M	0	0
5559	HET	1wk	4.5N	Loaded	M	0	0
5558	HET	1wk	4.5N	Loaded	M	0	0
5562	HET	1wk	4.5N	Loaded	M	0	0
5565	HET	1wk	4.5N	Loaded	M	0	0
5472	HET	2wk	4.5N	Loaded	M	0	0
5474	HET	2wk	4.5N	Loaded	M	0	0
5475	HET	2wk	4.5N	Loaded	M	0	0
5490	HET	2wk	4.5N	Loaded	M	0	0
5491	HET	2wk	4.5N	Loaded	M	0	0
5493	HET	2wk	4.5N	Loaded	M	0	0
5531	HET	6wk	4.5N	Loaded	M	0	0
5526	HET	6wk	4.5N	Loaded	M	0	0
5527	HET	6wk	4.5N	Loaded	M	0	0
5536	HET	6wk	4.5N	Loaded	M	0	0
5544	HET	6wk	4.5N	Loaded	M	0	0
5560	HET	6wk	4.5N	Loaded	M	0	0
5564	HET	1wk	9N	Loaded	M	97	2
5577	HET	1wk	9N	Loaded	M	164	1
5574	HET	1wk	9N	Loaded	M	57	1
5580	HET	1wk	9N	Loaded	M	125	1
5573	HET	1wk	9N	Loaded	M	65	1
5569	HET	1wk	9N	Loaded	M	76	1
5482	HET	2wk	9N	Loaded	M	172	2
5483	HET	2wk	9N	Loaded	M	402	1
5520	HET	2wk	9N	Loaded	M	94	2
5550	HET	2wk	9N	Loaded	M	447	2
5551	HET	2wk	9N	Loaded	M	303	2
5553	HET	2wk	9N	Loaded	M	318	2
5510	HET	6wk	9N	Loaded	M	772	3
5511	HET	6wk	9N	Loaded	M	1080	2
5516	HET	6wk	9N	Loaded	M	321	3
5530	HET	6wk	9N	Loaded	M	538	2
5533	HET	6wk	9N	Loaded	M	315	2
5525	HET	6wk	9N	Loaded	M	389	3

Subchondral Bone Plate MicroCT Data: Subchondral bone plate thickness (Th) and tissue mineral density (TMD) in the medial (Med) and lateral (Lat) aspects of the tibial plateau in wildtype (WT) and *cho*/+ (HET) mice.

					Med		Lat	
ID	Genotype	Duration	Magnitude	Limb	Th (mm)	TMD (mg HA/ccm)	Th (mm)	TMD (mg HA/ccm)
5546	WT	1 Week	4.5N	Control	0.096	912.4	0.082	892.2
5547	WT	1 Week	4.5N	Control	0.091	895.6	0.085	892.5
5554	WT	1 Week	4.5N	Control	0.103	951.8	0.09	915.1
5556	WT	1 Week	4.5N	Control	0.096	918.7	0.083	886
5557	WT	1 Week	4.5N	Control	0.099	925.5	0.082	899.3
5567	WT	1 Week	4.5N	Control	0.088	898.9	0.089	891.2
5546	WT	1 Week	4.5N	Loaded	0.09	923.1	0.08	897.4
5547	WT	1 Week	4.5N	Loaded	0.089	893.7	0.082	895
5554	WT	1 Week	4.5N	Loaded	0.113	966.4	0.084	928.4
5556	WT	1 Week	4.5N	Loaded	0.093	901.3	0.075	861.9
5557	WT	1 Week	4.5N	Loaded	0.099	933.9	0.085	903.1
5567	WT	1 Week	4.5N	Loaded	0.093	891	0.091	889.1
5561	HET	1 Week	4.5N	Control	0.092	917.1	0.09	913.3
5545	HET	1 Week	4.5N	Control	0.092	922.4	0.086	904.9
5559	HET	1 Week	4.5N	Control	0.091	903.8	0.082	897.4
5558	HET	1 Week	4.5N	Control	0.092	899.1	0.084	898.9
5565	HET	1 Week	4.5N	Control	0.098	904.7	0.092	907.5
5562	HET	1 Week	4.5N	Control	0.087	898.9	0.081	887.5
5561	HET	1 Week	4.5N	Loaded	0.104	929.5	0.084	898.4
5545	HET	1 Week	4.5N	Loaded	0.104	935.5	0.082	902.1
5559	HET	1 Week	4.5N	Loaded	0.096	913.8	0.081	881.3
5558	HET	1 Week	4.5N	Loaded	0.087	868.9	0.084	883.6
5565	HET	1 Week	4.5N	Loaded	0.099	895.5	0.09	898.1
5562	HET	1 Week	4.5N	Loaded	0.09	901.5	0.081	899.3
5537	WT	2 week	4.5N	Control	0.107	962.5	0.088	904.9
5538	WT	2 week	4.5N	Control	0.12	963.8	0.092	908.2
5539	WT	2 week	4.5N	Control	0.094	924.1	0.089	898
5541	WT	2 week	4.5N	Control	0.113	945.9	0.102	937.7
5518	WT	2 week	4.5N	Control	0.086	883.7	0.082	877
5522	WT	2 week	4.5N	Control	0.088	880.7	0.082	894.7
5537	WT	2 week	4.5N	Loaded	0.1	957.1	0.088	933.1
5538	WT	2 week	4.5N	Loaded	0.11	982.1	0.083	915.6
5539	WT	2 week	4.5N	Loaded	0.087	904.3	0.083	901.4
5541	WT	2 week	4.5N	Loaded	0.119	966.6	0.098	937
5518	WT	2 week	4.5N	Loaded	0.088	875.4	0.08	857.7

5522	WT	2 Week	4.5N	Loaded	0.084	887.5	0.081	879.8
5472	HET	2 week	4.5N	Control	0.091	931.2	0.078	898.7
5474	HET	2 week	4.5N	Control	0.092	903.8	0.08	884
5490	HET	2 week	4.5N	Control	0.107	964.1	0.086	935.1
5491	HET	2 week	4.5N	Control	0.097	926.3	0.086	905.4
5493	HET	2 week	4.5N	Control	0.097	923.4	0.083	907
5475	HET	2 week	4.5N	Control	0.102	925	0.087	901.3
5472	HET	2 week	4.5N	Loaded	0.093	901.7	0.082	883.8
5474	HET	2 week	4.5N	Loaded	0.084	903.2	0.073	888.3
5490	HET	2 week	4.5N	Loaded	0.109	949.7	0.083	924.7
5491	HET	2 week	4.5N	Loaded	0.089	906.6	0.087	910.8
5493	HET	2 week	4.5N	Loaded	0.096	903.4	0.091	905.9
5475	HET	2 week	4.5N	Loaded	0.107	934.6	0.084	913.5
5532	WT	6 Week	4.5N	Control	0.09	871.5	0.085	856.4
5534	WT	6 Week	4.5N	Control	0.095	961.8	0.085	923.2
5524	WT	6 Week	4.5N	Control	0.1	936.1	0.086	921.1
5535	WT	6 Week	4.5N	Control	0.105	963.3	0.089	937.2
5528	WT	6 Week	4.5N	Control	0.083	889.9	0.083	886.1
5529	WT	6 Week	4.5N	Control	0.087	891.4	0.078	879.2
5532	WT	6 Week	4.5N	Loaded	0.085	878.6	0.084	881.9
5534	WT	6 Week	4.5N	Loaded	0.098	926.9	0.088	906.9
5524	WT	6 Week	4.5N	Loaded	0.104	950.8	0.091	908.6
5535	WT	6 Week	4.5N	Loaded	0.102	928.4	0.087	895.4
5528	WT	6 Week	4.5N	Loaded	0.087	891	0.083	895.9
5529	WT	6 Week	4.5N	Loaded	0.084	884.4	0.08	864
5526	HET	6 Week	4.5N	Control	0.098	957.1	0.086	919.1
5527	HET	6 Week	4.5N	Control	0.106	933.8	0.092	911.6
5536	HET	6 Week	4.5N	Control	0.084	886.5	0.082	892.4
5544	HET	6 Week	4.5N	Control	0.099	911.7	0.086	893.7
5560	HET	6 Week	4.5N	Control	0.094	901.7	0.084	900.8
5531	HET	6 Week	4.5N	Control	0.089	881.9	0.081	888.7
5526	HET	6 Week	4.5N	Loaded	0.101	948.2	0.087	909.7
5527	HET	6 Week	4.5N	Loaded	0.102	914.1	0.077	896.6
5536	HET	6 Week	4.5N	Loaded	0.08	867	0.084	906.5
5544	HET	6 Week	4.5N	Loaded	0.092	915.5	0.082	899
5560	HET	6 Week	4.5N	Loaded	0.099	918.8	0.09	904.6
5531	HET	6 Week	4.5N	Loaded	0.09	879.7	0.083	901.2
5570	WT	1 Week	9N	Control	0.106	918.1	0.086	906.6
5571	WT	1 Week	9N	Control	0.112	948.3	0.095	905.2
5578	WT	1 Week	9N	Control	0.122	970.2	0.098	916.9

5576	WT	1 Week	9N	Control	0.116	969.4	0.103	924.5
5579	WT	1 Week	9N	Control	0.108	972.6	0.103	930.6
5572	WT	1 Week	9N	Control	0.104	958.5	0.087	921.4
5570	WT	1 Week	9N	Loaded	0.107	906.3	0.082	868.8
5571	WT	1 Week	9N	Loaded	0.116	955.5	0.1	917.8
5578	WT	1 Week	9N	Loaded	0.108	928.2	0.087	913.8
5576	WT	1 Week	9N	Loaded	0.117	955.2	0.099	916
5579	WT	1 Week	9N	Loaded	0.11	953	0.093	914.4
5572	WT	1 Week	9N	Loaded	0.108	912.9	0.086	862.1
5577	HET	1 Week	9N	Control	0.109	940.3	0.082	900.1
5580	HET	1 Week	9N	Control	0.086	931.9	0.091	915
5574	HET	1 Week	9N	Control	0.108	931.1	0.1	912.8
5573	HET	1 Week	9N	Control	0.103	952.5	0.087	902.1
5569	HET	1 Week	9N	Control	0.097	904.4	0.087	901.7
5564	HET	1 Week	9N	Control	0.09	883.8	0.087	917.5
5577	HET	1 Week	9N	Loaded	0.104	952.8	0.085	916.2
5580	HET	1 Week	9N	Loaded	0.102	939.1	0.095	922.6
5574	HET	1 Week	9N	Loaded	0.107	919	0.086	899.8
5573	HET	1 Week	9N	Loaded	0.108	922.7	0.09	901.3
5569	HET	1 Week	9N	Loaded	0.111	918.6	0.088	892
5564	HET	1 Week	9N	Loaded	0.097	921.53	0.087	913.6
5521	WT	2 Week	9N	Control	0.092	953.4	0.094	933.5
5519	WT	2 Week	9N	Control	0.084	877.6	0.081	874
5563	WT	2 Week	9N	Control	0.092	885.8	0.082	876.4
5566	WT	2 Week	9N	Control	0.083	869.4	0.077	873.9
5549	WT	2 Week	9N	Control	0.09	900.8	0.082	856.2
5523	WT	2 Week	9N	Control	0.104	971.5	0.096	945
5521	WT	2 Week	9N	Loaded	0.089	909.7	0.083	876.6
5519	WT	2 Week	9N	Loaded	0.074	851.9	0.069	845.7
5563	WT	2 Week	9N	Loaded	0.091	885.8	0.082	881.7
5566	WT	2 Week	9N	Loaded	0.087	858	0.081	865.6
5549	WT	2 Week	9N	Loaded	0.085	871.7	0.074	872.8
5523	WT	2 Week	9N	Loaded	0.094	906.7	0.075	876.8
5550	HET	2 Week	9N	Control	0.116	936	0.096	901.8
5551	HET	2 week	9N	Control	0.088	913.2	0.085	893.5
5553	HET	2 Week	9N	Control	0.097	897.6	0.083	880.4
5483	HET	2 Week	9N	Control	0.092	887.7	0.085	889.8
5482	HET	2 Week	9N	Control	0.099	938.2	0.091	910.8
5520	HET	2 Week	9N	Control	0.083	858.2	0.077	867.2
5550	HET	2 Week	9N	Loaded	0.081	854.9	0.075	853.6

5551	HET	2 Week	9N	Loaded	0.099	891.6	0.079	864.6
5553	HET	2 Week	9N	Loaded	0.082	855.2	0.077	863.3
5483	HET	2 Week	9N	Loaded	0.093	870.6	0.082	864.4
5482	HET	2 Week	9N	Loaded	0.103	914.5	0.087	903.9
5520	HET	2 Week	9N	Loaded	0.086	855.2	0.075	849.9
5509	WT	6 Week	9N	Control	0.088	877.1	0.075	879.1
5512	WT	6 Week	9N	Control	0.091	927.3	0.087	912.9
5513	WT	6 Week	9N	Control	0.093	897.6	0.089	893.9
5517	WT	6 Week	9N	Control	0.084	882.3	0.083	879.6
5514	WT	6 Week	9N	Control	0.09	926.2	0.086	902.5
5509	WT	6 Week	9N	Loaded	0.07	842.4	0.066	804.8
5512	WT	6 Week	9N	Loaded	0.087	871.7	0.078	874.4
5513	WT	6 Week	9N	Loaded	0.081	888.2	0.073	860.3
5517	WT	6 Week	9N	Loaded	0.083	889.2	0.072	828.4
5514	WT	6 Week	9N	Loaded	0.094	900.8	0.095	911.8
5510	HET	6 Week	9N	Control	0.093	910	0.081	879.3
5511	HET	6 Week	9N	Control	0.08	884	0.08	888.9
5516	HET	6 Week	9N	Control	0.085	880.2	0.082	900.4
5525	HET	6 Week	9N	Control	0.1	964.2	0.086	906.8
5533	HET	6 Week	9N	Control	0.093	888.6	0.088	894.8
5530	HET	6 Week	9N	Control	0.088	902	0.079	875.8
5510	HET	6 Week	9N	Loaded	0.071	816.4	0.07	860.4
5511	HET	6 Week	9N	Loaded	0.066	822.1	0.059	802.6
5516	HET	6 Week	9N	Loaded	0.078	846.1	0.082	858.5
5525	HET	6 Week	9N	Loaded	0.08	874.8	0.084	876.7
5533	HET	6 Week	9N	Loaded	0.075	839	0.07	814.8
5530	HET	6 Week	9N	Loaded	0.083	853.8	0.083	873.4

Epiphyseal Cancellous Bone MicroCT Data: Indices of cancellous bone architecture proximal to the growth plate in wildtype (WT) and *cho*/+ (HET) mice. Outcome measures: bone volume fraction (BV/TV), trabecular thickness (Tb.Th), trabecular separation (Tb.Sp), and tissue mineral density (TMD).

ID	Genotype	Duration	Magnitude	Limb	BV/TV	Tb.Th (mm)	Tb.Sp (mm)	TMD (mg HA/ccm)
5546	WT	1 Week	4.5N	Control	0.2643	0.0586	0.2137	935.59
5547	WT	1 Week	4.5N	Control	0.266	0.0548	0.1985	932.99
5554	WT	1 Week	4.5N	Control	0.2884	0.0551	0.1769	928.43
5556	WT	1 Week	4.5N	Control	0.2807	0.0608	0.2307	932.08
5557	WT	1 Week	4.5N	Control	0.2637	0.0533	0.1837	928.89
5567	WT	1 Week	4.5N	Control	0.3059	0.0529	0.1765	917.82
5546	WT	1 Week	4.5N	Loaded	0.2767	0.0575	0.2079	954.8
5547	WT	1 Week	4.5N	Loaded	0.2601	0.0541	0.199	945.42
5554	WT	1 Week	4.5N	Loaded	0.2984	0.0547	0.1819	946.14
5556	WT	1 Week	4.5N	Loaded	0.2567	0.0582	0.226	934.29
5557	WT	1 Week	4.5N	Loaded	0.2693	0.0525	0.1861	931.42
5567	WT	1 Week	4.5N	Loaded	0.3135	0.0532	0.176	935.46
5561	HET	1 Week	4.5N	Control	0.3318	0.0583	0.1883	933.12
5545	HET	1 Week	4.5N	Control	0.288	0.0583	0.1983	950.5
5559	HET	1 Week	4.5N	Control	0.2968	0.0556	0.1844	933.96
5558	HET	1 Week	4.5N	Control	0.2918	0.0571	0.1842	945.1
5565	HET	1 Week	4.5N	Control	0.3056	0.0574	0.1926	946.99
5562	HET	1 Week	4.5N	Control	0.2702	0.0531	0.1794	919.7
5561	HET	1 Week	4.5N	Loaded	0.3275	0.0585	0.1789	935.66
5545	HET	1 Week	4.5N	Loaded	0.2685	0.0575	0.2124	956.75
5559	HET	1 Week	4.5N	Loaded	0.2455	0.0515	0.203	931.75
5558	HET	1 Week	4.5N	Loaded	0.2759	0.0558	0.1935	932.34
5565	HET	1 Week	4.5N	Loaded	0.2824	0.0575	0.208	937.09
5562	HET	1 Week	4.5N	Loaded	0.2576	0.054	0.1904	938.72
5537	WT	2 week	4.5N	Control	0.3175	0.0581	0.1692	933.38
5538	WT	2 week	4.5N	Control	0.2511	0.0544	0.2078	932.01
5539	WT	2 week	4.5N	Control	0.3033	0.0522	0.1995	949.07
5541	WT	2 week	4.5N	Control	0.3753	0.0548	0.1693	949.92
5518	WT	2 week	4.5N	Control	0.2641	0.046	0.1924	910.98
5522	WT	2 week	4.5N	Control	0.2818	0.0486	0.1977	900.236
5537	WT	2 week	4.5N	Loaded	0.3353	0.0599	0.1646	942.04
5538	WT	2 week	4.5N	Loaded	0.2558	0.057	0.2165	940.54
5539	WT	2 week	4.5N	Loaded	0.27	0.0514	0.2081	943.47
5541	WT	2 week	4.5N	Loaded	0.3827	0.0546	0.1879	964.18
5518	WT	2 week	4.5N	Loaded	0.2324	0.0474	0.1965	900.562

5522	WT	2 week	4.5N	Loaded	0.2529	0.0458	0.197	924.588
5472	HET	2 week	4.5N	Control	0.2406	0.0504	0.1966	968.54
5474	HET	2 week	4.5N	Control	0.2507	0.0502	0.1953	946.33
5490	HET	2 week	4.5N	Control	0.2892	0.0462	0.2006	959.096
5491	HET	2 week	4.5N	Control	0.2844	0.0475	0.21	958.315
5493	HET	2 week	4.5N	Control	0.3247	0.0533	0.1807	954.278
5475	HET	2 week	4.5N	Control	0.2424	0.0438	0.2034	952.064
5472	HET	2 week	4.5N	Loaded	0.229	0.0495	0.2022	950.18
5474	HET	2 week	4.5N	Loaded	0.2365	0.047	0.1948	951.28
5490	HET	2 week	4.5N	Loaded	0.2437	0.047	0.2211	955.775
5491	HET	2 week	4.5N	Loaded	0.2743	0.0498	0.2056	964.891
5493	HET	2 week	4.5N	Loaded	0.3212	0.0523	0.1942	960.593
5475	HET	2 week	4.5N	Loaded	0.2426	0.0465	0.2024	943.925
5532	WT	6 Week	4.5N	Control	0.2405	0.051	0.1899	915.54
5534	WT	6 Week	4.5N	Control	0.3247	0.0624	0.1928	960.14
5524	WT	6 Week	4.5N	Control	0.2384	0.0555	0.2128	933.12
5535	WT	6 Week	4.5N	Control	0.2391	0.0542	0.2058	957.47
5528	WT	6 Week	4.5N	Control	0.2238	0.0539	0.2147	936.7
5529	WT	6 Week	4.5N	Control	0.2287	0.0498	0.2242	946.33
5532	WT	6 Week	4.5N	Loaded	0.2256	0.0507	0.1967	923.61
5534	WT	6 Week	4.5N	Loaded	0.2662	0.0537	0.2037	952.78
5524	WT	6 Week	4.5N	Loaded	0.2163	0.0511	0.2064	937.48
5535	WT	6 Week	4.5N	Loaded	0.2156	0.0515	0.1991	935.07
5528	WT	6 Week	4.5N	Loaded	0.2057	0.0503	0.2053	927.39
5529	WT	6 Week	4.5N	Loaded	0.2411	0.049	0.2159	931.23
5526	HET	6 Week	4.5N	Control	0.3108	0.0592	0.1968	946.53
5527	HET	6 Week	4.5N	Control	0.2523	0.0534	0.209	935.98
5536	HET	6 Week	4.5N	Control	0.2359	0.0523	0.1897	935.46
5544	HET	6 Week	4.5N	Control	0.1974	0.0504	0.2218	916.06
5560	HET	6 Week	4.5N	Control	0.2042	0.0548	0.2337	922.9
5531	HET	6 Week	4.5N	Control	0.2102	0.0529	0.2316	916.91
5526	HET	6 Week	4.5N	Loaded	0.2814	0.0592	0.2157	958.77
5527	HET	6 Week	4.5N	Loaded	0.2214	0.052	0.2128	930.71
5536	HET	6 Week	4.5N	Loaded	0.2075	0.0496	0.1914	933.64
5544	HET	6 Week	4.5N	Loaded	0.2038	0.0527	0.2286	939.89
5560	HET	6 Week	4.5N	Loaded	0.2443	0.0564	0.2049	950.11
5531	HET	6 Week	4.5N	Loaded	0.2112	0.0502	0.2032	922.57
5570	WT	1 Week	9N	Control	0.2691	0.0561	0.1934	925.24
5571	WT	1 Week	9N	Control	0.2609	0.0565	0.2081	915.08
5578	WT	1 Week	9N	Control	0.3169	0.061	0.1809	937.81

5576	WT	1 Week	9N	Control	0.2913	0.0571	0.1785	937.55
5579	WT	1 Week	9N	Control	0.3031	0.0557	0.2008	946.14
5572	WT	1 Week	9N	Control	0.2741	0.0542	0.1828	931.55
5570	WT	1 Week	9N	Loaded	0.2971	0.0571	0.1852	913.91
5571	WT	1 Week	9N	Loaded	0.2462	0.0568	0.2148	919.05
5578	WT	1 Week	9N	Loaded	0.2838	0.0571	0.1913	933.18
5576	WT	1 Week	9N	Loaded	0.2633	0.052	0.1915	917.95
5579	WT	1 Week	9N	Loaded	0.2752	0.0556	0.1878	928.3
5572	WT	1 Week	9N	Loaded	0.2833	0.0561	0.1872	912.15
5577	HET	1 Week	9N	Control	0.2644	0.0533	0.1871	926.02
5580	HET	1 Week	9N	Control	0.2982	0.0575	0.1825	939.3
5574	HET	1 Week	9N	Control	0.2953	0.0569	0.1838	935.96
5573	HET	1 Week	9N	Control	0.2744	0.0524	0.1788	913.58
5569	HET	1 Week	9N	Control	0.2528	0.0536	0.1959	926.02
5564	HET	1 Week	9N	Control	0.2839	0.0508	0.1904	930.12
5577	HET	1 Week	9N	Loaded	0.3036	0.0558	0.1873	936.44
5580	HET	1 Week	9N	Loaded	0.3281	0.0585	0.1856	930.71
5574	HET	1 Week	9N	Loaded	0.2592	0.0526	0.2048	890.93
5573	HET	1 Week	9N	Loaded	0.2642	0.0527	0.1868	936.7
5569	HET	1 Week	9N	Loaded	0.253	0.0521	0.1884	914.04
5564	HET	1 Week	9N	Loaded	0.3147	0.0553	0.1857	942.36
5521	WT	2 week	9N	Control	0.2714	0.056	0.2011	959.1
5519	WT	2 week	9N	Control	0.2299	0.0484	0.1836	914.04
5563	WT	2 week	9N	Control	0.3085	0.0532	0.1911	921.33
5566	WT	2 week	9N	Control	0.2445	0.048	0.2144	910.39
5549	WT	2 week	9N	Control	0.2346	0.0472	0.202	924
5523	WT	2 week	9N	Control	0.3323	0.0605	0.1984	973.3555
5521	WT	2 week	9N	Loaded	0.2257	0.0529	0.2044	895.22
5519	WT	2 week	9N	Loaded	0.165	0.0448	0.2015	885.26
5563	WT	2 week	9N	Loaded	0.2778	0.0508	0.1925	919.57
5566	WT	2 week	9N	Loaded	0.2384	0.0472	0.1997	890.73
5549	WT	2 week	9N	Loaded	0.2524	0.0489	0.197	908.9
5523	WT	2 week	9N	Loaded	0.2917	0.0526	0.1982	925.76
5550	HET	2 week	9N	Control	0.2664	0.0528	0.188	922.5
5551	HET	2 week	9N	Control	0.2157	0.0491	0.2015	919.77
5553	HET	2 week	9N	Control	0.2994	0.0504	0.1761	910.39
5483	HET	2 week	9N	Control	0.2606	0.0512	0.2068	941.256
5482	HET	2 week	9N	Control	0.304	0.0518	0.1987	978.043
5520	HET	2 week	9N	Control	0.2573	0.0473	0.1873	900.041
5550	HET	2 week	9N	Loaded	0.196	0.048	0.2032	891.19

5551	HET	2 week	9N	Loaded	0.2317	0.0514	0.1963	916.38
5553	HET	2 week	9N	Loaded	0.2337	0.0409	0.1789	867.94
5483	HET	2 week	9N	Loaded	0.2704	0.0479	0.2005	948.418
5482	HET	2 week	9N	Loaded	0.3111	0.0529	0.2106	959.877
5520	HET	2 week	9N	Loaded	0.2008	0.0472	0.2093	887.41
5509	WT	6 Week	9N	Control	0.2433	0.0537	0.2079	931.49
5512	WT	6 Week	9N	Control	0.2597	0.0575	0.2095	969.51
5513	WT	6 Week	9N	Control	0.238	0.0563	0.221	927.71
5515	WT	6 Week	9N	Control	0.2346	0.0514	0.2006	954.02
5517	WT	6 Week	9N	Control	0.2343	0.0528	0.2076	930.25
5514	WT	6 Week	9N	Control	0.2672	0.0523	0.2065	960.07
5509	WT	6 Week	9N	Loaded	0.1372	0.0514	0.2348	907.27
5512	WT	6 Week	9N	Loaded	0.1503	0.05	0.2378	894.38
5513	WT	6 Week	9N	Loaded	0.2396	0.0636	0.2027	916.77
5515	WT	6 Week	9N	Loaded	0.1491	0.0465	0.2317	892.16
5517	WT	6 Week	9N	Loaded	0.2047	0.0506	0.2098	920.29
5514	WT	6 Week	9N	Loaded	0.3418	0.0718	0.153	950.57
5510	HET	6 Week	9N	Control	0.2585	0.0555	0.199	918.79
5511	HET	6 Week	9N	Control	0.2147	0.0523	0.2141	937.35
5516	HET	6 Week	9N	Control	0.2407	0.0558	0.2226	923.87
5525	HET	6 Week	9N	Control	0.2583	0.0543	0.2037	944.06
5533	HET	6 Week	9N	Control	0.2558	0.0558	0.1968	931.36
5530	HET	6 Week	9N	Control	0.2548	0.0537	0.1951	940.28
5510	HET	6 Week	9N	Loaded	0.1651	0.048	0.2233	880.7
5511	HET	6 Week	9N	Loaded	0.1235	0.0482	0.239	863.32
5516	HET	6 Week	9N	Loaded	0.2492	0.0574	0.2099	894.57
5525	HET	6 Week	9N	Loaded	0.1785	0.05	0.2104	908.25
5533	HET	6 Week	9N	Loaded	0.1606	0.0487	0.2115	887.08
5530	HET	6 Week	9N	Loaded	0.2252	0.0572	0.2009	898.74

Metaphyseal Cancellous Bone MicroCT Data: Indices of cancellous bone architecture distal to the growth plate in wildtype (WT) and *cho*/+ (HET) mice. Outcome measures: bone volume fraction (BV/TV), trabecular thickness (Tb.Th), trabecular separation (Tb.Sp), and tissue mineral density (TMD).

ID	Genotype	Duration	Magnitude	Limb	BV/TV	Tb.Th (mm)	Tb.Sp (mm)	TMD (mg HA/ccm)
5546	WT	1 Week	4.5N	Control	0.0744	0.046	0.288	808.561
5547	WT	1 Week	4.5N	Control	0.0826	0.0467	0.2748	786.749
5554	WT	1 Week	4.5N	Control	0.1564	0.0624	0.273	851.3392
5556	WT	1 Week	4.5N	Control	0.153	0.0625	0.2403	850.2323
5557	WT	1 Week	4.5N	Control	0.1309	0.0523	0.2501	844.307
5567	WT	1 Week	4.5N	Control	0.0969	0.0488	0.2438	760.575
5546	WT	1 Week	4.5N	Loaded	0.0859	0.0494	0.2603	852.315
5547	WT	1 Week	4.5N	Loaded	0.0801	0.0458	0.2759	822.56
5554	WT	1 Week	4.5N	Loaded	0.1685	0.0628	0.2558	853.0972
5556	WT	1 Week	4.5N	Loaded	0.1352	0.0585	0.2468	833.564
5557	WT	1 Week	4.5N	Loaded	0.1379	0.0531	0.2467	845.414
5567	WT	1 Week	4.5N	Loaded	0.0911	0.0441	0.2537	823.472
5561	HET	1 Week	4.5N	Control	0.0953	0.0501	0.2723	836.754
5545	HET	1 Week	4.5N	Control	0.1105	0.06	0.2823	850.7532
5559	HET	1 Week	4.5N	Control	0.1101	0.0483	0.2624	801.725
5558	HET	1 Week	4.5N	Control	0.1237	0.055	0.264	823.407
5565	HET	1 Week	4.5N	Control	0.1348	0.0495	0.2318	826.402
5562	HET	1 Week	4.5N	Control	0.0951	0.0477	0.2574	809.733
5561	HET	1 Week	4.5N	Loaded	0.1197	0.0514	0.2462	828.29
5545	HET	1 Week	4.5N	Loaded	0.1053	0.0569	0.272	868.658
5559	HET	1 Week	4.5N	Loaded	0.1155	0.0533	0.2568	835.777
5558	HET	1 Week	4.5N	Loaded	0.1239	0.052	0.2412	823.537
5565	HET	1 Week	4.5N	Loaded	0.111	0.0489	0.2622	807.389
5562	HET	1 Week	4.5N	Loaded	0.1051	0.0481	0.2523	823.146
5537	WT	2 week	4.5N	Control	0.1811	0.056	0.2396	837.21
5538	WT	2 week	4.5N	Control	0.1301	0.0608	0.3268	834.9315
5539	WT	2 week	4.5N	Control	0.0937	0.0485	0.2888	840.335
5541	WT	2 week	4.5N	Control	0.1967	0.0609	0.284	832.1317
5518	WT	2 week	4.5N	Control	0.0741	0.0416	0.2513	792.349
5522	WT	2 week	4.5N	Control	0.0746	0.0455	0.269	801.139
5537	WT	2 week	4.5N	Loaded	0.1702	0.0566	0.2701	833.564
5538	WT	2 week	4.5N	Loaded	0.107	0.0531	0.3059	852.641
5539	WT	2 week	4.5N	Loaded	0.1104	0.0572	0.2968	828.29
5541	WT	2 week	4.5N	Loaded	0.1953	0.0623	0.2485	861.0406
5518	WT	2 week	4.5N	Loaded	0.0845	0.0481	0.2483	775.225

5522	WT	2 week	4.5N	Loaded	0.0833	0.0445	0.2633	822.886
5472	HET	2 week	4.5N	Control	0.0665	0.0438	0.2505	891.707
5474	HET	2 week	4.5N	Control	0.0765	0.04	0.2434	855.701
5490	HET	2 week	4.5N	Control	0.1181	0.0507	0.256	897.697
5491	HET	2 week	4.5N	Control	0.1	0.0433	0.2377	831.285
5493	HET	2 week	4.5N	Control	0.1556	0.0518	0.2304	837.601
5475	HET	2 week	4.5N	Control	0.084	0.0454	0.2615	866.054
5472	HET	2 week	4.5N	Loaded	0.077	0.0466	0.2429	892.488
5474	HET	2 week	4.5N	Loaded	0.0888	0.0469	0.2445	892.098
5490	HET	2 week	4.5N	Loaded	0.1021	0.0469	0.2599	876.211
5491	HET	2 week	4.5N	Loaded	0.1096	0.0466	0.2453	860.584
5493	HET	2 week	4.5N	Loaded	0.1404	0.0514	0.2343	842.614
5475	HET	2 week	4.5N	Loaded	0.0818	0.0452	0.2626	866.249
5532	WT	6 Week	4.5N	Control	0.0465	0.0451	0.3071	812.728
5534	WT	6 Week	4.5N	Control	0.1494	0.059	0.2738	833.499
5524	WT	6 Week	4.5N	Control	0.127	0.0547	0.2723	801.334
5535	WT	6 Week	4.5N	Control	0.1006	0.0502	0.2984	844.567
5528	WT	6 Week	4.5N	Control	0.0489	0.0451	0.323	824.318
5529	WT	6 Week	4.5N	Control	0.0574	0.045	0.306	831.09
5532	WT	6 Week	4.5N	Loaded	0.0575	0.0456	0.2948	812.403
5534	WT	6 Week	4.5N	Loaded	0.1142	0.0525	0.2985	831.61
5524	WT	6 Week	4.5N	Loaded	0.1523	0.0577	0.2526	838.317
5535	WT	6 Week	4.5N	Loaded	0.1131	0.0519	0.2831	846
5528	WT	6 Week	4.5N	Loaded	0.0584	0.0467	0.3556	814.617
5529	WT	6 Week	4.5N	Loaded	0.0577	0.0478	0.3018	810.775
5526	HET	6 Week	4.5N	Control	0.1346	0.0562	0.2638	841.898
5527	HET	6 Week	4.5N	Control	0.0817	0.046	0.293	808.757
5536	HET	6 Week	4.5N	Control	0.0874	0.048	0.2527	821.714
5544	HET	6 Week	4.5N	Control	0.0692	0.044	0.3089	776.137
5560	HET	6 Week	4.5N	Control	0.103	0.0486	0.2619	836.624
5531	HET	6 Week	4.5N	Control	0.0485	0.0469	0.3218	802.376
5526	HET	6 Week	4.5N	Loaded	0.1333	0.0575	0.2576	866.965
5527	HET	6 Week	4.5N	Loaded	0.0857	0.0463	0.2812	830.569
5536	HET	6 Week	4.5N	Loaded	0.084	0.0471	0.2619	847.497
5544	HET	6 Week	4.5N	Loaded	0.0701	0.049	0.2947	835.452
5560	HET	6 Week	4.5N	Loaded	0.0969	0.0492	0.255	851.664
5531	HET	6 Week	4.5N	Loaded	0.0401	0.0499	0.328	852.25
5570	WT	1 Week	9N	Control	0.1277	0.0502	0.2837	789.614
5571	WT	1 Week	9N	Control	0.1376	0.0613	0.3061	818.0679
5578	WT	1 Week	9N	Control	0.1983	0.0627	0.2911	853.618

5576	WT	1 Week	9N	Control	0.1619	0.0578	0.2768	827.834
5579	WT	1 Week	9N	Control	0.1835	0.0649	0.3304	839.4891
5572	WT	1 Week	9N	Control	0.1251	0.0596	0.2774	853.943
5570	WT	1 Week	9N	Loaded	0.1244	0.0493	0.2703	800.488
5571	WT	1 Week	9N	Loaded	0.1326	0.0591	0.3	829.006
5578	WT	1 Week	9N	Loaded	0.1412	0.05	0.286	804.069
5576	WT	1 Week	9N	Loaded	0.1512	0.0551	0.3025	800.683
5579	WT	1 Week	9N	Loaded	0.199	0.0627	0.2634	846.2606
5572	WT	1 Week	9N	Loaded	0.1144	0.0518	0.2829	806.869
5577	HET	1 Week	9N	Control	0.1306	0.0592	0.3164	815.137
5580	HET	1 Week	9N	Control	0.1384	0.0534	0.2981	814.682
5574	HET	1 Week	9N	Control	0.1655	0.0606	0.2661	809.9291
5573	HET	1 Week	9N	Control	0.1194	0.0599	0.2793	851.209
5569	HET	1 Week	9N	Control	0.1145	0.0523	0.323	796.256
5564	HET	1 Week	9N	Control	0.0849	0.0462	0.2664	823.146
5577	HET	1 Week	9N	Loaded	0.1332	0.0574	0.3	821.714
5580	HET	1 Week	9N	Loaded	0.1416	0.052	0.2706	821.649
5574	HET	1 Week	9N	Loaded	0.15	0.0575	0.2929	806.283
5573	HET	1 Week	9N	Loaded	0.1091	0.0615	0.2813	864.8821
5569	HET	1 Week	9N	Loaded	0.0955	0.0497	0.3424	814.031
5564	HET	1 Week	9N	Loaded	0.0996	0.0515	0.2723	840.921
5521	WT	2 week	9N	Control	0.1338	0.0612	0.3197	870.2211
5519	WT	2 week	9N	Control	0.0533	0.038	0.2715	836.168
5563	WT	2 week	9N	Control	0.1077	0.049	0.2467	819.891
5566	WT	2 week	9N	Control	0.0707	0.0423	0.2988	774.769
5549	WT	2 week	9N	Control	0.0605	0.0429	0.2827	818.393
5523	WT	2 week	9N	Control	0.1591	0.0625	0.2692	849.0604
5521	WT	2 week	9N	Loaded	0.1075	0.0511	0.3053	812.077
5519	WT	2 week	9N	Loaded	0.0739	0.0587	0.2895	836.363
5563	WT	2 week	9N	Loaded	0.1395	0.0617	0.2503	857.134
5566	WT	2 week	9N	Loaded	0.0804	0.0504	0.2885	815.658
5549	WT	2 week	9N	Loaded	0.0775	0.0549	0.2821	852.901
5523	WT	2 week	9N	Loaded	0.1347	0.0571	0.2727	820.932
5550	HET	2 week	9N	Control	0.1139	0.0506	0.2442	810.319
5551	HET	2 week	9N	Control	0.0752	0.0412	0.2596	777.799
5553	HET	2 week	9N	Control	0.1146	0.0479	0.239	770.928
5483	HET	2 week	9N	Control	0.0743	0.0437	0.2843	840.596
5482	HET	2 week	9N	Control	0.107	0.043	0.2396	858.892
5520	HET	2 week	9N	Control	0.0788	0.0453	0.259	784.926
5550	HET	2 week	9N	Loaded	0.0916	0.0534	0.2636	832.652

5551	HET	2 week	9N	Loaded	0.0921	0.0501	0.2677	817.416
5553	HET	2 week	9N	Loaded	0.1077	0.0479	0.2463	800.162
5483	HET	2 week	9N	Loaded	0.1073	0.0545	0.2663	874.583
5482	HET	2 week	9N	Loaded	0.1366	0.0566	0.2558	874.127
5520	HET	2 week	9N	Loaded	0.0943	0.0553	0.2633	816.44
5509	WT	6 Week	9N	Control	0.0645	0.0446	0.3148	801.009
5512	WT	6 Week	9N	Control	0.0579	0.0416	0.3679	826.532
5513	WT	6 Week	9N	Control	0.0816	0.0488	0.2884	785.578
5515	WT	6 Week	9N	Control	0.0703	0.0451	0.2918	871.783
5517	WT	6 Week	9N	Control	0.061	0.0424	0.3047	792.219
5514	WT	6 Week	9N	Control	0.0752	0.05	0.3121	850.492
5509	WT	6 Week	9N	Loaded	0.1003	0.06787	0.3131	867.0959
5512	WT	6 Week	9N	Loaded	0.1056	0.0762	0.2934	872.9557
5513	WT	6 Week	9N	Loaded	0.0932	0.0646	0.2951	850.3625
5515	WT	6 Week	9N	Loaded	0.0351	0.0615	0.3574	837.601
5517	WT	6 Week	9N	Loaded	0.0841	0.0625	0.3023	847.5628
5514	WT	6 Week	9N	Loaded	0.0814	0.064	0.3448	798.6651
5510	HET	6 Week	9N	Control	0.096	0.0434	0.2526	794.433
5511	HET	6 Week	9N	Control	0.0546	0.038	0.2757	827.964
5516	HET	6 Week	9N	Control	0.0758	0.0475	0.3016	786.033
5525	HET	6 Week	9N	Control	0.1133	0.0527	0.2818	833.043
5533	HET	6 Week	9N	Control	0.07	0.0482	0.3026	813.705
5530	HET	6 Week	9N	Control	0.0766	0.0451	0.2749	838.382
5510	HET	6 Week	9N	Loaded	0.1074	0.0555	0.2621	795.018
5511	HET	6 Week	9N	Loaded	0.0765	0.0589	0.2948	819.565
5516	HET	6 Week	9N	Loaded	0.1017	0.0599	0.2671	801.92
5525	HET	6 Week	9N	Loaded	0.1276	0.0629	0.292	829.918
5533	HET	6 Week	9N	Loaded	0.0782	0.0609	0.2925	822.4954
5530	HET	6 Week	9N	Loaded	0.1155	0.0592	0.2556	822.69

Metaphyseal Cortical Shell MicroCT Data: Metaphyseal cortical shell tissue mineral density (TMD) and thickness (Ct.Th) of the tibia in wildtype (WT) and *cho*/+ (HET) mice.

ID	Genotype	Duration	Magnitude	Limb	TMD (mg HA/ccm)	Ct.Th (mm)
5546	WT	1 Week	4.5N	Control	1024.076	0.165
5547	WT	1 Week	4.5N	Control	1019.063	0.154
5554	WT	1 Week	4.5N	Control	1019.128	0.172
5556	WT	1 Week	4.5N	Control	1014.961	0.173
5557	WT	1 Week	4.5N	Control	1004.999	0.155
5567	WT	1 Week	4.5N	Control	993.0187	0.16
5546	WT	1 Week	4.5N	Loaded	1011.054	0.156
5547	WT	1 Week	4.5N	Loaded	1021.667	0.155
5554	WT	1 Week	4.5N	Loaded	1023.165	0.17
5556	WT	1 Week	4.5N	Loaded	996.5347	0.169
5557	WT	1 Week	4.5N	Loaded	1006.106	0.153
5567	WT	1 Week	4.5N	Loaded	1012.877	0.155
5561	HET	1 Week	4.5N	Control	1002.981	0.168
5545	HET	1 Week	4.5N	Control	1009.036	0.166
5559	HET	1 Week	4.5N	Control	999.2693	0.154
5558	HET	1 Week	4.5N	Control	986.3775	0.146
5565	HET	1 Week	4.5N	Control	991.0655	0.168
5562	HET	1 Week	4.5N	Control	982.7964	0.152
5561	HET	1 Week	4.5N	Loaded	999.3996	0.164
5545	HET	1 Week	4.5N	Loaded	1013.008	0.164
5559	HET	1 Week	4.5N	Loaded	998.6834	0.154
5558	HET	1 Week	4.5N	Loaded	984.0987	0.149
5565	HET	1 Week	4.5N	Loaded	1008.189	0.151
5562	HET	1 Week	4.5N	Loaded	996.9905	0.145
5537	WT	2 week	4.5N	Control	1006.171	0.166
5538	WT	2 week	4.5N	Control	986.3775	0.151
5539	WT	2 week	4.5N	Control	993.4095	0.141
5541	WT	2 week	4.5N	Control	1009.882	0.16
5518	WT	2 week	4.5N	Control	963.3286	0.132
5522	WT	2 week	4.5N	Control	973.5508	0.141
5537	WT	2 week	4.5N	Loaded	1003.697	0.161
5538	WT	2 week	4.5N	Loaded	1011.119	0.157
5539	WT	2 week	4.5N	Loaded	1003.111	0.147
5541	WT	2 week	4.5N	Loaded	1028.634	0.175
5518	WT	2 week	4.5N	Loaded	952.1948	0.138
5522	WT	2 week	4.5N	Loaded	984.9451	0.139

5472	HET	2 week	4.5N	Control	992.1723	0.134
5474	HET	2 week	4.5N	Control	971.9882	0.126
5490	HET	2 week	4.5N	Control	999.8554	0.143
5491	HET	2 week	4.5N	Control	977.0668	0.137
5493	HET	2 week	4.5N	Control	1005.064	0.156
5475	HET	2 week	4.5N	Control	993.4745	0.139
5472	HET	2 week	4.5N	Loaded	970.5558	0.124
5474	HET	2 week	4.5N	Loaded	997.3161	0.131
5490	HET	2 week	4.5N	Loaded	975.8948	0.142
5491	HET	2 week	4.5N	Loaded	985.466	0.139
5493	HET	2 week	4.5N	Loaded	988.5262	0.149
5475	HET	2 week	4.5N	Loaded	982.0803	0.135
5532	WT	6 Week	4.5N	Control	977.0016	0.137
5534	WT	6 Week	4.5N	Control	999.5298	0.156
5524	WT	6 Week	4.5N	Control	985.6613	0.147
5535	WT	6 Week	4.5N	Control	1005.911	0.145
5528	WT	6 Week	4.5N	Control	985.1404	0.136
5529	WT	6 Week	4.5N	Control	971.0115	0.127
5532	WT	6 Week	4.5N	Loaded	970.8814	0.137
5534	WT	6 Week	4.5N	Loaded	980.3223	0.142
5524	WT	6 Week	4.5N	Loaded	982.5361	0.142
5535	WT	6 Week	4.5N	Loaded	1003.827	0.147
5528	WT	6 Week	4.5N	Loaded	997.6417	0.138
5529	WT	6 Week	4.5N	Loaded	975.9599	0.132
5526	HET	6 Week	4.5N	Control	1000.246	0.165
5527	HET	6 Week	4.5N	Control	986.3775	0.142
5536	HET	6 Week	4.5N	Control	963.0682	0.132
5544	HET	6 Week	4.5N	Control	963.5239	0.137
5560	HET	6 Week	4.5N	Control	995.4279	0.146
5531	HET	6 Week	4.5N	Control	965.2819	0.132
5526	HET	6 Week	4.5N	Loaded	1007.473	0.161
5527	HET	6 Week	4.5N	Loaded	990.6749	0.145
5536	HET	6 Week	4.5N	Loaded	986.8333	0.128
5544	HET	6 Week	4.5N	Loaded	974.5275	0.139
5560	HET	6 Week	4.5N	Loaded	993.6699	0.146
5531	HET	6 Week	4.5N	Loaded	955.7758	0.125
5570	WT	1 Week	9N	Control	991.1957	0.156
5571	WT	1 Week	9N	Control	988.982	0.156
5578	WT	1 Week	9N	Control	1006.757	0.163
5576	WT	1 Week	9N	Control	998.6182	0.165

5579	WT	1 Week	9N	Control	1016.133	0.16
5572	WT	1 Week	9N	Control	1010.078	0.161
5570	WT	1 Week	9N	Loaded	985.466	0.151
5571	WT	1 Week	9N	Loaded	990.805	0.171
5578	WT	1 Week	9N	Loaded	994.1907	0.157
5576	WT	1 Week	9N	Loaded	994.2559	0.169
5579	WT	1 Week	9N	Loaded	1010.989	0.169
5572	WT	1 Week	9N	Loaded	985.2707	0.163
5577	HET	1 Week	9N	Control	974.267	0.142
5580	HET	1 Week	9N	Control	997.5114	0.151
5574	HET	1 Week	9N	Control	990.805	0.153
5573	HET	1 Week	9N	Control	982.6663	0.152
5569	HET	1 Week	9N	Control	983.9034	0.154
5564	HET	1 Week	9N	Control	992.1723	0.148
5577	HET	1 Week	9N	Loaded	988.4611	0.16
5580	HET	1 Week	9N	Loaded	987.4844	0.158
5574	HET	1 Week	9N	Loaded	985.9218	0.176
5573	HET	1 Week	9N	Loaded	991.3911	0.158
5569	HET	1 Week	9N	Loaded	979.4759	0.158
5564	HET	1 Week	9N	Loaded	1009.752	0.167
5521	WT	2 week	9N	Control	1014.505	0.163
5519	WT	2 week	9N	Control	969.3839	0.126
5563	WT	2 week	9N	Control	998.8787	0.161
5566	WT	2 week	9N	Control	964.3703	0.135
5549	WT	2 week	9N	Control	976.611	0.131
5523	WT	2 week	9N	Control	980.4526	0.154
5521	WT	2 week	9N	Loaded	973.2905	0.168
5519	WT	2 week	9N	Loaded	953.1714	0.161
5563	WT	2 week	9N	Loaded	1011.64	0.181
5566	WT	2 week	9N	Loaded	967.5607	0.162
5549	WT	2 week	9N	Loaded	968.2119	0.15
5523	WT	2 week	9N	Loaded	1019.974	0.156
5550	HET	2 week	9N	Control	970.4256	0.134
5551	HET	2 week	9N	Control	949.5252	0.129
5553	HET	2 week	9N	Control	890.7308	0.113
5483	HET	2 week	9N	Control	984.5545	0.141
5482	HET	2 week	9N	Control	1000.116	0.144
5520	HET	2 week	9N	Control	926.8669	0.123
5550	HET	2 week	9N	Loaded	961.4404	0.151
5551	HET	2 week	9N	Loaded	947.572	0.143

5553	HET	2 week	9N	Loaded	968.5374	0.153
5483	HET	2 week	9N	Loaded	971.5976	0.151
5482	HET	2 week	9N	Loaded	985.9218	0.155
5520	HET	2 week	9N	Loaded	935.6916	0.138
5509	WT	6 Week	9N	Control	974.9182	0.148
5512	WT	6 Week	9N	Control	1004.608	0.139
5513	WT	6 Week	9N	Control	981.1037	0.154
5515	WT	6 Week	9N	Control	1011.185	0.132
5517	WT	6 Week	9N	Control	983.7081	0.135
5514	WT	6 Week	9N	Control	1015.482	0.143
5509	WT	6 Week	9N	Loaded	981.0385	0.153
5512	WT	6 Week	9N	Loaded	1002.981	0.166
5513	WT	6 Week	9N	Loaded	997.1859	0.187
5515	WT	6 Week	9N	Loaded	1017.565	0.132
5517	WT	6 Week	9N	Loaded	1014.505	0.188
5514	WT	6 Week	9N	Loaded	1000.441	0.167
5510	HET	6 Week	9N	Control	953.6271	0.129
5511	HET	6 Week	9N	Control	976.2204	0.122
5516	HET	6 Week	9N	Control	970.8814	0.137
5525	HET	6 Week	9N	Control	979.9317	0.142
5533	HET	6 Week	9N	Control	981.6246	0.138
5530	HET	6 Week	9N	Control	987.9402	0.138
5510	HET	6 Week	9N	Loaded	960.5939	0.159
5511	HET	6 Week	9N	Loaded	975.1135	0.158
5516	HET	6 Week	9N	Loaded	986.2474	0.173
5525	HET	6 Week	9N	Loaded	982.5361	0.166
5533	HET	6 Week	9N	Loaded	948.4835	0.147
5530	HET	6 Week	9N	Loaded	975.5693	0.161

Matrix metalloproteinase (MMP)-13 Immunostaining: MMP-13 levels in articular cartilage of the medial tibial plateau determined by immunohistochemistry with anti-MMP13 antibodies. MMP-13 levels reported as percentage of positive immunostaining per cartilage area.

ID	Genotype	Duration	Magnitude	Limb	Percent MMP13 per Cartilage Area
5579	WT	1wk	9.0N	Control	0.051044
5572	WT	1wk	9.0N	Control	1.944739
5579	WT	1wk	9.0N	Loaded	0.19419
5571	WT	1wk	9.0N	Loaded	0.268459
5572	WT	1wk	9.0N	Loaded	1.141847
5570	WT	1wk	9.0N	Loaded	1.656129
5574	HET	1wk	9.0N	Control	1.89645
5573	HET	1wk	9.0N	Control	1.595822
5564	HET	1wk	9.0N	Loaded	0.305861
5574	HET	1wk	9.0N	Loaded	0.011749
5580	HET	1wk	9.0N	Loaded	0.685305
5573	HET	1wk	9.0N	Loaded	3.1385
5523	WT	2wk	9.0N	Control	0.501446
5566	WT	2wk	9.0N	Control	0.528736
5523	WT	2wk	9.0N	Loaded	1.262565
5563	WT	2wk	9.0N	Loaded	0.47223
5566	WT	2wk	9.0N	Loaded	6.531734
5549	WT	2wk	9.0N	Loaded	1.722938
5520	HET	2wk	9.0N	Control	1.692745
5551	HET	2wk	9.0N	Control	2.388889
5520	HET	2wk	9.0N	Loaded	0.236063
5550	HET	2wk	9.0N	Loaded	1.602997
5551	HET	2wk	9.0N	Loaded	3.855533
5553	HET	2wk	9.0N	Loaded	0.423343

Discoidin Domain Receptor (DDR)-2 Immunostaining: DDR-2 levels in articular cartilage of the medial tibial plateau determined by immunohistochemistry with anti-DDR2 antibodies. DDR-2 levels reported as percentage of positive immunostaining per cartilage area.

ID	Genotype	Duration	Magnitude	Limb	Percent DDR2 per Cartilage Area
5578	WT	1wk	9.0N	Control	0.094971
5572	WT	1wk	9.0N	Control	2.596529
5570	WT	1wk	9.0N	Control	0.23227
5578	WT	1wk	9.0N	Loaded	3.90657
5572	WT	1wk	9.0N	Loaded	0.371918
5570	WT	1wk	9.0N	Loaded	1.138243
5564	HET	1wk	9.0N	Control	0.470486
5573	HET	1wk	9.0N	Control	0.081419
5569	HET	1wk	9.0N	Control	3.710968
5564	HET	1wk	9.0N	Loaded	1.320071
5573	HET	1wk	9.0N	Loaded	2.181808
5569	HET	1wk	9.0N	Loaded	0.208747
5519	WT	2wk	9.0N	Control	1.994681
5566	WT	2wk	9.0N	Control	0.206309
5549	WT	2wk	9.0N	Control	0.047784
5519	WT	2wk	9.0N	Loaded	0.098778
5566	WT	2wk	9.0N	Loaded	1.582475
5549	WT	2wk	9.0N	Loaded	1.626953
5482	HET	2wk	9.0N	Control	7.455687
5551	HET	2wk	9.0N	Control	2.272
5553	HET	2wk	9.0N	Control	1.095361
5482	HET	2wk	9.0N	Loaded	0.087044
5551	HET	2wk	9.0N	Loaded	0.749114
5553	HET	2wk	9.0N	Loaded	0.010569

Chondrocyte apoptosis: Chondrocyte apoptosis determined by TUNEL assay in articular cartilage in the medial tibial plateau. Chondrocyte apoptosis reported as percent positive TUNEL staining per DAPI area.

ID	Genotype	Duration	Magnitude	Limb	Percent TUNEL per DAPI Area
5578	WT	1wk	9.0N	control	0.091463
5579	WT	1wk	9.0N	control	0.85443
5572	WT	1wk	9.0N	control	0.626374
5578	WT	1wk	9.0N	loaded	0.367647
5576	WT	1wk	9.0N	loaded	1.13913
5579	WT	1wk	9.0N	loaded	2.449275
5571	WT	1wk	9.0N	loaded	1.679245
5572	WT	1wk	9.0N	loaded	1.736364
5570	WT	1wk	9.0N	loaded	0.066116
5574	HET	1wk	9.0N	control	1.506944
5573	HET	1wk	9.0N	control	0.023077
5569	HET	1wk	9.0N	control	0
5564	HET	1wk	9.0N	loaded	0.666667
5577	HET	1wk	9.0N	loaded	0.431034
5574	HET	1wk	9.0N	loaded	2.945455
5580	HET	1wk	9.0N	loaded	1
5573	HET	1wk	9.0N	loaded	1.344262
5569	HET	1wk	9.0N	loaded	0.28169
5519	WT	2wk	9.0N	control	0.18239
5523	WT	2wk	9.0N	control	1.53211
5566	WT	2wk	9.0N	control	0.384058
5519	WT	2wk	9.0N	loaded	0.478632
5521	WT	2wk	9.0N	loaded	0.620253
5523	WT	2wk	9.0N	loaded	2.917647
5563	WT	2wk	9.0N	loaded	0.181818
5566	WT	2wk	9.0N	loaded	0.495413
5549	WT	2wk	9.0N	loaded	0.394737
5482	HET	2wk	9.0N	control	1.623288
5520	HET	2wk	9.0N	control	0.056818
5551	HET	2wk	9.0N	control	0.261538
5482	HET	2wk	9.0N	loaded	0.963768
5483	HET	2wk	9.0N	loaded	4.140496
5520	HET	2wk	9.0N	loaded	0.719512
5550	HET	2wk	9.0N	loaded	0.175926
5551	HET	2wk	9.0N	loaded	1.378378
5553	HET	2wk	9.0N	loaded	3.207547

Modified Mankin Score: Mankin scoring of articular cartilage measured by Safranin O/Fast Green stain for wildtype (WT) and *cho*/+ (HET) mice. Individual and average scores reported for articular cartilage in the medial and lateral tibial plateaus.

ID	Genotype	Duration	Magnitude	Limb	Medial	Lateral	Average
5578	WT	1wk	9N	control	4	4.222222	4.111111
5576	WT	1wk	9N	control	4.2	4.2	4.2
5579	WT	1wk	9N	control	3.111111	3.555556	3.333333
5571	WT	1wk	9N	control	2.333333	2.375	2.354167
5572	WT	1wk	9N	control	3	3.571429	3.285714
5570	WT	1wk	9N	control	2.6	3.2	2.9
5519	WT	2wk	9N	control	2.75	4.142857	3.446429
5521	WT	2wk	9N	control	3.375	4.222222	3.798611
5523	WT	2wk	9N	control	2.636364	3.454545	3.045455
5563	WT	2wk	9N	control	3.111111	4.222222	3.666667
5566	WT	2wk	9N	control	2.777778	3.25	3.013889
5549	WT	2wk	9N	control	2.888889	3.333333	3.111111
5509	WT	6wk	9N	control	4	4.625	4.3125
5512	WT	6wk	9N	control	3.545455	4.1	3.822727
5513	WT	6wk	9N	control	3.076923	3	3.038462
5514	WT	6wk	9N	control	2.363636	3.5	2.931818
5515	WT	6wk	9N	control	3.4	4.375	3.8875
5517	WT	6wk	9N	control	3.454545	4	3.727273
5564	HET	1wk	9N	control	3.888889	4.2	4.044444
5577	HET	1wk	9N	control	5.666667	5.142857	5.404762
5574	HET	1wk	9N	control	3.428571	4.166667	3.797619
5580	HET	1wk	9N	control	3.714286	3	3.357143
5573	HET	1wk	9N	control	4	3.75	3.875
5569	HET	1wk	9N	control	4.125	3.5	3.8125
5482	HET	2wk	9N	control	3.727273	4.5	4.113636
5483	HET	2wk	9N	control	4.090909	4.8	4.445455
5520	HET	2wk	9N	control	3.666667	3.75	3.708333
5550	HET	2wk	9N	control	3.444444	4.125	3.784722
5551	HET	2wk	9N	control	3.5	3.5	3.5
5553	HET	2wk	9N	control	4.666667	4.666667	4.666667
5510	HET	6wk	9N	control	4.333333	4.6	4.466667
5511	HET	6wk	9N	control	2.75	3.555556	3.152778
5516	HET	6wk	9N	control	3.818182	4	3.909091
5530	HET	6wk	9N	control	4.307692	4.2	4.253846
5533	HET	6wk	9N	control	2.714286	3.333333	3.02381

5525	HET	6wk	9N	control	3.461538	3.75	3.605769

APPENDIX B: CHAPTER 3 DATA

Histological (OARSI) Score: OARSI scoring of articular cartilage damage measured by Safranin O/Fast Green stain. Each column corresponds to a slide separated at a 90 μm interval. Scores reported for articular cartilage in the medial (M) and lateral (L) tibial plateaus.

ID	Group	Plateau	1	7	13	19	25	31	37	43	49	55	61	67	73	79	85	91	Average	Max
B1L	control	M		0	0	0	0	1	0.5	1	0	0	0	0.5					0.272727	1
		L	0.5	0.5	0.5	1	0	0	0	0.5									0.375	1
B2L	control	M		0	0	0	0	0	0	0.5	1	0.5	0	0.5					0.227273	1
		L	0	0.5	1	1	0.5	1	1	0	0	0.5							0.55	1
B3L	control	M		0	0	0	0	0	0	1	0	1	0	0					0.181818	1
		L	0	0.5	0.5	0.5	0	0	0	0	0								0.166667	0.5
F1R	control	M		0	0.5	0	0	0	1	1	2	0	0	0.5	0				0.416667	2
		L	0	1	2	1	1	1	1		0	0	0.5						0.75	2
F2R	control	M	0.5	0	0	0	0	0.5	1	0.5	1	0	0	0.5					0.333333	1
		L	0	2	2	2	2	0.5	0.5	1	0	0	0.5						0.954545	2
B1R	saline	M				0.5	0.5	0	0	0	0	0	0.5	0	0.5	0			0.181818	0.5
		L			3	0.5	0	1	0.5	0	0.5	0	0.5	0					0.6	3
B2R	saline	M		0.5	0	0	0	0	0	0	0.5	0.5	0	0.5					0.181818	0.5
		L			0.5	3	1	0.5	0.5	2	0.5	0	0	0					0.8	3
B3R	saline	M				5	5	4	4	1	0	0	0	0	0	0.5			1.772727	5
		L				3	1	0	1	0.5	0.5	0	0	0.5					0.722222	3
F1L	saline	M				6	5	5	5	6	5	3	0	2	0	0	0		3.083333	6
		L				6	5	4	2	1	0.5	0.5	1	0.5	0	0			1.863636	6
F2L	saline	M						5	5	5	5	4	3	2	0	0.5			3.277778	5
		L				5	4	2	2	1	0.5	0.5	0.5	0					1.722222	5
D1R	bolus	M				4	4	4	3	3	0	0	0.5	0	0.5				1.9	4
		L					4	1	2	0.5	0	0	0.5	0	0				0.888889	4
D2R	bolus	M								5	5	4	4	3	3	2	1	0	3	5
		L					3	4	3	3	2	1	1	1	0				2	4
D3R	bolus	M			6	6	2	0	0	0	0	0	0	0	0.5				1.318182	6
		L		0	0	0.5	1	0.5	0.5	0	0	0	0						0.25	1
H1L	bolus	M						4	4	3	0.5	0	0	0	0	0	0.5	0	1.090909	4
		L				3	2	0.5	0.5	0	0.5	0	0	0.5					0.777778	3
H2L	bolus	M					5	5	5	4	2	1	2	0	0.5	0			2.45	5
		L		6	4	2	1	1	2	2	0.5	0.5							2.111111	6
C1R	NPs	M						5	5	4	4	3	2	2					3.571429	5
		L			0.5	4	3	2	1	0.5	0.5	0.5	0.5	0					1.25	4
C2R	NPs	M			5	5	2	0	0	0	0	0	0.5	0	0.5				1.181818	5
		L						6	2	2	0	0	0.5	1	0.5				1.5	6
C3R	NPs	M		5	4	4	4	3	3	0	0.5	0.5	0	0.5					2.227273	5

		L	4	3	1	2	1	1	1	0	0								1.444444	4
G1L	NPs	M				5	5	4	3	3	0	0	0	0	0	0	0.5		1.708333	5
		L			2	2	2	2	0	1	1	1	0	0					1.1	2
G2L	NPs	M						5	5	5	4	3	3	2	0	0.5	0.5		2.8	5
		L			3	3	2	2	0.5	0.5	0.5	0.5							1.5	3
A1R	gel+NPs	M		2	3	0	0	0	0	0	0.5	0.5	0.5	0.5	0				0.583333	3
		L			0	0	0.5	0.5	0.5	0.5	1	0.5	0.5	0.5					0.45	1
A2R	gel+NPs	M							6	6	5	2	0	0	0.5	0	0.5		2.222222	6
		L								6	4	1	2	1	0	0.5	0.5		1.875	6
A3R	gel+NPs	M			0.5	0	0	0	0	0	0	0	0	0.5	0	0			0.083333	0.5
		L	0.5	0	0	0.5	0.5	0.5	1	0	0.5	0							0.35	1
E1L	gel+NPs	M					4	4	3	3	2	0	0	0.5	0.5	0.5			1.75	4
		L	3	2	0.5	1	0	0.5	0.5	0									0.9375	3
E2L	gel+NPs	M		4	3	0	0	0.5	0	0	0.5	0.5							0.944444	4
		L						2	2	0.5	1	0	0	1	1				0.9375	2
I1R	gel only	M				6	5	4	0.5	0	0	0.5	0	0	0.5				1.65	6
		L			4	2	2	2	0.5	0.5	1	0	0.5	0					1.25	4
I2R	gel only	M						0.5	0	0	0	0	0	1	5	6			1.388889	6
		L		0	0	0.5	0	1	0	0.5	2	0	4						0.8	4
I3R	gel only	M	3	0	0	0.5	0	0	0	0.5	0	0.5	0.5	0					0.416667	3
		L		3	0.5	1	1	0.5	0.5	1	0.5	0.5	0	0					0.772727	3
G4L	gel only	M							0	0	0	0	0	0	0.5	0.5	0.5		0.166667	0.5
		L			3	2	1	1	0.5	0.5	0	0.5	0.5						1	3
H4L	gel only	M					3	0	0	0	0.5	1	0	0.5	0.5				0.611111	3
		L			3	2	2	2	0.5	1	1	2	0.5	0.5					1.45	3

Osteophyte Measurements: Osteophyte size and maturity (mat) measured by Safranin O/Fast Green stain. Size reported as absolute width (μm); maturity reported on a scale of 0 to 3. Measurements reported for osteophytes in the posterior (post), middle (mid), and anterior (ant) regions of the medial (M) tibial plateau, and average (avg) of all three regions.

						post		mid		ant		avg	
ID	Group	Plateau	post	mid	ant	Size	Mat	Size	Mat	Size	Mat	Size	Mat
B1L	control	M	13	37	61	0	0	0	0	0	0	0	0
B2L	control	M	13	37	61	0	0	0	0	0	0	0	0
B3L	control	M	13	37	61	0	0	0	0	0	0	0	0
F1R	control	M	13	37	67	0	0	0	0	0	0	0	0
F2R	control	M	7	31	61	0	0	0	0	0	0	0	0
B1R	saline	M	25	49	73	248.3	1	225.4	1	210.7	2	228.1333	1.333333
B2R	saline	M	13	37	61	43.9	1	81.4	1	62.9	1	62.73333	1
B3R	saline	M	25	49	73	454.2	1	286	1	160.8	2	300.3333	1.333333
F1L	saline	M	25	49	79	498.7	1	413.3	1	309.9	2	407.3	1.333333
F2L	saline	M	37	55	73	386	1	344.3	1	335.9	2	355.4	1.333333
D1R	bolus	M	25	43	67	221.2	1	175.3	1	96.1	1	164.2	1
D2R	bolus	M	49	67	85	391.8	1	367.3	1	358.9	1	372.6667	1
D3R	bolus	M	19	43	67	277.5	1	288.2	1	219.1	1	261.6	1
H1L	bolus	M	37	61	85	296.4	1	232.2	2	208.7	1	245.7667	1.333333
H2L	bolus	M	31	49	73	248.3	1	237.9	1	180.4	1	222.2	1
C1R	NPs	M	37	49	61	309.8	1	248.3	1	240.1	1	266.0667	1
C2R	NPs	M	19	43	67	196.2	1	171.2	2	0	0	122.4667	1
C3R	NPs	M	13	37	61	286	1	306.7	1	240	1	277.5667	1
G1L	NPs	M	25	49	79	233.7	1	156.5	1	31.3	1	140.5	1
G2L	NPs	M	37	55	79	415.6	1	277.2	1	429.9	2	374.2333	1.333333
A1R	gel+NPs	M	13	43	67	194.5	1	81.5	1	0	0	92	0.666667
A2R	gel+NPs	M	43	61	79	202.6	1	175.3	2	200.3	2	192.7333	1.666667
A3R	gel+NPs	M	19	49	73	110.6	1	52.2	1	0	0	54.26667	0.666667
E1L	gel+NPs	M	31	49	73	211	1	150.4	1	225.4	2	195.6	1.333333
E2L	gel+NPs	M	13	31	49	81.5	1	233.8	2	35.5	1	116.9333	1.333333
I1R	gel only	M	25	43	67	356.8	1	273.5	1	211	1	280.4333	1
I2R	gel only	M	73	55	37	400.7	1	210.9	2	113.2	2	241.6	1.666667
I3R	gel only	M	7	31	61	136.3	1	59.9	2	62.6	1	86.26667	1.333333
G4L	gel only	M	43	61	79	121.3	1	185.7	1	200.3	2	169.1	1.333333
H4L	gel only	M	31	49	67	41.7	1	102.2	1	194.1	2	112.6667	1.333333

Synovitis Scoring: Synovitis scores reflecting thickness and cell density of the synovium measured by Safranin O/Fast Green stain. Measurements reported for synovium in the posterior (post), middle (mid), and anterior (ant) regions of the medial (M) tibial plateau, and average (avg) of all three regions.

ID	Group	Plateau	post	mid	ant	post	mid	ant	avg
B1L	control	M	13	37	61	1	0	2	1
B2L	control	M	13	37	61	1	1	0	0.666667
B3L	control	M	13	37	61	0	0	0	0
F1R	control	M	13	37	67	1	1	0	0.666667
F2R	control	M	7	31	61	0	0	0	0
B1R	saline	M	25	49	73	2	3	5	3.333333
B2R	saline	M	13	37	61		2	5	3.5
B3R	saline	M	25	49	73	4	4	3	3.666667
F1L	saline	M	25	49	79	4	3	4	3.666667
F2L	saline	M	37	55	73	5	5		5
D1R	bolus	M	25	43	67	4	2	1	2.333333
D2R	bolus	M	49	67	85	3	5	4	4
D3R	bolus	M	19	43	67		3	5	4
H1L	bolus	M	37	61	85		3	4	3.5
H2L	bolus	M	31	49	73	5	4	3	4
C1R	NPs	M	37	49	61	2	5	3	3.333333
C2R	NPs	M	19	43	67	5	5	3	4.333333
C3R	NPs	M	13	37	61	5	5	5	5
G1L	NPs	M	25	49	79	3	5	5	4.333333
G2L	NPs	M	37	55	79	5	4	4	4.333333
A1R	gel+NPs	M	13	43	67	5	4	5	4.666667
A2R	gel+NPs	M	43	61	79	3	4	4	3.666667
A3R	gel+NPs	M	19	49	73	3	2		2.5
E1L	gel+NPs	M	31	49	73	5	5	4	4.666667
E2L	gel+NPs	M	13	31	49	4	3	4	3.666667
I1R	gel only	M	25	43	67	4	3	3	3.333333
I2R	gel only	M	73	55	37				
I3R	gel only	M	7	31	61	3	3		3
G4L	gel only	M	43	61	79	2	3	4	3
H4L	gel only	M	31	49	67	3	4	4	3.666667

Particle Release and Mechanical Properties of Hydrogels following *In Vitro* Dynamic Cyclic Compression: Particle release measured by flow cytometry. Storage and loss modulus (Pa) measured by rheometry.

Gel ID	PEG-MAL wt%	Loading Condition	% Particle Release	Storage Modulus	Loss Modulus
1	2.50%	Control	31	109.5685	7.10443
2	2.50%	Control	1	234.09575	10.521875
3	2.50%	Control	5	205.06125	19.411
4	2.50%	Control	0	219.99925	8.0105225
5	2.50%	Control	0	151.633	6.1430225
6	2.50%	Control	9	107.9185	3.2986025
7	5%	Control	0	1793.5225	56.125275
8	5%	Control	0	780.268	37.3024
9	5%	Control	0	1066.3	52.4038
10	5%	Control	0	651.68375	47.6812
11	5%	Control	0	439.9895	22.84645
12	5%	Control	0	443.216	27.06755
13	10%	Control	0	1934.3025	62.281725
14	10%	Control	0	1944.8275	77.077275
15	10%	Control	0	1531.13	61.057725
16	10%	Control	3	1054.2125	121.31625
17	10%	Control	0	782.673	49.832575
18	10%	Control	22	1191.08	73.99235
19	20%	Control	1	860.909	501.694
20	20%	Control	0	1390.175	499.60025
21	20%	Control	0	1125.11	494.10725
22	20%	Control	0	1296.735	400.52125
23	20%	Control	0	2422.695	1228.165
24	20%	Control	0	765.08075	312.866
25	2.50%	20% Strain	16	361.5945	25.670525
26	2.50%	20% Strain	15	262.497	13.038625
27	2.50%	20% Strain	21	264.475	10.848475
28	2.50%	20% Strain	29	184.1305	9.1982275
29	2.50%	20% Strain	39	176.25875	9.2238275
30	2.50%	20% Strain	36	148.66275	6.9662575
31	5%	20% Strain	3	766.79325	36.0171
32	5%	20% Strain	8	647.32275	24.33475
33	5%	20% Strain	2	845.3625	31.95695
34	5%	20% Strain	5	306.24075	9.4040775
35	5%	20% Strain	15	568.49	27.00565
36	5%	20% Strain	14	482.4935	22.748025

37	10%	20% Strain	9	1205.14	128.42025
38	10%	20% Strain	0	1378.545	75.829375
39	10%	20% Strain	4	1818.915	71.967125
40	10%	20% Strain	11	1980.9825	77.669725
41	10%	20% Strain	13	1232.0825	52.697625
42	10%	20% Strain	9	1048.82	63.419125
43	20%	20% Strain	0	684.71525	433.7
44	20%	20% Strain	0	1897.7425	551.4145
45	20%	20% Strain	0	3632.6475	683.171
46	20%	20% Strain	0	2496.5	224.682
47	20%	20% Strain	1	2020.0825	1040.1
48	20%	20% Strain	0	3386.8775	302.87775
49	2.50%	40% Strain	26	150.731	6.4832325
50	2.50%	40% Strain	12	239.00925	11.47355
51	2.50%	40% Strain	18	194.2005	11.6767
52	2.50%	40% Strain	12	184.763	10.12335
53	2.50%	40% Strain	36	173.298	7.896695
54	2.50%	40% Strain	26	129.11175	7.69943
55	5%	40% Strain	0	1941.3925	144.70975
56	5%	40% Strain	27	1219.0275	33.491775
57	5%	40% Strain	20	410.33075	19.937575
58	5%	40% Strain	27	427.542	30.25605
59	5%	40% Strain	0	1062.085	42.14945
60	5%	40% Strain	0	620.186	28.726525
61	10%	40% Strain	0	2256.8325	414.394
62	10%	40% Strain	0	1478.07	145.9215
63	10%	40% Strain	23	1609.4175	106.78125
64	10%	40% Strain	0	1744.3775	147.10525
65	10%	40% Strain	27	1416.145	235.47025
66	10%	40% Strain	23	1630.5775	129.11025
67	20%	40% Strain	34	1937.65	886.56075
68	20%	40% Strain	21	1762.9675	712.3045
69	20%	40% Strain	35	1135.3375	424.41925
70	20%	40% Strain	12	3108.75	414.6015
71	20%	40% Strain	1	2391.4575	1005.51825
72	20%	40% Strain	0	1928.5125	664.98175
73	2.50%	80% Strain	56	137.8735	10.3264375
74	2.50%	80% Strain	87	119.11625	4.5019475
75	2.50%	80% Strain	73	57.488	2.4981525
76	2.50%	80% Strain	59	135.575	4.4262775

77	2.50%	80% Strain	58	179.5685	6.3305125
78	2.50%	80% Strain	44	93.6641	4.6108425
79	5%	80% Strain	45	615.432	42.38195
80	5%	80% Strain	59	532.34575	26.991475
81	5%	80% Strain	68	625.95375	18.56935
82	5%	80% Strain	69	555.031	21.80035
83	5%	80% Strain	55	513.10125	28.9666
84	5%	80% Strain	37	529.93025	24.592425
85	10%	80% Strain	45	1309.305	184.36275
86	10%	80% Strain	34	996.1095	58.632775
87	10%	80% Strain	43	1138.96	189.702
88	10%	80% Strain	15	1047.7125	61.315175
89	10%	80% Strain	44	1543.6125	81.6793
90	10%	80% Strain	28	774.38925	55.97795
91	20%	80% Strain	40	2588.6925	205.7315
92	20%	80% Strain	39	1809.9475	207.71225
93	20%	80% Strain	46	1119.655	325.2665
94	20%	80% Strain	78	1934.78	346.9705
95	20%	80% Strain	58	2231.435	121.0615
96	20%	80% Strain	67	2332.8425	234.938

Hydrogel Mass Changes and Swelling Ratio: Daily changes in hydrogel mass (g) in excess PBS and corresponding swelling ratios compared to initial mass.

Sample #	PEG-MAL wt%	Outcome	Day 0	Day 1	Day 2	Day 3	Day 4	Day 5	Day 6	Day 7	Day 8	Day 9	Day 10	Day 16
1	2.50%	Mass	38.5	46.7	46.7	47.2	47	48.8	46.6	46.7	44.7	44	41.9	38.5
2	2.50%	Mass	32	44.8	42.9	43.6	42.9	43.4	44.1	45.4	44.8	26.9	23.2	21.9
3	2.50%	Mass	36.4	47	44.5	43.5	44	43.9	43	46.9	46.8	42	36.4	29.5
4	2.50%	Mass	40.7	49	52.2	53.6	51.4	50.2	51.5	50.1	54.1	39	37.9	35.3
5	2.50%	Mass	31.2	36.8	39.5	34.1	34.6	31.2	35.7	34.8	32.9	34.7	30.7	30.8
6	2.50%	Mass	37.6	31.7	33	32.7	32.8	32.6	32.6	32.8	25.8	25.1	23.5	24.5
1	5%	Mass	39.6	63.7	69.2	69.5	73.1	76.4	69.1	69.1	77.7	70.6	78.9	72.2
2	5%	Mass	40.6	80.6	80.3	75.1	82.3	79.8	83.6	80.7	86.7	85.4	83.2	82.7
3	5%	Mass	42.6	72.9	77.7	83.5	88.2	83.9	84.4	85.8	81.9	84.2	78.8	76.5
4	5%	Mass	40.9	68.1	68.5	70.8	73.4	74.6	74.9	76.1	74.5	73	72.4	62.6
5	5%	Mass	42.7	77.4	78	78.9	82.1	78.6	90.5	85.5	81.4	83.1	85.1	76.4
6	5%	Mass	39.5	70.2	72.5	72.2	69.6	70.5	71.3	72.3	72.1	70.4	70.4	65.6
1	10%	Mass	37.1	99.3	107.4	112.6	115.3	108	118.8	127.6	109.1	120.5	124.5	116.9
2	10%	Mass	39.9	99.5	105.8	103.4	117	109.4	111.8	113.8	115.4	118.1	126	117.4
3	10%	Mass	39.2	111.6	115.1	124.8	121.1	122.1	131.6	128.7	122.2	126.6	123.7	121.2
4	10%	Mass	43.7	88.1	103.2	101.9	102.6	103.8	105.5	115	114.8	112.9	106.6	105.6
5	10%	Mass	42.9	98.3	102.4	104.7	101.8	106.1	108.8	106.2	106.6	110.1	100.6	104.4
6	10%	Mass	41.4	94.8	107.8	99.7	106.7	105.7	105.3	105.7	105.1	107.8	93.4	95.8
1	20%	Mass	39.1	128.7	144.7	151.3	154.5	154.9	151.1	150.3	147.4	152.5	149.6	174.4
2	20%	Mass	40	123.2	154.7	134.8	139.1	148	155	155.1	139	148.1	161.9	149.5
3	20%	Mass	41.5	141.1	159.4	152.7	158.3	149.2	159.1	166.1	165.7	170.8	170.9	169.2
4	20%	Mass	38.8	136.4	153.5	151.1	138.5	152.5	146.1	146.5	147.5	145.9	152.7	166.8
5	20%	Mass	40.6	151.5	168.1	154.6	154.4	166.8	153.2	159.3	166.4	148.3	168.4	153.2
6	20%	Mass	42.1	131.5	166.8	174.2	170.5	170.4	167.1	166.1	169.1	181.9	183.8	178
1	2.50%	Swelling Ratio	100.0	121.3	121.3	122.6	122.1	126.8	121.0	121.3	116.1	114.3	108.8	100.0
2	2.50%	Swelling Ratio	100.0	140.0	134.1	136.3	134.1	135.6	137.8	141.9	140.0	84.1	72.5	68.4
3	2.50%	Swelling Ratio	100.0	129.1	122.3	119.5	120.9	120.6	118.1	128.8	128.6	115.4	100.0	81.0
4	2.50%	Swelling Ratio	100.0	120.4	128.3	131.7	126.3	123.3	126.5	123.1	132.9	95.8	93.1	86.7
5	2.50%	Swelling Ratio	100.0	117.9	126.6	109.3	110.9	100.0	114.4	111.5	105.4	111.2	98.4	98.7
6	2.50%	Swelling Ratio	100.0	84.3	87.8	87.0	87.2	86.7	86.7	87.2	68.6	66.8	62.5	65.2
1	5%	Swelling Ratio	100.0	160.9	174.7	175.5	184.6	192.9	174.5	174.5	196.2	178.3	199.2	182.3
2	5%	Swelling Ratio	100.0	198.5	197.8	185.0	202.7	196.6	205.9	198.8	213.5	210.3	204.9	203.7

3	5%	Swelling Ratio	100.0	171.1	182.4	196.0	207.0	196.9	198.1	201.4	192.3	197.7	185.0	179.6
4	5%	Swelling Ratio	100.0	166.5	167.5	173.1	179.5	182.4	183.1	186.1	182.2	178.5	177.0	153.1
5	5%	Swelling Ratio	100.0	181.3	182.7	184.8	192.3	184.1	211.9	200.2	190.6	194.6	199.3	178.9
6	5%	Swelling Ratio	100.0	177.7	183.5	182.8	176.2	178.5	180.5	183.0	182.5	178.2	178.2	166.1
1	10%	Swelling Ratio	100.0	267.7	289.5	303.5	310.8	291.1	320.2	343.9	294.1	324.8	335.6	315.1
2	10%	Swelling Ratio	100.0	249.4	265.2	259.1	293.2	274.2	280.2	285.2	289.2	296.0	315.8	294.2
3	10%	Swelling Ratio	100.0	284.7	293.6	318.4	308.9	311.5	335.7	328.3	311.7	323.0	315.6	309.2
4	10%	Swelling Ratio	100.0	201.6	236.2	233.2	234.8	237.5	241.4	263.2	262.7	258.4	243.9	241.6
5	10%	Swelling Ratio	100.0	229.1	238.7	244.1	237.3	247.3	253.6	247.6	248.5	256.6	234.5	243.4
6	10%	Swelling Ratio	100.0	229.0	260.4	240.8	257.7	255.3	254.3	255.3	253.9	260.4	225.6	231.4
1	20%	Swelling Ratio	100.0	329.2	370.1	387.0	395.1	396.2	386.4	384.4	377.0	390.0	382.6	446.0
2	20%	Swelling Ratio	100.0	308.0	386.8	337.0	347.8	370.0	387.5	387.8	347.5	370.3	404.8	373.8
3	20%	Swelling Ratio	100.0	340.0	384.1	368.0	381.4	359.5	383.4	400.2	399.3	411.6	411.8	407.7
4	20%	Swelling Ratio	100.0	351.5	395.6	389.4	357.0	393.0	376.5	377.6	380.2	376.0	393.6	429.9
5	20%	Swelling Ratio	100.0	373.2	414.0	380.8	380.3	410.8	377.3	392.4	409.9	365.3	414.8	377.3
6	20%	Swelling Ratio	100.0	312.4	396.2	413.8	405.0	404.8	396.9	394.5	401.7	432.1	436.6	422.8

APPENDIX C: CHAPTER 4 DATA

Histological (OARSI) Score: OARSI scoring of articular cartilage damage measured by Safranin O/Fast Green stain. Each column corresponds to a slide separated at a 90 μm interval. Scores reported for articular cartilage in the medial (M) and lateral (L) tibial plateaus.

Mouse ID	Group	Duration	Plateau	1	7	13	19	25	31	37	43	49	55	61	67	73	79	85	91	97	103	109	Avg	Max
K1L	control	+0-weeks	M				0	0	0	0	0	1	0	0	0								0.111	1
			L		0	0	0.5	0.5	0	0.5	0												0.214	0.5
K2L	control	+0-weeks	M	0	0	0	0	0.5	0	0	0	0											0.056	0.5
			L		0	0	1	0.5	0	0	0	0	0	0									0.150	1
K3L	control	+0-weeks	M	0	0	0	0	0	0	0.5	0	0	0	0.5									0.091	0.5
			L	0	0	0.5	0.5	0.5	1	0.5	0	0	0										0.300	1
N1L	control	+0-weeks	M					0	0	0	0	0	0	0	0	0	0	0.5					0.045	0.5
			L		0	0.5	0.5	0.5	0.5	0	0.5	0											0.313	0.5
N2L	control	+0-weeks	M			0	0	0	0	0	0	0.5	0	0	0	0.5							0.091	0.5
			L		0	0	0	0.5	0	0	0.5	0	0										0.111	0.5
N3L	control	+0-weeks	M		0	0	0	0	0	0.5	0	0	0	0.5									0.100	0.5
			L		0	0	0.5	1	1	0.5	0	0	0										0.333	1
O1L	control	+0-weeks	M			0	0	0	0	0	0.5	0	0	0	0	0.5							0.091	0.5
			L	0.5	0.5	0	0.5	0	0	0	0	0											0.167	0.5
K1R	DMM-only	+0-weeks	M				0	0	0	0	0	0	0	0	0	0							0.000	0
			L	0	0	0	0	0	0	0													0.000	0
K2R	DMM-only	+0-weeks	M			0	0	0	0	0.5	0.5	0	2	2	0								0.500	2
			L	1	0.5	0.5	0	0	0	0													0.286	1
K3R	DMM-only	+0-weeks	M		0	0	0	0	0	0	0.5	1	0.5	1	0.5								0.318	1
			L	0	0	1	0	0	0	0	0.5	0	0.5										0.200	1
N1R	DMM-only	+0-weeks	M	0	0	0	0	0	0	0	0	0	0	0.5									0.045	0.5
			L		0	0	0.5	0.5	0.5	0	0	0	0.5										0.222	0.5
N2R	DMM-only	+0-weeks	M			0	0	0	0	0	0.5	0	0	0.5	0.5								0.150	0.5
			L	0	0	0	0	0.5	1	0	0	0											0.167	1
N3R	DMM-only	+0-weeks	M		0	0	0	0	0	0.5	0.5	0	0	0	0								0.091	0.5
			L			0	0.5	0.5	0	0.5	0	0	0	0									0.167	0.5
O1R	DMM-only	+0-weeks	M			0	0	0	0	0	0	0	0.5	0	2	2							0.409	2
			L			2	2	0.5	0.5	0	0	0	0										0.625	2
J1L	control	+2-weeks	M			0	0	0	0	0	0.5	1	0.5	0	0.5	0.5							0.273	1
			L	0	0	1	0.5	0.5	0	0	0	0											0.222	1
J2L	control	+2-weeks	M				0	0	0	0	0.5	0.5	0.5	0.5	0	0.5	0.5						0.273	0.5
			L	0	0	2	1	1	0.5	0.5	0.5	2	0.5										0.800	2
J3L	control	+2-weeks	M		0	0	0	0	0	0.5	2	1	0.5	0	0								0.364	2

			L	1	1	1	1	1	0	0														0.714	1
P1L	control	+2-weeks	M			0	0	0	0	0	0.5	0.5	0.5	0	0									0.150	0.5
			L			0.5	1	0.5	0	0	0	0	0											0.250	1
P2L	control	+2-weeks	M		0	0	0	0	0	0.5	0.5	0	0	0										0.100	0.5
			L		0.5	0.5	0.5	0.5	0	0	0	0												0.250	0.5
P3L	control	+2-weeks	M	0	0	0	0.5	0.5	0.5	0	0	0												0.167	0.5
			L		0	0.5	0.5	0.5	0	0	0	0												0.188	0.5
O3L	control	+2-weeks	M		0	0	0	0	0	2	0.5	0	0	0										0.250	2
			L		0.5	1	0	0	0.5	0.5	0	0	0											0.278	1
J1R	DMM-only	+2-weeks	M							0	0	0	1	0	0.5	0.5	2	0						0.444	2
			L			0	1	0.5	2	0	0	0												0.500	2
J2R	DMM-only	+2-weeks	M			0	0	0	0	1	0.5	0.5	0.5	0.5	2									0.500	2
			L	0	0	1	1	1	0	2	0													0.625	2
J3R	DMM-only	+2-weeks	M					0	1	2	2	2	0.5	0	0.5									1.000	2
			L		0	1	2	1	1	1	0													0.857	2
P1R	DMM-only	+2-weeks	M						0	0	0	1	0	0.5	0.5	0.5	0							0.278	1
			L			0	0	1	0.5	0	1	0	0.5											0.375	1
P2R	DMM-only	+2-weeks	M					0	0	0	0	0	0	0.5	0.5	0.5								0.167	0.5
			L		0	0	0.5	0.5	0	0.5	0	0												0.188	0.5
P3R	DMM-only	+2-weeks	M				0	0	0	0	0.5	0.5	0.5	1	0.5	1								0.400	1
			L	0	0	0	0	1	1	0														0.286	1
O3R	DMM+1.0N	+2-weeks	M			0	0	2	1	1	1	2	2	2										1.222	2
			L		0	1	1	0	0	0.5	0	0.5												0.375	1
L1R	DMM+1.0N	+2-weeks	M							0	0	0	0	0	0.5	0.5	0.5	0						0.167	0.5
			L			0	0	0.5	0	1	0.5	0												0.286	1
L2R	DMM+1.0N	+2-weeks	M				0	0	0	0	0	0.5	0.5	0.5	0	0.5								0.200	0.5
			L		0	0	0	0	0	0.5	0	0	0											0.056	0.5
L3R	DMM+1.0N	+2-weeks	M						0	0	0	0	0	0.5	0.5	0.5								0.188	0.5
			L	0	0	0	0.5	1	0.5	0														0.286	1
M1R	DMM+1.0N	+2-weeks	M				0	0	0	0	0	0	0	0.5	0.5									0.111	0.5
			L		0	0	1	0.5	1	0	1	0.5												0.500	1
M2R	DMM+1.0N	+2-weeks	M					0	0	0	0.5	0.5	0.5	0	0.5	1	0.5							0.350	1
			L		0	0	0.5	0.5	0	0	0													0.143	0.5
M3R	DMM+1.0N	+2-weeks	M					0	0	0	0	0	0	1	0	0.5	0							0.150	1
			L		0	0	0.5	0	0.5	0	0													0.143	0.5
O2R	DMM+1.0N	+2-weeks	M		0	0	0	0	1	2	1	2	0.5	0	2									0.773	2
			L		0	1	1	0.5	0.5	0	0	0												0.375	1
A1L	control	+6-weeks	M		0	0	0	0	0.5	1	0.5	0	0	0	0.5									0.227	1

			L			0.5	0.5	0.5	1	1	1	0	0										0.563	1
A2L	control	+6-weeks	M											0	0.5	0	0	0	0	0.5	1	0	0.222	1
			L						0	0.5	1	0.5	0	0.5	0.5								0.429	1
A3L	control	+6-weeks	M		0	0	0	1	0.5	2	1	0	0	0	0								0.409	2
			L		0	0	1	1	1	2	0	1	0										0.667	2
I1L	control	+6-weeks	M		0	0.5	0	2	1	0.5	1	0.5	0	0	0								0.500	2
			L		0	0.5	0.5	0.5	0.5	2	2	0	0										0.667	2
I2L	control	+6-weeks	M		0	0.5	0	0.5	1	0.5	0	0.5	0	0	0	0							0.250	1
			L		0	0	0.5	1	0.5	2	2	2	0	0									0.800	2
I4L	control	+6-weeks	M			0.5	0	1	0.5	0.5	0	0	0	0									0.278	1
			L					0.5	0.5	0.5	1	0.5	0.5	0	0								0.438	1
I5L	control	+6-weeks	M	0	0	0	0	0.5	0.5	0.5	0	0											0.167	0.5
			L		0.5	0.5	0.5	0.5	0.5	0	0	0											0.313	0.5
A1R	DMM-only	+6-weeks	M							0	0	0	0	1	2	1	3	2	2				1.100	3
			L	0	0	1	1	1	1	2													0.857	2
A2R	DMM-only	+6-weeks	M	0	0	0	1	1	2	2	2	1	0.5	2	2								1.125	2
			L	0	0	0	0.5	1	0.5	0.5	0	0	0										0.250	1
A3R	DMM-only	+6-weeks	M								0	0	0	2	2	1	3	3	2	2	0		1.364	3
			L	0	2	2	0.5	2	2	0.5													1.286	2
I1R	DMM-only	+6-weeks	M		0	0	0	1	2	2	2	0.5	0.5	0.5	2								0.955	2
			L		1	2	2	1	1	1	1	0											1.125	2
I2R	DMM-only	+6-weeks	M						0	0	1	1	2	3	3	2	1						1.444	3
			L	0	1	0.5	0	2	2														0.917	2
I4R	DMM-only	+6-weeks	M				0	0	0	0.5	0.5	0.5	0.5	0.5	2								0.500	2
			L			1	0.5	0.5	1	1	0												0.667	1
I5R	DMM-only	+6-weeks	M			0.5	0.5	0.5	0.5	0.5	2	1	1										0.813	2
			L			0.5	1	1	2	0.5	1	0											0.857	2
C1R	DMM+1.0N	+6-weeks	M	0	0	0	0	0.5	0.5	0.5	0.5	0.5	1	0.5	0								0.333	1
			L	0	0	1	0.5	0.5	0.5	0	0	0	0.5										0.300	1
C2R	DMM+1.0N	+6-weeks	M			0	0	0	0	0.5	0.5	2	2	2	1	0							0.727	2
			L	2	0.5	0.5	0.5	0	0	0													0.500	2
C3R	DMM+1.0N	+6-weeks	M								0	0	0	0	0	0.5	0.5	0.5	0.5	0.5			0.250	0.5
			L	0	0.5	2	2	1	1	2	0												1.063	2
D1R	DMM+1.0N	+6-weeks	M			0	0	0	0	0	0.5	0.5	2	0.5	0	0.5	0						0.333	2
			L	0	0.5	0.5	0.5	0.5	1	0.5	0	0											0.389	1
D2R	DMM+1.0N	+6-weeks	M		0.5	0.5	0	0.5	0.5	0.5	0.5	0.5	1	2	2	1							0.792	2
			L				0	0.5	1	1	1	1	0	0	0	0							0.450	1
D3R	DMM+1.0N	+6-weeks	M						0	0	0	1	0.5	0.5	0.5	0.5	0.5	0	0				0.318	1

			L			0	1	2	0.5	0	1	0	0										0.563	2
G1R	DMM+1.0N	+6-weeks	M						0	0	0	0	0	0	0	0	0						0.000	0
			L	0	1	1	2	0															0.800	2
E1R	DMM+2.0N	+6-weeks	M					0	1	0	0.5	0	2	0.5	0.5	0.5	0						0.500	2
			L	0	1	0.5	1	0	0	0													0.357	1
E2R	DMM+2.0N	+6-weeks	M					0	0	0	0	1	2	0	0	0	0						0.300	2
			L	2	0	0.5	1	0	0	0.5													0.571	2
E3R	DMM+2.0N	+6-weeks	M		0	0	0.5	1	1	2	2	2	2	2	2								1.318	2
			L			0.5	1	0.5	0.5	0.5	2	2	0										0.875	2
F1R	DMM+2.0N	+6-weeks	M				0	0	0	0	1	0.5	0	0	0	0							0.150	1
			L	0.5	0	0	1	1	2	0	0	0											0.500	2
F2R	DMM+2.0N	+6-weeks	M	0	0	0.5	1	2	0	0.5	0.5	0											0.500	2
			L			0.5	0	2	2	0	0	0	0	0									0.500	2
F3R	DMM+2.0N	+6-weeks	M						0	0	0	0	0	0.5	1	0.5	0.5	2	0.5				0.455	2
			L	0.5	0	0.5	1	0.5	0														0.417	1
G2R	DMM+2.0N	+6-weeks	M					0.5	0	0	0	0	0.5	0.5	0.5	0	0						0.200	0.5
			L	0	0	0.5	0.5	0.5	0.5	0	0												0.250	0.5
B1R	DMM+4.5N	+6-weeks	M							0.5	0	0	0.5	0.5	0.5	1							0.429	1
			L	1	0	0.5	0.5	0.5	0	0.5													0.429	1
B2R	DMM+4.5N	+6-weeks	M								0	0.5	0	0	0.5	2	0.5	2	2				0.833	2
			L		2	3	0.5	1	0	0.5													1.167	3
B3R	DMM+4.5N	+6-weeks	M				0	0	0	1	1	1	2	2	2	1	0.5						0.955	2
			L	2	2	2	1	2	1	0	0.5	0.5											1.222	2
H1R	DMM+4.5N	+6-weeks	M			0	0	0.5	0.5	0.5	0.5	1	0.5										0.438	1
			L			0.5	0.5	0	0.5	0.5	0.5	0	0										0.313	0.5
H2R	DMM+4.5N	+6-weeks	M							0	0	0	0.5	0	2	2	1	2	2	0			0.864	2
			L	3	2	2	1	1	0.5														1.583	3
H3R	DMM+4.5N	+6-weeks	M		0	0	0	0.5	0.5	0.5	2	2	2	1	1								0.864	2
			L	0.5	0.5	1	1	2	0.5	2	0												0.938	2
H4R	DMM+4.5N	+6-weeks	M		0	1	0	0.5	0	0.5	1	1	2	2									0.800	2
			L		0.5	1	0.5	2	2	2	0.5												1.214	2
H5R	DMM+4.5N	+6-weeks	M				0	0	0	0.5	1	0.5	1	0.5	2	0.5	0						0.545	2
			L		3	0	2	0.5	1	1	0.5	0.5	0										0.944	3

Osteophyte Measurements: Osteophyte size and maturity (mat) measured by Safranin O/Fast Green stain. Size reported as absolute width (μm); maturity reported on a scale of 0 to 3. Measurements reported for osteophytes in the posterior, middle, and anterior regions of the medial tibial plateau, and average of all three regions.

				Slide Numbers			Post		Mid		Ant		Avg	
Mouse ID	**Group**	**Duration**	**Plateau**	**Post**	**Mid**	**Ant**	**Size**	**Mat**	**Size**	**Mat**	**Size**	**Mat**	**Size**	**Mat**
K1L	control	+0-weeks	M	25	43	61	0	0	0	0	0	0	0.00	0.00
K2L	control	+0-weeks	M	7	25	43	0	0	0	0	0	0	0.00	0.00
K3L	control	+0-weeks	M	13	31	49	0	0	0	0	0	0	0.00	0.00
N1L	control	+0-weeks	M	37	55	73	0	0	0	0	0	0	0.00	0.00
N2L	control	+0-weeks	M	25	43	61	0	0	0	0	0	0	0.00	0.00
N3L	control	+0-weeks	M	19	37	55	0	0	0	0	0	0	0.00	0.00
O1L	control	+0-weeks	M	25	43	61	0	0	0	0	0	0	0.00	0.00
K1R	DMM-only	+0-weeks	M	31	49	67	0	0	45.5	1	0	0	15.17	0.33
K2R	DMM-only	+0-weeks	M	25	43	61	77.9	1	164.3	1	132.4	1	124.87	1.00
K3R	DMM-only	+0-weeks	M	19	37	55	0	0	86.3	1	75.1	1	53.80	0.67
N1R	DMM-only	+0-weeks	M	13	31	49	0	0	45.2	1	59.5	1	34.90	0.67
N2R	DMM-only	+0-weeks	M	25	43	61	62.6	1	105.7	1	117	1	95.10	1.00
N3R	DMM-only	+0-weeks	M	19	37	55	0	0	0	0	0	0	0.00	0.00
O1R	DMM-only	+0-weeks	M	25	43	61	102.5	1	108.7	1	94.5	1	101.90	1.00
J1L	control	+2-weeks	M	25	43	61	0	0	0	0	0	0	0.00	0.00
J2L	control	+2-weeks	M	31	49	67	0	0	0	0	0	0	0.00	0.00
J3L	control	+2-weeks	M	19	37	55	0	0	0	0	0	0	0.00	0.00
P1L	control	+2-weeks	M	25	43	61	0	0	0	0	0	0	0.00	0.00
P2L	control	+2-weeks	M	19	37	55	0	0	0	0	0	0	0.00	0.00
P3L	control	+2-weeks	M	7	35	43	0	0	0	0	0	0	0.00	0.00
O3L	control	+2-weeks	M	19	37	55	0	0	0	0	0	0	0.00	0.00
J1R	DMM-only	+2-weeks	M	43	61	79	73.7	1	94.5	1	167.4	2	111.87	1.33
J2R	DMM-only	+2-weeks	M	25	43	61	83.4	1	177.7	1	165.3	1	142.13	1.00
J3R	DMM-only	+2-weeks	M	37	49	61	132.7	1	188.9	1	231.8	1	184.47	1.00
P1R	DMM-only	+2-weeks	M	37	55	73	0	0	112.3	2	134.4	1	82.23	1.00
P2R	DMM-only	+2-weeks	M	31	49	67	0	0	0	0	82.1	1	27.37	0.33
P3R	DMM-only	+2-weeks	M	31	49	67	49.3	1	112.1	1	113.9	2	91.77	1.33

O3R	DMM+1.0 N	+2-weeks	M	19	37	55	133.4	1	187.7	2	177.5	2	166.20	1.67
L1R	DMM+1.0 N	+2-weeks	M	43	61	79	0	0	62.7	1	110.8	1	57.83	0.67
L2R	DMM+1.0 N	+2-weeks	M	31	49	67	0	0	64.7	1	98.5	1	54.40	0.67
L3R	DMM+1.0 N	+2-weeks	M	43	55	67	0	0	108.8	1	141.7	2	83.50	1.00
M1R	DMM+1.0 N	+2-weeks	M	25	43	55	0	0	97.7	1	96.6	1	64.77	0.67
M2R	DMM+1.0 N	+2-weeks	M	37	55	73	0	0	61.2	1	73.9	1	45.03	0.67
M3R	DMM+1.0 N	+2-weeks	M	37	55	73	0	0	29.2	1	73.8	1	34.33	0.67
O2R	DMM+1.0 N	+2-weeks	M	19	37	55	60.5	1	114.8	1	138.5	2	104.60	1.33
A1L	control	+6-weeks	M	13	37	61	0	0	0	0	0	0	0.00	0.00
A2L	control	+6-weeks	M	67	79	97	0	0	0	0	0	0	0.00	0.00
A3L	control	+6-weeks	M	13	37	61	0	0	0	0	0	0	0.00	0.00
I1L	control	+6-weeks	M	13	37	61	0	0	0	0	0	0	0.00	0.00
I2L	control	+6-weeks	M	19	43	67	0	0	0	0	0	0	0.00	0.00
I4L	control	+6-weeks	M	19	37	55	0	0	0	0	0	0	0.00	0.00
I5L	control	+6-weeks	M	7	25	43	0	0	0	0	0	0	0.00	0.00
A1R	DMM-only	+6-weeks	M	49	67	85	0.1087	2	0.1505	2	0.18	3	0.15	2.33
A2R	DMM-only	+6-weeks	M	13	37	61	0.1085	2	0.1293	1	0.1951	3	0.14	2.00
A3R	DMM-only	+6-weeks	M	55	79	97	0.1059	2	0.1841	2	0.237	2	0.18	2.00
I1R	DMM-only	+6-weeks	M	19	37	55	0.1904	2	0.1912	2	0.1706	3	0.18	2.33
I2R	DMM-only	+6-weeks	M	37	55	73	0.116	3	0.1981	2	0.2618	2	0.19	2.33
I4R	DMM-only	+6-weeks	M	25	43	61	0.1092	2	0.092	2	0.1318	3	0.11	2.33
I5R	DMM-only	+6-weeks	M	19	31	49	0.0633	2	0.1501	2	0.1711	3	0.13	2.33
C1R	DMM+1.0 N	+6-weeks	M	19	37	55	0.0326	2	0.0553	1	0.23	3	0.11	2.00
C2R	DMM+1.0 N	+6-weeks	M	25	43	61	0.0965	2	0.0943	2	0.1475	3	0.11	2.33
C3R	DMM+1.0 N	+6-weeks	M	55	73	91	0.0865	2	0.1262	2	0.1398	2	0.12	2.00
D1R	DMM+1.0 N	+6-weeks	M	31	49	67	0.0938	3	0.0622	1	0.0885	3	0.08	2.33
D2R	DMM+1.0 N	+6-weeks	M	19	43	67	0.0647	2	0.1153	2	0.1341	3	0.10	2.33
D3R	DMM+1.0 N	+6-weeks	M	37	61	85	0.076	2	0.0999	2	0.064	3	0.08	2.33
G1R	DMM+1.0 N	+6-weeks	M	37	55	73	0	0	0	0	0.0588	2	0.02	0.67
E1R	DMM+2.0 N	+6-weeks	M	37	55	73	0.0805	3	0.1222	2	0.0845	3	0.10	2.67
E2R	DMM+2.0 N	+6-weeks	M	37	55	73	0.0887	2	0.0615	2	0.1404	2	0.10	2.00
E3R	DMM+2.0 N	+6-weeks	M	13	37	61	0.1108	2	0.1496	2	0.18	3	0.15	2.33
F1R	DMM+2.0 N	+6-weeks	M	25	43	61	0	0	0	0	0.0938	3	0.03	1.00

F2R	DMM+2.0 N	+6-weeks	M	7	25	43	0.0229	2	0.0957	2	0.1762	3	0.10	2.33
F3R	DMM+2.0 N	+6-weeks	M	37	61	85	0.0907	3	0.0725	2	0.107	2	0.09	2.33
G2R	DMM+2.0 N	+6-weeks	M	37	55	73	0.0511	2	0.0407	2	0.13	3	0.07	2.33
B1R	DMM+4.5 N	+6-weeks	M	49	61	73	0.0478	2	0	0	0	0	0.02	0.67
B2R	DMM+4.5 N	+6-weeks	M	55	73	91	0.1107	2	0.1347	3	0.1785	2	0.14	2.33
B3R	DMM+4.5 N	+6-weeks	M	31	49	67	0.0759	2	0.1332	3	0.1158	2	0.11	2.33
H1R	DMM+4.5 N	+6-weeks	M	19	37	49	0.0895	2	0.1262	2	0.2054	3	0.14	2.33
H2R	DMM+4.5 N	+6-weeks	M	43	67	91	0.1195	3	0.1194	2	0.1084	2	0.12	2.33
H3R	DMM+4.5 N	+6-weeks	M	19	37	55	0.0691	2	0.1541	2	0.1889	3	0.14	2.33
H4R	DMM+4.5 N	+6-weeks	M	13	37	55	0.0734	3	0.1449	3	0.1192	3	0.11	3.00
H5R	DMM+4.5 N	+6-weeks	M	31	49	67	0.0786	2	0.067	2	0.1116	3	0.09	2.33

Subchondral Bone Plate MicroCT Data: Subchondral bone plate thickness (Th) and tissue mineral density (TMD) in the medial (Med) and lateral (Lat) aspects of the tibial plateau.

				Med		Lat	
Mouse ID	**Group**	**Duration**	**Limb**	**Th (mm)**	**TMD (mg HA/ccm)**	**Th (mm)**	**TMD (mg HA/ccm)**
K1	DMM-only	+0-weeks	control	0.107	868.5	0.098	873.4
K2	DMM-only	+0-weeks	control	0.116	883.5	0.1	841.6
K3	DMM-only	+0-weeks	control	0.111	889.8	0.097	876.6
N1	DMM-only	+0-weeks	control	0.107	861.4	0.101	868.9
N2	DMM-only	+0-weeks	control	0.108	895	0.098	856
N3	DMM-only	+0-weeks	control	0.094	841.7	0.094	834.4
O1	DMM-only	+0-weeks	control	0.114	891.6	0.098	852.5
J1	DMM-only	+2-weeks	control	0.114	890	0.102	863.6
J2	DMM-only	+2-weeks	control	0.118	903.9	0.1	891.5
J3	DMM-only	+2-weeks	control	0.112	898.6	0.099	892.2
P1	DMM-only	+2-weeks	control	0.108	900.9	0.096	872.6
P2	DMM-only	+2-weeks	control	0.093	844.4	0.091	856.2
P3	DMM-only	+2-weeks	control	0.099	886.9	0.094	864.8
O3	DMM+1.0N	+2-weeks	control	0.117	898.4	0.101	884.1
L1	DMM+1.0N	+2-weeks	control	0.108	879.4	0.097	849.2
L2	DMM+1.0N	+2-weeks	control	0.103	869.7	0.088	861.4
L3	DMM+1.0N	+2-weeks	control	0.099	857	0.09	868.1
M1	DMM+1.0N	+2-weeks	control	0.096	858.5	0.086	843.6
M2	DMM+1.0N	+2-weeks	control	0.1	852	0.091	849
M3	DMM+1.0N	+2-weeks	control	0.088	836.6	0.102	869
O2	DMM+1.0N	+2-weeks	control	0.107	899.6	0.095	874.1
A1	DMM-only	+6-weeks	control	0.121	910.8	0.093	878.5
A2	DMM-only	+6-weeks	control	0.122	912.3	0.103	879.5
A3	DMM-only	+6-weeks	control	0.124	914.4	0.097	887.8
I1	DMM-only	+6-weeks	control	0.111	893.4	0.101	892.7
I2	DMM-only	+6-weeks	control	0.123	932.6	0.097	880.5
I3	DMM-only	+6-weeks	control	0.101	885.9	0.087	868.2
I4	DMM-only	+6-weeks	control	0.109	875.4	0.093	870.5
I5	DMM-only	+6-weeks	control	0.098	848.2	0.09	863
C1	DMM+1.0N	+6-weeks	control	0.107	868.4	0.088	862.3
C2	DMM+1.0N	+6-weeks	control	0.106	895.1	0.088	873.9
C3	DMM+1.0N	+6-weeks	control	0.099	872.8	0.082	859.4
D1	DMM+1.0N	+6-weeks	control	0.097	860.5	0.089	879.9
D2	DMM+1.0N	+6-weeks	control	0.106	892.2	0.095	899.2
D3	DMM+1.0N	+6-weeks	control	0.106	870.7	0.088	862.7

G1	DMM+1.0N	+6-weeks	control	0.103	888.4	0.09	854.1
E1	DMM+2.0N	+6-weeks	control	0.124	909	0.099	880.9
E2	DMM+2.0N	+6-weeks	control	0.112	914.3	0.096	865
E3	DMM+2.0N	+6-weeks	control	0.116	899.9	0.094	865.3
F1	DMM+2.0N	+6-weeks	control	0.109	897.5	0.092	850.2
F2	DMM+2.0N	+6-weeks	control	0.102	884.7	0.095	867.8
F3	DMM+2.0N	+6-weeks	control	0.085	856.9	0.087	856.6
G2	DMM+2.0N	+6-weeks	control	0.113	899.1	0.095	873.1
B1	DMM+4.5N	+6-weeks	control	0.1	894.5	0.09	870.7
B2	DMM+4.5N	+6-weeks	control	0.102	873.2	0.088	870.9
B3	DMM+4.5N	+6-weeks	control	0.102	892.8	0.091	872.8
H1	DMM+4.5N	+6-weeks	control	0.1	868.4	0.098	863.6
H2	DMM+4.5N	+6-weeks	control	0.116	897.2	0.104	900.6
H3	DMM+4.5N	+6-weeks	control	0.106	905.1	0.094	876.4
H4	DMM+4.5N	+6-weeks	control	0.108	880.8	0.09	854.3
H5	DMM+4.5N	+6-weeks	control	0.102	881.2	0.085	880.6
K1	DMM-only	+0-weeks	DMM-treated	0.111	886.1	0.101	854.1
K2	DMM-only	+0-weeks	DMM-treated	0.107	869.6	0.094	863.1
K3	DMM-only	+0-weeks	DMM-treated	0.109	873.6	0.099	860.2
N1	DMM-only	+0-weeks	DMM-treated	0.11	873.2	0.093	854
N2	DMM-only	+0-weeks	DMM-treated	0.116	892.5	0.099	865
N3	DMM-only	+0-weeks	DMM-treated	0.098	854.9	0.089	849.7
O1	DMM-only	+0-weeks	DMM-treated	0.114	890.4	0.096	879.4
J1	DMM-only	+2-weeks	DMM-treated	0.114	894.3	0.092	869.6
J2	DMM-only	+2-weeks	DMM-treated	0.104	869.6	0.098	863.4
J3	DMM-only	+2-weeks	DMM-treated	0.115	902.2	0.095	876.2
P1	DMM-only	+2-weeks	DMM-treated	0.109	883	0.094	844.6
P2	DMM-only	+2-weeks	DMM-treated	0.103	878	0.095	864.2
P3	DMM-only	+2-weeks	DMM-treated	0.111	912.1	0.094	864.8
O3	DMM+1.0N	+2-weeks	DMM-treated	0.125	926.5	0.099	884.2
L1	DMM+1.0N	+2-weeks	DMM-treated	0.107	884.4	0.096	859.5
L2	DMM+1.0N	+2-weeks	DMM-treated	0.107	881.1	0.088	851.3
L3	DMM+1.0N	+2-weeks	DMM-treated	0.103	871.5	0.092	865.4
M1	DMM+1.0N	+2-weeks	DMM-treated	0.109	894	0.087	865.4
M2	DMM+1.0N	+2-weeks	DMM-treated	0.106	891.4	0.09	862.3
M3	DMM+1.0N	+2-weeks	DMM-treated	0.098	864	0.085	843.2
O2	DMM+1.0N	+2-weeks	DMM-treated	0.109	906.7	0.091	866.2
A1	DMM-only	+6-weeks	DMM-treated	0.123	934.3	0.096	890
A2	DMM-only	+6-weeks	DMM-treated	0.127	926.8	0.097	874.6
A3	DMM-only	+6-weeks	DMM-treated	0.135	941.4	0.119	912.3

I1	DMM-only	+6-weeks	DMM-treated	0.133	931.2	0.099	887.9
I2	DMM-only	+6-weeks	DMM-treated	0.123	940.3	0.111	904.9
I3	DMM-only	+6-weeks	DMM-treated	0.117	924.2	0.093	875.9
I4	DMM-only	+6-weeks	DMM-treated	0.119	898.8	0.098	866.5
I5	DMM-only	+6-weeks	DMM-treated	0.11	903.9	0.098	882.7
C1	DMM+1.0N	+6-weeks	DMM-treated	0.117	891.2	0.094	850
C2	DMM+1.0N	+6-weeks	DMM-treated	0.111	913.7	0.103	881.2
C3	DMM+1.0N	+6-weeks	DMM-treated	0.103	878.2	0.09	878
D1	DMM+1.0N	+6-weeks	DMM-treated	0.103	861.9	0.088	858.5
D2	DMM+1.0N	+6-weeks	DMM-treated	0.117	910.3	0.092	864.4
D3	DMM+1.0N	+6-weeks	DMM-treated	0.116	897.6	0.092	859.4
G1	DMM+1.0N	+6-weeks	DMM-treated	0.127	929	0.089	860.9
E1	DMM+2.0N	+6-weeks	DMM-treated	0.122	891.3	0.096	879.8
E2	DMM+2.0N	+6-weeks	DMM-treated	0.117	932.6	0.092	863.4
E3	DMM+2.0N	+6-weeks	DMM-treated	0.142	934.6	0.121	905.9
F1	DMM+2.0N	+6-weeks	DMM-treated	0.106	909.9	0.092	865.7
F2	DMM+2.0N	+6-weeks	DMM-treated	0.113	895.1	0.1	906.7
F3	DMM+2.0N	+6-weeks	DMM-treated	0.099	879.7	0.09	876.5
G2	DMM+2.0N	+6-weeks	DMM-treated	0.107	882.4	0.109	889.1
B1	DMM+4.5N	+6-weeks	DMM-treated	0.103	866.7	0.085	856.5
B2	DMM+4.5N	+6-weeks	DMM-treated	0.114	879.4	0.087	848.1
B3	DMM+4.5N	+6-weeks	DMM-treated	0.11	892.2	0.097	870.5
H1	DMM+4.5N	+6-weeks	DMM-treated	0.097	862.7	0.095	833.2
H2	DMM+4.5N	+6-weeks	DMM-treated	0.111	898.2	0.104	898.3
H3	DMM+4.5N	+6-weeks	DMM-treated	0.106	912.5	0.1	883.6
H4	DMM+4.5N	+6-weeks	DMM-treated	0.114	913.7	0.092	877.1
H5	DMM+4.5N	+6-weeks	DMM-treated	0.108	893.4	0.084	844.3

Epiphyseal Cancellous Bone MicroCT Data: Indices of cancellous bone architecture proximal to the growth plate. Outcome measures: bone volume fraction (BV/TV), trabecular number (Tb.N), trabecular thickness (Tb.Th), trabecular separation (Tb.Sp), and tissue mineral density (TMD).

Mouse ID	Group	Duration	Limb	BV/TV	Tb.N	Tb.Th (mm)	Tb.Sp (mm)	TMD (mg HA/ccm)
A1	DMM-only	+6-weeks	control	0.2766	6.0152	0.0475	0.1651	943.485
A2	DMM-only	+6-weeks	control	0.3112	6.5956	0.0498	0.1546	954.859
A3	DMM-only	+6-weeks	control	0.3596	6.2192	0.0513	0.1631	951.447
I1	DMM-only	+6-weeks	control	0.3214	6.6313	0.0507	0.1573	970.402
I2	DMM-only	+6-weeks	control	0.3535	6.4142	0.0536	0.1561	968.064
I3	DMM-only	+6-weeks	control	0.2949	5.9289	0.0498	0.1718	956.312
I4	DMM-only	+6-weeks	control	0.2632	6.0283	0.0456	0.1692	939.694
I5	DMM-only	+6-weeks	control	0.2705	6.5197	0.0456	0.1572	955.806
C1	DMM+1.0N	+6-weeks	control	0.2604	5.8743	0.0451	0.1728	934.892
C2	DMM+1.0N	+6-weeks	control	0.2863	6.5181	0.0447	0.155	945.381
C3	DMM+1.0N	+6-weeks	control	0.2809	6.0151	0.0483	0.1671	925.225
D1	DMM+1.0N	+6-weeks	control	0.2886	6.3085	0.0488	0.1597	937.546
D2	DMM+1.0N	+6-weeks	control	0.3464	6.2554	0.0555	0.1633	950.183
D3	DMM+1.0N	+6-weeks	control	0.3129	6.239	0.0516	0.1618	929.648
G1	DMM+1.0N	+6-weeks	control	0.2694	5.9706	0.0464	0.1671	929.648
E1	DMM+2.0N	+6-weeks	control	0.3285	6.3625	0.0488	0.1597	945.128
E2	DMM+2.0N	+6-weeks	control	0.3496	7.0135	0.0482	0.1442	951.952
E3	DMM+2.0N	+6-weeks	control	0.3423	6.0714	0.0518	0.166	936.535
F1	DMM+2.0N	+6-weeks	control	0.3098	6.1335	0.0503	0.1617	936.282
F2	DMM+2.0N	+6-weeks	control	0.3026	5.8837	0.0505	0.1714	938.051
F3	DMM+2.0N	+6-weeks	control	0.2716	6.2087	0.0471	0.1605	923.835
G2	DMM+2.0N	+6-weeks	control	0.3137	6.1186	0.0517	0.1622	939.694
B1	DMM+4.5N	+6-weeks	control	0.322	6.1038	0.0503	0.164	944.623
B2	DMM+4.5N	+6-weeks	control	0.2797	6.0106	0.0504	0.1673	937.104
B3	DMM+4.5N	+6-weeks	control	0.3171	6.4492	0.0479	0.1558	936.914
H1	DMM+4.5N	+6-weeks	control	0.3114	6.6713	0.0489	0.1495	937.04
H2	DMM+4.5N	+6-weeks	control	0.372	7.1083	0.0553	0.146	970.844
H3	DMM+4.5N	+6-weeks	control	0.3652	6.1303	0.0552	0.1606	947.782
H4	DMM+4.5N	+6-weeks	control	0.3362	6.7845	0.0507	0.1465	934.197
H5	DMM+4.5N	+6-weeks	control	0.2942	5.9455	0.0506	0.1707	947.592
A1	DMM-only	+6-weeks	DMM-treated	0.2599	6.0856	0.0447	0.166	960.924
A2	DMM-only	+6-weeks	DMM-treated	0.2869	6.0735	0.0491	0.1671	954.859

A3	DMM-only	+6-weeks	DMM-treated	0.3209	6.0625	0.0499	0.1653	958.144
I1	DMM-only	+6-weeks	DMM-treated	0.3431	6.5636	0.0525	0.1519	952.394
I2	DMM-only	+6-weeks	DMM-treated	0.3111	6.0579	0.0515	0.1655	960.861
I3	DMM-only	+6-weeks	DMM-treated	0.2664	5.7122	0.0485	0.1778	953.721
I4	DMM-only	+6-weeks	DMM-treated	0.2741	5.7599	0.0515	0.1764	946.013
I5	DMM-only	+6-weeks	DMM-treated	0.2913	5.96	0.0475	0.1698	957.702
C1	DMM+1.0N	+6-weeks	DMM-treated	0.2694	5.7972	0.0474	0.175	944.433
C2	DMM+1.0N	+6-weeks	DMM-treated	0.2825	5.8259	0.0494	0.1724	954.669
C3	DMM+1.0N	+6-weeks	DMM-treated	0.2553	5.7053	0.0498	0.1786	941.59
D1	DMM+1.0N	+6-weeks	DMM-treated	0.2849	5.9009	0.0496	0.1697	943.738
D2	DMM+1.0N	+6-weeks	DMM-treated	0.2969	6.2845	0.0487	0.1609	938.873
D3	DMM+1.0N	+6-weeks	DMM-treated	0.2861	6.1093	0.0497	0.17	933.881
G1	DMM+1.0N	+6-weeks	DMM-treated	0.2435	5.7032	0.0461	0.1737	927.499
E1	DMM+2.0N	+6-weeks	DMM-treated	0.3116	6.1153	0.0487	0.1675	945.76
E2	DMM+2.0N	+6-weeks	DMM-treated	0.3036	6.4458	0.0454	0.1554	950.309
E3	DMM+2.0N	+6-weeks	DMM-treated	0.3296	6.0585	0.054	0.1645	952.078
F1	DMM+2.0N	+6-weeks	DMM-treated	0.337	6.1375	0.0524	0.1646	951.32
F2	DMM+2.0N	+6-weeks	DMM-treated	0.2586	5.3876	0.0499	0.1865	934.26
F3	DMM+2.0N	+6-weeks	DMM-treated	0.3013	5.8645	0.0515	0.1709	958.144
G2	DMM+2.0N	+6-weeks	DMM-treated	0.2977	5.6878	0.0565	0.1722	960.545
B1	DMM+4.5N	+6-weeks	DMM-treated	0.2957	6.1472	0.0508	0.16	942.537
B2	DMM+4.5N	+6-weeks	DMM-treated	0.2566	5.7034	0.0489	0.1768	937.988
B3	DMM+4.5N	+6-weeks	DMM-treated	0.314	6.3082	0.0515	0.1603	942.601
H1	DMM+4.5N	+6-weeks	DMM-treated	0.2404	6.4562	0.043	0.1563	943.548
H2	DMM+4.5N	+6-weeks	DMM-treated	0.3991	6.8792	0.0561	0.1468	951.331
H3	DMM+4.5N	+6-weeks	DMM-treated	0.3384	6.3229	0.0531	0.1594	944.18
H4	DMM+4.5N	+6-weeks	DMM-treated	0.3336	6.3333	0.0557	0.1571	954.353
H5	DMM+4.5N	+6-weeks	DMM-treated	0.2584	6.053	0.0467	0.1702	953.279

Metaphyseal Cancellous Bone MicroCT Data: Indices of cancellous bone architecture distal to the growth plate. Outcome measures: bone volume fraction (BV/TV), trabecular number (Tb.N), trabecular thickness (Tb.Th), trabecular separation (Tb.Sp), and tissue mineral density (TMD).

Mouse ID	Group	Duration	Limb	BV/TV	Tb.N	Tb.Th (mm)	Tb.Sp (mm)	TMD (mg HA/ccm)
A1	DMM-only	+6-weeks	control	0.2327	5.3686	0.0544	0.1797	888.135
A2	DMM-only	+6-weeks	control	0.2323	4.747	0.0577	0.2128	881.88
A3	DMM-only	+6-weeks	control	0.2487	4.6271	0.0591	0.2166	900.709
I1	DMM-only	+6-weeks	control	0.2559	5.2364	0.0609	0.1902	891.1682
I2	DMM-only	+6-weeks	control	0.2734	5.1422	0.0659	0.1896	905.4481
I3	DMM-only	+6-weeks	control	0.2059	5.424	0.0556	0.1808	904.058
I4	DMM-only	+6-weeks	control	0.1811	5.0476	0.0558	0.1968	885.607
I5	DMM-only	+6-weeks	control	0.2042	5.1699	0.055	0.1917	888.767
C1	DMM+1.0N	+6-weeks	control	0.1748	5.3586	0.0504	0.1848	880.047
C2	DMM+1.0N	+6-weeks	control	0.1714	5.0782	0.0495	0.1947	890.852
C3	DMM+1.0N	+6-weeks	control	0.1531	4.9121	0.0485	0.201	881.121
D1	DMM+1.0N	+6-weeks	control	0.1531	4.7109	0.0484	0.2128	882.385
D2	DMM+1.0N	+6-weeks	control	0.1882	5.1761	0.0509	0.1892	896.223
D3	DMM+1.0N	+6-weeks	control	0.1662	5.0496	0.0494	0.1957	888.198
G1	DMM+1.0N	+6-weeks	control	0.1727	5.306	0.0495	0.184	891.484
E1	DMM+2.0N	+6-weeks	control	0.2303	5.5237	0.0551	0.1756	878.088
E2	DMM+2.0N	+6-weeks	control	0.2178	5.671	0.0519	0.1708	879.036
E3	DMM+2.0N	+6-weeks	control	0.236	5.3052	0.0552	0.1827	885.987
F1	DMM+2.0N	+6-weeks	control	0.2004	5.1174	0.0544	0.1908	889.083
F2	DMM+2.0N	+6-weeks	control	0.1868	5.0076	0.0523	0.1956	891.484
F3	DMM+2.0N	+6-weeks	control	0.154	5.0251	0.0474	0.1972	881.827
G2	DMM+2.0N	+6-weeks	control	0.1894	5.0081	0.0543	0.1961	892.432
B1	DMM+4.5N	+6-weeks	control	0.1497	4.6205	0.0485	0.2145	878.152
B2	DMM+4.5N	+6-weeks	control	0.1594	4.6746	0.0509	0.2141	886.176
B3	DMM+4.5N	+6-weeks	control	0.1811	5.2599	0.0513	0.1866	898.813
H1	DMM+4.5N	+6-weeks	control	0.1813	5.3128	0.0497	0.1843	856.289
H2	DMM+4.5N	+6-weeks	control	0.2551	5.6587	0.0562	0.1752	872.275
H3	DMM+4.5N	+6-weeks	control	0.2684	4.8715	0.0654	0.2003	911.8931
H4	DMM+4.5N	+6-weeks	control	0.2673	5.5275	0.0619	0.1745	909.7448
H5	DMM+4.5N	+6-weeks	control	0.224	4.8479	0.0627	0.202	881.0586
A1	DMM-only	+6-weeks	DMM-treated	0.2135	5.2157	0.0538	0.188	876.446
A2	DMM-only	+6-weeks	DMM-treated	0.2155	4.5658	0.0552	0.219	880.805
A3	DMM-only	+6-weeks	DMM-treated	0.2345	4.5142	0.0594	0.2207	892.305

I1	DMM-only	+6-weeks	DMM-treated	0.2612	4.9343	0.0652	0.1988	893.7588
I2	DMM-only	+6-weeks	DMM-treated	0.2493	4.8321	0.0641	0.2057	904.4371
I3	DMM-only	+6-weeks	DMM-treated	0.1785	5.1822	0.0533	0.1907	883.143
I4	DMM-only	+6-weeks	DMM-treated	0.1696	4.9807	0.0519	0.1986	874.234
I5	DMM-only	+6-weeks	DMM-treated	0.1876	5.5148	0.0506	0.1775	894.137
C1	DMM+1.0N	+6-weeks	DMM-treated	0.1649	5.0366	0.05	0.1978	873.792
C2	DMM+1.0N	+6-weeks	DMM-treated	0.1646	4.9857	0.049	0.1978	895.78
C3	DMM+1.0N	+6-weeks	DMM-treated	0.1341	4.5654	0.0469	0.2192	874.045
D1	DMM+1.0N	+6-weeks	DMM-treated	0.1437	4.8565	0.0466	0.2039	880.679
D2	DMM+1.0N	+6-weeks	DMM-treated	0.1758	5.0415	0.0517	0.1966	897.36
D3	DMM+1.0N	+6-weeks	DMM-treated	0.1553	5.0567	0.0483	0.1946	877.772
G1	DMM+1.0N	+6-weeks	DMM-treated	0.1749	5.0409	0.0511	0.1959	876.193
E1	DMM+2.0N	+6-weeks	DMM-treated	0.2172	5.2173	0.0552	0.1896	866.526
E2	DMM+2.0N	+6-weeks	DMM-treated	0.206	5.5214	0.0517	0.1739	887.187
E3	DMM+2.0N	+6-weeks	DMM-treated	0.2218	5.3333	0.0555	0.1816	867.979
F1	DMM+2.0N	+6-weeks	DMM-treated	0.192	5.1828	0.0528	0.1888	895.78
F2	DMM+2.0N	+6-weeks	DMM-treated	0.1752	4.7635	0.0524	0.2083	877.141
F3	DMM+2.0N	+6-weeks	DMM-treated	0.1529	4.9037	0.049	0.2017	896.981
G2	DMM+2.0N	+6-weeks	DMM-treated	0.1812	4.9364	0.055	0.2003	900.393
B1	DMM+4.5N	+6-weeks	DMM-treated	0.1492	4.6889	0.0492	0.2115	876.193
B2	DMM+4.5N	+6-weeks	DMM-treated	0.1568	4.5193	0.0528	0.2217	883.775
B3	DMM+4.5N	+6-weeks	DMM-treated	0.1721	4.8515	0.0534	0.2054	882.764
H1	DMM+4.5N	+6-weeks	DMM-treated	0.1511	4.9328	0.0485	0.2018	853.32
H2	DMM+4.5N	+6-weeks	DMM-treated	0.2515	5.6391	0.056	0.1721	886.239
H3	DMM+4.5N	+6-weeks	DMM-treated	0.2638	5.107	0.0641	0.1885	895.844
H4	DMM+4.5N	+6-weeks	DMM-treated	0.2522	5.5394	0.058	0.1741	896.918
H5	DMM+4.5N	+6-weeks	DMM-treated	0.2094	4.5142	0.0611	0.2223	887.314

Meniscal Ossicle MicroCT Data: Volume (BV) and tissue mineral density (TMD) of medial meniscal ossicle.

Mouse ID	Group	Duration	Limb	BV	TMD (mg HA/ccm)
A1	DMM-only	+6-weeks	control	0.0873	698.8
A2	DMM-only	+6-weeks	control	0.0863	689.7
A3	DMM-only	+6-weeks	control	0.0925	752.8
I1	DMM-only	+6-weeks	control	0.0938	771.9
I2	DMM-only	+6-weeks	control	0.0975	813.3
I3	DMM-only	+6-weeks	control	0.0866	690.5
I4	DMM-only	+6-weeks	control	0.0902	775.2
I5	DMM-only	+6-weeks	control	0.0988	793.2
C1	DMM+1.0N	+6-weeks	control	0.0835	771
C2	DMM+1.0N	+6-weeks	control	0.0885	795.1
C3	DMM+1.0N	+6-weeks	control	0.0892	774.6
D1	DMM+1.0N	+6-weeks	control	0.0904	768.2
D2	DMM+1.0N	+6-weeks	control	0.0848	708.9
D3	DMM+1.0N	+6-weeks	control	0.0893	679.7
G1	DMM+1.0N	+6-weeks	control	0.0861	709.6
E1	DMM+2.0N	+6-weeks	control	0.0919	681
E2	DMM+2.0N	+6-weeks	control	0.0784	731.2
E3	DMM+2.0N	+6-weeks	control	0.088	686.5
F1	DMM+2.0N	+6-weeks	control	0.091	715
F2	DMM+2.0N	+6-weeks	control	0.0926	783
F3	DMM+2.0N	+6-weeks	control	0.0746	687
G2	DMM+2.0N	+6-weeks	control	0.0968	712.5
B1	DMM+4.5N	+6-weeks	control	0.0871	693.8
B2	DMM+4.5N	+6-weeks	control	0.0975	706.2
B3	DMM+4.5N	+6-weeks	control	0.0865	705.8
H1	DMM+4.5N	+6-weeks	control	0.0888	792.2
H2	DMM+4.5N	+6-weeks	control	0.094	788.9
H3	DMM+4.5N	+6-weeks	control	0.0936	710.3
H4	DMM+4.5N	+6-weeks	control	0.0939	779.2
H5	DMM+4.5N	+6-weeks	control	0.0854	771.4
A1	DMM-only	+6-weeks	DMM-treated	0.1609	756.3
A2	DMM-only	+6-weeks	DMM-treated	0.2098	710.1
A3	DMM-only	+6-weeks	DMM-treated	0.2152	716.5
I1	DMM-only	+6-weeks	DMM-treated	0.1454	681.2
I2	DMM-only	+6-weeks	DMM-treated	0.1276	676.3
I3	DMM-only	+6-weeks	DMM-treated	0.1191	741.4

I4	DMM-only	+6-weeks	DMM-treated	0.1144	678.7
I5	DMM-only	+6-weeks	DMM-treated	0.135	734.8
C1	DMM+1.0N	+6-weeks	DMM-treated	0.1513	709.1
C2	DMM+1.0N	+6-weeks	DMM-treated	0.143	762.4
C3	DMM+1.0N	+6-weeks	DMM-treated	0.1453	703.6
D1	DMM+1.0N	+6-weeks	DMM-treated	0.1278	682
D2	DMM+1.0N	+6-weeks	DMM-treated	0.1342	685.5
D3	DMM+1.0N	+6-weeks	DMM-treated	0.1677	716.2
G1	DMM+1.0N	+6-weeks	DMM-treated	0.1202	737.9
E1	DMM+2.0N	+6-weeks	DMM-treated	0.1572	674
E2	DMM+2.0N	+6-weeks	DMM-treated	0.1101	712.9
E3	DMM+2.0N	+6-weeks	DMM-treated	0.1517	671.7
F1	DMM+2.0N	+6-weeks	DMM-treated	0.1056	767.6
F2	DMM+2.0N	+6-weeks	DMM-treated	0.1448	691.8
F3	DMM+2.0N	+6-weeks	DMM-treated	0.1418	754.2
G2	DMM+2.0N	+6-weeks	DMM-treated	0.1307	727.6
B1	DMM+4.5N	+6-weeks	DMM-treated	0.0964	686.9
B2	DMM+4.5N	+6-weeks	DMM-treated	0.1313	651.4
B3	DMM+4.5N	+6-weeks	DMM-treated	0.1414	693
H1	DMM+4.5N	+6-weeks	DMM-treated	0.144	673.4
H2	DMM+4.5N	+6-weeks	DMM-treated	0.1689	734
H3	DMM+4.5N	+6-weeks	DMM-treated	0.1395	729.1
H4	DMM+4.5N	+6-weeks	DMM-treated	0.1362	728.3
H5	DMM+4.5N	+6-weeks	DMM-treated	0.1581	672.9

Chondrocyte number and apoptosis: Chondrocyte number and apoptosis determined by DAPI staining and TUNEL assay in articular cartilage in the medial (M) tibial plateau. Chondrocyte number reported as percent positive DAPI staining per cartilage area. Chondrocyte apoptosis reported as percent positive TUNEL staining per DAPI area.

Mouse ID	Group	Duration	Plateau	Percent DAPI per Cartilage Area	Percent TUNEL per DAPI Area
K1L	control	+0-weeks	M	12.863	1.267
K2L	control	+0-weeks	M	12.754	1.151
K3L	control	+0-weeks	M	6.047	1.305
N2L	control	+0-weeks	M	14.085	2.986
N3L	control	+0-weeks	M	7.347	3.543
K1R	DMM-only	+0-weeks	M	10.986	4.089
K2R	DMM-only	+0-weeks	M	6.352	5.896
K3R	DMM-only	+0-weeks	M	8.075	5.351
N1R	DMM-only	+0-weeks	M	8.907	4.858
N2R	DMM-only	+0-weeks	M	8.274	3.289
N3R	DMM-only	+0-weeks	M	12.418	0.400
J1R	DMM-only	+2-weeks	M	9.234	8.382
J2R	DMM-only	+2-weeks	M	10.361	19.080
J3R	DMM-only	+2-weeks	M	5.362	17.553
P1R	DMM-only	+2-weeks	M	6.049	8.810
P2R	DMM-only	+2-weeks	M	11.612	1.878
P3R	DMM-only	+2-weeks	M	7.143	8.275
L1R	DMM+1.0N	+2-weeks	M	7.741	2.627
L2R	DMM+1.0N	+2-weeks	M	7.685	10.080
M1R	DMM+1.0N	+2-weeks	M	8.578	1.224
M2R	DMM+1.0N	+2-weeks	M	9.528	4.708
M3R	DMM+1.0N	+2-weeks	M	9.946	1.079
A1R	DMM-only	+6-weeks	M	5.298	7.938
A2R	DMM-only	+6-weeks	M	6.487	20.693
A3R	DMM-only	+6-weeks	M	3.754	31.501
I1R	DMM-only	+6-weeks	M	5.673	6.094
I2R	DMM-only	+6-weeks	M	3.317	54.564
I4R	DMM-only	+6-weeks	M	4.584	13.025
C1R	DMM+1.0N	+6-weeks	M	8.766	5.829
C2R	DMM+1.0N	+6-weeks	M	4.887	23.803
C3R	DMM+1.0N	+6-weeks	M	5.751	18.213
D1R	DMM+1.0N	+6-weeks	M	5.292	8.338
D2R	DMM+1.0N	+6-weeks	M	2.874	54.522
D3R	DMM+1.0N	+6-weeks	M	5.469	15.101

E1R	DMM+2.0N	+6-weeks	M	3.311	8.204
E2R	DMM+2.0N	+6-weeks	M	5.985	14.238
E3R	DMM+2.0N	+6-weeks	M	5.082	19.252
F1R	DMM+2.0N	+6-weeks	M	2.815	21.741
F2R	DMM+2.0N	+6-weeks	M	4.467	38.646
F3R	DMM+2.0N	+6-weeks	M	2.247	34.253
B1R	DMM+4.5N	+6-weeks	M	11.105	2.155
B2R	DMM+4.5N	+6-weeks	M	3.349	33.799
B3R	DMM+4.5N	+6-weeks	M	5.297	0.984
H1R	DMM+4.5N	+6-weeks	M	5.207	6.701
H2R	DMM+4.5N	+6-weeks	M	2.320	76.321
H3R	DMM+4.5N	+6-weeks	M	6.084	11.206

Picrosirius Red Staining: Aligned collagen content in cartilage surface of medial (M) tibial plateau determined by picrosirius red staining. Surface collagen content reported as percentage of positive picrosirius red staining on the cartilage surface.

Mouse ID	Group	Duration	Plateau	Picrosirius staining (% Cartilage Surface)
K1L	control	+0-weeks	M	33.5
K2L	control	+0-weeks	M	50.6
K3L	control	+0-weeks	M	70.2
N1L	control	+0-weeks	M	57.4
N2L	control	+0-weeks	M	43.6
N3L	control	+0-weeks	M	67.8
K1R	DMM-only	+0-weeks	M	51.5
K2R	DMM-only	+0-weeks	M	33.7
K3R	DMM-only	+0-weeks	M	73.3
N1R	DMM-only	+0-weeks	M	55.8
N2R	DMM-only	+0-weeks	M	73.7
N3R	DMM-only	+0-weeks	M	71.3
J1L	control	+2-weeks	M	63.3
J2L	control	+2-weeks	M	71.8
J3L	control	+2-weeks	M	51.1
P1L	control	+2-weeks	M	67.2
P2L	control	+2-weeks	M	55.9
P3L	control	+2-weeks	M	56.6
J1R	DMM-only	+2-weeks	M	49.1
J2R	DMM-only	+2-weeks	M	59.4
J3R	DMM-only	+2-weeks	M	34.4
P1R	DMM-only	+2-weeks	M	63.2
P2R	DMM-only	+2-weeks	M	47.6
P3R	DMM-only	+2-weeks	M	60.3
L1R	DMM+1.0N	+2-weeks	M	44.2
L2R	DMM+1.0N	+2-weeks	M	68.7
L3R	DMM+1.0N	+2-weeks	M	76.5
M1R	DMM+1.0N	+2-weeks	M	52.8
M2R	DMM+1.0N	+2-weeks	M	76.6
M3R	DMM+1.0N	+2-weeks	M	69.9
A1L	control	+6-weeks	M	42.7
A2L	control	+6-weeks	M	38.5
A3L	control	+6-weeks	M	42.6
I1L	control	+6-weeks	M	46
I2L	control	+6-weeks	M	47.3
I4L	control	+6-weeks	M	54.5

A2R	DMM-only	+6-weeks	M	58
A3R	DMM-only	+6-weeks	M	8.3
I1R	DMM-only	+6-weeks	M	37.5
I2R	DMM-only	+6-weeks	M	10.2
I4R	DMM-only	+6-weeks	M	53.8
C1R	DMM+1.0N	+6-weeks	M	33.2
C2R	DMM+1.0N	+6-weeks	M	21.4
C3R	DMM+1.0N	+6-weeks	M	48.9
D1R	DMM+1.0N	+6-weeks	M	37
D2R	DMM+1.0N	+6-weeks	M	25
D3R	DMM+1.0N	+6-weeks	M	36.2

Cleaved Aggrecan Immunostaining: Cleaved aggrecan levels in articular cartilage of the medial tibial plateau determined by immunohistochemistry with anti-NITEGE antibodies. Cleaved aggrecan levels reported as percentage of positive immunostaining per cartilage area.

Mouse ID	Group	Duration	Plateau	NITEGE Positive Signal (% Cartilage Area)
J1L	control	+2-weeks	M	0.441331
J2L	control	+2-weeks	M	0.132415
J3L	control	+2-weeks	M	0.356629
O3L	control	+2-weeks	M	0.83271
J1R	DMM-only	+2-weeks	M	0.241816
J2R	DMM-only	+2-weeks	M	1.055916
J3R	DMM-only	+2-weeks	M	1.221493
O3R	DMM-only	+2-weeks	M	1.541642
L1R	DMM+1.0N	+2-weeks	M	0.245954
L2R	DMM+1.0N	+2-weeks	M	0.36317
L3R	DMM+1.0N	+2-weeks	M	0.517325
M1R	DMM+1.0N	+2-weeks	M	1.620706
A1L	control	+6-weeks	M	0.325998
A2L	control	+6-weeks	M	0.157626
A3L	control	+6-weeks	M	0.114579
I2L	control	+6-weeks	M	0.193819
A1R	DMM-only	+6-weeks	M	0.18561
A2R	DMM-only	+6-weeks	M	0.374999
A3R	DMM-only	+6-weeks	M	0.651711
I2R	DMM-only	+6-weeks	M	0.288624
C1R	DMM+1.0N	+6-weeks	M	0.218258
C3R	DMM+1.0N	+6-weeks	M	0.48381
D1R	DMM+1.0N	+6-weeks	M	0.153103
D3R	DMM+1.0N	+6-weeks	M	0.299251